

Analytic studies on the SYK models

FROM INSTANTANEOUS THERMALIZATION TO HOLOGRAPHIC DUALITY

Dissertation

for the award of the degree

Doctor rerum naturalium

of the Georg-August-Universität Göttingen

within the doctoral program *Physics*

of the Georg-August University School of Science (GAUSS)

submitted by

Jan Cillié Louw

from Cape Town

Göttingen, 2023

Thesis Advisory Committee

Prof. Dr. Stefan Kehrein

Institute for Theoretical Physics
Georg-August-Universität Göttingen

Prof. Dr. Fabian Heidrich-Meisner

Institute for Theoretical Physics
Georg-August-Universität Göttingen

Prof. Dr. Peter K. Sollich

Institute for Theoretical Physics
Georg-August-Universität Göttingen

Members of the Examination Board

Reviewer: Prof. Dr. Stefan Kehrein

Institute for Theoretical Physics
Georg-August-Universität Göttingen

Second Reviewer: Prof. Dr. Fabian Heidrich-Meisner

Institute for Theoretical Physics
Georg-August-Universität Göttingen

Further Members of the Examination Board

Prof. Dr. Peter K. Sollich

Institute for Theoretical Physics
Georg-August-Universität Göttingen

Priv.-Doz. Dr. Salvatore R. Manmana

Institute for Theoretical Physics
Georg-August-Universität Göttingen

Prof. Dr. Claus Ropers

IV. Physikalisches Institut
Georg-August-Universität Göttingen

Prof. Dr. Thomas Weitz

I. Physikalisches Institut
Georg-August-Universität Göttingen

Date of the oral examination: 23-06-2023

Abstract

The quasiparticle picture is so prominent in condensed matter physics that it is almost taken as an axiom. Without this simplification, the physics becomes nearly intractable. However, the physics also becomes remarkable, leading to holographic connections to gravity found in such *strange* metals lacking a quasiparticle description. In this thesis we present analytic, i.e., mathematical results on the fermionic charged Sachdev-Ye-Kitaev (cSYK) models which capture these interesting features. We provide results on fast thermalization, chaotic-to-regular phase transitions, and charge dynamics in a lattice of such models. We also provide a concrete holographic mapping onto gravity showing how the partition functions of both charged dilaton gravity and the complex SYK model overlap exactly.

Contents

Abstract	I
Contents	II
1 Introduction and motivation	5
1.1 Fermi liquids	7
1.1.1 Mathematical Framework of Fermi-liquid theory	7
1.1.2 Quasiparticle poles and the Green's functions	9
1.2 Non-Fermi-Liquids	11
1.3 The solvable nonintegrable SYK models	14
1.3.1 Aspects of strange metals	16
1.3.2 Lack of quasiparticles	17
1.3.3 Chaos and holography	17
1.3.4 Experimental proposals for flat banded SYK models	18
1.4 Outline and main results of the thesis	19
2 Analytical methods for SYK models	21
2.1 Many many-body interactions	22
2.2 The kinetic SYK model	24
2.2.1 Existence of quasiparticles	26
2.3 Disordered action and self averaging	27
2.3.1 The G - Σ path integral	31
2.3.2 The near-conformal invariance in SYK	31
2.4 Exact solvability of the large- q SYK model	33
2.4.1 IR comparison	35
2.4.2 Solvable competing large- q SYK models	35
Appendix 2.A: Grassmann path integrals	36
Appendix 2.B: Lack of self-averaging in free particles	38
Appendix 2.C: Averaged Hamiltonian	39
Appendix 2.D: Conformal group	40
3 Dynamics in charged SYK models	41
3.1 Chaos and Lyapunov exponents	43

3.1.1	Motivation for regularized correlations	46
3.1.2	Large- q Lyapunov exponent	46
3.2	The Keldysh formalism	47
3.2.1	Kadanoff-Baym equations	49
3.2.2	SYK thermalization	50
3.2.3	Publication: Thermalization of many many-body interacting SYK models	52
3.3	Charge dynamics on a lattice	61
3.3.1	Current and charge density from continuity equation	62
3.3.1.1	Response to a thermoelectric gradient	63
3.3.1.2	Response to an electrical field	64
3.4	Analytical results for dynamics on a lattice	65
3.4.1	Preprint: Dynamics and Charge Fluctuations in Large- q Sachdev-Ye-Kitaev Lattices	67
	Appendix 3.A: Connectedness and lower bound on thermalization time	80
	Appendix 3.B: Momentum space transformation	81
	Appendix 3. C: Kubo's formula for conductivity	82
4	SYK Thermodynamics	85
4.1	Phase diagram of the complex SYK model	86
4.1.1	Obtaining the equation of state	87
4.1.2	Comparing KMS relations	88
4.1.3	Charged SYK Green's functions	89
4.2	A liquid-gas phase transition in the cSYK model	90
4.2.1	Publication: Shared universality of charged black holes and the complex large- q Sachdev-Ye-Kitaev model	93
4.3	Scaling and field mixing	102
4.3.1	Comparison to numerics	103
4.4	Motivation for studying the large- q case	105
	Appendix 4.A: Numerical calculation of the phase diagram	106
5	Black hole thermodynamics	107
5.1	Bekenstein bound and the implication of holography	107
5.1.1	Simplest model for holography	108
5.2	Regularity of the spherically symmetric metric	109
5.2.1	Black hole temperature from the Euclidean-trick	109
5.3	Phase transitions in black holes	110
5.3.1	Black hole chemistry in vacuum pressure	111
5.3.1.1	Mass from the Smarr relation derivation	112
5.4	JT gravity and SYK	113
5.4.1	Eulerian-trick for AdS_2	114
5.4.2	Motivation from changing length scale	115
5.5	Holographic mappings beyond the zero temperature limit	115

5.5.1	Preprint: Matching partition functions of deformed JT gravity and the charged SYK model	117
6	Summary and outlook	133
	Bibliography	137
	Acknowledgments	147
	CV	150

Preface

Author's Note: Publications

During this doctorate, I contributed to a selection of publications and preprints included in this thesis

- **Thermalization of many many-body interacting SYK models** (included in Sec. 3.2.3)
Jan C. Louw and Stefan Kehrein
Phys. Rev. B 105, 075117 (2022)
<https://doi.org/10.48550/arXiv.2111.08671>
Author contributions: J. C. L. did the analytic calculations and wrote the article. S. K. suggested the project, wrote part of the introduction, and independently did many of the analytical calculations. Both authors discussed the results.
- **Shared universality of charged black holes and the complex large-q Sachdev-Ye-Kitaev model** (included in Sec. 4.2.1)
Jan C. Louw and Stefan Kehrein
Phys. Rev. B 107, 075132 (2023)
<https://doi.org/10.1103/PhysRevB.107.075132>
Author contributions: J. C. L. suggested the direct rescaling of the charge density $Q \rightarrow \tilde{Q}q^{-1/2}$, did the analytic calculations, and wrote the article. S. K. suggested rescaling the chemical potential as $\mu = \hat{\mu}q^{-1/2}$, which inspired the consideration of multiple eventual rescalings in the paper, and also provided input on the manuscript. Both authors discussed the results and possible interpretations.
- **Dynamics and Charge Fluctuations in Large-q Sachdev-Ye-Kitaev Lattices** (included in Sec. 3.4.1)
Rishabh Jha and Jan C. Louw
Phys. Rev. B 107, 235114 (2023)
<https://doi.org/10.1103/PhysRevB.107.235114>
Author contributions: J. C. L. set up an early outline of the manuscript, having set up the analytic equations to be solved. Both authors together found the main results and revised the manuscript.
- **Matching partition functions of deformed JT gravity and the cSYK model** (included in Sec. 5.5.1)

Jan C. Louw, Sizheng Cao, and Xian-Hui Ge
arXiv:2305.05394

<https://doi.org/10.48550/arXiv.2305.05394>

Author contributions: J. C. L. did the analytic calculations and wrote the manuscript. S. C. verified some of the analytical calculations and produced all figures. X-H. G. revised parts of the manuscript and suggested linear stability analysis to extract the Lyapunov exponent. All authors contributed parts to the manuscript and discussed the results.

I also contributed to the following:

- **Thermalization of a Lipkin-Meshkov-Glick model coupled to a bosonic bath**

Jan C. Louw, Johannes N. Kriel, and Michael Kastner
Phys. Rev. A 100, 022115 (2019)

<https://doi.org/10.1103/PhysRevA.100.022115>

Author contributions: J. C. L. wrote the early draft of the manuscript and did all of the analytical calculations. M.K. suggested the project and contributed to the manuscript. H.K. suggested the methods using derivations and produces some of the numerical results. All authors discussed the methods and contributed to the manuscript and discussed the results.

- **Bosonic representation of a Lipkin-Meshkov-Glick model with Markovian dissipation**

Jan C. Louw, Johannes N. Kriel, and Michael Kastner
Phys. Rev. B 102, 094430 (2020)

<https://doi.org/10.1103/PhysRevB.102.094430>

Author contributions: J. C. L. wrote the early draft of the manuscript and did most of the analytical calculations. M.K. suggested the project and contributed to the manuscript. H.K. suggested the factorization method and solved the problem via an SU(1,1) Bogoliubov transform allowing one to directly study the heating of the system. All authors discussed the methods and contributed to the manuscript and discussed the results.

A note on natural units

The values of physical constants of nature depend on the units we use to measure them. In this thesis, we will discuss quantum mechanics, gravity, and statistical mechanics. For this, there is a particularly convenient set of units—the Planck units.

Planck unit	time	length	mass	temperature	charge
Expression	$t_P = \frac{\hbar}{m_P c^2}$	$\ell_P = ct_P$	$m_P = \sqrt{\frac{\hbar c}{G_N}}$	$T_P = \hbar / (k_B t_P)$	$Q_P = \sqrt{\frac{\alpha \hbar c}{k_e}}$
SI magnitude	10^{-43} [s] 10^{-25} [as]	10^{-35} [m] 10^{-15} [fm]	$\alpha 10^{-8}$ [kg] 10 [μ g]	10^{32} [K] 10^{30} [kK]	$\sqrt{\alpha} 10^{-18}$ [A·s] $\sqrt{\alpha} 10^0$ [A·as]

Figure 0.1: Planck units.

Our goal is to express the constants of nature in terms of natural units of length, time, energy ($E_P = m_P c^2$), charge, and temperature

$$c = \frac{\ell_P}{t_P}, \quad \hbar = \frac{E_P \ell_P}{c} = E_P t_P, \quad G_P = \frac{E_P \ell_P}{m_P^2}, \quad k_e = \frac{1}{4\pi\epsilon_0} = \frac{\alpha E_P \ell_P}{Q_P^2}, \quad k_B = \frac{E_P}{T_P}.$$

The above also reflects the energy competitions stemming from the various aspects of nature.

To motivate their usefulness let us consider the two crucial length scales involved in these fields. One is the reduced Compton wavelength, $\lambda = \hbar/(mc)$, which marks the length scale where many-body quantum effects become significant, and the other is the Schwarzschild radius, $r_s = 2mG_N/c^2$, which denotes the scale where gravity becomes important. The solution to $r_s = 2\lambda$ is the Planck mass, $m_P = \sqrt{\frac{\hbar c}{G_N}}$, which implies that a particle with Planck mass has a Compton wavelength of $\ell_P = \hbar/(cm_P)$. A theory of quantum gravity would then be necessary for such a localized mass, and the Planck temperature can be related to a wavelength of ℓ_P for black-body radiation.

The Planck time is 26 orders of magnitude shorter than the current record for (attosecond-lasers) ultrashort pulsed lasers [1]. The Planck length is approximately 20 orders of magnitude smaller than the root-mean-square radius of a proton. The Planck temperature is 27 orders of magnitude hotter than the hottest star. By setting $\alpha \approx 1/137$, i.e., setting it equal to the fine-structure constant, we have normalized the Planck charge such that the electron charge e is equal to $1Q_P$.

Throughout this thesis, we will work in natural Planck units, listed in Figure 0.1, which correspond to units where the Planck length, time, mass, temperature, and charge are set to unity. We will restore the units when necessary for specific reasons.

Chapter 1

Introduction and motivation

The holy grail of condensed matter physics is room-temperature superconductivity—metals that conduct electricity without any resistance whatsoever below a critical temperature of 300 degrees Kelvin. A significant stride towards this goal was achieved in 1986 with the discovery of high- T_c ceramics, with measured resistivity plotted in Fig. 1.1 [3]. This breakthrough had a dual nature; not only did it introduce high- T_c superconductivity, but it also revealed the existence of an unusual phase above the critical temperature T_c , characterized by its abnormal linear in T resistivity. Moreover, it appears increasingly probable that this enigmatic *strange* metal phase is not only crucial for understanding high-temperature superconductivity but could also provide insights into fundamental questions in quantum gravity [4].

The term “strange metal” is often used synonymously with “non-Fermi-liquid”, a near-definition that illustrates the core of this strangeness. It illustrates how different it is from what has been studied and understood over the last century, so much so that we define strange metals by what they are not. This apophatic definition underscores the prevalence and foundational nature of the quasiparticle concept in Fermi-liquid theory. As such, it only seems appropriate that we start by discussing such *normal* metals. Inspired by Mattuck [5], we contrast the two types of matter by considering three horses seen in Fig. 1.2.

The first image is that of a cartoon horse, with well-defined properties, like an ordinary particle. Bring many horses together, however, and they can become nearly impossible to predict. With the dust kicked up, hiding the horses, one focuses on the properties of the herd. If one is lucky, the collective behavior of the herd is simple, behaving as one quasi-horse with slightly altered properties¹. Similarly, the quasiparticles are collective excitations that arise in many-body systems due to the interactions between the original “bare” particles. Their influence on their neighbors effectively creates a surrounding cloud of excited particles. This particle cloud conceals/screens the

¹A school of fish might be a more intuitive picture.

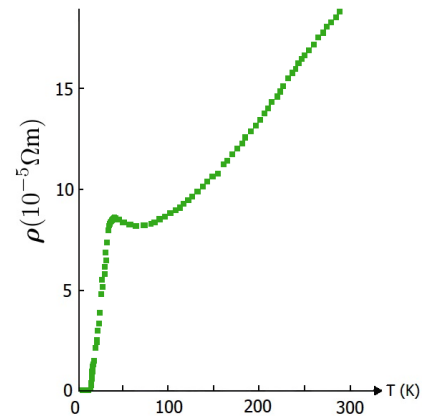


Figure 1.1: Measured resistivity of Lanthanum-Barium-Copper Oxide (adapted from [2])

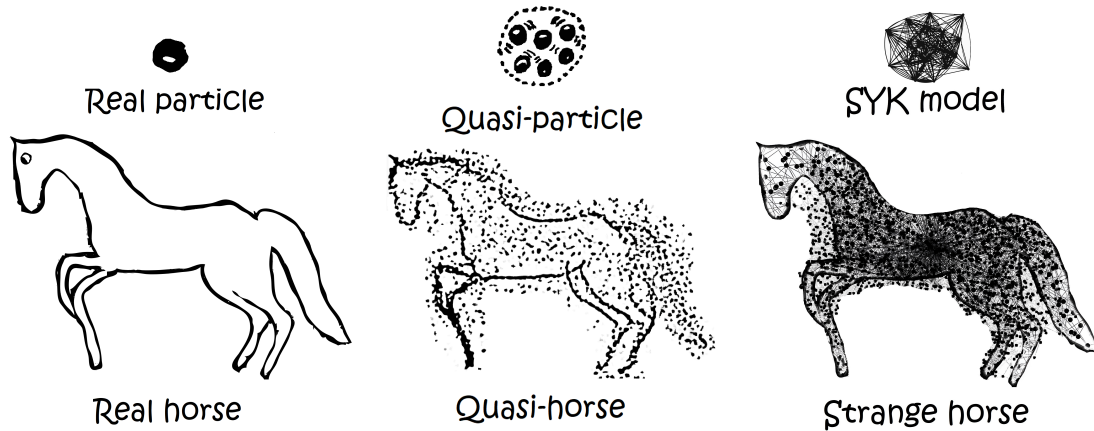


Figure 1.2: The three horses of condensed matter. On the left is a horse, in the middle is Mattuck’s quasi-horse, and on the right is a strange horse.

bare particles, much like the dust cloud obscures the horse, leading to weak interactions between quasiparticles. The cloud’s presence contributes additional mass to the real particle, resulting in a new renormalized mass m^* and bestowing it with a measurable finite lifetime.

The miracle of quasiparticles is the extent to which this behavior is reflected in reality [6]. For instance, this picture often remains valid even for strongly interacting systems. An intuitive explanation for this phenomenon is that the mean free path diverges at low temperatures, and as such, even a strongly interacting fluid (with diffuse scattering) can behave like a gas of ballistic²/free quasiparticles. This framework has been used to successfully describe a wide range of phenomena. Given our topic, an appropriate example of such quasiparticles is that of Cooper pairs. They are stable bosonic excitations that emerge in superconducting materials when electron pairs are bound together due to attractive phononic interactions [7], as described by Bardeen–Cooper–Schrieffer (BCS) theory. Other examples include the bosons in one-dimensional Tomonaga–Luttinger liquids [8], the anyons exhibiting fractional statistics in the fractional quantum Hall effect [9], and the renormalized fermions forming a Fermi-liquid in lattices.

Our third and final *strange* horse represents the unpredictable collective behavior of a chaotic herd. Its all-to-all graph-like structure represents the strongly correlated fermions, collectively entangled, leading to a whole state of matter. While the study of such a material is a difficult task, a whole class of solvable models has emerged over the last couple of decades that captures some of its aspects. These are the Sachdev–Ye–Kitaev (SYK) models. Throughout this thesis, we will present analytical results on such matter, stretching from thermalization behavior to holographic dualities with gravity.

Before introducing the SYK models, we first introduce the standard Fermi-liquid formalism which views strongly interacting systems as a collection of dressed nearly free quasiparticles. This puts everything in a greater context and allows us to provide contrast to systems lacking such a quasiparticle picture.

²Only scattering with the boundary needs to be considered

1.1 Fermi liquids

Physical systems typically consist of particles with many degrees of freedom described by nonlinear equations. Given this complex structure, the task of predicting the dynamics seems impossible. One might imagine that chaos could lead to some averaging behavior, hence uncorrelated statistics. Remarkably, assuming such *molecular chaos*, Boltzmann was able to write down a tractable equation describing the particles' momentum distribution n_k . Assuming spatial uniformity, this equation is given by $\dot{n}_k + F \cdot \nabla_k n_k = \mathcal{C}[n]$. While the left-hand side amounts to Newton's law for individual molecules³ subject to a force F , the right-hand side captures the complicated collisions between particles [4]. Boltzmann reduced this to the weighted average over all momentum conserving two-body scattering processes⁴, illustrated in Fig. 1.3,

$$n_k n_{k_1} - n_{k_2} n_{k_3}. \quad (1.1)$$

1.1.1 Mathematical Framework of Fermi-liquid theory

While the classical example already seemed daunting, the problem increases exponentially in complexity given a quantum system. Take for example a standard interacting (spinless) fermionic many-body Hamiltonian

$$\mathcal{H} = \sum_k \varepsilon_k^{(0)} c_k^\dagger c_k + \sum_{k_1, k_2, k_3, k_4} J_{k_3, k_4}^{k_1, k_2} c_{k_1}^\dagger c_{k_2}^\dagger c_{k_3} c_{k_4}. \quad (1.2)$$

By the spin-statistics theorem, the fermionic creation and annihilation operators satisfy the canonical anti-commutation relations

$$\{c_i, c_j^\dagger\} = \delta_{ij}, \quad \{c_i, c_j\} = 0 = \{c_i^\dagger, c_j^\dagger\}.$$

Given this, the only allowed fermion occupation numbers are 0 and 1 for each of the \mathcal{N} modes. Thus the space is spanned by $2^{\mathcal{N}}$ states. Numerically, such an exponentially large Hilbert space in system size limits us to considering small system sizes, i.e., far away from the regime of interest—the thermodynamics limit $\mathcal{N} \rightarrow \infty$. This is because standard methods, such as exact diagonalization, have a complexity that scales at least linearly with the size of the Hilbert space⁵ [10].

Let us start with the simplest case, namely a gas of free fermions. We then adiabatically introduce interactions that result in the free particles having re-normalized properties. In certain cases, the corresponding excitations can be viewed as particles dressed with a cloud of electrons, which can be described by a unitary transformation of the original fermions [11]. In particular, by

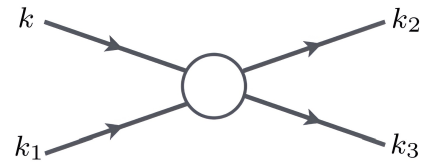


Figure 1.3: Two body scattering with momentum $(k, k_1) \rightarrow (k_2, k_3)$, where $k + k_1 = k_2 + k_3$.

³To see this, note that it is just Hamilton's equation for a position-independent phase space distribution n_k where the force is the negative gradient of the Hamiltonian. In other words, it is Newton's law for a distribution over momentum.

⁴Note the lack of contribution to \mathcal{C} when no scattering occurs, i.e., for equal incoming and outgoing momenta. The probability of scattering merely swapping momentum can be ignored since it has a measure of zero in comparison.

⁵One can, however, limit the size of the Hilbert space by considering subsectors. Although, these subsectors are usually still exponentially large in \mathcal{N} .

focusing on small excitations around the Fermi surface, one may define new fermionic operators. Such low-lying excitations are identified with a set of quasiparticles, each with energy ε_k and momentum distribution n_k . Remarkably, Boltzmann's simplification often holds even for such a dilute gas of dressed/quasi-particles in dimensions $d > 1$, with one important difference. Because of Pauli's exclusion principle, the particles can only evolve to unoccupied momentum modes, hence a reduced scattering phase space. Taking the probability of these modes being unoccupied into account modifies the expression in $\mathcal{C}[n]$ to

$$n_k n_{k_1} (1 - n_{k_2}) (1 - n_{k_3}) - n_{k_2} n_{k_3} (1 - n_k) (1 - n_{k_1}). \quad (1.3)$$

This marks the start of Landau's phenomenological⁶ Fermi-liquid theory. It offers a robust representation of quasiparticles and is crucial for understanding quantum many-body systems. Due to their weak interactions (small Landau parameters f_{k_1, k_2}) the total energy of these excitations is nearly linearly additive

$$E[\vec{n}] = E[\vec{0}] + \sum_k \varepsilon_k n_k + \sum_{k_1, k_2} f_{k_1, k_2} n_{k_1} n_{k_2} + \mathcal{O}(n^3) \quad (1.4)$$

which effectively parameterizes the energy of exponentially many low-lying states, $\sim e^{\alpha N}$, by a polynomial number of occupations $|n_1, n_2, \dots\rangle$. One consequence of Eq.(1.4) is that the many-body level spacings are polynomial $\delta E \sim 1/N$ for low energies. These collective excitations have a rather long lifetime, owing to the limited number of scattering processes available for fermions around the Fermi surface, at the Fermi energy ε_{k_F} . At zero temperature, all states are filled below the Fermi surface, and hence the exclusion principle and momentum conservation, reflected in (1.3), drastically restricts the scattering phase space. Consider again the process illustrated in Fig. 1.3, this time with one electron above the Fermi surface, $\xi_k \equiv \varepsilon_k - \varepsilon_{k_F} > 0$, which scatters with a particle in the Fermi sea, $\xi_{k_1} < 0$, the post-scattering particles must occupy unoccupied sites, i.e., above the Fermi surface $\xi_{k_2}, \xi_{k_3} > 0$. If the initial electron is close to the Fermi surface, then $\xi_{k_1}, \xi_{k_2}, \xi_{k_3}$ must also be close to it. In fact, at the surface, the scattering phase space goes to zero. At non-zero temperatures, the probability of finding two suitable fermions for scattering depends on the number of electrons in the thin outer and inner shells, with thickness proportional to T . Hence, the probability of *two* such scattering events is proportional to T^2 . Formally, the above analysis amounts to Fermi's golden rule, yielding the scattering rate [12, 13]

$$\Gamma_k \propto \pi^2 T^2 / \varepsilon_{k_F} + \xi_k^2 / \varepsilon_{k_F}. \quad (1.5)$$

Note that the scattering phase space volume goes to zero as $T \rightarrow 0$, implying an infinite quasiparticle lifetime at the Fermi surface; hence the above picture does not rely on interactions being weak.

Given that resistivity is directly related to transport, it is influenced by the probability of these scattering events. One might assume that electron-electron interactions generate resistivity with a T^2 dependence. This can be seen directly in the Drude formula in two dimensions, $\rho_e = m^* \Gamma / (n q_e^2)$ with transport scattering rate Γ and density of electrons n [12]. As such, the quadratic dependence

⁶It is phenomenological in the sense that it describes the empirical relationship of phenomena to each other, in a way that is consistent with fundamental theory, although it is not derived from first principles.

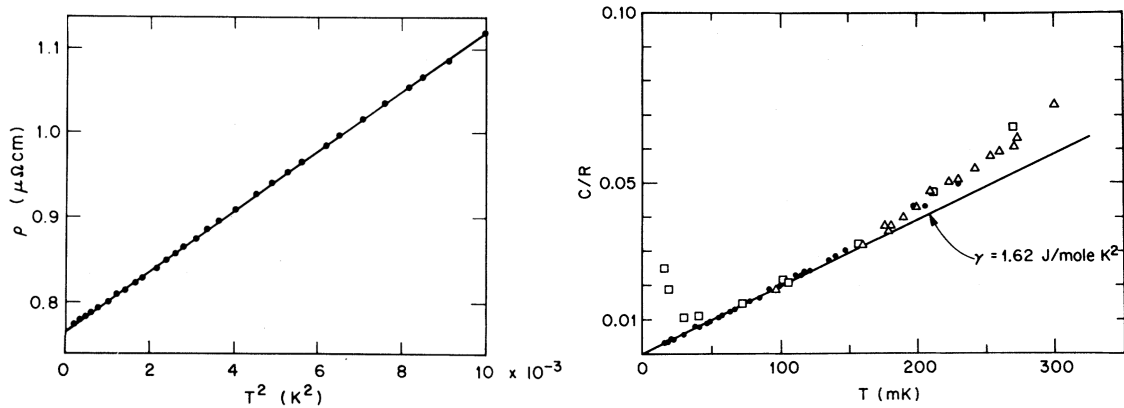


Figure 1.4: (Left) Electrical resistivity of CeAl_{13} in the millikelvin regime as a function of T^2 . (Right) Specific heat of CeAl_{13} in millikelvin regime, in zero field (\bullet , \triangle) and in $10^4 \text{Oe} = (4\pi)^{-1} 10^7 \text{A/m}$ (\square). Figures adapted from [14]

on T is indeed present for Fermi-liquids, since near the Fermi-surface $\Gamma \propto T^2$ [15]. This, and many other Fermi liquid predictions, can be seen in many materials at *low* temperatures [12]. Take for instance cerium-aluminum-13 (CeAl_{13}), with experimental data plotted in Fig. 1.4. On the left is the resistivity plotted as a function of T^2 . The strong linear behavior of this function, as predicted, illustrates the power of this formalism. Further, a Sommerfeld expansion around the Fermi surface yields the linear specific heat $C \propto T$, again matching with the data on the right.

Since the temperature is also related to the mean scattering rate of these electrons, it is expected that both electrical and thermal conductivity should be functions of temperature. Indeed, one usually finds $\rho_e = LT\rho_{\text{th}}$, where L is known as the Lorentz number or Wiedemann–Franz (WF) ratio. Fermi-liquid theory predicts the Sommerfeld value $L_0 = \pi^2 e^{-2}/3$ for L , which is the WF law [16, 17]. Again, this is experimentally verified in many compounds, see for instance Fig. 1.5. This result rests on the fact that heat and charge are both transported via the quasiparticles at low temperatures, where phononic contributions can be ignored. Typically, deviations away from the Sommerfeld value again become small at larger temperatures [18], i.e., the law fails in the intermediate regime.

1.1.2 Quasiparticle poles and the Green’s functions

To simplify the analysis, one often focuses on correlation functions. Here we give a brief introduction to such correlation functions such that we may contrast them with those found in non-Fermi-liquids. As an example, consider the process where a fermion with momentum k is “created” (added) at a time $t = 0$ and allowed to propagate until a time t when the excitation is destroyed (removed). The independence of the single particle momentum mode k in the interacting system [21] is then measured by the retarded Green’s function

$$G_k^R(t) = -i\Theta(t)\langle\{c_k(t), c_k^\dagger\}\rangle \quad (1.6)$$

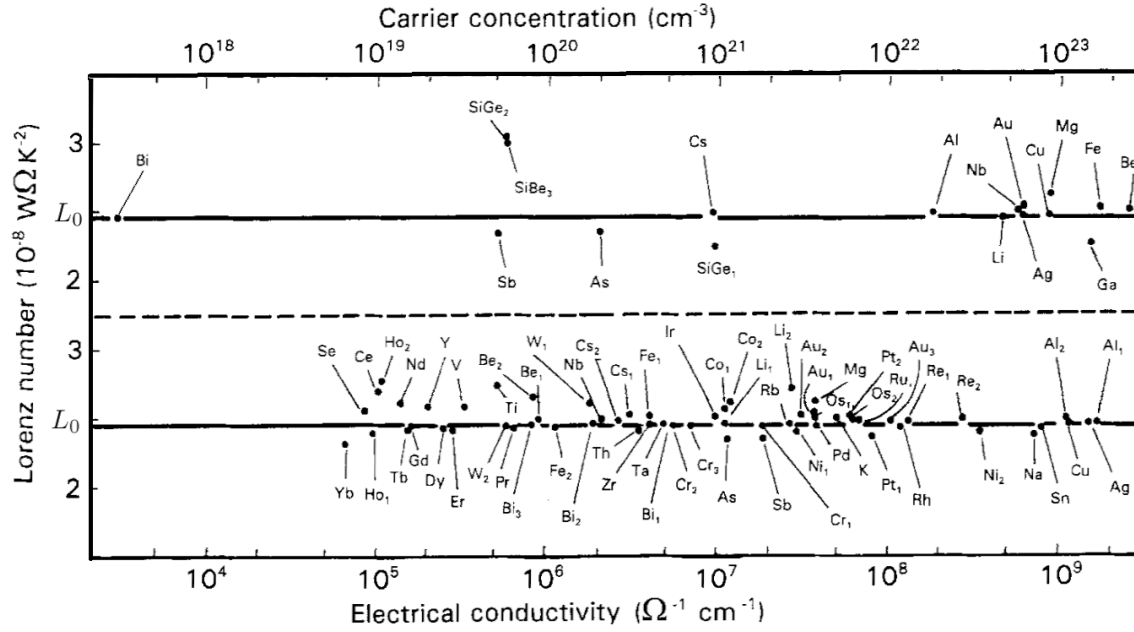


Figure 1.5: Experimentally measured Lorenz number of normal metals in the low-temperature residual resistance regime. Figure adapted from [19, 20].

which would merely yield a phase in the case without any interactions $\langle \{c_k(t), c_k^\dagger\} \rangle = e^{-i\xi_k^{(0)}t}$. In frequency space we have

$$G_{k;0}^R(\omega + i0^+) = \frac{1}{\omega + i0^+ - \xi_k^{(0)}} = -i\delta(\omega - \xi_k^{(0)}) + \mathcal{P} \frac{1}{\omega - \xi_k^{(0)}},$$

where we have used the Sokhotski–Plemelj theorem to write the fraction in terms of a Cauchy principal value \mathcal{P} and a delta spectral function $A_{k;0}(\omega) \equiv -\Im G_{k;0}^R(\omega)/\pi$. In general the spectral function $A_k(\omega) = -\Im G_k^R(\omega)/\pi$ is a positive function and is normalized over $\omega \in \mathbb{R}$. In fact, it represents the probability of finding a single particle excitation with momentum k and energy ω . So, a delta spectral function means that the excitation energy of the particle must correspond to the dispersion relation $\xi_k^{(0)}$. From the above, one can define the Fermi-surface $\xi_k^{(0)} = 0$ as all k such that in frequency space $G_{k;0}^R(0) \rightarrow \infty$.

Interaction can be included via a self-energy Σ , which appears in Dyson's equation

$$G^R(\omega)^{-1} = G_0^R(\omega)^{-1} - \Sigma^R(\omega). \quad (1.7)$$

The self-energy can be identified with the sum of all irreducible diagrams, as we see in Sec. 1.3 and again in Sec. 2.2. To gain some idea of the role that the self-energy plays, let us consider a minimal example, suppressing the k subscripts,

$$\Sigma^R(\omega) = -(\omega - \xi - i\Gamma)/Z + \omega - \xi^{(0)},$$

where Z is the spectral weight. From (1.7) we then have $G^R(\omega) = Z/(\omega - i\Gamma - \xi)$, or $G^R(t) \propto e^{-(i\xi + \Gamma)t}$ for $t > 0$, i.e., the imaginary part of Σ yields the quasiparticle's scattering rate, while the real part renormalizes its energy.

At $T = 0$ and close to the Fermi surface, we may ignore the imaginary contribution, since the scattering rate (1.5) is $\Gamma = \mathcal{O}(\xi^2)$. This yields the leading order contribution

$$G_k^R(\omega) = \frac{Z_k}{\omega - \xi_k} + G_{k;\text{inc}}^R(\omega), \quad (1.8)$$

where $G_{k;\text{inc}}^R(\omega)$ has no poles. With this one can define the Fermi surface even for the interacting system, again as all k such that $G_k^R(0)$ diverges at $T = 0$.

One can study the self-energy experimentally via angle-resolved photoemission spectroscopy (ARPES), where electrons are ejected from materials via the photoelectric effect. Their measured energy and momentum are then used to determine the spectral function $A_k(\omega)$ as plotted in Fig. 1.6. Note that as k tends to the Fermi momentum k_F , the peaks narrow. This reflects the fact that quasiparticles close to the surface have longer lifetimes. The peak has a width proportional to the temperature, reflecting the thermal broadening of the Fermi distribution function. Here, the temperatures correspond to energies several orders of magnitude smaller than the typical energy of the interactions. It is only as $T \rightarrow 0$ that the peak tends to a sharp Lorentzian function.

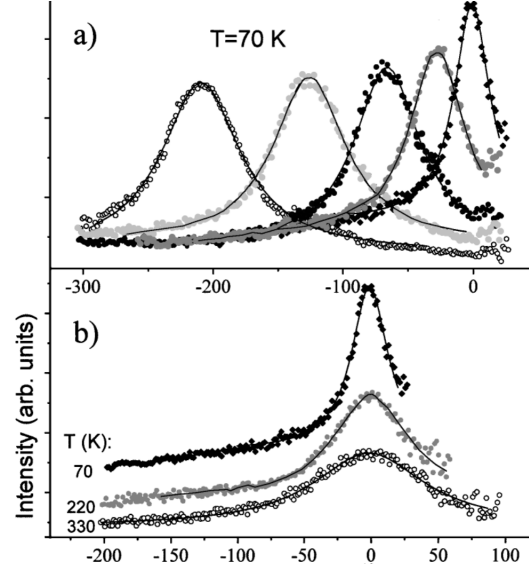


Figure 1.6: The spectral function $A_k(\omega)$ of Mo(110) [21, 22]. The horizontal axis is ω , where the Fermi energy is at $\omega = 0$. (a) For different momenta k . (b) For different temperatures T .

1.2 Non-Fermi-Liquids

Let us now return to the topic of high- T_c superconductors, like cuprates (copper-oxides) mentioned at the start. Such ceramics are typically insulating [2], however, for Lanthanum-Copper-Oxide La_2CuO_4 , with a random set of Lanthanum atoms replaced by barium $\text{La}_{2-x}\text{Ba}_x\text{CuO}_4$, it was discovered to have a superconductive phase [3]. At optimal doping $x = 0.15$, where the critical temperature T_c is maximized, it has $T_c = 35$ Kelvin, more than double the previous record.

Using BCS theory, given some assumptions on the electronic band structure, one can prove a theoretical upper bound on T_c of $T_c^* = 28\text{K}$ [23], with the highest known single-gap⁷ BCS

⁷Multi-gap (multi-banded) superconductors can overshoot this bound, e.g., V_3Si [24] with $T_c^* = 40\text{K}$ [23]. The largest experimentally observed T_c in such a material is $T_c = 39\text{K}$ in Magnesium diboride MgB_2 . This is due to two different bands contributing to the superconducting state, with strong electron-phonon coupling in one band and weaker coupling in the other.

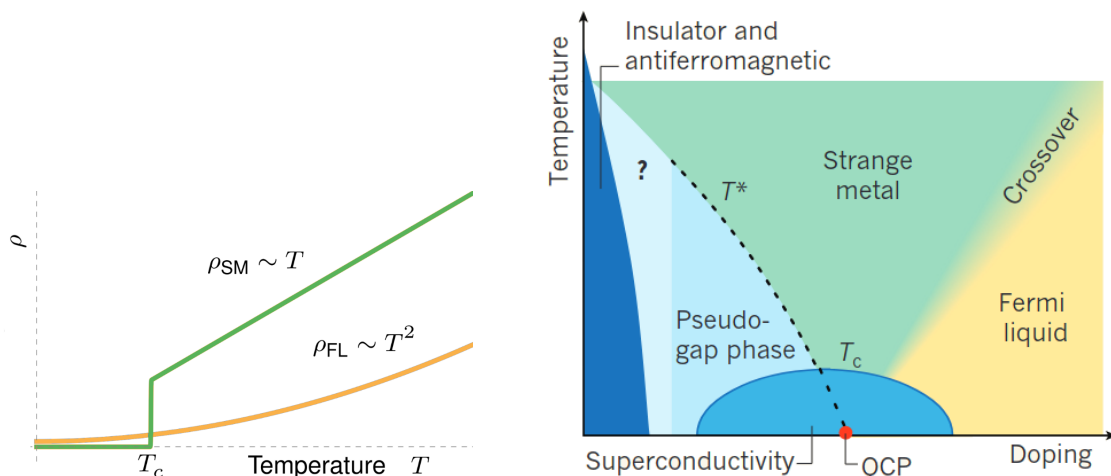


Figure 1.7: (Left) Resistivity of strange and normal metals. (Right) Phase diagram of cuprate (adapted from [26]). For certain materials, the doping can be simulated via a pressure [27].

superconductor being niobium germanium Nb₃Ge with $T_c = 24K$ [25]. Thus, such high T_c -superconductors require a different mathematical approach than ordinary Fermi-liquid and BCS theory.

The typical phase diagram of a cuprate is plotted in Fig. 1.7. At low temperatures, one sees a whole dome covering the superconductive phase spanning a range of doping. For low doping, the cuprates are insulating. Between T_c and T_c^* , lies the pseudogap phase, named due to a dip in the density of states to some non-zero value [26]. In terms of this phase diagram, our focus is on the green area, where the quasiparticle picture completely breaks down. In particular, at near-optimal doping, for $T > T_c$, the resistivity becomes linear in temperature T , plotted in Fig. 1.7. Such linear resistance is also common to so-called bad metals. They are also called non-saturating metals since their resistance does not saturate to the Mott-Ioffe-Regel bound $\rho_e = k_F^{d-2} e^2 / \hbar$ [28] but rather linearly overshoots it at high temperatures [29]. A quasiparticle picture would then imply that their mean-free path has become smaller than a lattice constant. At higher doping, the Fermi-liquid is restored as reflected in a quadratic temperature resistivity at low temperatures [30]. The contrast between the two cases was plotted in Fig.1.2. In the green region the Wiedemann–Franz law [31–33] is no longer satisfied. Due to these deviations from ordinary materials, this is termed the *strange metals* phase. The resistivity $\rho_e = \rho_0 + A_{SM}T + A_{FL}T^2$ corresponding to the right-hand side of the phase diagram is nicely seen in the quasi-one-dimensional Bechgaard-salts, where the constant A_{FL} scales with the critical temperature T_c [34]. What this means is that when the critical temperature is tuned to zero, via either pressure or doping, the resistivity is quadratic in temperature at low temperatures, corresponding to the yellow part. Otherwise, one is left with zero resistivity in the superconductive phase and a leading order linear in T resistivity above, corresponding to the strange metal phase.

Such strange metals thermalize rapidly due to their Planckian transport $\tau_{SM} = \alpha \hbar \beta \ll \Gamma_{FL}^{-1}$, where $\hbar \beta$ is the Planckian/Boltzmann time. Experimentally α is usually close to 1 for many

materials with high- T_c phases [35]:

Material	Bi2212	Bi2201	LSCO	Nd-LSCO	PCCO	LCCO	TMTSF
α	1.1 ± 0.3	1 ± 0.4	0.9 ± 0.3	0.7 ± 0.4	0.8 ± 0.2	1.2 ± 0.3	1 ± 0.3

Importantly, note that τ_{SM} has no dependence on the coupling strength between the electrons since α is just a number. This occurs when a system lacks quasiparticles, in which case the only relevant energy scale is the temperature T . One then finds that the equally important quantum fluctuations (which arise due to the uncertainty principle) and thermal fluctuations (which arise due to the finite temperature) can conspire to yield Planckian dynamics [36]. This timescale thus provides an upper bound on the thermalization rate [36, 37], also see [38, App. B].

To theoretically study such strange phenomena, we require a mathematical model which goes beyond Fermi-liquid theory. A starting point is to ask why Landau’s robust quasiparticle picture might break down in the first place. To understand this, let us focus on the foundation of Fermi-liquid theory—the existence of the Fermi-surface. Clearly, this surface exists for a non-interacting system. We have before considered how the Green’s functions are changed when switching on interactions. One may prove that this surface still exists in that case. Not only does it exist, but it was shown by Luttinger that the enclosed volume remains invariant. The proof of Luttinger’s theorem, however, relies on a perturbative series to all orders in the interactions [39]. Note that this is a non-perturbative result, in other words, the result does not rely on small interactions. It rather depends on the fermionic scattering limitations around the Fermi surface we mentioned before. This makes it applicable even at strong interactions, hence the robust nature of quasiparticles. However, while interactions need not be small, one does require the perturbative series to be valid. Indeed, the series no longer converges in the presence of quantum phase transitions [40] or more generally when there exists some singularity in the series. The latter occurs in a 1D electron gas which is no longer described by fermions, but rather by a bosonic (Luttinger) liquid [8].

Let us attempt to classify these cases by considering the self-energy. There are three main ways in which the theory can break down [41]. The first is when dealing with a non-analytic self-energy, found in marginal Fermi liquids (MFL), e.g.,

$$\Sigma(k_F, \omega) \sim \ln(\omega_c/\omega) + i\omega.$$

An example of this would be the 2-dimensional Hubbard model [42–44]. At $T = 0$ and at the Fermi energy, the MFL form of the self-energy implies a diverging m^* .

Another breakdown occurs for multipole singularities, as found in BCS states. Lastly, the Green’s functions

$$\mathcal{G}(\omega) \sim \omega^{2\Delta-1}, \tag{1.9}$$

and hence the self-energy, could have a branch cut $\Delta < 1/2$ instead of a pole $\Delta = 1/2$. We now move on to the SYK models, which fit this third example [45].

1.3 The solvable nonintegrable SYK models

One important aspect of both strange metals and Fermi-liquids are their energy level statistics⁸, i.e., the distribution function $P(\delta E)$ describing the gaps between consecutive energy level $\delta E = E_{i+1} - E_i$. Systems with uncorrelated eigenvalues are integrable [46], i.e., they have Poissonian level statistics $P_P(\delta E) \propto e^{-\alpha\delta E}$ [47]. Typically, one may find the eigenstates of such systems via Bethe ansatz. For instance, a harmonic oscillator with a non-linearity perturbation satisfies Poissonian statistics [48]. Typically, integrable systems map onto non-chaotic systems in the classical limit. This is the Berry-Tabor conjecture [49].

For classical systems, solvability usually implies integrability [50], which typically holds true in quantum systems as well. Indeed, Fermi-liquid theory describes these low-lying integrable excitations of certain models. An exception to this is the class of SYK models [51], which serve as tractable nonintegrable models [33, 51–53]. They have nonintegrable Wigner-Dyson level statistics

$$P_{\text{WD}}(\delta E) \propto \delta E^\beta e^{-\alpha\delta E^2}, \quad (1.10)$$

where $\beta = 1, 2, 4$ correspond to the orthogonal, unitary, and symplectic Gaussian ensembles respectively. The SYK models will fit all three of these ensembles depending on the number of fermions in the system \mathcal{N} . This \mathcal{N} -dependent β is due to differences in Clifford algebras, it will be modular 8 for real fermions [54] and modular 4 for complex fermions [55].

The tractability in the SYK models arises, in part, from their *quenched* disorder. In other words, their interactions are described by quenched (constants fixed at some initial time $t = t_0$) random disorder X , with a mean of zero. The random variables X are typically assumed to be Gaussian, although this is not necessary. Such *quenched* random interactions are commonly used to model impurity systems where the coupling varies from point to point in an uncontrolled way. This is unusual in QFT, where we usually assume homogeneity and fixed couplings. The study of these solvable models originates in the Sachdev-Ye (SY) model [51], which consists of a lattice with \mathcal{N} randomly interacting spins. We will focus on the fermionic variant of the SY model, known as the SYK model. The simplest version consists of \mathcal{N} interacting Majorana fermions [56]

$$\mathcal{H}_{\text{SYK}} \equiv J \sum_{i_1, i_2, i_3, i_4=1}^{\mathcal{N}} X_{i_1, i_2, i_3, i_4} \chi_{i_1} \chi_{i_2} \chi_{i_3} \chi_{i_4}. \quad (1.11)$$

Here χ are (hermitian) Majorana fermionic operators, which are their own anti-particles ($\chi_i^\dagger = \chi_i$) and are thus defined by a single anti-commutation relation

$$\{\chi_i, \chi_j\} = 2\delta_{ij}.$$

Since the interactions are all-to-all, i.e., infinite-range exchange interactions, the term flavor may be more appropriate than lattice site for the labels i .

⁸It is important to remove any symmetry influences on this function by calculating level spacings in symmetry sub-sectors. Further, to obtain an honest representation of $P(\delta E)$ an “unfolding” procedure is first done on the spectrum.

Importantly, all couplings X_{i_1, i_2, i_3, i_4} are independent and identical random (IID) variables. In the large \mathcal{N} regime, a diagrammatic expansion, illustrated in Fig. 1.8, indicates that the melon diagrams dominate over all other diagrams⁹. The important point is that these melons are examples of planar diagrams, which have no “intersecting” dashed lines corresponding to averaged random variables, such as those found in the second line in Fig. 1.8. We will return to this topic again in the next chapter. Such reducible diagrams are particularly simple to re-sum, in this case yielding a self-energy $\Sigma = J^2 G^3$.

For low energies, we typically study ordinary electrons described by complex Dirac fermions. Their annihilation operators are related to real Majorana fermions via $2c_i = \chi_{2i} + \imath\chi_{2i+1}$, with corresponding creation operators $2c_i^\dagger = \chi_{2i} - \imath\chi_{2i+1}$. Extending (1.11) to include such fermions yields the complex SYK (cSYK) model¹⁰ [53, 58]

$$\mathcal{H}_4 = J_4 \sum_{\substack{1 \leq i_1 < i_2 \leq \mathcal{N} \\ 1 \leq j_1 < j_2 \leq \mathcal{N}}} X_{j_1 j_2}^{i_1 i_2} c_{i_1}^\dagger c_{i_2}^\dagger c_{j_2} c_{j_1}, \quad (1.12)$$

where $(X_{j_1, j_2}^{i_1, i_2})^* = X_{i_1, i_2}^{j_1, j_2}$ ensures the hermiticity of the Hamiltonian.

For this Hamiltonian there is a U(1) symmetry, corresponding to a conserved charge density

$$\mathcal{Q} = \frac{1}{\mathcal{N}} \sum_{i=1}^{\mathcal{N}} \langle c_i^\dagger c_i \rangle - \frac{1}{2}. \quad (1.13)$$

From this one can assign charges of plus or minus half to particles and holes respectively. One can then view the terms in (1.12) as exchanging charges between lattice sites, depicted schematically in Fig. 1.9. By tuning a chemical potential, we can force the system to arbitrary filling. The diagrams re-sum to yield a self-energy matching that of the SY model $\Sigma(t) = -J_4^2 G(t)^2 G(-t)$. Here half filling corresponds to charge neutrality $\mathcal{Q} = 0$, for which the KMS relation yields $G(-t) = -G(t)$, hence reducing to the Majorana case, where one can ignore the arrows in Fig. 1.8.

⁹The directions of the arrows will be important for the Dirac fermionic case. For the Majorana case, the arrows can be ignored due to time-reflection symmetry.

¹⁰Note that, as written here, this Hamiltonian does not respect particle-hole symmetry [57].

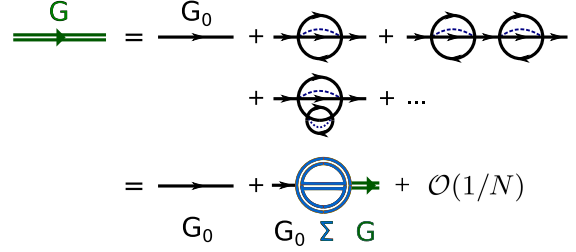


Figure 1.8: Leading order Feynman diagrams for the SYK model. The dashed blue lines indicate RVs averaging together, the black lines with arrows are the non-interacting Green’s functions.

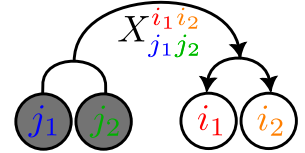


Figure 1.9: Schematic representation of the effect of the terms in (1.12) leading to the swapping of positive and negative “charges”, i.e., particles and holes.

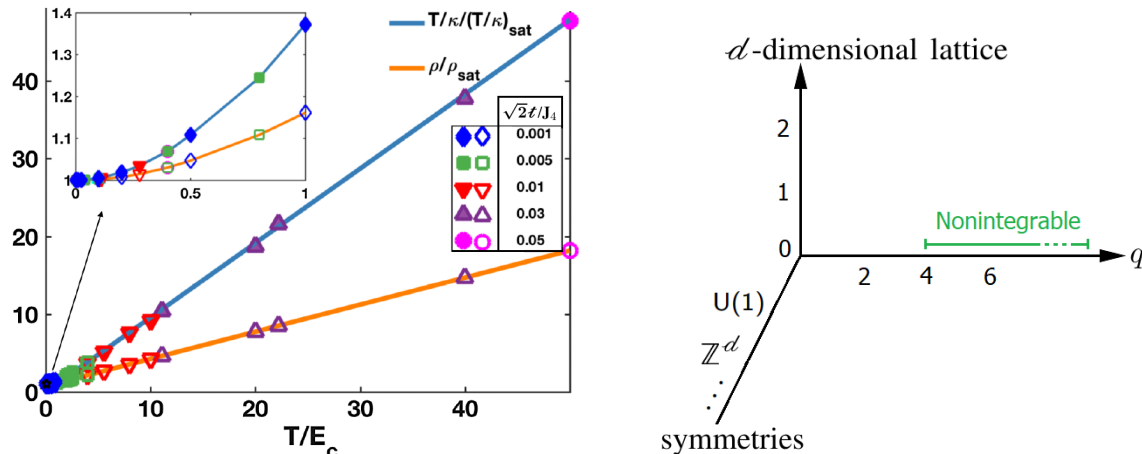


Figure 1.10: (Left) Thermal (κ^{-1}) and electrical (ρ) resistivities for different temperatures T of an SYK sheet, taken from [33]. (Right) Various generalizations of the SYK models, for instance by adding symmetries or considering $q/2$ -body interactions or dimensions $d > 0$.

1.3.1 Aspects of strange metals

In the motivation for these models, we placed a strong emphasis on modeling strange metals. However, up to this point, we have only introduced models with all-to-all IID interactions. As such, they have *no* built-in sense of locality and hence can be considered to be zero-dimensional. Such a local structure is included by studying coupling cSYK models via SYK-type hopping terms

$$\mathcal{H}_2^{x,x'} = t \sum_{ij=1}^{\mathcal{N}} Y_j^i(x, x') c_{x';i}^\dagger c_{x;j} + \text{H.C.},$$

to form a d -dimensional lattice.

The self-energy of such coupled models remains rather simple. This is because the independence in the zero mean random variables decouples the various Hamiltonians from one another. Hence, one can easily combine a near arbitrary set of SYK models and study their behavior [45]. Due to the simplicity of combining and extending different SYK models, various generalizations have been considered. The various directions in which the models have been extended are depicted in Fig. 1.10. For instance, by adding additional symmetries in the disorder, one even allows for a superconducting instability [59]. Coupling to bosons has also been studied in the Yukawa-SYK model [60]. By considering $q/2$ -body interactions, one finds similar chaotic properties [45], while having more access to analytical results [61]. And by considering d -dimensional lattices, one can study transport properties.

The strange metal behavior can then be found in the electrical and thermal resistivity [33]. To see this, consider the plots in Fig. 1.2. At low temperatures, below a coherence energy $E_c = 2t^2/J_4$, the hopping dominates. The residual entropy density $\mathcal{S}(T)$ stemming from the interaction is then rapidly quenched to zero. This implies a large Sommerfeld coefficient $\gamma = \mathcal{S}'(0)$, which is proportional to the effective mass. Hence, at low temperatures, the system is a heavy Fermi liquid

with a large mass renormalization. As expected, it also yields the standard quadratic in temperature resistivity. This reverses above a coherence temperature $T > E_c$, where the interactions dominate, leaving a linear resistivity $\rho_e \propto T$, consistent with an incoherent metal (strange metal-like) phase. By considering the ratios of resistivities, one notes how the Wiedemann-Franz law holds at low temperatures $L = L_0$ and is smoothly broken beyond the coherence temperature $L \rightarrow 3L_0/8$.

1.3.2 Lack of quasiparticles

These SYK models all have a rather peculiar feature, namely that their entropy density $\mathcal{S}_{\mathcal{N}}(T) \equiv -\langle \ln \varrho \rangle / \mathcal{N}$, remains finite in the thermodynamic limit $\mathcal{S}(T) \equiv \mathcal{S}_{\infty}(T)$, even at zero temperature $\mathcal{S}(0) \neq 0$. A quick check shows that a D -fold degenerate ground state $\varrho_0 = \mathbb{1}_D/D$ yields an entropy $\mathcal{N}\mathcal{S}_{\mathcal{N}}(T) = D \ln D$. Hence, if $D \sim e^{\mathcal{W}(\mathcal{N}\mathcal{S}_0)}$, where \mathcal{W} is the product log, then we are left with a residual entropy density $\mathcal{S}(T=0) = \mathcal{S}_0$ in the thermodynamic limit. Here, however, the disorder and lack of symmetries in the SYK model prevent the needed properties to produce such an extensively degenerate ground state. As such, one may wonder how a system with a non-degenerate ground state can have a non-zero (even extensively large) entropy at zero kelvin.

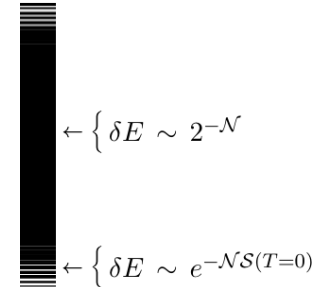


Figure 1.11: Energy level spacings of SYK models.

The solution to this mystery lies in their lack of quasiparticles.

This is seen in their level spacings plotted in Fig. 1.11. The exponentially small level spacings in the bulk of the spectrum are typical for many-body Hamiltonians. The novelty is that their level spacings remain exponentially small down to above the ground state, $\delta E \sim e^{-\mathcal{N}\mathcal{S}(T=0)}$ [62]. A comparison to the polynomial level spacings found in Fermi-liquids (1.4) is an immediate sign that the quasiparticle picture fails. In other words, the exponentially small level spacings are an indication that the Fermi-liquid quasiparticle picture cannot even hold right above the ground state. With such exponentially small level spacings, one can obtain $\mathcal{S}_{\infty}(T) \xrightarrow{T \rightarrow 0} \mathcal{S}(T=0)$. The limits do not commute, however, $\mathcal{N}\mathcal{S}_{\mathcal{N}}(0) \sim D \ln(D)$ is indeed zero because there is only a single ground state $D = 1$.

1.3.3 Chaos and holography

The above lack of degeneracy also hints at a different feature of the model. When considering the full distribution function over eigenvalues, one finds a measure of zero corresponding to overlapping eigenvalues. This is partially reflected in the Wigner-Dyson level spacing distribution $P_{\text{WD}}(0) = 0$, i.e., a measure of zero for degenerate eigenvalues. Such level repulsion is a typical feature found in quantum systems with a chaotic classical counterpart. Typically a system that satisfies Wigner-Dyson statistics also displays chaos under the classical limit. This observation inspired the Bohigas-Giannoni-Schmit (BGS) conjecture, stating that (single-body¹¹) quantum models with

¹¹In other words, the statement is not about the many-body quantum systems we consider here. For such second quantized models, the correspondence between quantum and classical chaos becomes more complex. We will return to this point again in Sec. 4.1.2

chaotic classical limits, with properties such as ergodicity, will be nonintegrable [63, 64]. The SYK models are even maximally chaotic, saturating the Maldacena-Stanford-Shenker (MSS) bound on the Lyapunov exponent $\lambda_{\text{MMS}} = 2\pi T$ [65]. The resurgence of interest in these models was primarily driven by this feature since it hints at a possible simple model for holography. This is in part because this chaotic nature is a key feature of gravity, with a saturated Lyapunov exponent $\lambda_L = 2\pi T$ found in most (if not all) non-extremal black holes. This together with an emergent conformal symmetry at low energies makes it a candidate for an anti-de-Sitter (AdS)/conformal field theory (CFT) correspondence. Not only would this be a candidate for holography, but its simplicity would also allow us to gain a more concrete understanding of the mapping. This is because the correspondence typically manifests itself as an S-duality¹², meaning when the coupling strength is strong on one side of the duality, it is weak on the other. In other words, when one theory is easy to solve, the other is nearly intractable, and vice versa. This is, in fact, one of the most appealing features of AdS/CFT, since it gives us a possible alternative to understanding strongly correlated quantum systems via classical Einstein gravity. It does, however, also pose a problem, namely a concrete verification and understanding of the duality. Here the proposal is between a rare tractable model for a strongly interacting quantum system, which would again be dual to a weakly interacting, i.e., classical gravity. Hence, one can in principle find the exact mapping between the two theories.

Motivation.— The combination of the above features: lack of quasiparticles, strange metal properties, a conformal symmetry, non-integrability, maximally chaotic, and yet still tractable in the thermodynamic limit, makes this SYK models a remarkable rarity. They stand in stark contrast to traditional quantum many-body physics where exact solutions exist only for integrable models, leaving only numerical options for nonintegrable models. These numerical methods are then plagued by the curse of dimensionality, with a growing Hilbert space of size [degrees of freedom] ^{\mathcal{N}} restricting studies to small particle numbers \mathcal{N} . By sidestepping this, these models have opened the pathway to analytical insights into quantum chaotic models as well as quantum gravity.

1.3.4 Experimental proposals for flat banded SYK models

Given the discussed relation between strange metals and SYK model chains in Sec. 1.3.1, one might wonder what further relations are seen between these models and real materials¹³. For instance, one hopes to somehow simulate some $q = 4$ SYK-type model. There is indeed a range of simulation/digital approaches usually focused on the Majorana case [67–69].

In terms of a more standard notion of “experimental” setups, the problem becomes more difficult. There are essentially four features of the SYK model that make it physically unusual. The first is its lack of kinetic (quadratic) term. Experimentally this would correspond to a flat banded system, as opposed to a non-flat dispersion relation, e.g., $\epsilon_k = |k|^2/(2m)$. Approximate flat bands are found in real materials, for instance, magic-angle graphene [70–72], or in a Kagome optical lattice [73]. Other methods to create such flat bands are discussed in [73]. The second and third unusual features are the *all-to-all* and *random* couplings which seem rather far removed from microscopic

¹²The first of such dualities was the Kramers–Wannier duality for the two-dimensional Ising model [66]. The strong and weak coupling corresponds to low and high temperatures, respectively.

¹³Unfortunately creating a black hole in the lab is beyond our current capability.

Hamiltonians. The all-to-all couplings, i.e., infinite-range couplings, could be approximated with sufficiently long-ranged interactions. The randomness was also partially addressed by considering an ensemble of sampled graphene flakes with pseudo-random irregular boundaries [74] or via various other protocols for generating randomness in certain materials summarized in [75]. The fourth aspect, and possibly the most important, is its chaotic nature, or rather its *maximally* chaotic nature. Proposals for this again involve disordered graphene materials [72, 74].

There are various experimental proposals for mimicking a subset of these four SYK features. These include solid state materials [72, 74, 76–78], as well as both cold atoms and optical lattice proposals [75, 79].

1.4 Outline and main results of the thesis

The thesis will be outlined as follows: In Chapter 2, we describe various *analytical methods* for dealing with the $q/2$ -body interacting Sachdev-Ye-Kitaev (SYK) models. These methods include the integrable kinetic case $q = 2$, the use of near-conformal symmetry to extract infrared results and a $1/q$ expansion. We compare the analytically obtained leading-order $1/q$ results to numerically obtained results for $q = 4$, highlighting the strong overlap. Such overlap holds for rather general SYK models and settings, hence will continue to be found in all subsequent chapters.

In Chapter 3, we consider the non-equilibrium dynamics of the SYK model, leaving the equilibrium physics for the next chapter. This chapter will be useful in understanding the results in the subsequent chapters since the chaotic nature of the SYK models will be an important characteristic throughout this thesis. The Lyapunov exponent characterizing the degree of chaos is found by considering certain correlators which we review. We then focus on the thermalization behavior of the SYK models by exploring various dynamical protocols that knock the system out of equilibrium. Our first main result is that the large- q SYK model thermalizes instantaneously given a near-arbitrary dynamical protocol [80].

We also consider the extensions of the SYK model onto a d -dimensional lattice, allowing us to study its relation to metals, for instance how it captures aspects of strange metals like T -linear resistivity. We then show how the large- q SYK model again simplifies the equations of motion. This yields our second novel result which encompasses concrete statements about the charge dynamics and lack of instantaneous thermalization in such d -dimensional SYK lattices [81].

Chapter 4 continues with the *thermodynamics* of the large- q SYK model while using the results from the previous chapters. The third result of this thesis is that the large- q SYK model has a fully analytically solvable phase transition that bears a striking similarity to those found in gravity [61]. We compare the analytically obtained large q results to the numerically obtained finite q results. We find some overlap but also discuss important differences that favor the analytical analysis of the large- q SYK model. For instance, we discuss the concretely shown mean-field universality class and how it points to an extension of the holographic mapping.

Inspired by the results of Chapter 4, we focus on *black hole thermodynamics* in Chapter 5. We discuss the known $(d + 1)$ -dimensional black hole phase transitions in so-called black hole *chemistry* for $d > 1$. This chemistry refers to the presence of a variable vacuum pressure (the cosmological constant Λ). We then move onto the $d = 1$ case, which should be holographically dual to the $(0 + 1)$ -dimensional SYK model. A key motivation for treating $-\Lambda$ as a thermodynamic

pressure is that it preserves the correct scaling in the energy/mass of the gravitation system. There are, however, some discrepancies that arise when considering $(1 + 1)$ -dimensional gravity. We address this and give a novel scaling function to the mass. The scaling form preserves all known results for $d > 1$ but also yields the correct mass for $d = 1$. We finish the chapter by finding the gravitational model with the *same* partition function as the large- q SYK model, which is the fourth novel result of this study.

We conclude in Chapter 6 with a summary while providing an outlook for future study.

Chapter 2

Analytical methods for SYK models

In this chapter, we wish to highlight the mathematical aspects which make the SYK models solvable for large system sizes \mathcal{N} . In standard quantum mechanics one often focuses on the problem of diagonalizing a Hamiltonian. One may then write any observable of interest in that basis. Evaluating the time-dependent expectation value then amounts to summing matrix elements with time-dependent phases. In this sense, the quantum system is then fully solvable with any solutions immediately available. In many-body quantum systems, the problem is far more complex. To make sense out of the physics one rather looks at correlation functions which capture key aspects of the system. We introduced one such function, the retarded Green's function, in the previous chapter and mentioned its relation to the spectral function. There exists a whole range of such correlation functions. The ones we are interested in can be constructed via combinations of the (flavor averaged) greater and lesser Green's functions respectively given by

$$\mathcal{G}^>(t, t') = -\frac{1}{\mathcal{N}} \sum_{\nu=1}^{\mathcal{N}} \langle c_{\nu}(t) c_{\nu}^{\dagger}(t') \rangle, \quad \mathcal{G}^<(t, t') = \frac{1}{\mathcal{N}} \sum_{\nu=1}^{\mathcal{N}} \langle c_{\nu}^{\dagger}(t') c_{\nu}(t) \rangle. \quad (2.1)$$

For instance, the time-ordered Green's function is given by $\mathcal{G}(t, t') = \Theta(t - t')\mathcal{G}^>(t, t') + \Theta(t' - t)\mathcal{G}^<(t, t')$. For our purposes, we will, unless specified otherwise, work in the Heisenberg picture, e.g., $c(t) = e^{i\mathcal{H}t} c e^{-i\mathcal{H}t}$. In the thermodynamic setting, one focuses on the imaginary time ($t = \tau/i$) evolution of the fermions¹ $c(\tau/i)$. The thermal Green's functions are then given by $\mathcal{G}(\tau) \equiv \mathcal{G}(\tau/i, 0)$.

As we will see throughout this thesis, these functions allow one to obtain all the information we are interested in. Using them, one may calculate the energy density, the density of states, and even the partition function. As stated in the introduction, the time evolution of the interacting Green's functions is described by a self-energy which enters Dyson's equation

$$\mathcal{G}^{-1} = \mathcal{G}_0^{-1} - \Sigma. \quad (2.2)$$

The SYK models are *solvable* in the sense that the defining equations for the Green's functions are closed to leading order in $1/\mathcal{N}$, i.e., in the thermodynamic limit. This is because, on top of Dyson's

¹Often the imaginary time evolution is defined as just a function of τ , i.e., $c(\tau) = e^{\tau\mathcal{H}} c e^{-\tau\mathcal{H}}$ and $c^{\dagger}(\tau) = e^{\tau\mathcal{H}} c e^{-\tau\mathcal{H}}$. This, unfortunately, breaks the hermiticity in the relation $c(\tau)^{\dagger} \neq c^{\dagger}(\tau)$. With our notation, this issue does not occur since $c(\tau/i)^{\dagger} = e^{-\tau\mathcal{H}} c^{\dagger} e^{\tau\mathcal{H}} = c^{\dagger}(-\tau/i)$.

equation, we also have an additional relation for the self-energy $\Sigma = \tilde{\Sigma}$. This second relation is only dependent on the Green's function $\tilde{\Sigma}[\mathcal{G}]$ to leading order in $1/\mathcal{N}$. As such, the defining equations, *Dyson's equation* and the self-consistency relation $\tilde{\Sigma}[\mathcal{G}]$ are exactly known in the thermodynamic limit, and form a closed set of equations determining the Green's function. This allows one to then solve a nontrivial problem, with exponential complexity $2^{\mathcal{N}}$, via *numerics*, given \mathcal{N} is large.

In this thesis, however, we are focused on the *analytical* aspects of these models. There are three well-known cases in which such analytical results are available. In this chapter, we will discuss all three. The first is the rather trivial *kinetic SYK model*, discussed in Sec. 2.2. Due to its quadratic interactions, it is integrable, hence analytically solvable. Although this model is integrable, its diagrammatic expansion highlights the features which make the more general SYK models solvable.

The second solvable regime relies on a *near-conformal symmetry* in the SYK model, discussed in Sec. 2.3.2. This symmetry appears in the deep infrared (IR), low energy, late time, regime. By taking symmetry-breaking into account, one finds a Schwarzian action describing pseudo-Goldstone bosons. Such an action is also commonly found in gravitational theories. One may map the SYK Schwarzian directly onto certain dimensionally reduced black hole systems². While these results are indeed remarkable, one should note their limitation. In finding the correct action, one is again forced to make use of numerics. Further, the results are only valid at certain time scales and low energies.

2.1 Many many-body interactions

The third analytical method uses a more general model with $q/2$ many-body interactions:

Def 1 (charged $q/2$ -body interacting cSYK model) *The charged $q/2$ -body interacting cSYK model is defined by the Hamiltonian*

$$\mathcal{H}_q = J_q \sum_{\{\mu\}_1^{q/2}, \{\nu\}_1^{q/2}} X_{\nu_1 \dots \nu_{q/2}}^{\mu_1 \dots \mu_{q/2}} c_{\mu_1}^\dagger \dots c_{\mu_{q/2}}^\dagger c_{\nu_{q/2}} \dots c_{\nu_1}, \quad \overline{|X|^2} = \frac{2^q [(q/2)!]^2}{2q^2 \mathcal{N}^{q-1}} \quad (2.3)$$

summed over all ordered flavors $\{\nu\}_1^{q/2} \equiv 1 \leq \nu_1 < \dots < \nu_{q/2} \leq \mathcal{N}$. Here couplings $X_{\nu_1 \dots \nu_{q/2}}^{\mu_1 \dots \mu_{q/2}}$ are independent and identically distributed (IID) random variables (RVs).

The appropriate variance of X is found by accounting for the combinatorics involved in the possible scattering processes involved in \mathcal{H}_q at large \mathcal{N} via Stirling's formula.

Taking $q \rightarrow \infty$ yields the many³ many body interacting cSYK model [80]. Remarkably, the many many body interacting SYK model is analytically solvable. This solution holds in all regimes,

²There exists a large class of different $(d+1)$ -dimensional black hole systems which, when dimensionally reduced, yields a particular $d=1$ bulk together with the boundary term containing the Schwarzian.

³The first "many" here, as usual, refers to the large \mathcal{N} limit. So, it can be read as thermodynamically many bodies with $q/2$ -body interactions where q is large.

i.e., it is not limited to low energies or certain time scales. For this reason, it will be the main model of interest throughout this thesis.

A fast converging large- q expansion. The results one finds when replacing q with finite values greater than or equal to 4 often overlap strongly with the numerical results [61, 82, 83]. Hence, in considering large- q -body interactions, we learn qualitative features of the $q \geq 4$ SYK models. This provides the first motivation for considering such a seemingly unphysical system, namely that the $q \rightarrow \infty$ limit retains many of the interesting properties of the $q = 4$ case (like the behavior of the Lyapunov exponents, which we will discuss in Sec. 3.1.2). These are analytical results and therefore lack the numerical errors which we will see occur in the $q = 4$ numerical studies, which we will discuss in Sec. 4.3.1.

As to understanding why it can be reflective of the $q \geq 4$ case, one may view the solutions to the q -body SYK model as a $1/q$ expansion. The large- q limit is then the leading order solution to the finite q problem. The known strong overlap between the large- q (in a resummed form) and $q = 4$ model [83], is indicative of how fast the series converges. If this expansion is resummed in the right way [84], for instance replacing some leading order expression $1 + g(\tau)/\tau$ with $e^{g(\tau)/q}$, then it can capture more of the higher order corrections in $1/q$. Such an example is precisely what we find for the q -body SYK model. Doing so, in the low-energy limit, the Green's function derived under this method, in fact, exactly overlaps, up to a proportionality constant, with any $q \geq 4$ results, when q is set to the desired value. As such, it also yields quantitative results. Given these results, one sees how the $1/q$ expansion provides a well-behaved, systematic way of calculating the finite q physics.

An effective model for underlying physics. Aside from the $q \geq 4$ aspects captured by the many many-body SYK model, one may ask whether such interactions can be at all reflective of any real physics. From a renormalization perspective, interactions involving more than two particles (i.e. q -body interactions where $q > 4$) are expected to be sub-leading. Typically, kinetic terms $q = 2$ dominate⁴ over 2-body interactions and the hierarchy continues, with higher order scattering process decreasing in rarity. Such a hierarchy stems from fundamental interactions corresponding to $q = 4$. An exception would thus imply a fine-tuning of parameters forcing $q \leq 4$ contributions to be small. However, one should note that the SYK model is an *effective* model, not a microscopic model, a point we will return to in Chapter 6. Hence, it is nontrivial to assess which value q should take as an effective model for a particular real material. One way in which one may guesstimate this is by comparing violations in the Wiedemann-Franz (WF) law $L = L_0$ ($L_0 = \pi^2/(3e^2)$) of real correlated materials [32]. For instance, the q -body SYK model has Lorenz ratio $L = 4L_0/q^2$ for large q [85]. As stated before, such violations of the WF law are indicative of strange metals lacking quasiparticles or quantum systems close to critical points. As such, one may view such general q -body SYK models as effective models capturing quantitative and qualitative aspects of such systems. We will return to this topic again when discussing lattices consisting of coupled SYK models/dots in Sec. 3.3.

To simplify the analysis throughout this chapter, we often focus on the half-filling $\mu = 0$ (uncharged) case for the more explicit calculation, meaning that the non-interacting Green's functions are given by $\mathcal{G}_0(\tau) = \text{sgn}(\tau)/2$. For the equations given in this chapter, not much will change for a non-zero charge. We will, however, mention the important differences that occur

⁴They are more relevant under the renormalization group flow.

where appropriate. We will then return to the charged case in Sec. 3.2.3 and in Sec. 4.1 where it becomes particularly important for the thermodynamics.

2.2 The kinetic SYK model

The SYK models all owe their solvability to their quenched disorder-dependent couplings. A quenched system considers a realization of the system with a certain fixed⁵ disorder X , corresponding to impurities, and calculating the corresponding free energy by tracing out the fermions. As such, the disorder average is thought of as averaging different ensembles. In this section, we study how this averaging leads to a closed form expression for the self-energy by focusing on the simple kinetic case⁶

$$\mathcal{H}_2 = \sum_{i,j=1}^{\mathcal{N}} t_{ij} c_i^\dagger c_j, \quad \overline{|t_{ij}|^{2p}} = t^{2p} / \mathcal{N}^p. \quad (2.4)$$

Although integrable, the calculations reflect the key features of why the SYK model is solvable, which is the domination of the so-called melon diagrams.

Here we will focus on the Matsubara Green's functions $\mathcal{G}(i\omega_n)$ which are related to the thermal Green's functions via Fourier transform

$$\mathcal{G}(i\omega_n) = \int_0^\beta d\tau e^{i\omega_n \tau} \mathcal{G}(\tau).$$

For fermions, the Matsubara frequencies are given by $\omega_n = (2n + 1)\pi/\beta$. These Green's functions are related to retarded Green's functions introduced in Chapter 1 as $\mathcal{G}^R(\omega \rightarrow i\omega_n) = \mathcal{G}^>(\omega_n)$. This is shown by explicitly taking the trace of (2.1) with respect to the eigenstates $\{|E_n\rangle\}$ of the Hamiltonian, known as the Källén-Lehmann representation.

For such a quadratic Hamiltonian, the Heisenberg equations of motion are closed under the creation and annihilation operators. For instance,

$$\frac{dc_{k_0}(t)}{dt} = i[\mathcal{H}, c_{k_0}] = - \sum_{k_1} t_{k_0 k_1} c_{k_1}(t).$$

From this one can obtain a similar equation for the imaginary time Green's functions. In Matsubara frequency space it is given by

$$\mathcal{G}_{k_0 k_2}(i\omega_n) = \mathcal{G}_0(i\omega_n) + \sum_{k_1} \mathcal{G}_0(i\omega_n) t_{k_0 k_1} \mathcal{G}_{k_1 k_2}(i\omega_n),$$

where the non-interacting Green's function is given by $\mathcal{G}_0(\omega) = 1/\omega$. Here the subscripts indicate that the expectation values are with respect to c_{k_0} and $c_{k_2}^\dagger$, instead of the averaged diagonal sum, e.g., (2.1). We would like to solve for the flavor averaged Green's functions

$$\mathcal{G}(i\omega_n) \equiv \frac{1}{\mathcal{N}} \sum_{k_0=1}^{\mathcal{N}} \mathcal{G}_{k_0 k_0}(i\omega_n). \quad (2.5)$$

⁵Physically such randomness fluctuates on a slow timescale if fluctuating at all.

⁶Note the difference in the symbol t from t , which should remind the reader that this is not a time parameter.

By iteratively placing in the right-hand-side expression for the full Green's functions, one obtains the solution to the flavor averaged Green's functions as [86]

$$\mathcal{G}(\omega_n) = \mathcal{G}_0(\omega_n) + \mathcal{G}^{(1)}(\omega_n) + \mathcal{G}^{(2)}(\omega_n) + \dots, \quad (2.6)$$

where the superscript indicates the order in t . Explicitly the higher orders are given by

$$\mathcal{G}^{(n)} = \frac{1}{\mathcal{N}} \sum_{k_0, k_1, k_2, \dots, k_{n-1}} \mathcal{G}_0 t_{k_0 k_1} \mathcal{G}_0 t_{k_1 k_2} \dots \mathcal{G}_0 t_{k_{n-1} k_0} \mathcal{G}_0$$



where we have suppressed the ω_n dependence. We have also included a suggestive diagrammatic sketch. Now we disorder average over all possible RVs

$$\overline{\mathcal{G}^{(n)}} = \frac{1}{\mathcal{N}} \sum_{k_0, k_1, k_2, \dots, k_{n-1}} \overline{\mathcal{G}_0 t_{k_0 k_1} \mathcal{G}_0 t_{k_1 k_2} \dots \mathcal{G}_0 t_{k_{n-1} k_0} \mathcal{G}_0}$$

Odd products of t vanish since $\overline{t_{ij}} = 0$ and different RV's are independent. Let us consider some particular contributions. Graphically, we represent random variables that sum together via red dashed curves, and the averaged (and summed) version has solid curves. For instance

$$\overline{\mathcal{G}^{(2)}} = \frac{1}{\mathcal{N}} \sum_{k_0, k_1} \overline{\mathcal{G}_0 t_{k_0 k_1} \mathcal{G}_0 t_{k_1 k_0} \mathcal{G}_0} = \mathcal{G}_0 t \mathcal{G}_0 t \mathcal{G}_0$$



The important simplification from the averaging arises from the fact that each crossing line in the diagram indicates that one less index is being summed over. To understand why, consider the simplest example:

$$\frac{1}{\mathcal{N}} \sum_{k_0, k_1} \overline{\mathcal{G}_0 t_{k_0 k_1} \mathcal{G}_0 t_{k_1 k_0} \mathcal{G}_0 t_{k_0 k_1} \mathcal{G}_0 t_{k_1 k_0} \mathcal{G}_0} \sim \frac{1}{\mathcal{N}}$$



Importantly, we note that when lines cross, it indicates that more than two indices are summing together. In other words, they do not each freely sum over the all $i \in \{1, \dots, \mathcal{N}\}$. In the above we have four indices summing together, leading to one less summation than that of the reducible two circles in $\overline{\mathcal{G}^{(4)}}$. With one less sum, they also lose a factor \mathcal{N} . Together with the variance of the random variables $\overline{|t_{ij}|^{2p}} = t^{2p} \mathcal{N}^{-p}$, this implies that these kinds of diagrams are of lower

order in \mathcal{N} than the diagrams which do not cross. Such non-crossing diagrams are known as planar diagrams or melon diagrams for $q \geq 4$. Hence, this model, and all SYK models, is dominated by planar diagrams. This yields a drastic simplification already seen from the reduction in the combinatorics of the problem. The leading order (in \hat{t}) rainbow diagrams are

$$\overline{\mathcal{G}^{(4)}} = \begin{array}{c} \text{---} \text{---} \text{---} \text{---} \\ \text{---} \text{---} \text{---} \end{array} + \begin{array}{c} \text{---} \text{---} \text{---} \text{---} \\ \text{---} \text{---} \end{array} \quad \overline{\mathcal{G}^{(6)}} = \begin{array}{c} \text{---} \text{---} \text{---} \text{---} \text{---} \text{---} \\ \text{---} \text{---} \text{---} \end{array} + \begin{array}{c} \text{---} \text{---} \text{---} \text{---} \text{---} \text{---} \\ \text{---} \text{---} \end{array} \\ + \begin{array}{c} \text{---} \text{---} \text{---} \text{---} \text{---} \text{---} \\ \text{---} \text{---} \end{array} + \begin{array}{c} \text{---} \text{---} \text{---} \text{---} \text{---} \text{---} \\ \text{---} \text{---} \end{array}$$

Note that each diagram appears once and only once. Now comes the important realization, by multiplying by t^2 , the effect is to nest the diagrams

$$t^2 \overline{\mathcal{G}^{(0)}} = \text{---} \quad t^2 \overline{\mathcal{G}^{(2)}} = \begin{array}{c} \text{---} \text{---} \\ \text{---} \end{array} \quad t^2 \overline{\mathcal{G}^{(4)}} = \begin{array}{c} \text{---} \text{---} \text{---} \text{---} \\ \text{---} \end{array} + \begin{array}{c} \text{---} \text{---} \text{---} \text{---} \\ \text{---} \end{array}$$

Such nested diagrams are known as irreducible diagrams since they cannot be cut in two by cutting a (black) leg associated with the non-interacting Green's functions. By definition, the sum over all such irreducible diagrams

$$t^2 \sum_{i=0}^{\infty} \overline{\mathcal{G}^{(i)}},$$

is the self-energy Σ . Further note that this sum is just the average of (2.6) multiplied by t^2 , i.e., it is equal to $t^2 \overline{\mathcal{G}}$, and as such we are left with the self-energy directly in terms of the averaged Green's functions

$$\Sigma = t^2 \overline{\mathcal{G}}. \quad (2.7)$$

This now, together with Dyson's equation, yields the close form equation $\overline{\mathcal{G}}^{-1} = \mathcal{G}_0 - t^2 \overline{\mathcal{G}}$ which is solved by

$$\overline{\mathcal{G}}(\omega) \propto \mathcal{G}_0^{-1}(\omega) \pm \sqrt{\mathcal{G}_0^{-2}(\omega) - 4t^2}. \quad (2.8)$$

2.2.1 Existence of quasiparticles

Note that there are no poles in the above Green's function (2.8). In this sense, one might claim that there is no Fermi surface. However, this statement is rather about the averaged system. To see this, let us take a step back and reconsider \mathcal{H}_2 . We can diagonalize a quadratic Hamiltonian such as (2.4). This is done via a unitary⁷ Bogoliubov transform $\mathcal{B} = \sum_i |\epsilon_i\rangle\langle i|$, where ϵ_i are the eigenvalues of \hat{t} , which defines the old fermions in terms of the new ones $c_\beta = \mathcal{B}_{\beta\nu} a_\nu$, where we have used the Einstein summation convention. For fermions, we wish to preserve the canonical commutation

⁷While this transformation is orthogonal for fermions, it would be symplectic for bosons [87]. Such a transform occurs in the derivation of Hawking radiation, where the strongly curved space-time from the black hole alters the vacuum. The bosonic excitations of the new vacuum are related to the old ones via a Bogoliubov transform [88].

relations, e.g., $\{a_i, a_j^\dagger\} = \delta_{ij}$, implying that \mathcal{B} is a unitary transform. The Hamiltonian then maps to

$$c_\alpha^\dagger \hat{t}_{\alpha\beta} c_\beta = b_\mu^\dagger [\mathcal{B}^\dagger]_{\mu\alpha} \hat{t}_{\alpha\beta} \mathcal{B}_{\beta\nu} a_\nu = \epsilon_\alpha a_\alpha^\dagger a_\alpha.$$

As such, the imaginary time evolved fermionic operators are $a_\nu(\tau/\iota) = e^{-\tau\epsilon_\nu} a_\nu$. The mean flavor Green's functions simply transform as

$$\mathcal{G}(\tau) = \frac{1}{\mathcal{N}} \sum_{\nu=1}^{\mathcal{N}} \mathcal{T} \langle a_\nu(\tau/\iota) a_\nu^\dagger \rangle, \quad \mathcal{G}(i\omega_n) = \frac{1}{\mathcal{N}} \sum_{\nu=1}^{\mathcal{N}} \frac{1}{i\omega_n - \epsilon_\nu}. \quad (2.9)$$

As expected, the poles in each Green's function are there. To get a well-defined average, one must consider regularized Green's functions by considering complex frequencies $\omega + i\eta$. This has the effect of smoothening each realization, which may then be averaged together to yield (2.8).

Lastly, the couplings \hat{t}_{ij} are the components of a standard (Hermitian) Gaussian random matrix \hat{t} . It is a large random matrix of order \mathcal{N} , with mean zero, variance \hat{t}/\mathcal{N} , and its n th moments are bounded. As such, from Wigner's semicircle law, the eigenvalues ϵ_α are distributed according to

$$P(\epsilon_\alpha) = \frac{1}{\pi \hat{t}} \sqrt{1 - \left(\frac{\epsilon_\alpha}{2\hat{t}}\right)^2},$$

which is also reflected in (2.8). To see how well these averages capture the non-averaged functions, one looks at higher order moments $\overline{\mathcal{G}(i\omega_n)^m}$ to find the full Green's function distribution $p(\mathcal{G})$. Ideally, one would find something like $p(\mathcal{G}) \propto e^{-\mathcal{N}(\mathcal{G}-\bar{\mathcal{G}})^2 + \mathcal{O}(\mathcal{N}^0)}$ indicating a self-averaging behavior which we discuss next.

2.3 Disordered action and self averaging

Throughout this thesis, we will study the equilibrium and even non-equilibrium properties of the disorder models by focusing on the partition function $\mathcal{Z}(X)$. This function can be related to the unitary evolution operator

$$\mathcal{U}(t, 0) = e^{-i\mathcal{H}(t-\delta)\iota\delta} e^{-i\mathcal{H}(t-2\delta)\delta} \dots e^{-i\mathcal{H}(t-N\delta)\delta} e^{-i\mathcal{H}(0)\delta}$$

where $N \rightarrow \infty$ and the infinitesimal steps are $\delta = t/N$. For instance, the standard partition function is simply $\mathcal{U}(-i\beta, 0)$. In particular, imaginary and real-time evolution can be performed along some contour \mathcal{C} via the contour-ordered exponential known as the S -matrix

$$\mathcal{U}_{\mathcal{C}} \equiv \lim_{N \rightarrow \infty} \prod_{i=1}^{2N} e^{-i\delta t_i \mathcal{H}(t_i)} = \mathcal{T}_{\mathcal{C}} \exp\left(-i \int_{\mathcal{C}} dt \mathcal{H}(t)\right) \quad (2.10)$$

where $\delta t \sim 1/N$. The typical contour we consider is plotted in Fig. 3.4. Typically, \mathcal{C} is chosen based on what one wishes to calculate. Since we are interested in thermodynamics, our contour will be along the imaginary leg from $t = 0$ straight to $t = -i\beta$, in which case the thermodynamic partition function is the trace $\mathcal{Z}(X) = \text{Tr}\{\mathcal{U}_{\mathcal{C}}\}$. General contours will also allow us to extract the nonequilibrium dynamics of observables or Green's functions, as we will see in Chapter 3.

We formally write this as a coherent state path integral over Grassmann fields,

$$\mathcal{Z}(X) = \int \mathcal{D}(\bar{\psi}, \psi) e^{\sqrt{\mathcal{N}} S[\bar{\psi}, \psi; X]}$$

where S is the disorder-dependent action. A brief overview of such fields and integrals is given in App. 2.A. The constant $\sqrt{\mathcal{N}}$ has been factored to make the action intensive after averaging. It is a functional of $\bar{\psi}, \psi$

$$S[\bar{\psi}, \psi; X] = -\text{Tr}\{\hat{\mathcal{G}}_0^{-1} \circ G\} - \int_{\mathcal{C}} dt \mathcal{H}(\bar{\psi}(t), \psi(t)) / \sqrt{\mathcal{N}}. \quad (2.11)$$

Here we have defined the quadratic bilocal⁸ field

$$G(t_1, t_2) \equiv -\frac{1}{\mathcal{N}} \sum_{\mu=1}^{\mathcal{N}} \bar{\psi}_{\mu}(t_1) \psi_{\mu}(t_2). \quad (2.12)$$

Such bilocal fields have a continuous matrix type of multiplication over some chosen contour \mathcal{C}

$$(\hat{A} \circ \hat{B})(t_i, t_j) \equiv \int_{\mathcal{C}} dt_k \hat{A}(t_i, t_k) \hat{B}(t_k, t_j). \quad (2.13)$$

With this, the trace's definition is then merely an extension from the trace over discrete matrices indices to continuous time parameters

$$\text{Tr}\{\hat{A} \circ \hat{B}\} \equiv \int_{\mathcal{C}} dt (\hat{A} \circ \hat{B})(t, t). \quad (2.14)$$

There are two typical kinds of disorder that are often considered. The first is annealed disorder, which stems from temporal fluctuations which oscillate on a fast timescale, hence averaging itself. In other words, annealed disorder stems from dynamical degrees of freedom which, when traced over, corresponds to an open quantum system. Here we focus on the quenched disorder, which corresponds to unknown and uncontrollable impurities in various samples. For disorder X distributed according to $p(X)$, the *annealed* and *quenched* generating functions are given by

$$\ln \overline{\mathcal{Z}(X)} = \ln \int dX p(X) \mathcal{Z}(X), \quad \overline{\ln \mathcal{Z}(X)} = \int dX p(X) \ln \mathcal{Z}(X) \quad (2.15)$$

respectively. In the annealed case X and ψ fluctuate together, described by an effective Euclidean action where the Lagrangian gains a term proportional to $\ln p(X)$, seen for instance by rewriting $p(X) = e^{-\beta[-T \ln p(x)]}$.

The disorder average is then an ensemble average $\overline{\ln \mathcal{Z}}$, where $\mathcal{Z} = \text{Tr}\{e^{-\beta \mathcal{H}}\}$. However, evaluating this can be tricky. One option is to consider the power series

$$\overline{\ln \mathcal{Z}} = \sum_{k>0} \overline{(1 - \mathcal{Z})^k} / k,$$

⁸The fields are not local in time, since two different times enter, this makes them bilocal.

but this series converges slowly due to the $1/k$ instead of the usual $1/k!$. A second alternative is via the derivative formula for the logarithm

$$\overline{\ln \mathcal{Z}} = \lim_{\Lambda \rightarrow 0} \frac{\overline{\mathcal{Z}^\Lambda} - 1}{\Lambda}.$$

One notes that the average $\overline{\mathcal{Z}^\Lambda}$, amounts to considering the annealed average of Λ replica systems

$$\overline{\mathcal{Z}^\Lambda} = \overline{\text{Tr}\{e^{-\beta \sum_{\ell=1}^{\Lambda} \mathcal{H}_{\ell}}\}},$$

where we have defined the Hamiltonian \mathcal{H}_{ℓ} , which all share the same disorder X . As such, it is often called the “replica trick”. For instance, for the $q = 4$ -body SYK model

$$\sum_{\ell=1}^{\Lambda} \mathcal{H}_{4;\ell} = \sum_{\substack{1 \leq i_1 < i_2 \leq \mathcal{N} \\ 1 \leq j_1 < j_2 \leq \mathcal{N}}} X_{j_1 j_2}^{i_1 i_2} \sum_{\ell=1}^{\Lambda} c_{\ell, i_1}^\dagger c_{\ell, i_2}^\dagger c_{\ell, j_2} c_{\ell, j_1},$$

which can also be viewed as a lattice of Λ SYK dots with exact translation invariance with simple *annealed* disorder. One then analytically continues this partition function from integer Λ to a real number, such that one may take the limit as $\Lambda \rightarrow 0$. This process can be challenging and can also fail for certain systems. When employing the above trick, one introduces correlations over the different replicas i, j , for instance,

$$\mathcal{G}_{ij}(t, t') = -\frac{1}{\mathcal{N}} \sum_{\mu=1}^{\mathcal{N}} \langle \mathcal{T} c_{i;\mu}(t) c_{j;\mu}^\dagger(t') \rangle.$$

Often the assumption of replica diagonal symmetry $\mathcal{G}_{ij}(\tau, \tau') = \delta_{ij} \mathcal{G}(\tau, \tau')$ allows one to then solve the problem, as was done in the $q = 4$ SYK model [53]. This diagonal assumption, while holding in the fermionic SYK model [89], is not always valid. Such replica diagonal symmetry breaking is, in fact, a defining feature of a system condensing into a spin glass phase. One of the most notable classical spin glass models is the Sherrington-Kirkpatrick (SK) model [90]. The Sachdev-Ye (SY) model [51]

$$\mathcal{H}_{\text{SY}} = J \sum_{i_1, i_2=1}^{\mathcal{N}} X_{i_1 i_2} \sum_{\mu, \nu=1}^M \hat{S}_{i_1}^{\mu\nu} \hat{S}_{i_2}^{\nu\mu}, \quad (2.16)$$

is an extension of the SK model. Here the operators $\hat{S}^{\mu\nu}$ are the generators⁹ of the group $\text{SU}(M)$ [91]. This model becomes exactly solvable in the thermodynamic limit with large spin degrees of freedom. It has the same closure relation as the complex $q = 4$ SYK model. Indeed, like the SK model, by reducing the temperature (or increasing the spin angular momentum) this model will condense into a spin glass [92]. Numerical evidence suggests that replica symmetry is also

⁹The size of the algebra is $M^2 - 1$, since angular momentum conservation provides one additional restriction on the M^2 operators. In the case where $M = 2$, these generators are merely the three Pauli matrices.

broken in the bosonic SYK model, i.e., the same model, but with the fermionic operators replaced by hard-core bosons [62].

One signature of when the replica diagonal assumption fails is a negative entropy. For the fermionic SYK model, the entropy remains positive at all temperatures.

We now come to the important topic of self-averaging which is related to replica symmetry. An observable for a disordered model is said to be self-averaging if the large \mathcal{N} limit means that it tends to its averaged value [93]. In this sense, it is the law of large numbers for quantum systems. In other words, it is an observable which is connected in a way such that the presence of *many* couplings (sampled from some distribution) has the effect of averaging itself. For such observables, the annealed and quenched averages coincide. A system is said to be self-averaging if the same holds for the partition function

$$\overline{\ln \mathcal{Z}} \xrightarrow{\mathcal{N} \rightarrow \infty} \ln \overline{\mathcal{Z}}. \quad (2.17)$$

This condition is stronger than replica diagonal symmetry. Considering the respective power series, one notes that this will occur if $\overline{\mathcal{Z}^\Lambda} \xrightarrow{\mathcal{N} \rightarrow \infty} \overline{\mathcal{Z}}^\Lambda$, i.e. when all replicas are independent of another. The importance of this, and the reason for this particular definition of a self-averaging *system*, is that one can then calculate observables from the annealed partition function. Further, it gives new relevance to the system, since the ensemble average now encodes a single thermodynamically large system. While neither free bosonic nor free fermionic models are self-averaging at any intensive temperature, it can already be seen that the breaking is stronger in the bosonic case due to their condensation, see App. 2.B. Indeed, unlike the bosonic SYK models, the fermionic case does preserve replica symmetry [94].

For the fermionic SYK model, in the large \mathcal{N} regime, for intensive temperatures $T = \mathcal{O}(\mathcal{N}^0)$, one can estimate $\ln \overline{\mathcal{Z}} - \overline{\ln \mathcal{Z}}$ via the leading order replica off-diagonal melon diagrams which scale as $\mathcal{N}^{2-q}\beta^2$ [57, 95]. At large temperatures the system becomes only weakly dependent on the disorder, seen in the extreme where $\mathcal{Z} \xrightarrow{T \rightarrow \infty} \text{Tr}\{\mathbb{1}\}$. The reverse is true at low temperatures. As expected, replica symmetry breaking would occur at low temperatures, however, in first taking the large \mathcal{N} limit, they never contribute. An exception is the kinetic $q = 2$ case from Sec. 2.2. Given some interaction ($q > 2$) term, however, we only have to focus on the averaged Green's functions, which are equal to the actual Green's function to leading order in $1/\mathcal{N}$

$$\mathcal{G} \sim \overline{\mathcal{G}}.$$

As we saw in Sec. 2.2, the planar dominance leads to many terms being of sub-leading order in $1/\mathcal{N}$. In the end, the problem is one of combinatorics—counting the various averages that can occur together with their weight given by the number of sums over \mathcal{N} indices left over. In doing this one notes that only the variances contribute to the action. Counting all the contributions, as is done in Sec. 3.4.1, one is left with the effective averaged action

$$S_I[G] \sim \int dt_1 \int dt_2 \frac{\overline{\mathcal{H}(\overline{\psi}(t_1), \psi(t_1))\mathcal{H}(\overline{\psi}(t_2), \psi(t_2))}}{2\mathcal{N}}. \quad (2.18)$$

Evaluating the above variance one finds that it may be written purely in terms of the bilocal fields G (2.12). For instance, for the q -body SYK model (2.3) one finds

$$\overline{\mathcal{H}(\overline{\psi}(t_1), \psi(t_1))\mathcal{H}(\overline{\psi}(t_2), \psi(t_2))} = \frac{J_q^2}{2q^2} [-2G(t_1, t_2)2G(t_2, t_1)]^{q/2},$$

as shown in App. 2.C. This leaves us with an action $S_I[G] = \text{Tr}\{\tilde{\Sigma}[G]/q \circ G\}$, where

$$q\tilde{\Sigma}[G](t_1, t_2) = \mathcal{L}(t_1, t_2)2G(t_1, t_2), \quad \mathcal{L}(t_1, t_2) \equiv J_q^2[-2G(t_1, t_2)2G(t_2, t_1)]^{q/2-1}. \quad (2.19)$$

2.3.1 The G- Σ path integral

Even for such a general $q/2$ -body interaction, one may write down the general effective action in terms of two bilocal fields \mathcal{G} , Σ . Their on-shell values will end up being the flavor averaged Green's function and self-energy. Even upon combining various SYK models, the averaged partition function will take the form

$$\bar{\mathcal{Z}} = \int \mathcal{D}(\bar{\psi}, \psi) e^{-\mathcal{N}S_I[G] + \mathcal{N} \text{Tr}\{\mathcal{G}_0^{-1} \circ G\}}, \quad (2.20)$$

with the quadratic field G (2.12). Lagrange multipliers are then introduced via a delta functional

$$\begin{aligned} \bar{\mathcal{Z}} &= \int \mathcal{D}(\bar{\psi}, \psi) \int d\mathcal{G} \delta[\mathcal{G} - G] e^{\mathcal{N} \text{Tr}\{\mathcal{G}_0^{-1} \circ G\}} e^{-\mathcal{N}S_I[\mathcal{G}]} \\ &= \int \mathcal{D}(\bar{\psi}, \psi) \int d\mathcal{G} \int d\Sigma e^{\mathcal{N} \text{Tr}\{\Sigma \circ [\mathcal{G} - G]\}} e^{\mathcal{N} \text{Tr}\{\mathcal{G}_0^{-1} \circ G\}} e^{-\mathcal{N}S_I[\mathcal{G}]}. \end{aligned}$$

Integrating the above Gaussian type integral of Grassmann fields in G , yields

$$\bar{\mathcal{Z}} = \int \mathcal{D}\mathcal{G} \int \mathcal{D}\Sigma e^{-\mathcal{N}\bar{S}[\mathcal{G}, \Sigma]}, \quad (2.21)$$

where we have gained an invaluable (averaged) action for our model

$$\bar{S}[\mathcal{G}, \Sigma] \equiv \text{Tr}\{\tilde{\Sigma}[\mathcal{G}]/q - \Sigma \circ \mathcal{G} - \ln[\mathcal{G}_0^{-1} - \Sigma]\}. \quad (2.22)$$

This allows us to gain a whole wealth of knowledge about the theory, for instance, its symmetries. By varying the action, w.r.t. Σ , we obtain Dyson's equation (2.2) $\mathcal{G} = [\mathcal{G}_0^{-1} - \Sigma]^{-1}$. Varying this action with \mathcal{G} yields $\delta\bar{S} = \text{Tr}\{\tilde{\Sigma} - \Sigma \circ \delta\mathcal{G}\}$ which identifies the self-energy as $\Sigma(t_1, t_2) = \tilde{\Sigma}[\mathcal{G}](t_1, t_2)$.

2.3.2 The near-conformal invariance in SYK

Let us now find the symmetries in the action (2.22). First, let us make the following change in the integration variable in (2.21): $\Sigma = \Sigma_C + \mathcal{G}_0^{-1}$. This redefinition of self-energy changes Dyson's equation to $\mathcal{G} = -\Sigma_C^{-1}$. The action (2.22) may then be separated into two parts $\bar{S} = S_{\text{CFT}} + S_{\text{Sc}}$

$$S_{\text{CFT}} = \text{Tr}\{\tilde{\Sigma}[\mathcal{G}]/q - \Sigma_C \circ \mathcal{G} - \ln[-\Sigma_C]\}, \quad S_{\text{Sc}} = -\text{Tr}\{\mathcal{G}_0^{-1} \circ \mathcal{G}\}. \quad (2.23)$$

The first action is extremized given the field Σ_C takes on the "value" of the self-energy $\Sigma_C = \tilde{\Sigma}[\mathcal{G}]$. Together with the modified Dyson's equation $\Sigma_C \mathcal{G} = -1$, we have

$$\delta_C(t_1 - t_2) = \int_{\mathcal{C}} dt' J_q^2[-4\mathcal{G}(t_1, t')\mathcal{G}(t', t_2)][-4\mathcal{G}(t', t_2)\mathcal{G}(t_2, t')]^{q/2-1}. \quad (2.24)$$

Note that any solution to (2.24) remains a solution even upon arbitrary time reparametrization [53] $t \rightarrow u(t)$, as long as the Green's function and self-energy transform as

$$\mathcal{G}(t_1, t_2) \rightarrow e^{i[\phi(t_1) - \phi(t_2)]} \mathcal{G}(u(t_1), u(t_2)) [\dot{u}(t_1) \dot{u}(t_2)]^\Delta \quad (2.25)$$

$$\Sigma_C(t_1, t_2) \rightarrow e^{i[\phi(t_1) - \phi(t_2)]} \Sigma_C(u(t_1), u(t_2)) [\dot{u}(t_1) \dot{u}(t_2)]^{1-\Delta}, \quad (2.26)$$

respectively and $\Delta = 1/q$. The only effect is to yield the new delta function [96]

$$\delta_C(u(t_1) - u(t_2)) = \frac{2\delta(t_1 - t_2)}{u(t_1) + u(t_2)}.$$

In other words, the action is invariant under diffeomorphisms. The conformal group consists of all transformations which preserve angles, see e.g., App. 2.D. Note that there exists no notion of angles in one dimension, as such any smooth transformation ‘‘preserves’’ angles and is considered conformal [97]. Written in group theoretic language¹⁰, we have $\text{Conf}_1 \simeq \text{Diff}_1$, i.e., the group of all conformal transformations is isomorphic to the group of all diffeomorphisms in $0 + 1$ dimensions. Here we have an (anomalous) conformal dimension $\Delta = 1/q$.

In the IR regime, one finds the local (instead of bilocal) conformal solution $\mathcal{G}_C(t) \propto \text{sgn}(t)|t|^{-2\Delta}$.

The remaining details we wish to reflect on can be found in the simpler Majorana SYK model [45], corresponding to the neutral-charge case of the cSYK model. The charge cSYK discussion can be found in [57]. Let us now focus on the contour along the imaginary leg $t \in [0, -i\beta]$, meaning the imaginary time Green's functions \mathcal{G}_C . One can also infer the IR form at small T [45]

$$\mathcal{G}_C(\tau) \propto b_q \mathcal{G}_0(\tau) \left[\frac{\pi}{\beta J_q \sin(\pi|\tau|/\beta)} \right]^{2\Delta}, \quad b_q = \left[(1 - 2\Delta) \frac{\tan(\pi\Delta)}{\pi\Delta} \right]^\Delta. \quad (2.27)$$

Now we focus on the correction terms which we have ignored so far

$$S_{\text{Sc}}[u] = \frac{1}{2} \int dt dt_{12} \dot{\delta}(t_{12}) \mathcal{G}(t_1, t_2), \quad (2.28)$$

which select out solutions near equal times, i.e., small $t_{12} \equiv t_1 - t_2$. Defining the average time $t = (t_1 + t_2)/2$ we have

$$\mathcal{G}(t_1, t_2) = \mathcal{G}_C(t_{12}) \left[1 + \frac{\Delta}{6} t_{12}^2 \text{Sch}(u(t), t) + \mathcal{O}(t_{12}^3) \right], \quad (2.29)$$

where we have defined the Schwarzian derivative

$$\text{Sch}(u(t), t) \equiv \left[\frac{\ddot{u}(t)}{\dot{u}(t)} \right]' - \frac{1}{2} \left[\frac{\ddot{u}(t)}{\dot{u}(t)} \right]^2. \quad (2.30)$$

With some reasoning and collecting some diverging functions, one finds the contribution [96, 98]

$$S_{\text{Sc}}[u] = \frac{\alpha_S(q)}{J_q} \int dt \text{Sch}(u(t), t) \quad (2.31)$$

¹⁰The field over which the group acts will be either \mathbb{R} or \mathbb{C} depending on the time domain/contour \mathcal{C} [80].

to leading order in t_{12} . The only solution to which $\text{Sch}(u(z), z) = 0$ is the Möbius transform¹¹

$$u(z) = \frac{az + b}{cz + d}, \quad \begin{bmatrix} a & b \\ c & d \end{bmatrix} \in \text{SL}_2, \quad (2.32)$$

where the special linear group SL_2 consists of matrices with determinant 1, i.e., $ad - bc = 1$. Thus, the Schwarzian derivative measures deviations away from a Möbius transform. As such S_{Sc} leads to a breaking of the Conf_1 symmetry down to an SL_2 symmetry.

The reparametrization modes u causing this symmetry breaking are pseudo-Nambu–Goldstone bosons. Evaluating the total action leaves the low-energy path integral over all scalar fields¹² [45]

$$\mathcal{Z}_{\text{IR}} = \int \mathcal{D}u e^{-\mathcal{N}[\beta E(T=0) - \mathcal{S}(T=0) - S_{\text{Sc}}[u]]}.$$

The on-shell contributions then yield the leading free energy (per lattice site)

$$-T \ln \mathcal{Z}_{\text{IR}}/\mathcal{N} \sim E(T=0) - T\mathcal{S}(T=0) - 2\pi^2 \alpha_S(q) T^2/J_q,$$

where we note that the Schwarzian contribution is of order $\mathcal{O}(T^2)$. One still has to find α_S numerically, except for large q , where one may analytically show $\alpha_S(q) \sim \Delta^2/4$ [45].

2.4 Exact solvability of the large- q SYK model

Now we focus on the large q case of (2.3) and see how a $1/q$ expansion provides a leading order closed-form solution. We start by writing the Green's function as

$$\mathcal{G}(\tau) = \mathcal{G}_0(\tau) e^{\mathcal{G}(\tau)/q}, \quad \mathcal{G}_0(\tau) = \text{sgn}(\tau)/2 \quad (2.33)$$

with boundary condition $\mathcal{G}(0^+) = 0$. Next, we assume that, for the large q case, the \mathcal{G} 's are of order $\mathcal{O}(q^0)$. Then the exponential may be expanded as $1 + \mathcal{G}/q + \mathcal{O}(q^{-2})$. The exponential form can then be viewed as a leading order resummation of the $1/q$ expansion, thus minimizing the error in the series $1 + g/q \rightarrow e^{g/q}$. As before, the self-energy Σ is related to \mathcal{G} via Dyson's equation (2.2) $\mathcal{G}_0^{-1} - \mathcal{G}^{-1} = \Sigma$. Now we expand the left-hand side in orders of $1/q$

$$\mathcal{G}_0(i\omega_n)^{-1} - \frac{1}{\mathcal{G}_0(i\omega_n) + \frac{1}{q}[\mathcal{G}_0 \times g](i\omega_n)} = \mathcal{G}_0(i\omega_n)^{-2} \frac{[\mathcal{G}_0 \times g](i\omega_n)}{q} + \mathcal{O}(q^{-2}),$$

where, recalling that $\mathcal{G}_0(i\omega_n)^{-1} = i\omega_n$, the Fourier transform may be written as

$$[i\omega_n]^2 [\mathcal{G}_0 \times g](i\omega_n) = [(-\partial_\tau)^2 \mathcal{G}_0(\tau) \mathcal{G}(\tau)](i\omega_n). \quad (2.34)$$

¹¹Technically the symmetry is the quotient group $\text{PSL}_2 = \text{SL}_2/\{\pm 1\}$ known as the projective special linear group. This is because the Möbius transform corresponding to $M \in \text{SL}_2$ and $-M$ are the same, as such we consider the equivalence class of elements $M \equiv_R -M$, which is PSL_2 .

¹²The extension to arbitrary charge density would also include a functional integral over all phase fields ϕ [85].

Inverting this Fourier transform on both sides yields $\partial_\tau^2 \mathcal{G}(\tau)/2 = q\Sigma(\tau)$ for $\tau > 0$. In terms of (2.33) the self-energy (2.19) is then given by

$$q\Sigma(\tau) \sim J_q^2 e^{\mathcal{G}+(\tau)}, \quad \mathcal{G}+(\tau) \equiv \frac{\mathcal{G}(\tau) + \mathcal{G}(-\tau)}{2},$$

leaving the equation $\ddot{\mathcal{G}}(\tau) = 2J_q^2 e^{\mathcal{G}+(\tau)}$, which is the same for $\mathcal{G}(\pm\tau)$. As such, the only asymmetry that can occur is a possible linear term. The Majorana-like symmetry at half-filling means that no such term enters $\mathcal{G}(-\tau) = \mathcal{G}(\tau)$ [45]. As such we are only left with a Liouville equation

$$\ddot{\mathcal{G}}_+(\tau) = 2J_q^2 e^{\mathcal{G}+(\tau)}, \quad (2.35)$$

which is solved by the symmetric function¹³[99]

$$e^{\mathcal{G}+(\tau)} = \frac{(\lambda/2)^2}{J_q^2 \cos^2(\pi v/2 - \lambda|\tau|/2)}, \quad \lambda \geq 0. \quad (2.36)$$

One may further relate this to the energy by using the generalized Galitskii-Migdal sum rule [80] $q^2 \langle \mathcal{H}_q/N \rangle = -2J_q \sin(\pi v/2)$. This indicates that the ground state is at $v \rightarrow 1$, hence the positive temperature results correspond to $v \in [0, 1]$.

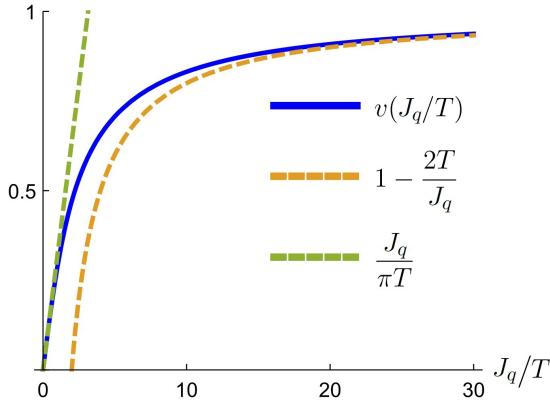


Figure 2.1: Plot of the solution v to the closure relation (2.39)

relation $2J_q = \lambda \sec(\pi v/2)$. Substituting (2.37) then yields $\beta J_q \cos(\pi v/2) = \pi[m + v]$, which has multiple solutions. In fact, in the range $m\pi \leq \beta J_q < (m+1)\pi$, one finds exactly $m+1$ solutions.

In the UV regime $\beta J_q \rightarrow 0$, one has a unique solution corresponding to $m = 0$, which corresponds to the smallest period in the Green's functions. Decreasing temperature further, one would not expect this definition to undergo any abrupt change; thus we have the relation

$$\lambda = 2\pi v T, \quad (2.38)$$

¹³Here, without loss of generality, we have taken $\lambda \geq 0$.

¹⁴If we had kept the negative temperature solutions, then this would only change by having to consider $m \rightarrow m + \Theta(-v)$, for $m \geq 0$

We would now like to relate the temperature to v and λ . At equilibrium, the temperature is related to the periodicity in the Green's functions. In particular, the Kubo-Martin-Schwinger (KMS) relation for fermions: $\mathcal{G}(-\tau) = -\mathcal{G}(-\tau + \beta)$. Via some trigonometric manipulation, the equation $\mathcal{G}_+(-\tau) = \mathcal{G}_+(-\tau + \beta)$ reduces to $\sin(\lambda[\tau - \beta/2]) \sin(\lambda\beta/2 - \pi v) = 0$, i.e.,

$$\lambda = 2\pi[m + v]T, \quad (2.37)$$

with $m \in \mathbb{Z}$, or $\lambda = 0$. The latter yields a constant Green's function; hence we focus on the former (2.37). Since both $\lambda, T \geq 0$, we only consider¹⁴ $m \geq 0$. From the boundary condition $e^{\mathcal{G}(0)} = 1$ on (2.36), we obtain the closure relation

where v is the solution to the closure relation

$$\pi v = \beta J_q \cos(\pi v/2). \quad (2.39)$$

We may invert (2.39) using the Lagrange inversion theorem. The solution $v(\beta J_q)$ is only dependent on βJ_q , plotted in Fig. 2.1. With this, we may write (2.36) as

$$e^{\mathcal{G}_+(\tau)} = \left[\frac{\pi v}{\beta J_q \cos(\pi v(1/2 - |\tau|/\beta))} \right]^2 \quad (2.40)$$

where the closure relation (2.39) ensures the boundary condition $\mathcal{G}_+(0) = 0$.

2.4.1 IR comparison

In the infrared (IR) regime $\beta J_q \rightarrow \infty$, we find $v \rightarrow 1$, as plotted in Fig. 2.1. With this, the solution (2.40) becomes

$$e^{\mathcal{G}_+(\tau)} = \left[\frac{\pi v}{\beta J_q \sin(\pi|\tau|/\beta)} \right]^2$$

for $\tau \neq 0, \beta$. This appears very similar to the finite q IR solution (2.27). Indeed, the only difference is the appearance of the proportionality constant

$$b_q = \left[(1 - 2\Delta) \frac{\tan(\pi\Delta)}{\pi\Delta} \right]^\Delta, \quad \Delta = \frac{1}{q}.$$

For large q , this proportionality constant behaves as $b_q \sim 1 - 2\Delta^2$, i.e., it rapidly saturates to 1. For instance, $b_4 > 0.89$ and already $b_6 > 0.95$. As such, this is our first explicit example of how the large q analytical result can be used to not only obtain qualitative features of small $q \geq 4$, but even quantitative estimates.

2.4.2 Solvable competing large- q SYK models

The solvable property of SYK models continues to hold even when combining such models. For instance, $\mathcal{H}_r + \mathcal{H}_q$ would yield a self-energy which is merely the sum of the individual models $\Sigma = \Sigma_r + \Sigma_q$. A standard example is to add a quadratic term $r = 2$, for which there is a chaotic-to-regular crossover [33, 100]. For the equilibrium Green's functions, for $r = \kappa q$, this then leaves the leading order equation $\ddot{\mathcal{G}}_+(\tau) = 2J_q^2 e^{\mathcal{G}_+(\tau)} + 2J_{\kappa q}^2 e^{\kappa \mathcal{G}_+(\tau)}$. For this particular case, one can, in fact, still find an exact analytical solution for the Green's functions $\mathcal{G}(\tau) \propto e^{\mathcal{G}_+(\tau)/q}$, when $\kappa \in \{1/2, 1, 2\}$. For instance, when $\kappa = 1/2$ we are left with the equation

$$\ddot{\mathcal{G}}_+(\tau) = 2J_q^2 e^{\mathcal{G}_+(\tau)} + 2J_{\kappa q} e^{\kappa \mathcal{G}_+(\tau)} \quad (2.41)$$

which has the solution

$$e^{\mathcal{G}_+(\tau)/2} = \frac{(\pi v)^2}{(\beta J_{\kappa q})^2 + \sqrt{(\pi v)^2 (\beta J_q)^2 + (\beta J_{\kappa q})^4} \cos(\pi v(1/2 + \tau/\beta))} \quad (2.42)$$

which reduces to the Liouville solution for $J_{\kappa q} = 0$. It is subject to the boundary condition that $\mathcal{G}_+(0) = 0$ which would yield the following closure relation for v

$$\pi v = \sqrt{1 + \left(\frac{(\beta J_{\kappa q})^2}{\pi v \beta J_q}\right)^2} \beta J_q \cos(\pi v/2) + \frac{(\beta J_{\kappa q})^2}{\pi v}. \quad (2.43)$$

From (2.42) one can explicitly confirm the intuition that the lower body scattering term, the $q/2$ -body term in this case, dominates at low temperatures. This is because the q -body and $q/2$ -body contributions are of the order βJ_q and $\beta^2 J_{q/2}^2$ respectively. As such, at low temperatures, the $J_{q/2}$ contributions dominate, while at higher temperatures the q -body scattering J_q dominates.

For $\kappa = 2$, we have essentially the same equation as before, with the roles of the couplings inverted. To see this we rewrite

$$2\mathcal{G}_+(\tau) \sim 4J_{\kappa q}^2 e^{2\mathcal{G}_+(\tau)} + 4J_q^2 e^{2\mathcal{G}_+(\tau)/2}, \quad (2.44)$$

which is (2.41) upon making the following re-definitions $(\mathcal{G}_+, J_{\kappa q}^2, J_q^2) \rightarrow 2(\mathcal{G}_+, J_q^2, J_{\kappa q}^2)$. For $\kappa = 1$, the equation reduces to a Liouville equation with the same solution with re-definitions $J_{\kappa q} \rightarrow 0$, $J_q^2 \rightarrow J_q^2 + J_{\kappa q}^2$, leaving the solution (2.39).

Appendix 2.A: Grassmann path integrals

A particularly useful tool for evaluating expectation values is Feynman's path integral formulation. To set up the path integral, however, one needs to insert resolutions of identity over appropriately continuous states. For bosons, these states are simply the over-determined and unnormalized Glauber coherent states $|\psi\rangle \equiv e^{-\psi \cdot \mathbf{c}^\dagger} |0\rangle$, where we have defined the dot product between the two arrays $\mathbf{c} \equiv (c_1, c_2, \dots, c_N)$ and $\psi \equiv (\psi_1, \psi_2, \dots, \psi_N)$ as $\psi \cdot \mathbf{c}^\dagger \equiv \sum_i \psi_i c_i^\dagger$. Since the states are over-determined they have a special resolution of identity

$$\mathbb{1} = \int d\mu(\psi) |\psi\rangle \langle \psi|, \quad \mu(\psi) = \left(\prod_{i=1}^N d\bar{\psi}_i d\psi_i \right) e^{-\bar{\psi} \cdot \psi} \quad (2.45)$$

with a measure $\mu(\psi)$. For fermions, there exists no such state. However, a particularly useful framework considers generalizing the parameters ψ_i to that of Grassmann variables, which are anti-commuting numbers. One can then define the unnormalized *fermionic coherent state* as before, where c_i are then fermionic creation and annihilation operators. Expanding the exponential yields

$$|\psi\rangle = |0\rangle - \psi \cdot \mathbf{c}^\dagger |0\rangle.$$

One usually normal orders the operators first before taking expectation values with respect to the Grassmann variables. In this case, one only requires the following relations: $c_i |\psi\rangle = \psi_i |\psi\rangle$, $\langle \psi | c_i^\dagger = \langle \psi | \bar{\psi}_i$, and $\langle \psi' | \psi \rangle \equiv e^{\psi' \cdot \psi}$. For any normally ordered operator $\mathcal{H}(\mathbf{c}^\dagger, \mathbf{c})$, we have

$$\langle \psi' | \mathcal{H}(\mathbf{c}^\dagger, \mathbf{c}) | \psi \rangle = \mathcal{H}(\bar{\psi}', \psi) e^{\psi' \cdot \psi}. \quad (2.46)$$

The process of normal ordering is also captured by defining $c_i^\dagger |\psi\rangle = -\partial_{\psi_i} |\psi\rangle$ and $\langle \psi | c_i = \partial_{\bar{\psi}_i} \langle \psi |$. We will define Grassmann integration merely as Grassmann differentiation

$$\int d\psi \psi^n = \partial_{\psi} \psi^n = \delta_{n1}. \quad (2.47)$$

We are in particular interested in the trace of S-matrix (2.10), which can be evaluated over fermionic coherent states

$$\mathcal{Z} = \frac{\text{Tr}\{\mathcal{U}_C \hat{\rho}\}}{\text{Tr}\{\hat{\rho}\}} = \frac{1}{\text{Tr}\{\hat{\rho}\}} \int d\mu(\psi(t_{2N})) (-\psi(t_{2N}) | \mathcal{U}_C \hat{\rho} | \psi(t_{2N})) \rightarrow \int \mathcal{D}(\bar{\psi}, \psi) e^{iS[\psi, \bar{\psi}]} \quad (2.48)$$

in particular as a path integral over these Grassmann fields as on the right. To achieve this we factor the S-matrix and insert multiple resolutions of identity (2.45). These are for Grassmann variables at different “times” $\psi(t)$. Inserting multiple resolutions of identities into the trace and using the property for ordered operators (2.46) yields terms like

$$e^{-\bar{\psi}(t_{i+1}) \cdot \psi(t_{i+1})} |\psi(t_{i+1})\rangle \langle \psi(t_{i+1})| e^{-i\delta t_i \mathcal{H}(t_i)} |\psi(t_i)\rangle \langle \psi(t_i)| = |\psi(t_{i+1})\rangle e^{i\delta t_i \mathcal{L}(t_i)} \langle \psi(t_i)| \quad (2.49)$$

where the Lagrangian \mathcal{L} becomes only dependent on t_i in the continuum limit. It is given by

$$i\bar{\psi}(t_{i+1}) \cdot \frac{\psi(t_{i+1}) - \psi(t_i)}{\delta t_i} - \mathcal{H}(\bar{\psi}(t_{i+1}), \psi(t_i)) \quad (2.50)$$

where the Lagrangian terms sum together to yield the total action

$$iS[\psi, \bar{\psi}] = i \sum_{i=1}^{2N-1} \delta t_i \mathcal{L}(t_i) - \bar{\psi}(t_1) \cdot (\psi(t_1) + \rho \psi(t_{2N})).$$

A natural question is whether one can define such a time derivative for Grassmann variables, for what does it mean to say $\psi(t) - \psi(t - \delta)$ is small? One solution treats the Grassmann variables as fermionic fields composed of fermions that do not appear in the original problem. In this case, one can write something like $\psi(t) = \lambda(t)a$, where $\lambda(t)$ is a scalar function and a is a fermionic annihilation operator. Then we have

$$\dot{\psi}(t) \equiv \lim_{\delta \rightarrow 0} \frac{\psi(t) - \psi(t - \delta)}{\delta} = \dot{\lambda}(t)a.$$

A second question is whether $\dot{\lambda}(t)$ is well-defined if we are integrating over all $\lambda(t)$, including non-differential and even discontinuous paths. This is not a novel problem but is also encountered in ordinary phase space path integrals. It is resolved by noting that when the path “jumps”, the action and thus the phase oscillates rapidly canceling out to tiny values. These cases can be well-defined using the Riemann Lebesgue lemma. As such in our formulation we need only consider all differentiable functions. Let us now define

$$\langle \psi, \hat{A} \psi \rangle \equiv \sum_{ij} \delta t_i \delta t_j \bar{\psi}^T(t_i) \hat{A}(t_i, t_j) \psi(t_j) \rightarrow \int dt_1 \int dt_2 \bar{\psi}^T(t_1) \hat{A}(t_1, t_2) \psi(t_2),$$

which allows one to prove identities like the Grassmann-Gaussian integral

$$\int \mathcal{D}(\bar{\psi}, \psi) e^{-\langle \psi, \hat{A} \psi \rangle} = e^{\text{Tr}\{\ln \hat{A}\}} \quad (2.51)$$

where we have used the relation $\det(\hat{A}) = e^{\text{Tr}\{\ln \hat{A}\}}$ and defined trace over bilinear matrices

$$\text{Tr}\{\hat{A}\} \equiv \int dt \text{Tr}\{\hat{A}(t, t)\},$$

where $\text{Tr}\{\hat{A}(t, t)\}$ is the standard matrix trace. For flavor independent diagonal bilocals $\hat{A}_{ij} = \delta_{ij} A$, we further have that $\text{Tr}\{\ln \hat{A}\} = \mathcal{N} \text{Tr}\{\ln A\}$, where $\text{Tr}\{\ln A\}$ is just the scalar bilinear trace. The bilinears may be multiplied as

$$(\hat{A} \circ \hat{B})(t_1, t_2) = \int dt_3 \hat{A}(t_1, t_3) \hat{B}(t_3, t_2), \quad (2.52)$$

however, given the context, we will often omit the \circ symbol, for instance, $(\mathcal{G}^{-1} \mathcal{G})(t, t_0) = \delta_{t, t_0}^{\mathcal{C}}$.

Appendix 2.B: Lack of self-averaging in free particles

For \mathcal{N} free particles the partition functions factorize as $\mathcal{Z} = \prod_{k=1}^{\mathcal{N}} \mathcal{Z}_k$. Assuming these are disordered models, we quantify the degree to which the system is self-averaging via the parameter

$$\mathcal{D} = \frac{\overline{\ln \mathcal{Z}} - \ln \overline{\mathcal{Z}}}{\mathcal{N}}.$$

Now due to the factorization and assuming all free particles are distributed in the same way, we find $\mathcal{D} = \ln \overline{\mathcal{Z}_1} - \overline{\ln \mathcal{Z}_1}$. Now we consider two cases, the one for fermions $\mathcal{Z}_F = 1 + y$ and for bosons

$$\mathcal{Z}_B = 1 + \sum_{n=1}^{\infty} y^n = [1 - y]^{-1}, \quad y \equiv e^{-\beta\xi}.$$

Here y is a random variable since ξ is distributed according to some distribution. In fact, the expectation value of y^n is the moment generating function of $\mu - \epsilon$, $M(n\beta) = \overline{e^{n\beta(\mu - \epsilon)}}$

We must have $\xi \equiv \epsilon - \mu > 0$ such that the particle density, given by the Bose-Einstein distribution $n_B(\xi) = 1/(e^{\beta\xi} - 1)$ is positive and finite. As such, we focus on random variables which have a lower bound. Since the variance can be pulled into β , we focus on distributions with unit variance and mean at ξ_0 . For instance, for semicircle distribution or Poisson distribution, we get the moment-generating functions

$$M(\beta) = e^{-\beta\xi_0} \frac{I_1(2\beta)}{\beta}, \quad M(\beta) = \exp(-\beta\xi_0(e^{-\beta} - 1)),$$

respectively. Here the Poisson distribution necessarily has a variance equal to its mean. We know that in the infinite temperature limit, the system is self-averaging, $\mathcal{D} = 0$. We wish to compare the degree to which the systems are self-averaging at high temperatures captured by a small δ , $y = \delta x$. We will focus on the cumulants of x , which are defined in terms of the series

$$\overline{\ln e^{tx}} = \sum_{n \geq 1} \kappa_n \frac{t^n}{n!}.$$

In terms of the moments, $\mu_n = \overline{x^n}$, the first three cumulants are $\kappa_1 = \mu_1$ and the centered means

$$\kappa_2 = \overline{(x - \mu_1)^2} = \mu_2 - \mu_1^2, \quad \kappa_3 = \overline{(x - \mu_1)^3} = \mu_3 - \mu_1^3 - 3\mu_1[\mu_2 - \mu_1^2] \quad (2.53)$$

which may be inverted to yield the expressions

$$\mu_2 = \kappa_2 + \kappa_1^2, \quad \mu_3 = \kappa_3 + 3\kappa_2\kappa_1 + \kappa_1^3.$$

Now since the random variable x is positive, $\kappa_1 \geq 0$. Next, the variance is necessarily non-negative $\kappa_2 \geq 0$. For fermions, we are simply left with

$$\mathcal{D}_F(\delta) = \sum_{n \geq 1} \delta^n (-1)^n \frac{\mu_n - \mu_1^n}{n} = \delta^2 \frac{\kappa_2}{2} + \delta^3 \frac{f_3}{3} + \mathcal{O}(\delta^4), \quad f_3 = \mu_1^3 - \mu_3.$$

By the generalized mean inequality, we have that if $q > p$, then $\mu_q \geq \mu_p^{q/p}$, as such f_3 is necessarily negative. In the bosonic case, we find

$$\mathcal{D}_B(\delta) = \ln(1 + \delta\chi) + \overline{-\ln(1 - y)}$$

where $\chi = \sum_{n \geq 1} \delta^{n-1} \mu_n$. Now using the Taylor series of the logarithm

$$-\ln(1 - y) = \sum_{n \geq 1} \frac{y^n}{n}$$

we are left with

$$\mathcal{D}_B(\delta) = \sum_{n=1}^{\infty} \delta^n \frac{(-1)^{n-1} \chi^n - \mu_n}{n} = \delta^2 \frac{\kappa_2}{2} + \delta^3 \frac{\kappa_3 - f_3}{3} + \mathcal{O}(\delta^4).$$

Note that the leading order expressions are rather similar, both are positive to leading order, and their difference only appears at cubic order $\mathcal{D}_B(\delta) - \mathcal{D}_F(\delta) = \delta^3[\kappa_3 + 2\kappa_1\kappa_2]$. If this is positive, then the bosons are less self-averaging. Explicitly, $\kappa_3 + 2\kappa_1\kappa_2 = \mu_3 - \mu_1\mu_2 \geq \mu_2(\mu_2^{1/2} - \mu_1)$, which non-negative by the generalized mean inequality. In fact, $\mathcal{D}_B(\delta) - \mathcal{D}_F(\delta)$ is strictly positive for non-zero cumulants

$$\mathcal{D}_B(\delta) > \mathcal{D}_F(\delta). \quad (2.54)$$

The reason is that $\kappa_3 + 2\kappa_1\kappa_2 > \kappa_3$, where the third cumulant is related to the skewness $\tilde{\mu}_3$ of the distribution $\kappa_3 = \kappa_2^{3/2}\tilde{\mu}_3$. In particular, the third cumulant is positive if and only if the distribution is skewed to the right, meaning that it has a longer tail on the right side of the mean than on the left side. For our exponential decaying function $y = e^{-\beta(\epsilon-\mu)}$ it will necessarily be skewed to the left since it reaches a maximum for minimum ϵ . In fact, for a strictly positive random variable, it is impossible to have a symmetric distribution, since the distribution must have a lower bound of zero. Therefore, the distribution must be either skewed to the right or the left. However, a distribution that is skewed to the left cannot have a positive third moment, since the left tail is longer than the right tail.

Appendix 2.C: Averaged Hamiltonian

Let us calculate the variance of the Hamiltonian (2.3)

$$\mathcal{H}_q = J_q \sum_{\{\mu\}_1^{q/2}, \{\nu\}_1^{q/2}} X_{\nu}^{\mu} c_{\mu}^{\dagger} c_{\nu}, \quad c_{\nu} \equiv c_{\nu_r} \cdots c_{\nu_1}, \quad \overline{|X|^2} = \frac{\mathcal{N}}{2q^2} \frac{[q/2]!^2 2^{q/2}}{[\mathcal{N}]^q}.$$

Taking the average, only the planar parts contribute, i.e, only when all the indices have a single partner

$$\overline{\mathcal{H}_q(t_1)\mathcal{H}_q(t_2)} = J_q^2 \overline{|X|^2} \sum_{\{\mu\}_1^{q/2}, \{\nu\}_1^{q/2}} c_{\mu}^{\dagger}(t_1)c_{\nu}(t_1)c_{\nu}^{\dagger}(t_2)c_{\mu}(t_2).$$

Let us now consider the operator

$$\hat{f}_{[q/2]}(t_1, t_2) \equiv \frac{[q/2]! 2^{q/2}}{[\mathcal{N}]^{q/2}} \sum_{\{\mu\}_1^{q/2}} c_{\nu}(t_1)c_{\nu}^{\dagger}(t_2) = \frac{2^{q/2}}{\mathcal{N}^{q/2}} c_{\nu}(t_1)c_{\nu}^{\dagger}(t_2)$$

where we are using the Einstein summation convention. What we have done in the second line above is to expand out each term into a sum over all permutations. For instance

$$2c_{\nu_2}(t_1)c_{\nu_1}(t_1)c_{\nu_1}^{\dagger}(t_2)c_{\nu_2}^{\dagger}(t_2) = c_{\nu_2}(t_1)c_{\nu_1}(t_1)c_{\nu_1}^{\dagger}(t_2)c_{\nu_2}^{\dagger}(t_2) + c_{\nu_1}(t_1)c_{\nu_2}(t_1)c_{\nu_2}^{\dagger}(t_2)c_{\nu_1}^{\dagger}(t_2).$$

Here we deviate to consider two different cases. If it is composed of creation and annihilation operators, at $t = 0$. For this case, we may use the commutation relation that $f(c^{\dagger}c)c = cf(c^{\dagger}c - 1)$, hence

$$\begin{aligned} f(\hat{n}) &= \frac{2^{q/2}}{[\mathcal{N}]^{q/2-1}} c_{\nu_r} \cdots c_{\nu_2} (1 - \hat{n}) c_{\nu_2}^{\dagger} \cdots c_{\nu_r}^{\dagger} \\ &= \frac{2^{q/2}}{[\mathcal{N}]^{q/2-1}} c_{\nu_r} \cdots c_{\nu_2} c_{\nu_2}^{\dagger} (1 - \hat{n} - 1/\mathcal{N}) \cdots c_{\nu_r}^{\dagger} \\ &= \frac{2^{q/2}}{[\mathcal{N}]^{q/2-2}} c_{\nu_r} \cdots (1 - \hat{n})(1 - \hat{n} - 1/\mathcal{N}) \cdots c_{\nu_r}^{\dagger} \\ &= 2^{q/2} (1 - \hat{n}) \cdots (1 - \hat{n} - ([q/2] + 2)/\mathcal{N})(1 - \hat{n} - ([q/2] + 1)/\mathcal{N}). \end{aligned}$$

Hence, in the limit of large \mathcal{N} , we find $f(\hat{n}) \rightarrow (1 - 2\hat{\mathcal{Q}})^{q/2}$. By performing the same permutations, we find that the variance of the Hamiltonian to leading order in \mathcal{N} takes the form $J_q^2 \mathcal{N} f(\hat{n}) f(1 - \hat{n}) / (2q^2)$, which implies

$$\overline{\mathcal{H}_q^2} / \mathcal{N} \xrightarrow{\mathcal{N} \rightarrow \infty} J_q^2 [1 - 4\hat{\mathcal{Q}}^2]^{q/2} / (2q^2). \quad (2.55)$$

The simplest is when c is replaced by Grassmann fields. In this case, we have

$$\hat{f} = \left[2 \frac{\psi_{\nu}(t_1) \bar{\psi}_{\nu}(t_2)}{\mathcal{N}} \right]^{q/2} = [-2G(t_2, t_1)]^r.$$

Appendix 2.D: Conformal group

For $d \geq 3$ the conformal group is described by an invariance under translation $\mathbf{r} \rightarrow \mathbf{r} + \mathbf{a}$, rotation $\mathbf{r} \rightarrow R\mathbf{r}$ and dilation $\mathbf{r} \rightarrow b^{-1}\mathbf{r}$ [90]. Additionally, there is also the special conformal transformation

$$\mathbf{r} \rightarrow \frac{\mathbf{r}/r^2 + \mathbf{a}}{[\mathbf{r}/r^2 + \mathbf{a}]^2}$$

which is a combination of all of the above. In two dimensions we define $z = r_1 + ir_2$, for which we find that all conformal transformations may be written as a Möbius transform

$$f(z) = \frac{az + b}{cz + d},$$

for complex coefficients a, b, c, d satisfying $ad - bc = 1$. Interestingly, any holomorphic mapping $z \rightarrow f(z) = r'_1 + ir'_2$ defines a local conformal transformation, which is due to the Cauchy-Riemann equations

$$\frac{\partial r'_2}{\partial r'_1} = -\frac{\partial r'_1}{\partial r_2}, \quad \frac{\partial r'_1}{\partial r_1} = \frac{\partial r'_2}{\partial r_2}.$$

As such, any model with Green's function $\mathcal{G}(r_1, r_2)$ which is holomorphic has local conformal invariance. If it is further invariant under Möbius transform, then it is conformally invariant.

Chapter 3

Dynamics in charged SYK models

The idea of thermal equilibrium is so ubiquitous in our daily lives that we often take it for granted. We know that our cup of hot coffee will eventually cool down to room temperature. Consider the same process on a mathematical level, and it becomes apparent that the very concepts of thermal equilibrium and thermalization are truly remarkable phenomena. How is it possible for a macroscopic object, such as a cup of coffee, to reach a state of thermal equilibrium with its surroundings seemingly forgetting its initial state? And why is it that the thermal behavior of macroscopic systems is so much simpler than that of their microscopic constituents encoded by 10^{23} numbers? These questions were already rather challenging to answer on a classical level, for instance via Boltzmann's H-theorem [101]. In quantum systems, with a Hilbert space size of $e^{10^{23}}$, this difficulty increases exponentially.

While equilibrium is often a good starting assumption, most phenomena are inherently nonequilibrium. Studying quantum systems that are not in equilibrium can provide valuable insight into unresolved issues regarding thermalization, chaos, and transport in quantum many-body. These are the topics we consider in this chapter.

In the Schrödinger picture, the dynamics of these states populating the Hilbert space is described by the von Neumann equation

$$\dot{\rho}_S(t) = -i[\mathcal{H}(t), \rho_S(t)]. \quad (3.1)$$

The initial system can be in some pure state $|\psi(t_0)\rangle\langle\psi(t_0)|$ or a mixed state such as a Gibbs thermal state¹ $\rho(t_0) = e^{-\beta\mathcal{H}(t_0)}$. Formally the solution is a similarity transform

$$\rho_S(t) = U(t, t_0)\rho(t_0)U(t, t_0)^\dagger, \quad U(t, t_0) = \mathcal{T} \exp\left(-i \int_{t_0}^t dt' \mathcal{H}(t')\right),$$

where the time-ordered exponential $U(t, t_0)$ is the unitary evolution operator. Given the time evolved state, the expectation value is then simply computed via

$$\langle\hat{O}\rangle(t) = \text{Tr}\{\hat{O}\rho_S(t)\}/\text{Tr}\{\rho(t_0)\}. \quad (3.2)$$

This unitary evolution implies that the dynamics of a quantum system is reversible. In other words, $U(t, t_0)^\dagger$, will reproduce the initial state. A subtle point, however, is the practical difficulty

¹Throughout this section we will allow for unnormalized states, a point which will become important later on.

in performing this reversal perfectly². What is the effect of some δ perturbation $U_\delta(t, t_0)^\dagger$ when attempting to reverse the time evolution? A measure of this is the Loschmidt echo [102]

$$\mathcal{L}(t) = |\langle \psi(t_0) | \mathcal{U}_C(t, t_0) | \psi(t_0) \rangle|^2,$$

with S -matrix $\mathcal{U}_C(t, t_0) = U_\delta(t, t_0)^\dagger U(t, t_0)$. Any deviation away from unity $\mathcal{L}(t) \neq 1$ reflects this difficulty.

However, this practical difficulty in time reversal does not address the full problem. This is because, given a constant Hamiltonian, Poincare recurrence implies that any (quantum or classical) system can get arbitrarily close to its original state again, sometimes called Zermelo's paradox [103]. This lack of thermalization can be directly observed in experiments. Perhaps the most famous example of this is the quantum Newton's cradle experiment. The classical Newton's cradle consists of a series of suspended balls. Releasing one it collides with the rest, transferring its energy and momentum, with both being conserved as the process repeats indefinitely (assuming no damping). The quantum version consists of a one-dimensional Bose gas of ultra-cold rubidium atoms confined to an optical lattice[104]. Again no appreciable damping is observed even when the system is prepared in an excited state. The key in both cases is integrability, i.e., the systems possess an extensive number of local³ conserved quantities $\{\hat{I}_i\}$ that restrict their dynamics. In the long-time limit, such integrable systems can be described by a generalized Gibbs ensemble $\rho \propto \exp(-\sum_i \beta_i \hat{I}_i)$, where the Lagrange multipliers β_i are also referred to as generalized inverse temperatures [105, 106].

Especially in the context of quantum mechanics, thermalization, the process by which entropy increases to a maximum allowed value seems at the very least counter-intuitive. To see this, consider a subsystem A by tracing out the Hilbert space corresponding to a subsystem B , \mathcal{H}_B , $\rho_A(t) = \text{Tr}_B\{\rho(t)\}$ which obeys the second law of thermodynamics, i.e., with increasing von Neumann entropy density $\mathcal{S}_A = -\langle \ln \rho_A \rangle / \mathcal{N}$. However, now the reversed solution, with decreasing entropy is again a solution. On top of this, the solution should eventually tend back to its low entropy state due to the recurrence relation. Zermelo's paradox is (partially) solved by noting that the recurrence time diverges with the size of the Hilbert space.

Quantum thermodynamics concerns itself with these problems and attempts to justify the macroscopically observed statistical laws from the microscopic laws of quantum mechanics. Much progress has been made in our understanding of the process by which a system becomes "thermal". The definition of what it means to be thermal in quantum mechanics can be subtle. In the framework of open quantum systems, certain subsystems can be shown to evolve towards a Gibbs thermal distribution [107].

If we are considering a small subsystem, where the full state is some randomly chosen pure state, one may show that most states are essentially thermal [108]. In particular one can show that any pure state, restricted to a sub-Hilbert space with Hamiltonian \mathcal{H}_A , which weakly interacts with the rest, is asymptotically given by $\text{Tr}_B\{|\psi\rangle\langle\psi|\} \sim e^{-\beta\mathcal{H}_A}$ for large Hilbert space dimension $|\mathcal{H}_B|$. The associated temperature is then related to the total energy of the system. Such arguments from

²There is an anecdotal story of Boltzmann claiming his H -theorem proved the second law, i.e., the arrow of time. Loschmidt then challenged this stating that reversing all momenta would eventually lead a system to its initial state. Boltzmann simply replied, "Then try and do it!"

³Note that the eigenstate projection operators, while conserved quantities are typically highly non-local.

typicality should, however, be considered with care. This is because, from the perspective of state preparations, not all states are necessarily equally likely. For instance, physical Hamiltonians are local which should be reflected in most states. On top of this, while any Hermitian operator formally corresponds to an observable \hat{O} , experimentally we only have access to local measurements. As such, what we physically experience as thermal equilibrium is when these observables fall within some range of their Gibbs expectation values. Thus, for a closed system to be thermal, it is neither required (nor anticipated) that $\rho(t) \xrightarrow{t \rightarrow \infty} e^{-\beta \mathcal{H}}$. These ideas form the starting point of the eigenstate thermalization hypothesis [109, 110]. It states that assuming nearby energy eigenstates $|E_n\rangle, |E_m\rangle$, with respective energies $\bar{E} \pm \omega/2$, cannot be distinguished by local observations, then the system will thermalize. More formally the assumption is that the matrix elements can be expressed as

$$O_{nm} = \bar{O}(\bar{E})\delta_{nm} + e^{-S_{\text{mc}}(\bar{E})/2} f(\bar{E}, \omega) R_{nm},$$

with smooth functions \bar{O} and f , microcanonical entropy S_{mc} and random matrix R with mean zero and unit variance. This is the expected behavior for nonintegrable systems.

3.1 Chaos and Lyapunov exponents

A good starting point to understand thermalization might be to consider how it occurs classically⁴. Classical thermalization is understood in terms of dynamical chaos leading to the system exploring its available phase space.

The Lyapunov exponent quantifies a specific signature of chaos, namely, exponential sensitivity to initial conditions. To motivate how one quantifies this in a quantum system, let us start by considering its classic version [111]. Take a particular trajectory $\mathbf{x}(t; \mathbf{x}_0)$, with initial position \mathbf{x}_0 . Next, we consider the trajectory which results from having slightly varied the initial conditions $\mathbf{x}(t; \mathbf{x}_0 + \delta)$. The effect of this small change can be read off from their difference in trajectories, illustrated in Fig. 3.1,

$$\lim_{\delta \rightarrow 0} \frac{\mathbf{x}(t; \mathbf{x}_0 + \delta) - \mathbf{x}(t; \mathbf{x}_0)}{\delta}$$

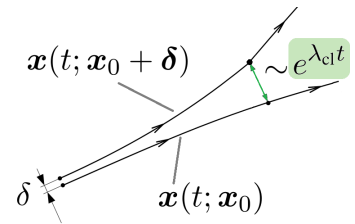


Figure 3.1: Two trajectories stemming from a perturbative change in initial conditions.

which is essentially the derivative of $\mathbf{x}(t)$ with respect to $\mathbf{x}(0)$. We are interested in the maximal sensitivity at *late* times, i.e., the component which influences another at a maximum

$$\left| \frac{\partial x_i(t)}{\partial x_j(0)} \right| \sim e^{\lambda_{\text{cl}} t}, \quad (3.3)$$

where we have suppressed with \mathbf{x}_0 . So for $\lambda_{\text{cl}} \leq 0$, the system is regular/integrable. The paths do not diverge and there is no exponential sensitivity to initial conditions. However, for $\lambda_{\text{cl}} > 0$, the

⁴Often chaos in quantum and classical physics are contrasted by the statement that quantum mechanics is linear, while classical equations are nonlinear. This is a false comparison, in fact, the two equations which one should contrast with another, the von Neumann equation (3.1) and the classical Liouville equation, where $[\cdot, \cdot]_{\text{vN}} \rightarrow \{\cdot, \cdot\}_{\text{PB}}$, are *both* linear.

trajectories will diverge exponentially, even given an infinitesimal difference in initial conditions⁵. We may rewrite this expression in terms of the Poisson bracket

$$\frac{\partial x_i(t)}{\partial x_j(0)} = \frac{\partial x_i(t)}{\partial x_k(0)} \frac{\partial p_j(0)}{\partial p_k(0)} - \frac{\partial x_i(t)}{\partial p_k(0)} \frac{\partial p_j(0)}{\partial x_k(0)} = \{x_i(t), p_j(0)\}_{\text{PB}}.$$

This then leaves us with the expression

$$|\{x_i(t), p_j(0)\}_{\text{PB}}| \sim e^{\lambda_{\text{cl}} t}. \quad (3.4)$$

Via the correspondence principle, we may relate this to its quantum mechanical counterpart

$$\frac{1}{i\hbar} [\hat{x}_i(t), \hat{p}_j(0)] \xrightarrow{\hbar \rightarrow 0} \{x_i(t), p_j(0)\}_{\text{PB}}. \quad (3.5)$$

This mapping can be made concrete via the use of coherent states, star products, and Moyal brackets [113]. To capture the magnitude, we focus on the expectation value $\langle |[\hat{x}_i(t), \hat{p}_j(0)]|^2 \rangle = -\langle [\hat{x}_i(t), \hat{p}_j(0)]^2 \rangle$ [114].

The above, however, requires a phase space representation; hence it does not apply to certain quantum systems, e.g., spin systems. As such, we allow for a broad class of (typically single-body) operators in $C_{\text{un}}(t) = \langle |[X(t), P(0)]|^2 \rangle$. For observables, this commutator serves as an influence measure of P on later measurements of X . In this way, they can be used to study the spread of information. For instance, in a spin system, one could consider initially commuting operators $\sigma_{z,i}$, $\sigma_{z,j}$. As such, given local operators (including the Hamiltonian), $C_{\text{un}}(t)$ may be bounded by a kind of light cone known as a Lieb-Robinson bound [115, 116]. While this process is not exactly that of thermalization, this scrambling rate, or information propagation rate usually gives some indication of the equilibration rate.

Let us partially restrict the discussion to hermitian operators (observables) for which we have $C_{\text{un}}(t) = \mathcal{F}_{\text{un}}^{(\text{TOC})}(t) - 2\Re\mathcal{F}_{\text{un}}(t)$ where we have defined

$$\mathcal{F}_{\text{un}}(t) = \text{Tr}\{(X(t)P)^2 \varrho\}, \quad \mathcal{F}_{\text{un}}^{(\text{TOC})}(t) = \|\varrho^{1/2} X(t) P\|_F^2 + \|X(t) P \varrho^{1/2}\|_F^2 \quad (3.6)$$

and the Frobenius norm $\|A\|_F \equiv \sqrt{\text{Tr}\{A^\dagger A\}}$. Indeed, studying the correlator C_{un} in nonintegrable⁶ models, with all-to-all interactions, one finds exponential growth. For early times $C_{\text{un}}(t) = \mathcal{O}(e^{2\lambda_L(t-t_*)})$, where t_* is the *Ehrenfest*/scrambling time [65, 119]. Here λ_L is the quantum Lyapunov exponent which would overlap with λ_{cl} in the semiclassical limit [96]. This can be seen in the behavior of the OTOC illustrated in Fig. (3.2), where initially, over the collision/dissipation timescale t_d , the OTOC factorizes at an exponential rate $\mathcal{O}(e^{-t/t_d})$. In most nonintegrable models, it will be given by $t_d = \mathcal{O}(1/\lambda_L)$ [65]. The correlation C_{un} becomes sizable at around⁷ the *Ehrenfest*/scrambling time $t_* \sim \lambda_L^{-1} \ln \mathcal{N}$. The logarithm in \mathcal{N} here indicates that

⁵This exponential sensitivity to initial conditions is often referred to as the ‘‘Butterfly effect’’ [112].

⁶In integrable models one finds power laws [118]

⁷Depending on the context, it is also sometimes referred to as the scrambling time. The term entering the logarithm is usually either $1/\hbar$ or \mathcal{N} , hence it is the large parameter, which, taken to infinity, yields the semi-classical limit. As such, the semi-classical approximation is only valid for $t < t_*$

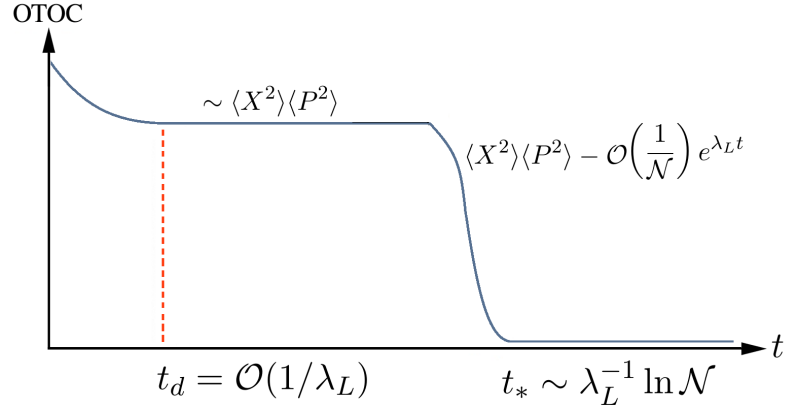


Figure 3.2: Schematic illustration of OTOC behavior for a nonintegrable Hamiltonian built from finite products of simple local operators and with many degrees of freedom [65, 117].

t_* can be much larger than t_d for large \mathcal{N} , indicated in the in-between flat line⁸ of Fig. (3.2). The growth in the correlations is due to the late-time decay in the OTOC [65, 121]

$$\mathcal{F}_{\text{un}}(t) \sim \langle X^2 \rangle \langle P^2 \rangle - \mathcal{O}(1/\mathcal{N}) e^{\lambda_L t}. \quad (3.7)$$

For the SYK model, the decay in the OTOC can be sensitive to the considered operators [62]. For instance, choosing Majorana type fermionic operators $X = c_i + c_i^\dagger$ and $P = c_j + c_j^\dagger$ yields a fast decay to zero. However, in choosing $X = c_i^\dagger c_i$ and $P = c_j^\dagger c_j$, one finds a notably slower decay in the OTOC [122, 123]. This can again be seen from the perspective of classifying a classical system of equations; Even though there may be some fixed points or orbitals, the system's chaos is determined by the *largest* exponent in the Lyapunov spectrum.

In the study of nonintegrable models, one usually focuses on the regularized correlator

$$C_{\text{reg}}(t) = -\text{Tr}\{(\varrho^{1/2}[X(t), P(0)])^2\}, \quad (3.8)$$

which is numerically better behaved, and avoids certain UV divergences. For a thermal initial state, this correlator may be written in terms of the regularized time and out-of-time ordered operators $C_{\text{reg}}(t) = \mathcal{F}_{\text{reg}}^{(\text{TOC})}(t) - 2\Re\mathcal{F}_{\text{reg}}(t + \imath\beta/4)$ [65, 96]⁹ where one smears out the density matrix in between the operators in (3.6)

$$\mathcal{F}_{\text{reg}}(t) = \text{Tr}\{(X(t)\varrho^{1/4}P\varrho^{1/4})^2\}, \quad \mathcal{F}_{\text{reg}}^{(\text{TOC})}(t) = 2\|\varrho^{1/4}X(t)P\varrho^{1/4}\|_F^2. \quad (3.9)$$

Here we have used the form of the unitary evolution operator $U(t) = e^{-\imath\mathcal{H}t}$ and its inverse to write $X(t + \imath\beta/4) = \varrho^{1/4}X(t)\varrho^{-1/4}$, hence

$$\mathcal{F}_{\text{reg}}(t + \imath\beta/4) = \text{Tr}\{X(t)P\varrho^{1/2}X(t)P\varrho^{1/2}\} = \mathcal{F}_{\text{reg}}(t - \imath\beta/4)^*,$$

⁸The limitation to small \mathcal{N} for numerics makes this rather difficult to notice in the numerical plots however [120].

⁹Note the mistake in [96, 2.13], where X and P should be swapped in one of the OTOC terms. In the Keldysh formalism, this smearing out would correspond to a deformation of the time contour by adding multiple “legs” into the imaginary time direction.

where we have permuted the unitary evolution operator passed the thermal density matrix.

It has been previously conjectured that the scrambling time $t_* \sim \lambda_L^{-1} \ln \mathcal{N}$ cannot be less than $C\beta \ln \mathcal{N}$, for some constant C [124]. This would imply a linear temperature bound on the Lyapunov exponent λ_L . Indeed, upon assuming the quantitative behavior in Fig. 3.2 one may prove that the regularized correlator necessarily satisfies a bound on its growth

$$|\partial_t \ln C_{\text{reg}}(t)| \leq 2\pi T/\hbar \quad (3.10)$$

known as the Maldacena-Shenker-Stanford bound [65, 125]. Most many-body quantum systems yield a Lyapunov exponent which is much smaller than the bound (3.10) [126]. Remarkably, in the low-energy limit, the SYK model saturates this bound on chaos $\lambda_L \rightarrow 2\pi T$. As an example, in the strongly coupled regime, for non-hermitian operators we find

$$\frac{1}{\mathcal{N}^2} \sum_{ij} \text{Tr} [\varrho^{1/2} \{c_i(t), c_j^\dagger\} \varrho^{1/2} \{c_i(t), c_j^\dagger\}^\dagger] \sim \frac{1}{\mathcal{N}} e^{2\pi T t}, \quad t \lesssim \beta \ln \mathcal{N} \quad (3.11)$$

for the SYK model [45, 127]. This bound is also saturated in black hole models [128–130], which is our second hint of holographic duality in the SYK model.

3.1.1 Motivation for regularized correlations

One should note that while C_{reg} often overlaps with C_{un} , this is not necessarily always the case. For instance, while the exponential growth in the regularized case follows the MSS bound, the unregularized case can exceed it [119].

With the dimensionful \hbar in (3.10), it is natural to ask what a more standard semi-classical analysis would yield. We have kept the dimensionful parameters just to indicate that this bound is consistent with classical chaos. Namely, as we take the classical limit $\hbar \rightarrow 0$, the bound no longer exists. Would the Lyapunov exponent from the regularized correlator overlap with a semi-classical phase space analysis (3.3)? For the unregularized correlator this does not seem to be the case for the quantum kicked rotor model, where typically $\lambda_L^{(\text{un})} > \lambda_{\text{cl}}$ [131]. The same holds true for both the Dicke and the Lipkin-Meshkov-Glick models. As one moves away from an unstable fixed point, the two exponents diverge, where the system can become classically regular ($\lambda_{\text{cl}} \leq 0$), while $\lambda_L^{(\text{un})} > 0$ [132]. There are also further relations that indicate that C_{reg} may capture aspects of microscopic quantum chaos not captured by the unregularized version C_{un} [119, 128, 133, 134].

3.1.2 Large- q Lyapunov exponent

In general, the OTOCs are related to the $1/\mathcal{N}$ corrections to the flavor averaged four-point functions of the SYK model [135]

$$\frac{1}{\mathcal{N}^2} \sum_{ij} \langle \mathcal{T} c_i(t) c_i^\dagger(t) c_j c_j^\dagger \rangle = \mathcal{G}(0)\mathcal{G}(0) + \mathcal{O}\left(\frac{1}{\mathcal{N}}\right) e^{\lambda_L t}.$$

These $1/\mathcal{N}$ corrections are obtained from a sum over the aforementioned ladder diagrams [45, 135].

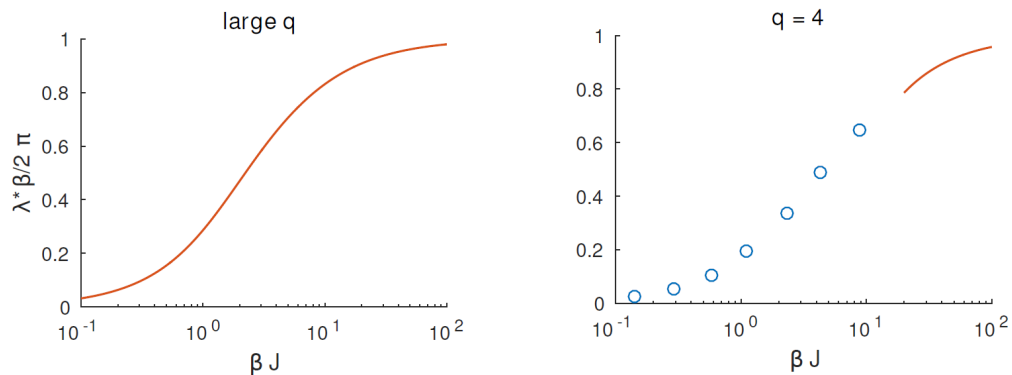


Figure 3.3: Large- q Lyapunov exponent (red curve). (Right) Numerically calculated Lyapunov exponent (blue circles) for the $q = 4$ SYK model. Both cases are for the Majorana SYK model, which corresponds to the charge-neutral complex SYK model. The Figure originates from [45].

Having just discussed the regularized versus unregularized OTOC, in particular the advantages of C_{reg} , it might seem strange that we are considering the unregularized version above. However, when models have a ladder-diagram dominated structure in the four-point functions, which is the case for the SYK model, then the Lyapunov exponent is, in fact, insensitive¹⁰ to the particular regularization as shown in the supplementary material of [120]. For the large- q SYK model, one may calculate this exponent analytically [133, 135, 136]. In particular, the OTOCs behave as $e^{2\pi T v t}$. This was, in fact, the λ (2.38) which entered the previously derived symmetric part of the large- q Green's functions (2.36). As such, we already know the Lyapunov exponent

$$\lambda_L = 2\pi T v, \quad (3.12)$$

for the large- q SYK model in all regimes since v is the solution to $\beta J_q = \pi v \sec(\pi v/2)$, which was plotted in Fig. 2.1. Thus, we note that this model is only maximally chaotic $v \rightarrow 1$, in the infrared limit $\beta J_q \rightarrow \infty$. In the high-temperature case, we find $v \rightarrow \beta J_q/\pi$, hence the system becomes regular (non-chaotic) $\lambda_L \rightarrow 2J_q$ for weak effective coupling, which we will further discuss in the next chapter. Such a linear-in-coupling Lyapunov exponent is also seen in weakly coupled open quantum systems [107]. One may also compare the large- q result with $q = 4$, as plotted in Fig. 3.3, and again one finds a notable overlap.

3.2 The Keldysh formalism

A major challenge in condensed matter physics is to understand how universal non-equilibrium behaviors can emerge in strongly interacting quantum systems. For instance, it is known that models with disorder typically equilibrate on the fast Planckian/Boltzmann timescale $\tau_{\text{eq}} \propto \alpha \hbar/\beta$ [37].

¹⁰The behavior in the OTOCs, for instance, the values of t_d and t_* can still differ greatly, however [120].

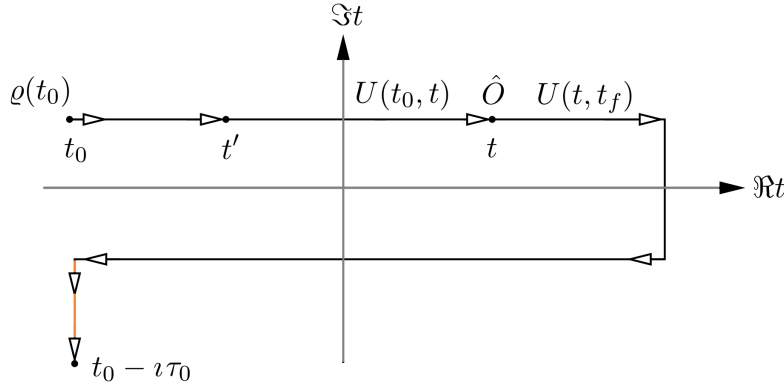


Figure 3.4: The Keldysh contour, with the observable (3.13) inserted at time t . The imaginary leg from t_0 to $t_0 - i\tau_0$ is given in orange. The distance from the horizontal axes seen in the forward and backward (real-time) contributions is purely for visual convenience.

For a strongly interacting quantum field theory, the standard approach is to study this in the Keldysh formalism. Its origin lies in the fact that the expectation value of some observable at a time t (3.2) can be rewritten as

$$\langle \hat{\mathcal{O}} \rangle(t) = \frac{\text{Tr}\{U(t_0, t)\hat{\mathcal{O}}U(t, t_f)U(t_f, t_0)\varrho(t_0)\}}{\text{Tr}\{\varrho(t_0)\}} \quad (3.13)$$

where one takes the evolution along some contour \mathcal{C} in the complex plane. A particularly useful example of such a contour is sketched in Fig. 3.4. The final contribution $[t_0, t_0 - i\tau_0]$, with $\tau_0 = \beta$, is the before mentioned imaginary leg for $t_0 = 0$, relevant for equilibrium physics. Ignoring this part of the contour, one is left with a closed time contour $U(t_0, \infty)U(\infty, t_0)$, where $t_f \rightarrow \infty$, which is merely the identity operator. However, the usefulness of this expression arises in our choice of (contour) time-dependent Hamiltonian. In particular the sourced Hamiltonian

$$\mathcal{H}_\lambda(t) = \mathcal{H}(t) \pm \mathcal{H}_s[\lambda(t)],$$

where \pm is used for the forward/backward part of the contour. Such a sourced Hamiltonian also has a physical interpretation as an applied field. The linear response to this field is given by Kubo's formula [137]

$$\langle \mathcal{O}(t) \rangle = \langle \mathcal{O} \rangle_0 + \int dt' \chi_{\mathcal{O}\mathcal{H}_s}(t, t'), \quad \chi_{\mathcal{O}\mathcal{H}_s}(t, t') \equiv \langle [\mathcal{O}(t), \mathcal{H}_s(t')] \rangle / i \quad (3.14)$$

Let us take the case where we couple to another external fermion via a Fano-type interaction [12]

$$\mathcal{H}_s[\lambda(t)] = \lambda(t) \frac{\eta c^\dagger(t) + c \eta^\dagger(t)}{\langle \eta^\dagger \eta \rangle}$$

where η is some external fermionic operator which anti-commutes with all c . In the simplest case, it is the annihilation operator of some fermion. In this case, the interaction injects/removes electrons

from the system, i.e., acting like a scanning tunneling microscope (STM) tip. Now if we consider the interaction to be weak, and switched on at $t = 0$, then via linear response theory, we would get¹¹

$$\langle \eta^\dagger c \rangle(t) = \int_{-\infty}^{\infty} dt' \lambda(t') [-i\Theta(t-t') \langle [\eta^\dagger c(t), \eta c^\dagger(t')] \rangle / \langle \eta^\dagger \eta \rangle] \quad (3.15)$$

where the response function is the expression inside the square brackets. Note that the contributions like $c(t')$ have vanished due to charge conservation in the unperturbed Hamiltonian. Now anti-commuting the operators past one another and factorizing the expectation values of the initial uncorrelated fermionic systems, we are left with the response function [21]

$$G^R(t, t') = \Theta(t-t') \langle \{c(t), c^\dagger(t')\} \rangle / i \quad (3.16)$$

which is nothing but the retarded Green's function. This highlights the point that Green's functions can be seen as yielding information about observables corresponding to an open quantum system.

We now have time evolution along a contour \mathcal{C} , $U_{\mathcal{C}}[\lambda] = U(t_0, \infty)U(\infty, t_0)$, where the perturbation stems from η . This is the start of the Schwinger-Keldysh formalism. Let us define the sourced partition function as

$$Z[\lambda] \equiv \frac{\text{Tr}\{U_{\mathcal{C}}[\lambda]\varrho(t_0)\}}{\text{Tr}\{\varrho(t_0)\}}, \quad (3.17)$$

which is our generating function for expectation values. For instance, choosing $\mathcal{H}_s[\lambda(t)] = \lambda(t)\hat{O}$, a functional derivative with respect to the coupling $\lambda(t)$ would yield

$$\langle \hat{O} \rangle(t) = \left. \frac{i}{2} \frac{\delta Z[\lambda]}{\delta \lambda(t)} \right|_{\lambda=0}. \quad (3.18)$$

This essentially amounts to inserting observables along the forward and backward contours (time evolving them) and computing their expectation value with respect to the initial state $\varrho(t_0)$.

If we now take $t_0 \rightarrow -\infty$, then $\varrho(-\infty)$ is the state of the system in the infinite past where interactions are switched off, only to be switched on adiabatically. If we considered disorder interactions, then the denominator is disorder-independent. As such, in the Keldysh formalism, the generating function with and without the logarithm, seen from the normalization identity $Z[0] = 1$ [138]. In other words, it gives us the ability to study both quenched and annealed disordered systems. As such, one does not have to introduce replicas in systems with quenched disorder as in Sec. 2.3. Further, if the system is strongly interacting and nonintegrable, then the system becomes insensitive to the initial state, this is the Bogoliubov assumption of weakening initial conditions.

3.2.1 Kadanoff-Baym equations

If we are just interested in the Green's functions, which are described by Dyson's equation, which in terms of the contour bilocal product (2.13), may be written as $\mathcal{G} = \mathcal{G}_0^{-1} + \mathcal{G}_0^{-1} \circ \Sigma \circ \mathcal{G}$. This can be evaluated along the contour where we would parameterize time by some s , $t(s)$. This is, however, rather inconvenient. As such, we use a set of rules, the Langreth rules, to rewrite our

¹¹This expectation value can be extracted from knowledge about the observables $\eta c^\dagger + \text{H.C.}$ and $\eta c + \text{H.C.}$.

equations in terms of only a single leg of the contour [139]. The resulting equations are known as the Kadanoff-Baym (KB) equations¹² [140]

$$\begin{aligned} \partial_{t_1} \mathcal{G}^{\gtrless}(t_1, t_2) = & - \int_{t_0}^{\infty} dt_3 \Sigma^{\gtrless}(t_1, t_3) \mathcal{G}^A(t_3, t_2) + \Sigma^R(t_1, t_3) \mathcal{G}^{\gtrless}(t_3, t_2) \\ & + \int_{t_0 - i\beta}^{t_0} dt_3 \Sigma^<(t_1, t_3) \mathcal{G}^>(t_3, t_2) \end{aligned}$$

which describes the time evolution of the non-equilibrium Green's functions. Here we have defined the advanced/retarded functions

$$\mathcal{G}^A(t_3, t_2) = \Theta(t_2 - t_3) [\mathcal{G}^<(t_3, t_2) - \mathcal{G}^>(t_3, t_2)] \quad (3.19)$$

$$\Sigma^R(t_1, t_3) = -\Theta(t_1 - t_3) [\Sigma^<(t_1, t_3) - \Sigma^>(t_1, t_3)]. \quad (3.20)$$

Under the Bogoliubov principle, the assumption that initial correlations become irrelevant as $t_0 \rightarrow -\infty$ [139, 141], the imaginary part of the contour is ignored. The KB equations then take the form

$$\int_{-\infty}^{t_2} dt_3 \Sigma^{\gtrless}(t_1, t_3) \mathcal{G}^A(t_3, t_2) + \int_{-\infty}^{t_1} dt_3 \Sigma^R(t_1, t_3) \mathcal{G}^{\gtrless}(t_3, t_2).$$

3.2.2 SYK thermalization

The KB equations are typically difficult to solve in full generality. Hence, a quasiparticle structure is frequently used to further reduce this to a quantum Boltzmann equation. A question is at what rate equilibrium is reached. As stated before, a quantum Boltzmann equation would predict a rate proportional to T^2 . This approach cannot be employed for final states lacking quasiparticle excitations. Fortunately, due to the disorder, we may set up the exact KB equations.

One possible way to study how a closed system reaches thermal equilibrium is by studying its response to a quench. The term originally comes from metallurgy, where one rapidly cools a metal, i.e., the quenched parameter is the temperature. In condensed matter, the quenched parameter is any model parameter such as the coupling strength. In particular any instantaneous change to this parameter. Experimental realizations of this are found in ultracold optical lattices [142]. This simplifies the problem from a continuous time-dependent problem to two different time-independent Hamiltonian problems connected at some time. One can then for instance consider knocking a system out of equilibrium and study the rate at which thermal equilibrium is reached once more. As for the KB equations, the full problem is broken into four quadrants as illustrated in Fig. 3.5. Numerical studies considering such quenches indicate that the Majorana SYK model, in the strong coupling regime $\beta_f J_4 \gg 1$, thermalizes at the Planckian rate [143, 144]

$$\beta_{\text{eff}}(t) = \beta_f + \alpha e^{-\alpha T_f t},$$

where β_f is the final inverse temperature. This is not unexpected given the above rate is proportional to the Lyapunov exponent.

¹²The minus sign stems from the way we define our Green's functions without the imaginary unit in from.

The dynamics of the Majorana SYK model corresponds to the uncharged, $Q = 0$ complex SYK model. One can also study the model under the influence of a flat banded “mass” term¹³ $\mathcal{H} \rightarrow \mathcal{H}_q - \eta \hat{Q}$ [145] generating a non-zero charge density. One could also merely refer to this as a chemical potential, however, we will distinguish between the mass term η and a chemical potential term μ on the basis that the latter does not appear in real-time evolution since it is a thermodynamic parameter. Such a non-zero charge density modifies the effective interaction strength to $\mathcal{J}(Q) = [1 - 4Q^2]^{(2-q)/4} J_q$ which we will call the “effective interaction”.

In this case, one finds that a larger mass term leads to slower thermalization [146, 147]. This can be understood by noticing that the effective coupling $\mathcal{J}(Q)$ is suppressed. Since a larger mass term leads to a larger charge density, we effectively have a weaker interacting SYK model, hence slower thermalization.

In the large- q limit, it was shown that quenching from $\mathcal{H}_{q/2} + \mathcal{H}_q \rightarrow \mathcal{H}_q$, the system thermalizes instantaneously [143]. In the following publication, we show how this remains true in the charged SYK model. Further, we show that this result is rather robust, in fact, it holds true for a wide range of dynamical protocols, where we sum together various SYK models, illustrated in Fig. 3.6,

$$\mathcal{H}(t) = \mathcal{H}_2(t) + \sum_{\kappa} \mathcal{H}_{\kappa q}(t)$$

as long as $\mathcal{H}(t > 0) = \mathcal{H}_q$. As such, the result not only holds for a near-arbitrary quench but also ramps. Such instantaneous jumps in equilibrium states can also be found in black holes, with jumps in their Hawking temperature after sending in a delta function “pulse” of energy [148, 3.21]. Such thermalization might feel unphysical, however, from the perspective of a connected graph it might make more sense. The connectivity of the graph, and thus the “speed” of information propagation, scales with q . As such, one might be able to show that such instantaneous thermalization is only possible in the case where $q \rightarrow \infty$. A more detailed discussion on this is provided in App. 3.A.

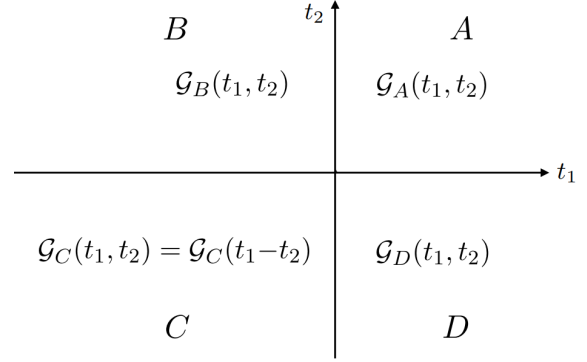


Figure 3.5: Four time quadrants of a quench out of equilibrium $\mathcal{G}_C(t_1, t_2) = \mathcal{G}_C(t_1 - t_2)$.

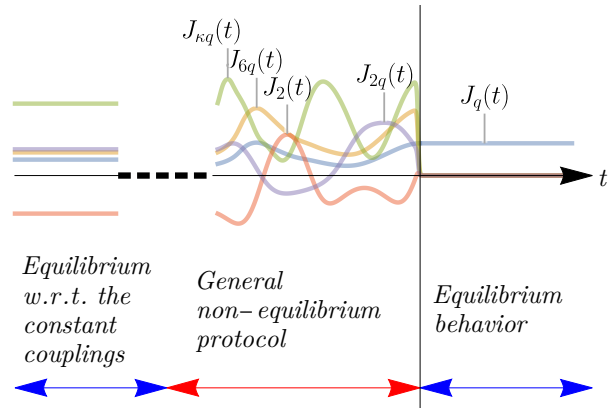


Figure 3.6: Various time protocols, leading to instantaneous thermalization

¹³The ordinary dispersion relation $k^2/(2\eta)$ has the mass entering the denominator. The term “mass” can, however, be motivated from the relativistic dispersion relation $\epsilon_k = \sqrt{k^2 + \eta^2} = \eta + \mathcal{O}(k^2/\eta)$, for a large rest mass.

3.2.3 Publication: Thermalization of many many-body interacting SYK models

Reprinted article with permission from

Jan C. Louw and Stefan Kehrein


Phys. Rev. B 105, 075117 (2022)

<https://doi.org/10.48550/arXiv.2111.08671>


Copyright (2022) by the American Physical Society.

Author contributions J. C. L. did the analytic calculations and wrote the article. S. K. suggested the project, wrote part of the introduction, and independently did many of the analytical calculations. Both authors discussed the results.

Thermalization of many many-body interacting Sachdev-Ye-Kitaev models

Jan C. Louw  and Stefan Kehrein

Institute for Theoretical Physics, Universität Göttingen, Friedrich-Hund-Platz 1, 37077 Göttingen, Germany

 (Received 30 November 2021; accepted 31 January 2022; published 7 February 2022)

We investigate the nonequilibrium dynamics of complex Sachdev-Ye-Kitaev (SYK) models in the $q \rightarrow \infty$ limit, where $q/2$ denotes the order of the random Dirac fermion interaction. We extend previous results by Eberlein *et al.* [*Phys. Rev. B* **96**, 205123 (2017)] to show that a single SYK $q \rightarrow \infty$ Hamiltonian for $t \geq 0$ is a perfect thermalizer in the sense that the local Green's function is instantaneously thermal. The only memories of the quantum state for $t < 0$ are its charge density and its energy density at $t = 0$. Our result is valid for all quantum states amenable to a $1/q$ expansion, which are generated from an equilibrium SYK state in the asymptotic past and acted upon by an arbitrary combination of time-dependent SYK Hamiltonians for $t < 0$. Importantly, this implies that a single SYK $q \rightarrow \infty$ Hamiltonian is a perfect thermalizer even for nonequilibrium states generated in this manner.

DOI: [10.1103/PhysRevB.105.075117](https://doi.org/10.1103/PhysRevB.105.075117)

I. INTRODUCTION

The thermalization of closed quantum many-body systems has become a major research topic due to its relevance both for the foundations of quantum statistical mechanics [1,2] and for experiments, especially in cold atomic gases [3]. Unitarity of time evolution in a closed system implies that a pure state can never evolve to a mixed state described by a thermal density operator. However, a time-evolved pure state can become indistinguishable from a thermal state from the point of view of local measurements or, more generally, measurements of few-body operators. It is in this sense that thermalization of closed quantum many-body systems is usually defined [4].

The two main categories of thermalization behavior are integrable systems, which generically time evolve to a non-thermal stationary state described by a generalized Gibbs ensemble [5–7], and nonintegrable systems, whose stationary state can be described by a thermal state. The generic underlying fundamental reason for the thermalization of non-integrable systems is the eigenstate thermalization hypothesis (ETH) [8–11]. In between these two categories are strongly disordered systems, which can show many-body localization with non-ETH behavior for large disorder and ETH behavior for weaker disorder [12].

The actual thermalization dynamics for nonintegrable systems is usually described by a quantum Boltzmann equation (QBE). However, the QBE is applicable only in systems that allow a quasiparticle description [13]. Within the QBE framework, the approach to equilibrium is exponential with a relaxation time τ that scales like $1/\tau \sim U^2 T^2$ at low temperatures, where U is the interaction strength and T is the temperature of the final state [14].

An important class of materials in which the quasiparticle picture of Fermi liquid theory is invalid is strange metals based on their linear in T electrical resistivity behavior [15,16]. In the past few years, the Sachdev-Ye-Kitaev (SYK)

model [17,18] has paved the way to a better understanding of such materials [19,20]. Apart from its lack of a quasiparticle description, the SYK model has other fascinating properties like being analytically solvable in the thermodynamic limit while at the same time being chaotic (even maximally chaotic in a well-defined sense at low temperatures [21]) [22] and connections to holographic theories and black holes [18,19]. The original SYK model contains only an interaction term for $q = 4$ Majorana fermions [18], but generalizations to general q -particle interaction terms and even superpositions of different q -interaction terms are possible while still retaining the analytic solvability in equilibrium [22]. The same is true for Dirac fermions instead of Majorana fermions [19]. Of particular interest is the many many-body limit $q \rightarrow \infty$, where calculations become analytically more manageable [22].

In this paper we are interested in the thermalization dynamics of the SYK model [23–33]. Due to its lack of quasiparticles the relaxation time is expected to be “Planckian,” $1/\tau = f k_B T/\hbar$, for low temperatures, where f is a constant of order 1 [14]. In the low-temperature limit the relaxation time is therefore both much shorter and universal with no dependence on the interaction strength compared to, e.g., Fermi liquid theory. The thermalization dynamics of the SYK model for Majorana fermions after a quench was first investigated by Eberlein *et al.* [23]. They showed how the analytic solvability of the SYK model in equilibrium carries over to nonequilibrium situations, which can be described by a finite set of integro-differential equations. These equations could then be solved numerically or even analytically in the limit of $q \rightarrow \infty$ interacting Majorana fermions. Specifically, they presented numerical results for a quench starting from an equilibrium state generated by an SYK $q = 2$ plus $q = 4$ model to a $q = 4$ model that are consistent with $1/\tau \propto T$.

In the $q \rightarrow \infty$ limit Eberlein *et al.* solved the Kadanoff-Baym equations analytically for a quench starting from an equilibrium state generated by an SYK q plus $2q$ model (or

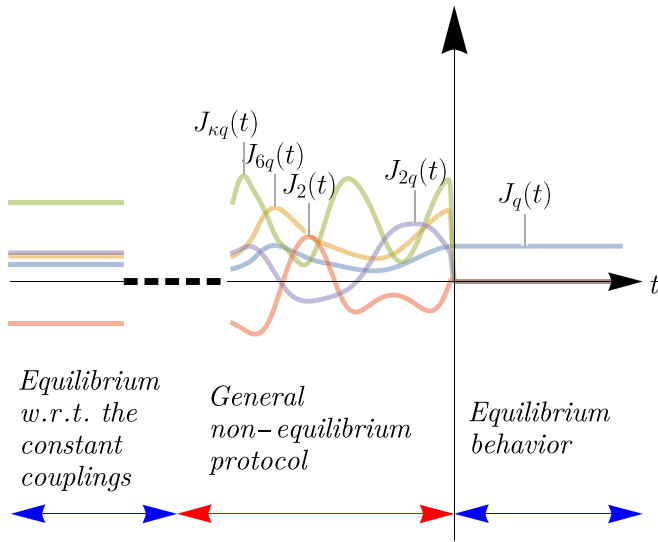


FIG. 1. A schematic summary of the key result of this work. In the asymptotic past, the system is prepared in a thermal Gibbs state with respect to initially time independent couplings [see (13)]. Afterwards, the state is time evolved under a general sum of SYK models. For times $t \geq 0$ only a single SYK term remains. Our key result is that the system is then instantaneously in equilibrium in the large- q limit.

alternatively, q plus $q/2$ model). The postquench Hamiltonian was a single SYK q model. The surprising result was instantaneous equilibrium behavior of the local Green's function after the quench [23], implying that there is no memory of the prequench state except for its energy density.

Our paper generalizes the large- q results in Ref. [23] along various lines. First of all, our analytic calculation holds generally for Dirac fermions (notice that the half-filled Dirac fermion SYK model is equivalent to the Majorana SYK model). More importantly, the system does not need to be in equilibrium before the quench but can be in a general nonequilibrium state generated by a superposition of arbitrary time-dependent SYK interaction terms. Finally, we do not require a quench but just some arbitrary time-dependent protocol (see Fig. 1) that leads to a single remaining SYK term for $t \geq 0$. In the asymptotic past, $t \rightarrow -\infty$, the system is in a thermal equilibrium Gibbs state. The protocol, with arbitrary time-dependent couplings, then leads to nonequilibrium (NEQ) physics, which prepare an NEQ initial state $\varrho(t=0)$. Under these conditions we show that the local Green's function is instantaneously in equilibrium for $t \geq 0$. The only memories of the quantum state for $t < 0$ are its charge density and its energy density at $t=0$. In this sense the $q \rightarrow \infty$ SYK Hamiltonian is a perfect thermalizer. The key requirements of our analytic calculation are the $q \rightarrow \infty$ limit and the existence of a single SYK term for $t \geq 0$.

Outline. We start by describing the general model in Sec. II. In Sec. III, we go on to study the nonequilibrium dynamics given by the Kadanoff-Baym (KB) equations. We make use of the particular expansion allowed in the many many-body regime, described in Sec. III A, which significantly simplifies the (KB) equations.

The main focus of our study, namely, studying the dynamics of a very general state under a single SYK $q \rightarrow \infty$ Hamiltonian, is presented in Sec. IV. For this case we obtain exact results for the local Green's function, which are shown to instantaneously satisfy all conditions of a thermal state in Sec. IV A 1. The equilibrium properties of this state, such as the energy density, are elaborated on in Sec. IV A 2. For completeness, we discuss the simplest case where all interactions are switched off, leaving only a kinetic term in Sec. IV B. Finally, in Sec. V we summarize the results.

II. MODEL

The complex $(p/2)$ -body interacting SYK model is defined by all-to-all interactions [19,34,35]

$$\mathcal{H}_p = \sum_{\substack{1 \leq i_1 < \dots < i_{p/2} \leq N \\ 1 \leq j_1 < \dots < j_{p/2} \leq N}} X_{j_1 \dots j_{p/2}}^{i_1 \dots i_{p/2}} c_{i_1}^\dagger \dots c_{i_{p/2}}^\dagger c_{j_{p/2}} \dots c_{j_1}.$$

Here c_k^\dagger and c_k are fermionic creation and annihilation operators, respectively, while N is the number of lattice sites. The couplings X are complex random variables with zero mean. Their variance is given by

$$\overline{|X_{j_1 \dots j_{p/2}}^{i_1 \dots i_{p/2}}|^2} = \frac{U_p^2 [(p/2)!]^2}{[N/2]^{p-1}},$$

where we allow for U_p to be time dependent. In this work we focus on a series of such $(p/2)$ -body interacting SYK models

$$\mathcal{H} = \sum_p \mathcal{H}_p. \quad (1)$$

Specifically, we will be interested in the *many* many-body case, that is to say, the case where p is large. However, the derivations which follow here are for the general case. We will introduce the details of the large- p case in Sec. III A.

By tuning a chemical potential, we are able to consider the system at arbitrary filling, encoded by the charge density

$$\mathcal{Q} \equiv \frac{1}{N} \sum_{k=1}^N \langle c_k^\dagger c_k \rangle - \frac{1}{2}, \quad (2)$$

which is a conserved quantity. For instance, half filling corresponds to charge neutrality $\mathcal{Q} = 0$, for which we will find the same equations as in the Majorana case [23].

We are interested in the nonequilibrium dynamics of (1), which, following [23], we will study in the Keldysh formalism [13]. In this framework one computes correlations, such as the Green's functions

$$\mathcal{G}(t_1, t_2) \equiv \frac{-1}{N} \sum_{k=1}^N \langle \mathcal{T}_C c_k(t_1) c_k^\dagger(t_2) \rangle, \quad (3)$$

by considering a closed time contour \mathcal{C} . Here \mathcal{T}_C is the contour time ordering operator. From this definition, we note that the Green's functions satisfy the conjugate relation

$$\mathcal{G}(t_1, t_2)^* = \mathcal{G}(t_2, t_1), \quad (4)$$

which we will use at a later stage. These functions encode various statistics of the model, such as the density of states and charge density. Their time evolution is determined by the

self-energy Σ via the Dyson equation $\Sigma(t_1, t_2) = \iota \delta_{\mathcal{C}}(t_1, t_2) - \mathcal{G}^{-1}(t_1, t_2)$. The SYK models are solvable in the sense that, in the thermodynamic limit, one can derive a closed-form expression for the self-energy in terms of the Green's functions. As an example, the $(p/2)$ -body interacting SYK model has a self-energy which is related to the Green's functions via [34,36]

$$\Sigma_p(t_1, t_2) = p2U_p^2[-4\mathcal{G}(t_1, t_2)\mathcal{G}(t_2, t_1)]^{p/2-1}\mathcal{G}(t_1, t_2) \quad (5)$$

to leading order in $1/N$. For a sum of SYK models, such as the model we consider (1), the self-energies are simply additive $\Sigma(t_1, t_2) = \sum_p \Sigma_p(t_1, t_2)$ [22].

III. REAL-TIME DYNAMICS

We are particularly interested in the relaxation dynamics of the Green's functions (3) for Hamiltonians (1), which take on a time dependence. To study this, it is convenient to work with time arguments defined along the real number line, instead of the closed time contour \mathcal{C} . In this real-time formalism, we focus on the forward and backward Green's functions, where t_1 and t_2 are chosen to lie on different halves of \mathcal{C} . These forward and backward Green's functions may be written explicitly as

$$\mathcal{G}^>(t_1, t_2) \equiv -\frac{1}{N} \sum_{k=1}^N \langle c_k(t_1) c_k^\dagger(t_2) \rangle, \quad (6)$$

$$\mathcal{G}^<(t_1, t_2) \equiv \frac{1}{N} \sum_{k=1}^N \langle c_k^\dagger(t_2) c_k(t_1) \rangle, \quad (7)$$

respectively. Their equations of motion, the KB equations, are obtained from the Dyson equation by applying the Langreth rules [37]

$$\partial_{t_1} \mathcal{G}^{\gtrless}(t_1, t_2) = \int_{t_1}^{t_2} dt_3 \Sigma^{\gtrless}(t_1, t_3) \mathcal{G}^A(t_3, t_2) + I(t_1, t_2). \quad (8)$$

Here we have defined the advanced Green's function, which for $t_3 < t_2$ is

$$\mathcal{G}^A(t_3, t_2) = \mathcal{G}^<(t_3, t_2) - \mathcal{G}^>(t_3, t_2). \quad (9)$$

In Appendix B, we elaborate on the process of writing the KB equations in this form. The final term is the integral

$$I(t_1, t_2) = \int_{-\infty}^{t_1} dt_3 \Sigma^>(t_1, t_3) \mathcal{G}^<(t_3, t_2) - \Sigma^<(t_1, t_3) \mathcal{G}^>(t_3, t_2), \quad (10)$$

which is the same for both forward and backward Green's functions. As $t_2 \rightarrow t_1$, it is the only remaining term in the KB equations (8) since the first integral drops out. It is also at such equal times that the left-hand side of (8) may be related to the energy via the Galitskii-Migdal sum rule [37,38]

$$\lim_{t_2 \rightarrow t_1} \partial_{t_1} \mathcal{G}^<(t_1, t_2) = -\iota \sum_{p>0} \frac{p}{2} E_p(t), \quad (11)$$

where $E_p(t) = \langle \mathcal{H}_p(t) \rangle / N$. We provide a proof for this relation in Appendix A. Comparing (11) to the right-hand side of (8) yields the following relation to the energy terms:

$$I(t, t) = -\iota \sum_{p>0} \frac{p}{2} E_p(t), \quad (12)$$

which will be key in solving the equations.

A. Many many-body case

In this work we focus on $(p = \kappa q)$ -body terms, for large q , which are particularly amenable to analytic calculation. In the regime where $1/q$ is small, the Green's functions take the form $\mathcal{G}^{\gtrless}(t_1, t_2) \propto 1 + g^{\gtrless}(t_1, t_2)/q + \mathcal{O}(1/q^2)$ [22,36]. Conveniently, by first rescaling the couplings as

$$U_p = \frac{J_p}{\sqrt{pq}}, \quad (13)$$

this structure is preserved even if we also have a competing kinetic term

$$\mathcal{H}_2 = \sum_{i=1}^N \sum_{j=1}^N X_j^i c_i^\dagger c_j, \quad \overline{|X_j^i|^2} = \frac{1}{N} \frac{J_2^2}{q}. \quad (14)$$

With this, the general Hamiltonian we consider is of the form

$$\mathcal{H}(t) = \mathcal{H}_2(t) + \sum_{\kappa>0} \mathcal{H}_{\kappa q}(t). \quad (15)$$

Here we again mention that at this point, the couplings $J_p(t)$ still have a general time dependence.

In this work we opt to write the $1/q$ expansion in an exponential form,

$$\mathcal{G}^{\gtrless}(t_1, t_2) = [\mathcal{Q} \mp \frac{1}{2}] e^{g^{\gtrless}(t_1, t_2)/q}, \quad (16)$$

which, together with higher-order corrections, has been found to have larger overlap with the exact $q = 4$ solution [39]. This form will also aid in the interpretation of our results. For instance, linear correction in g , like $\iota(t_1 - t_2)$, may then be identified with a phase in the Green's functions, instead of a secular (diverging) term. We stress, however, that to leading order in $1/q$, the results for both choices are the same.

For general p , we write the self-energy (5) as

$$\Sigma_p^{\gtrless}(t_1, t_2) = \frac{1}{q} \mathcal{L}_p^{\gtrless}(t_1, t_2) \mathcal{G}^{\gtrless}(t_1, t_2),$$

where we have defined

$$\mathcal{L}_p^{\gtrless}(t_1, t_2) \equiv 2J_p(t_1)J_p(t_2)[-4\mathcal{G}^{\gtrless}(t_1, t_2)\mathcal{G}^{\lesseqgtr}(t_2, t_1)]^{p/2-1}. \quad (17)$$

Since the total self-energy $\Sigma^{\gtrless} = \mathcal{L}^{\gtrless} \mathcal{G}^{\gtrless}/q$ is a sum over the individual terms, we have

$$\mathcal{L}^{\gtrless}(t_1, t_2) = 2J_2(t_1)J_2(t_2) + \sum_{\kappa>0} \mathcal{L}_{\kappa q}^{\gtrless}(t_1, t_2), \quad (18)$$

where we have written the kinetic term's contribution, which corresponds to $p = 2$, out explicitly.

Considering the definition (7), we note that at $t_1 = t_2 = 0$ the Green's functions are equal to the charge density up to a constant $\mathcal{G}^{\gtrless}(0, 0) = \mathcal{Q} \mp 1/2$, which implies the boundary conditions $g^{\gtrless}(0, 0) = 0$.

Inserting the large- q Green's function's expression (16) into the KB equations (8), the left-hand side simplifies to $\mathcal{G}^{\gtrless}(t_1, t_2) \partial_{t_1} g^{\gtrless}(t_1, t_2)/q$. Next, since the Green's functions are constant to leading order $\mathcal{G}^{\gtrless}(t_1, t_2) \sim \mathcal{G}^{\gtrless}(0, 0)$, the advanced Green's function is given by $\mathcal{G}^A(t_3, t_2) \sim 1$. With this, dividing (8) by $\mathcal{G}^{\gtrless}(0, 0)/q$, we are left with

$$\partial_{t_1} g^{\gtrless}(t_1, t_2) = \int_{t_1}^{t_2} dt_3 \mathcal{L}^{\gtrless}(t_1, t_3) + \frac{qI(t_1, t_2)}{\mathcal{G}^{\gtrless}(0, 0)}. \quad (19)$$

Using the definition (10) of I , the final term in (19) may be written as

$$\frac{qI(t_1, t_2)}{\mathcal{G}^{\geq}(t_1, t_2)} \sim 2\mathcal{G}^{\leq}(0, 0) \int_{-\infty}^{t_1} dt_3 \frac{\mathcal{L}^>(t_1, t_3) - \mathcal{L}^<(t_1, t_3)}{2},$$

which is remarkably independent of t_2 , to leading order in $1/q$. As such, it must be the same expression as that at $t_2 = t_1$,

$$\frac{qI(t_1, t_1)}{\mathcal{G}^{\geq}(t_1, t_1)} = 2\mathcal{G}^{\leq}(0, 0) \iota \alpha(t_1), \quad (20)$$

where we have labeled the integral by $\iota \alpha(t_1)$. Together with the Green's functions' relation to charge density (16), we are left with

$$\partial_{t_1} g^{\geq}(t_1, t_2) = \int_{t_1}^{t_2} dt_3 \mathcal{L}^{\geq}(t_1, t_3) + \mathcal{Q} \iota \alpha(t_1) \mp \frac{\iota \alpha(t_1)}{2}. \quad (21)$$

The most apparent simplification, due to the $1/q$ expansion, is that integrands have lost their t_2 dependence. This time argument makes an appearance only in the integral bound. Hence, by application of the fundamental theorem of calculus, one may obtain the second-order differential equation

$$\partial_{t_1} \partial_{t_2} g^>(t_1, t_2) = \mathcal{L}^>(t_1, t_2). \quad (22)$$

Using the form of the Green's functions (16), we may express $\mathcal{L}_{\kappa q}^>(t_1, t_2)$, defined in (17), as

$$2\mathcal{J}_{\kappa}(t_1)\mathcal{J}_{\kappa}(t_2) \exp\left[\kappa \frac{g^>(t_1, t_2) + g^<(t_2, t_1)}{2}\right]. \quad (23)$$

Here we have defined the *effective* couplings

$$\mathcal{J}_{\kappa}(t) \equiv [1 - 4\mathcal{Q}^2]^{\kappa q/4 - 1/2} J_p(t). \quad (24)$$

At half filling $\mathcal{Q} = 0$, they are equal to $J_p(t)$. For finite, nonzero charge densities, we have $1 - 4\mathcal{Q}^2 < 1$, leading to a suppression of the effective coupling

$$\mathcal{J}_1(t) \equiv [1 - 4\mathcal{Q}^2]^{q/4 - 1/2} J_q(t) \xrightarrow{q \rightarrow \infty} 0,$$

except for large $J_q \sim [1 - 4\mathcal{Q}^2]^{-q/4}$. As such, to maintain nontrivial interactions away from charge neutrality, the coupling can be rescaled by this factor [36]. For our results, however, we do not need to specify the scaling of J_q .

IV. SINGLE SYK TERM

Considering the relation between the integral I and the weighted sum over these terms (12), we note that $\alpha(t_1)$, defined in (20), is given by

$$(1 - 4\mathcal{Q}^2)\alpha(t) = qE_2(t) + q^2 \sum_{\kappa > 0} \kappa E_{\kappa q}(t). \quad (25)$$

Note here that all terms in this series contribute to the same order. This is because of the scaling in (13) leading to the kinetic term scaling like $1/q$, while the interaction terms scale like $1/q^2$. For a system in equilibrium, the individual terms $E_p(t)$ are all constant, leading to constant (25). Otherwise, even for constant couplings, the weighted sum (25) will generally not be constant since the individual terms $\mathcal{H}_p(t)$ are not conserved. In contrast, an equally weighted sum would correspond to the conserved (for constant couplings) total energy. With this we note the remarkable simplification which

occurs in the case where we switch off all but a single coupling in (15),

$$\mathcal{H}(t) = \begin{cases} \mathcal{H}_2(t) + \sum_{\kappa > 0} \mathcal{H}_{\kappa q}(t) & t < 0, \\ \mathcal{H}_p & t \geq 0. \end{cases}$$

In this case, the total interaction energy density is merely given by the single expectation value $E = \langle \mathcal{H}_p/N \rangle$. Since this is a conserved quantity, we find, using the relation (25), that $\alpha(t \geq 0)$ must also be a constant α_f .

To ensure the applicability of our KB equations, we require the system to be in equilibrium in the asymptotic past. Note, however, that we have *not* made any additional assumptions on the initial state $\varrho(0)$ of the system. The key to our proof is *only* that the final Hamiltonian consists of a single SYK term. This may be accomplished via a quench, as was considered in [23] for $\mathcal{H}_q + \mathcal{H}_{2q} \rightarrow \mathcal{H}_q$, via a ramp or any other time protocol, as shown in Fig. 1.

With this, the KB equations (21) simplify to

$$\partial_{t_1} g^>(t_1, t_2) = \int_{t_1}^{t_2} dt_3 \mathcal{L}^>(t_1, t_3) + \iota \alpha_f + 2\mathcal{Q} \iota \alpha_f, \quad (26)$$

$$\partial_{t_1} g^<(t_2, t_1) = \int_{t_1}^{t_2} dt_3 \mathcal{L}^>(t_1, t_3) + \iota \alpha_f - 2\mathcal{Q} \iota \alpha_f. \quad (27)$$

Here we have used the Green's function's conjugate relations (4) $\mathcal{G}(t_1, t_2)^* = \mathcal{G}(t_2, t_1)$, which imply that $g^{\geq}(t_1, t_2)^* = g^{\geq}(t_2, t_1)$, to replace $\mathcal{L}^<(t_1, t_3)^* \rightarrow \mathcal{L}^>(t_1, t_3)$. Equations (26) and (27) are remarkably similar, differing only by a constant. With the same boundary conditions, $g^{\geq}(0, 0) = 0$, their solutions can thus differ by only a linear term,

$$g^>(t_1, t_2) = g(t_1, t_2) + 2\mathcal{Q} \alpha_f \iota(t_1 - t_2), \quad (28)$$

$$g^<(t_2, t_1) = g(t_1, t_2) - 2\mathcal{Q} \alpha_f \iota(t_1 - t_2). \quad (29)$$

To derive the linear t_2 dependence, we have again used the Green's function's conjugate relations (4). From this we note that the Majorana relation $g^>(t_1, t_2) = g^<(t_2, t_1)$, found in [23], is reproduced as $\mathcal{Q} \rightarrow 0$. Considering the Green's functions (16), we note that such a linear result yields a phase

$$\mathcal{G}^>(t_1, t_2) \propto \exp\left(\iota \frac{2\mathcal{Q} \alpha_f (t_1 - t_2)}{q} + g(t_1, t_2)/q\right). \quad (30)$$

This corresponds to a frequency-independent shift in the self-energy $\Sigma(\omega)$. In the next section, we will show how this manifests itself as a shift in the chemical potential.

The addition of (28) and (29) yields the symmetric sum

$$g(t_1, t_2) \equiv \frac{g^>(t_1, t_2) + g^<(t_2, t_1)}{2}, \quad (31)$$

previously encountered in (23).

A. Single interaction term

We now consider the protocol where we are left with only a single interaction term, i.e., $\mathcal{H}(t > 0) = \mathcal{H}_q$. With this, as was found for Majorana fermions [23], (22) reduces to the Liouville equation

$$\partial_{t_1} \partial_{t_2} g(t_1, t_2) = 2\mathcal{J}^2 e^{g(t_1, t_2)}. \quad (32)$$

This equation is formally similar to the corresponding equilibrium equation $\ddot{g}(t) \propto e^{g(t)}$. The key difference, however, is

that we have two different time arguments, while in equilibrium only the relative time enters. For $g^*(t_1, t_2) = g(t_2, t_1)$, the solution of (32) may be written in the form [40]

$$e^{g(t_1, t_2)} = \frac{-\dot{u}(t_1)\dot{u}^*(t_2)}{\mathcal{J}^2[u(t_1) - u^*(t_2)]^2}. \quad (33)$$

We would next like to find the most general, *unique* solution (33). We may find $u(t)$ by considering the equal-time sum of (26) and (27),

$$\lim_{t_2 \rightarrow t} \partial_t \partial_t g(t, t_2) = \iota \alpha_f.$$

Substituting in expression (33) for g yields

$$\partial_t \ln \dot{u}(t) - 2 \frac{\dot{u}(t)}{u(t) - u^*(t^+)} = \iota \alpha_f. \quad (34)$$

Following [23], we make the ansatz

$$u(t) = \frac{a e^{i\pi v/2} e^{\sigma t} + \iota b}{c e^{i\pi v/2} e^{\sigma t} + \iota d}, \quad v \in [-1, 1], \quad (35)$$

which has five independent real parameters since the numerator and denominator are unique only up to an overall factor. Substituting (35) into (34), we are left with a constant $-\iota \sigma \tan(\pi v/2)$ on the left. Hence, identifying

$$\alpha_f = -\sigma \tan(\pi v/2), \quad (36)$$

we see that the ansatz solves the equation. This leaves only four free parameters, which are fully determined by the two complex initial conditions, implying that this ansatz is a valid and uniquely determined solution. By the Picard-Lindelöf (Cauchy-Lipschitz) theorem this is also the only solution to the nonlinear differential equation (34), determined by the two complex initial conditions $u(0)$ and $\dot{u}(0)$.

Substituting this into (33), the correction $g(t_1, t_2)$, for $t_1, t_2 \geq 0$, takes on the unique and *most* general form

$$e^{g(t_1, t_2)} = \frac{(\sigma/2)^2}{\mathcal{J}^2 \cos^2(\pi v/2 - \sigma \iota(t_1 - t_2)/2)}, \quad \sigma \geq 0. \quad (37)$$

Note that *all* solutions of (32) *only* depend on relative time $t_1 - t_2$, when both times are larger than zero because α_f is time independent. Remarkably, (37) is completely independent of a, b, c , and d , implying the $SL(2, \mathbb{C})$ invariance discussed in [23]. Here we have assumed without loss of generality that $\sigma > 0$, since $\sigma \rightarrow -\sigma$, is equivalent to taking $v \rightarrow -v$.

1. Comparison to equilibrium

As noted previously, like in the equilibrium case, the solution (37) depends on only time differences $g(t_1 - t_2) \equiv g(t_1, t_2)$. It is also a periodic function satisfying $g(t) = g(-t - \iota 2\pi v/\sigma)$. Such an equation is, in fact, a Kubo-Martin-Schwinger (KMS) relation for a system with inverse temperature $\beta_f \equiv 2\pi v/\sigma$. With this identification of the temperature, we have the expression

$$\sigma = \frac{2\pi v}{\beta_f}, \quad (38)$$

where σ is, in fact, the Lyapunov exponent of the system [22,41]. Inserting this into (37), the *correction* g takes on the

standard large- q thermal Green's function form [22]

$$e^{g(t)/2} = \frac{\pi v}{\beta_f \mathcal{J} \cos[\pi v(1/2 - \iota t/\beta_f)]}. \quad (39)$$

It must also satisfy the same boundary condition $g(0) = 0$, which yields the same closure relation

$$\beta_f \mathcal{J} = \frac{\pi v}{\cos(\pi v/2)}. \quad (40)$$

From this relation we are able to find v as a function of $\beta_f \mathcal{J}$. Given a particular energy density (36), one is then able to find the corresponding temperature.

One should note, however, that for the *total* system to be considered in thermal equilibrium, it is the *full* Green's functions that must satisfy the KMS relation. As such, we turn our attention to the full exact Green's functions, defined in (7). For $t > 0$ we find that the forward and backward Green's functions are related via

$$\frac{\mathcal{G}^<(t + \iota \beta_f)}{-\mathcal{G}^>(t)} = \frac{1 + 2Q}{1 - 2Q} e^{-\beta_f 2Q \alpha_f/q}. \quad (41)$$

For a standard KMS relation, the right-hand side is 1, while in the presence of a chemical potential this changes to [42]

$$\mathcal{G}_{\text{eq}}^<(t + \iota \beta) = -e^{\beta \mu} \mathcal{G}_{\text{eq}}^>(t). \quad (42)$$

This is because, when considering real-time dynamics, the chemical potential term enters the state $\propto e^{-\beta[\mathcal{H} - \mu N \hat{Q}]}$ but not the Hamiltonian.

As such, for $t \geq 0$, the system can be *immediately* identified as being in *thermal equilibrium*, with the new chemical potential term

$$\mu_f(Q) = T_f \ln \left[\frac{1 + 2Q}{1 - 2Q} \right] - 2Q \alpha_f/q. \quad (43)$$

2. The final energy range

As a final consistency check, we show that the energy densities of our solutions are always bounded by the lowest and highest eigenvalues of \mathcal{H}_q/N . We start by first writing the energy density in a simpler form by using the closure relation $g(0) = 0$, meaning $\sigma = 2\mathcal{J} \cos(\pi v/2)$. Recalling relation (36), $\alpha_f = -\sigma \tan(\pi v/2)$, the energy density (25), $q^2 E = (1 - 4Q^2) \alpha_f$, may then be expressed as

$$q^2 E = -(1 - 4Q^2) 2\mathcal{J} \sin(\pi v/2). \quad (44)$$

For $v \in [-1, 1]$, its range is then given by

$$q^2 E \in [-2\mathcal{J}(1 - 4Q^2), 2\mathcal{J}(1 - 4Q^2)].$$

Here, in fact, the lower bound corresponds to the ground state energy density [36]. Due to the symmetry of the SYK spectrum over the zero axis [43], the maximal energy is $-E_0$. As such, the allowable energies span the spectrum of the model.

In summary, given a state $\varrho(0)$, generated by a general protocol such as that shown in Fig. 1, we find the instantaneously thermal Green's function correction $g(t)$, given in (39),

$$e^{g(t)/2} = \frac{\pi v}{\beta_f \mathcal{J} \cos[\pi v(1/2 - \iota t/\beta_f)]}. \quad (45)$$

The system has memory of only two observables, namely, the charge density

$$\mathcal{Q} \equiv \frac{1}{N} \sum_{k=1}^N \text{Tr}\{c_k^\dagger c_k \varrho(0)\} - \frac{1}{2},$$

which is in the range $[-1/2, 1/2]$, where $\mathcal{Q} = 0$ at half filling, and the energy density

$$E_q \equiv \frac{1}{N} \text{Tr}\{\mathcal{H}_q \varrho(0)\}.$$

Together they uniquely determine the final thermal Green's function. In particular, the constant v is determined by both densities

$$\sin(\pi v/2) = \frac{q^2 E_q}{-(1 - 4\mathcal{Q}^2)2\mathcal{J}}.$$

The effective coupling \mathcal{J} , defined in (24), is given in terms of the charge density and coupling J_q . The final temperature is then determined by v from the closure relation (40),

$$T_f = \mathcal{J} \frac{\cos(\pi v/2)}{\pi v}.$$

B. Single kinetic term

Before concluding, we briefly discuss the case in which all interactions are switched off in (15), leaving only the kinetic term (14). With this, (22) reduces to only the leading term in (18), $\partial_{t_1} \partial_{t_2} g(t_1, t_2) = 2J_2^2$. This equation has a quadratic solution which, together with the boundary conditions $g(0, 0) = 0$ and $\partial_t g(t, t^+) = i\alpha_f$, is given by

$$g(t_1, t_2) = -J_2^2(t_1 - t_2)(t_1 - t_2 - i\alpha_f/J_2^2).$$

We again note that this is dependent on only time differences. The total Green's function is then given by

$$\mathcal{G}^>(t) \propto e^{t^2 2\mathcal{Q}\alpha_f t/q - J_2^2 t(t - i\alpha_f/J_2^2)/q}. \quad (46)$$

It again satisfies the KMS relation $g(t) = g(-t + i\alpha_f/J_2^2)$, identifying the inverse temperature as

$$\beta_f = -\alpha_f/J_2^2.$$

As such, even in this case, we find instantaneous thermalization to leading order in $1/q$.

V. CONCLUSION

In this paper we extended the previous results in Ref. [23] by studying the nonequilibrium dynamics of general Dirac fermion SYK models (15)

$$\mathcal{H}(t) = \mathcal{H}_2(t) + \sum_{\kappa > 0} \mathcal{H}_{\kappa q}(t) \quad (47)$$

in the $q \rightarrow \infty$ limit. Specifically, we were interested in the thermalization dynamics of a state ϱ at time $t = 0$, which was generated from an equilibrium state of a time-independent Hamiltonian of the form of (47) in the asymptotic past that is then acted upon by an arbitrary time-dependent $\mathcal{H}(t)$ for $t < 0$. For $t \geq 0$ we made the key assumption that only a single term in (47) remains. Under this assumption we could

show analytically that the local Green's function is instantaneously in equilibrium. The only properties of the state $\varrho(t = 0)$ that determine the $t \geq 0$ equilibrium behavior are the energy density and the charge density. In this sense a single $q \rightarrow \infty$ SYK term is a perfect thermalizer for a large class of states ϱ . Notice that it is unimportant whether one arrives at the single SYK term via a quench or a more general time-dependent protocol, as shown in Fig. 1.

We were able to prove this result by making use of the conserved quantities, namely, the q -body interaction energy and charge density, in combination with the Galitskii-Migdal sum rule. This forced the Green's function to be constant along the diagonal, leading to a differential equation with a unique solution depending on two initial conditions, which we identified as the energy density and the charge density at time $t = 0$. This unique solution turns out to be just the thermal Green's function of the Hamiltonian for $t \geq 0$.

ACKNOWLEDGMENTS

This work was funded by the Deutsche Forschungsgemeinschaft (DFG, German Research Foundation), 217133147/SFB 1073, project B03, and the Deutsche akademische Austauschdienst (DAAD, German Academic Exchange Service).

APPENDIX A: WEIGHTED ENERGY

In this Appendix, we prove the Galitskii-Migdal sum rule by considering the simplest case of n -body interactions, where n is even. From the explicit form of the backward Green's function

$$\begin{aligned} i\partial_t \mathcal{G}^<(t^+, t) &\equiv \frac{1}{N} \sum_k \langle \partial_t c_k^\dagger(t) c_k(t^+) \rangle \\ &= \frac{1}{N} \sum_k \langle [c_k^\dagger, \mathcal{H}] c_k \rangle(t). \end{aligned}$$

Explicitly, for any even n -body interaction term, we have

$$\begin{aligned} \sum_k [c_k^\dagger, c_1 \cdots c_n] c_k &= \sum_k \sum_{v=1}^n (-1)^{v-1} c_1 \cdots \{c_k^\dagger, c_v\} \cdots c_n c_k \\ &= - \sum_k \sum_{v=1}^n c_1 \cdots c_k \delta_{k,v} \cdots c_n \\ &= -n c_1 \cdots c_n. \end{aligned}$$

Using the same identity for a string of operators $c_1^\dagger \cdots c_n^\dagger$, one would find $[c_k^\dagger, c_1^\dagger \cdots c_n^\dagger] = 0$. As such, for some Hamiltonian

$$\mathcal{H} = \sum_{\substack{1 \leq i_1 < \cdots < i_{p/2} \leq N \\ 1 \leq j_1 < \cdots < j_{p/2} \leq N}} X_{j_1 \cdots j_n}^{i_1 \cdots i_n} c_{i_1}^\dagger \cdots c_{i_n}^\dagger c_{j_n} \cdots c_{j_1} \quad (A1)$$

using the identity $[c_k^\dagger, C^\dagger C] = C^\dagger [c_k^\dagger, C] + [c_k^\dagger, C^\dagger] C$, the second term will vanish. As such, the commutator evaluates to

$$[c_k^\dagger, \mathcal{H}] = \sum_{\substack{1 \leq i_1 < \cdots < i_{p/2} \leq N \\ 1 \leq j_1 < \cdots < j_{p/2} \leq N}} X_{j_1 \cdots j_n}^{i_1 \cdots i_n} [c_k^\dagger, c_{i_1}^\dagger \cdots c_{i_n}^\dagger] c_{j_n} \cdots c_{j_1}.$$

From the above expression $\sum_k [c_k^\dagger, \mathcal{H}]c_k$ is given by

$$-n \sum_{\substack{1 \leq i_1 < \dots < i_{p/2} \leq N \\ 1 \leq j_1 < \dots < j_{p/2} \leq N}} X_{j_1 \dots j_n}^{i_1 \dots i_n} c_{i_1}^\dagger \dots c_{i_n}^\dagger c_{j_1} \dots c_{j_n},$$

which is the Galitskii-Migdal sum rule [37] for n -body interactions

$$i \partial_t \mathcal{G}^<(t^+, t) = -\frac{n}{N} \langle \mathcal{H}(t) \rangle. \quad (\text{A2})$$

APPENDIX B: KADANOFF-BAYM EQUATIONS

Using the Langreth rule, the full Kadanoff-Baym (KB) equations are given by [37]

$$\begin{aligned} \partial_{t_1} \mathcal{G}^{\geq}(t_1, t_2) = & - \int_{t_0}^{\infty} dt_3 \Sigma^{\geq}(t_1, t_3) \mathcal{G}^A(t_3, t_2) \\ & + \Sigma^R(t_1, t_3) \mathcal{G}^{\geq}(t_3, t_2) \\ & + \int_{t_0 - i\beta}^{t_0} dt_3 \Sigma^<(t_1, t_3) \mathcal{G}^>(t_3, t_2), \end{aligned}$$

where we have defined the advanced and retarded functions

$$\begin{aligned} \mathcal{G}^A(t_3, t_2) &= \Theta(t_2 - t_3) [\mathcal{G}^<(t_3, t_2) - \mathcal{G}^>(t_3, t_2)], \\ \Sigma^R(t_1, t_3) &= -\Theta(t_1 - t_3) [\Sigma^<(t_1, t_3) - \Sigma^>(t_1, t_3)]. \end{aligned}$$

Under the Bogoliubov principle, the assumption that initial correlations become irrelevant as $t_0 \rightarrow -\infty$ [44,45], the imaginary part of the contour is ignored. The KB equations then take the form

$$\int_{-\infty}^{t_2} dt_3 \Sigma^{\geq}(t_1, t_3) \mathcal{G}^A(t_3, t_2) + \int_{-\infty}^{t_1} dt_3 \Sigma^R(t_1, t_3) \mathcal{G}^{\geq}(t_3, t_2).$$

This may be written as

$$\partial_{t_1} \mathcal{G}^{\geq}(t_1, t_2) = \int_{t_1}^{t_2} dt_3 \Sigma^{\geq}(t_1, t_3) \mathcal{G}^A(t_3, t_2) + I(t_1, t_2),$$

where we have pulled out part of the first integral and combined it with the second, yielding

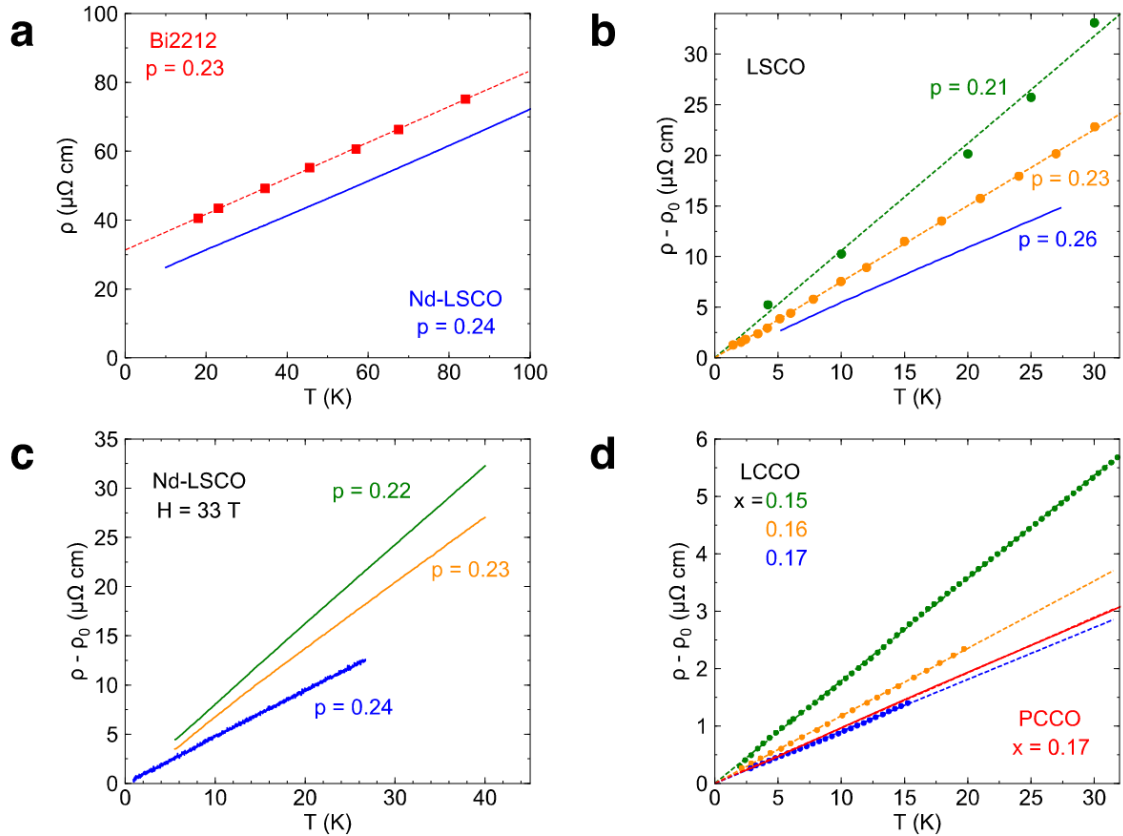
$$\begin{aligned} I(t_1, t_2) = & \int_{-\infty}^{t_1} dt_3 [\Sigma^{\geq}(t_1, t_3) [\mathcal{G}^<(t_3, t_2) - \mathcal{G}^>(t_3, t_2)] \\ & - [\Sigma^<(t_1, t_3) - \Sigma^>(t_1, t_3)] \mathcal{G}^{\geq}(t_3, t_2)]. \end{aligned}$$

In both \geq cases, this integral reduces to

$$I(t_1, t_2) = \int_{-\infty}^{t_1} dt_3 [\Sigma^>(t_1, t_3) \mathcal{G}^<(t_3, t_2) - \Sigma^<(t_1, t_3) \mathcal{G}^>(t_3, t_2)].$$

-
- [1] A. Polkovnikov, K. Sengupta, A. Silva, and M. Vengalattore, Colloquium: Nonequilibrium dynamics of closed interacting quantum systems, *Rev. Mod. Phys.* **83**, 863 (2011).
- [2] M. Ueda, Quantum equilibration, thermalization and prethermalization in ultracold atoms, *Nat. Rev. Phys.* **2**, 669 (2020).
- [3] T. Kinoshita, T. Wenger, and D. S. Weiss, A quantum Newton's cradle, *Nature (London)* **440**, 900 (2006).
- [4] C. Gogolin and J. Eisert, Equilibration, thermalisation, and the emergence of statistical mechanics in closed quantum systems, *Rep. Prog. Phys.* **79**, 056001 (2016).
- [5] M. Rigol, V. Dunjko, V. Yurovsky, and M. Olshanii, Relaxation in a Completely Integrable Many-Body Quantum System: An *Ab Initio* Study of the Dynamics of the Highly Excited States of 1D Lattice Hard-Core Bosons, *Phys. Rev. Lett.* **98**, 050405 (2007).
- [6] F. H. L. Essler and M. Fagotti, Quench dynamics and relaxation in isolated integrable quantum spin chains, *J. Stat. Mech.* (2016) 064002.
- [7] L. Vidmar and M. Rigol, Generalized Gibbs ensemble in integrable lattice models, *J. Stat. Mech.* (2016) 064007.
- [8] J. M. Deutsch, Quantum statistical mechanics in a closed system, *Phys. Rev. A* **43**, 2046 (1991).
- [9] M. Srednicki, Chaos and quantum thermalization, *Phys. Rev. E* **50**, 888 (1994).
- [10] M. Rigol, V. Dunjko, and M. Olshanii, Thermalization and its mechanism for generic isolated quantum systems, *Nature (London)* **452**, 854 (2008).
- [11] J. M. Deutsch, Eigenstate thermalization hypothesis, *Rep. Prog. Phys.* **81**, 082001 (2018).
- [12] D. A. Abanin, E. Altman, I. Bloch, and M. Serbyn, Colloquium: Many-body localization, thermalization, and entanglement, *Rev. Mod. Phys.* **91**, 021001 (2019).
- [13] A. Kamenev, *Field Theory of Non-equilibrium Systems* (Cambridge University Press, Cambridge, 2011).
- [14] S. Sachdev, *Quantum Phase Transitions* (Cambridge University Press, Cambridge, 2001).
- [15] R. L. Greene, P. R. Mandal, N. R. Poniatowski, and T. Sarkar, The strange metal state of the electron-doped cuprates, *Annu. Rev. Condens. Matter Phys.* **11**, 213 (2020).
- [16] A. Legros, S. Benhabib, W. Tabis, F. Laliberté, M. Dion, M. Lizaire, B. Vignolle, D. Vignolles, H. Raffy, Z. Z. Li, P. Auban-Senzier, N. Doiron-Leyraud, P. Fournier, D. Colson, L. Taillefer, and C. Proust, Universal T-linear resistivity and Planckian dissipation in overdoped cuprates, *Nat. Phys.* **15**, 142 (2019).
- [17] S. Sachdev and J. Ye, Gapless Spin-Fluid Ground State in a Random Quantum Heisenberg Magnet, *Phys. Rev. Lett.* **70**, 3339 (1993).
- [18] A. Kitaev, A simple model of quantum holography, Entanglement in Strongly-Correlated Quantum Matter (Part 1, Part 2), KITP (2015).
- [19] S. Sachdev, Bekenstein-Hawking Entropy and Strange Metals, *Phys. Rev. X* **5**, 041025 (2015).
- [20] X. Y. Song, C. M. Jian, and L. Balents, Strongly Correlated Metal Built from Sachdev-Ye-Kitaev Models, *Phys. Rev. Lett.* **119**, 216601 (2017).
- [21] J. Maldacena, S. H. Shenker, and D. Stanford, A bound on chaos, *J. High Energy Phys.* **08** (2016) 106.

- [22] J. Maldacena and D. Stanford, Remarks on the Sachdev-Ye-Kitaev model, *Phys. Rev. D* **94**, 106002 (2016).
- [23] A. Eberlein, V. Kasper, S. Sachdev, and J. Steinberg, Quantum quench of the Sachdev-Ye-Kitaev model, *Phys. Rev. B* **96**, 205123 (2017).
- [24] J. Sonner and M. Vielma, Eigenstate thermalization in the Sachdev-Ye-Kitaev model, *J. High Energy Phys.* **11** (2017) 149.
- [25] J. M. Magán, Black holes as random particles: Entanglement dynamics in infinite range and matrix models, *J. High Energy Phys.* **08** (2016) 081.
- [26] R. Bhattacharya, D. P. Jatkar, and N. Sorokhaibam, Quantum quenches and thermalization in SYK models, *J. High Energy Phys.* (2019) 66.
- [27] S. Bandyopadhyay, P. Urich, A. Paviglianiti, and P. Hauke, Universal equilibration dynamics of the Sachdev-Ye-Kitaev model, [arXiv:2108.01718](https://arxiv.org/abs/2108.01718).
- [28] C. Zanoci and B. Swingle, Energy Transport in Sachdev-Ye-Kitaev Networks Coupled to Thermal Baths, [arXiv:2109.03268](https://arxiv.org/abs/2109.03268).
- [29] Y. Cheipesh, A. I. Pavlov, V. Ohanesjan, K. Schalm, and N. V. Gnezdilov, Quantum tunneling dynamics in a complex-valued Sachdev-Ye-Kitaev model quench-coupled to a cool bath, *Phys. Rev. B* **104**, 115134 (2021).
- [30] A. Almheiri, A. Milekhin, and B. Swingle, Universal constraints on energy flow and SYK thermalization, [arXiv:1912.04912](https://arxiv.org/abs/1912.04912).
- [31] A. Halder, P. Halder, S. Bera, I. Mandal, and S. Banerjee, Quench, thermalization, and residual entropy across a non-Fermi liquid to Fermi liquid transition, *Phys. Rev. Res.* **2**, 013307 (2020).
- [32] C. Kuhlenskamp and M. Knap, Periodically Driven Sachdev-Ye-Kitaev Models, *Phys. Rev. Lett.* **124**, 106401 (2020).
- [33] A. Larzul and M. Schiró, Quenches and (pre)thermalisation in a mixed Sachdev-Ye-Kitaev model, [arXiv:2107.07781](https://arxiv.org/abs/2107.07781).
- [34] W. Fu, The Sachdev-Ye-Kitaev model and matter without quasiparticles, Ph.D. thesis, Harvard University, 2018.
- [35] Y. Gu, A. Kitaev, S. Sachdev, and G. Tarnopolsky, Notes on the complex Sachdev-Ye-Kitaev model, *J. High Energy Phys.* (2020) 157.
- [36] R. A. Davison, W. Fu, A. Georges, Y. Gu, K. Jensen, and S. Sachdev, Thermoelectric transport in disordered metals without quasiparticles: The Sachdev-Ye-Kitaev models and holography, *Phys. Rev. B* **95**, 155131 (2017).
- [37] G. Stefanucci and R. Van Leeuwen, *Nonequilibrium Many-Body Theory of Quantum Systems* (Cambridge University Press, Cambridge, 2013).
- [38] V. M. Galitskii and A. B. Migdal, Application of quantum field theory methods to the many body problem, *Sov. Phys. JETP* **7**, 96 (1958).
- [39] G. Tarnopolsky, Large q expansion in the Sachdev-Ye-Kitaev model, *Phys. Rev. D* **99**, 026010 (2019).
- [40] M. Tsutsumi, On solutions of Liouville's equation, *J. Math. Anal. Appl.* **76**, 116 (1980).
- [41] R. Bhattacharya, S. Chakrabarti, D. P. Jatkar, and A. Kundu, SYK model, chaos and conserved charge, *J. High Energy Phys.* **11** (2017) 180.
- [42] N. Sorokhaibam, Phase transition and chaos in charged SYK model, *J. High Energy Phys.* **07** (2020) 55.
- [43] A. M. García-García and J. J. M. Verbaarschot, Analytical spectral density of the Sachdev-Ye-Kitaev model at finite N , *Phys. Rev. D* **96**, 066012 (2017).
- [44] D. Semkat, D. Kremp, and M. Bonitz, Kadanoff-Baym equations with initial correlations, *Phys. Rev. E* **59**, 1557 (1999).
- [45] M. Pourfath, Numerical study of quantum transport in carbon nanotube-based transistors, Ph.D. thesis, Technical University of Vienna, 2007.

Figure 3.7: Resistivity of various cuprates at various dopings p, x taken from [35]

3.3 Charge dynamics on a lattice

A significant motivation for studying SYK models, as laid out in the introduction, was its similarities to the experimentally observed aspects of strange metals; for instance the linear in T resistivity in cuprates [34, 35, 149, 150], a selection of which is included in Fig. 3.7. Thus far, however, we have only considered a single (zero-dimensional) SYK dot (2.3), where the charge density has remained constant. This changes upon coupling multiple dots/sites together to form a lattice. Since strange metal behavior can be found in quasi-dimensions $\mathcal{d} \in \{1, 2, 3\}$ [34, 150], we start by focusing on the simplest case: $\mathcal{d} = 1$. Such chains are particularly appealing due to their tractability, with nontrivial solvable examples such as the Fermi-Hubbard, Tomonaga-Luttinger, spin-1/2 Heisenberg, and Kondo chains [151]. The fact that these models are integrable, unfortunately, limits their scope to a small subset of physical systems. To expand their applicability integrability can be broken, for example, by adding next-nearest-neighbor interactions [152]. This modification typically renders the model only perturbatively or numerically tractable [151]. Further, to see a change in the universal behavior (e.g., equilibrium properties such as critical exponents), one requires particular perturbations which are relevant. A perturbation is irrelevant if it shrinks under the renormalization group (RG) flow as the system is coarse-grained (when the length scale is

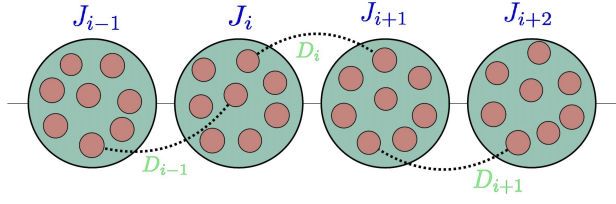


Figure 3.8: A chain where each blob contains a large- q cSYK model with inter-dot coupling strength for the i^{th} site given by J_i while the nearest neighbor coupling strength is given by D_i .

increased). It is marginal if it remains invariant under the flow. The relevant (growing) perturbations can significantly alter the low-energy (long-distance) behavior of the system and often lead to new phases or phase transitions.

With SYK-type chains, many large- \mathcal{N} problems become tractable despite a lack in integrability [33, 59, 127, 153–156]. Here we focus on such chains of coupled dots

$$\mathcal{H}_{q;i} = J_i \sum_{\{\mu\}_1^{q/2}, \{\nu\}_1^{q/2}} X(i)_{\nu}^{\mu} c_{i;\mu_1}^{\dagger} \cdots c_{i;\mu_{q/2}}^{\dagger} c_{i;\nu_{q/2}} \cdots c_{i;\nu_1}, \quad \overline{|X|^2} = \frac{[q^{-1}(q/2)!]^2}{(\mathcal{N}/2)^{q-1}} \quad (3.21)$$

where the operators $c_{i;\alpha}^{\dagger}$ and $c_{i;\alpha}$ are spinless fermionic creation and annihilation operators (associated with lattice site i and flavor α) respectively. Nearest neighbors can be coupled for instance via $r/2$ -body transport terms $\mathcal{H}_r^{i,i+1}$. The quadratic case¹⁴ $\mathcal{H}_2^{i,i+1} = \mathcal{H}_{2;i \rightarrow i+1} + \text{H.C.}$ has

$$\mathcal{H}_{2;i \rightarrow i+1} = D_i \sum_{\mu, \nu} Y(i)_{\nu}^{\mu} c_{i+1;\mu}^{\dagger} c_{i;\nu}, \quad \overline{|Y|^2} = \frac{1}{q} \frac{1}{2\mathcal{N}}, \quad (3.22)$$

as illustrated in Fig. 3.8. This yields the total Hamiltonian $\sum_i \mathcal{H}_{q;i} + \mathcal{H}_r^{i,i+1}$ forming a chain of length L . One can also include additional symmetries directly on the level of the random variables [157, 158]. For instance, one can impose exact translation invariance, $X(i)_{\nu}^{\mu} \rightarrow X(1)_{\nu}^{\mu}$, rather than the averaged translation invariance usually considered [59, 158].

3.3.1 Current and charge density from continuity equation

While the total charge density is still conserved, the local charge may move due to the coupling, hence the local charge density \hat{Q}_x on the lattice site x can fluctuate. In the continuum, the evolution of the charge density is given by a continuity equation $\dot{\hat{Q}}(x, t) = -\partial_x j(x, t)$, where $j(x, t)$ is the local current density. Since we are working on a lattice, we consider the discrete version $\dot{\hat{Q}}_i = j_i - j_{i+1}$ to define the local current density [151]. With this, Heisenberg's equation of motion reduces to

$$\partial_t \hat{Q}_i = \imath [\mathcal{H}, \hat{Q}_i] = \imath [\hat{Q}_i, \mathcal{H}^{i-1,i}] + \imath [\hat{Q}_i, \mathcal{H}^{i,i+1}],$$

¹⁴To ensure competition between the transport terms and the on-site interactions, we need to introduce a $1/q$ scaling in the variance for the random matrix $Y(i)$.

from which one would define the local current density as $\hat{j}_i = \iota[\hat{Q}_i, \mathcal{H}^{i-1,i}]$ associated with charge flow from site i to $i - 1$. Alternatively focusing on the second term, replacing i with $i - 1$, we have $\hat{j}_i = -\iota[\hat{Q}_{i-1}, \mathcal{H}^{i-1,i}]$ corresponding to charge flowing from $i - 1$ to i . This ambiguity is solved when the total charge is conserved, $[\hat{Q}_i + \hat{Q}_{i-1}, \mathcal{H}^{i-1,i}]$, meaning that the two definitions are equal. This may be explicitly checked for the tight-binding model with $\mathcal{H}^{i-1,i} = -t[c_{i-1}^\dagger c_i + c_i^\dagger c_{i-1}]$, with the dispersion relation $\epsilon_k = -2t \cos(k)$. For both cases reduce to $\hat{j}_i = t c_i^\dagger c_{i-1} / \iota + \text{H.C.}$, or $\hat{j}_k = \sum_p v_k c_p^\dagger c_{p+k}$ in momentum space¹⁵, with velocity $v_k = 2t \sin(k) = \partial_k \epsilon_k$. The above remains unchanged when adding any interactions which commute with the local charge densities, for instance, the spin-less Fermi-Hubbard chain interactions $H_{\text{int}} = U_0 \sum_{j=1}^L \hat{n}_j \hat{n}_{j+1}$. Generalizing (3.22) to $r/2$ -particle hopping $\mathcal{H}_{r;i \rightarrow i+1}$, the Galitskii-Migdal relations [81, 154] yields the following expression for the local electric current

$$j_i^{\mathcal{Q}}(t) = r \Im \langle \mathcal{H}_{r;i-1 \rightarrow i} / \mathcal{N} \rangle (t) / 2. \quad (3.23)$$

It can be read off from the momentum representation \hat{j}_k that a translationally invariant system implies a zero current $j_k = 0$. A current may still be induced in various ways. For instance, if one couple the dots via a time-periodic Rice-Mele Hamiltonian, one can implement a Thouless charge pump [155]. A slowly varying magnetic vector potential, included via Peierls substitution [33], with quadratic SYK hopping, also yields a current with a quadratic to linear in T resistivity crossover discussed in Sec. 1.3.1.

3.3.1.1 Response to a thermoelectric gradient

A potential difference leads to a gradient in charge $Q_x = Q + x \nabla Q$ and energy $E_x = E + x \nabla E$. One may also define a local energy current operator $\hat{j}_i^E = \iota[\mathcal{H}^{i-1,i}, \mathcal{H}^{i,i+1}]$ [154]. Analytically, this can be studied as a perturbation to equilibrium with small gradients in the local chemical potential $\mu_x = \mu + x \nabla \mu$ or temperature $T_x = T - x \nabla T$. The gradients are related via [28]

$$\begin{bmatrix} \nabla Q \\ \nabla E - \mu \nabla Q \end{bmatrix} = \hat{\chi}_s \begin{bmatrix} \nabla \mu \\ \nabla T \end{bmatrix}, \quad \hat{\chi}_s = \begin{bmatrix} K & \chi_{12} \\ T \chi_{12} & C_\mu \end{bmatrix}$$

with constant chemical potential heat capacity $C_\mu = T(\partial_T \mathcal{S})_\mu$, compressibility $K = (\partial_\mu Q)_T$ and χ_{12} related to $C_Q = T(\partial_T \mathcal{S})_Q = C_\mu - T \chi_{12}^2 / K$.

The linear response to the electrical and energy currents is then given by

$$\begin{bmatrix} j^{\mathcal{Q}} \\ j^E - \mu j^{\mathcal{Q}} \end{bmatrix} = -\hat{L} \begin{bmatrix} \nabla \mu \\ \nabla T \end{bmatrix}, \quad \hat{L} = \begin{bmatrix} \sigma & \alpha \\ \alpha T & \kappa + \alpha^2 T / \sigma \end{bmatrix}$$

where the general Einstein relation yields the conductivity matrix $\hat{L} = \hat{D} \hat{\chi}_s$, with diffusivity matrix \hat{D} . Here σ is the electrical conductivity, α is the thermoelectric conductivity and κ is the thermal conductivity. They describe the response of various observables to external forces or gradients. In other words, one can then investigate how parameters such as temperature, particle density, or interaction strength affect the transport behavior of the material. For transport of the same order as the inter-dot terms $\mathcal{H}_{q;i}$, $r = q$, the response to such a gradient has been studied both numerically and analytically, shown in Fig. 3.9.

¹⁵This form remains unchanged for higher dimensional lattices [159]. See App. 3.B for a refresher on momentum space and higher dimensional lattices.

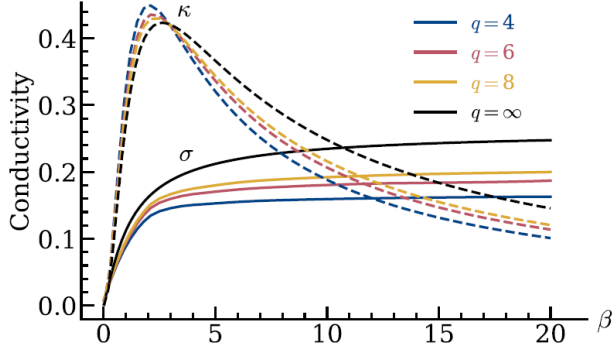


Figure 3.9: Conductivities of SYK chain with $q/2$ -body transport, taken from [154]. Here $J = D = 1$.

Perturbing away from half-filling, one finds the conductivities [154]

$$\sigma = \frac{D^2 \pi v}{4J_{\text{eff}}^2}, \quad \kappa = \frac{4\pi^2 v^2}{3q^2} T \sigma \quad (3.24)$$

to leading order in $1/q$, with $J_{\text{eff}} \equiv \sqrt{J^2 + 2D^2}$. At low temperatures we still have the expression $v \sim 1 - 2T/J_{\text{eff}}$, as was plotted in Fig. 2.1, hence a linear resistivity $\rho = 1/\sigma$. Considering Fig. 3.9, we again note how the large- q results are not only in qualitative agreement with the finite q results but also quantitatively predictive.

Lastly, we also have the Lorentz ratio differing from its Wiedemann-Franz value $L_0 \equiv \pi^2/3$ [154] $L = \beta\kappa/\sigma = (2v/q)^2 L_0$. In the limit as $v \rightarrow 1$ the result overlaps with gravitational (holographic) models with similar low energy limits $L = 4L_0/q^2$ [85], which is the Fermi-liquid Lorentz ratio for $q = 2$.

3.3.1.2 Response to an electrical field

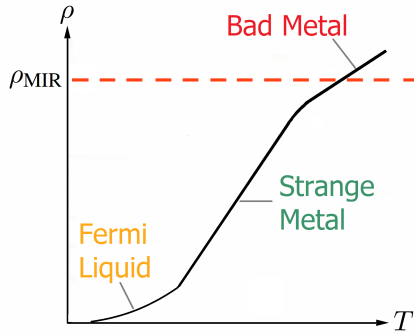


Figure 3.10: Schematic resistivity plot of $U_0, d \rightarrow \infty$ Hubbard model.

A current may also be seen as the response $J = \sigma \lambda_E$ to an applied electric field of magnitude λ_E , which can be recast into the familiar Ohm's law $I = V/R$. The response to an applied electric field $\lambda_E(t)$, $J^Q(\omega) = \sigma_{\text{opt}}(\omega) \lambda_E(\omega)$ [137], is given by Kubo's formula, see App. 3.C for additional details, with optical conductivity $\sigma_{\text{opt}}(\omega)$ [160]. The imaginary part of $\sigma_{\text{opt}}(\omega)$ describes the phase shift between the current and the electric field in the material. The real part is related to energy dissipation (as heat) in the material stemming from interactions with the incident electromagnetic radiation. As we take the frequency to zero, we are left with the direct current (DC) contribution $\rho^{-1} = \Re \sigma_{\text{opt}}(0^+)$ [160].

Let us now extend the analysis from a $d = 1$ chain to some d -dimensional lattice. Various experimentally observed resistivities are captured by the $U_0, d \rightarrow \infty$ Hubbard model [161], schematically plotted in Fig. 3.10. Our main focus is at higher temperatures where the quasi-particle picture completely breaks down. In particular, at near-optimal doping, for $T > T_c$, the resistivity becomes linear. Such a linear resistance is also common to so-called bad metals which, instead of saturating to the Mott-Ioffe-Regel bound¹⁶ $\rho_{\text{MIR}} = k_F^{d-2}$ [28], remains linear at high temperatures [29].

¹⁶The existence of this bound is motivated by the fact that a quasiparticle picture beyond it implies a mean-free-path smaller than a lattice constant.

The disorder averaging in the SYK model with quadratic hopping yields a rather simple¹⁷ formula [158]

$$\rho^{-1} = \int_{-\infty}^{\infty} d\omega \int d\mathbf{k} v_{\mathbf{k};x}^2 A_{\mathbf{k}}(\omega)^2 \frac{\beta \operatorname{sech}^2(\beta\omega/2)}{(2\pi)^d}, \quad (3.25)$$

where $A_{\mathbf{k}}(\omega) = -\Im G_{\mathbf{k}}^R(\omega)/\pi$ is the spectral function we encountered before in Sec. 1.1.2. At half filling, for $D^2/J \ll T \ll J$, one finds $\rho \propto T^{2(1-2/q)}/D^2$ [82]. This simplification can be extended to $r/2$ -particle transport, for which the resistivity is $\rho^{-1} \propto T^\alpha$, with $\alpha = 2(r/q - 1)$ beyond the coherent regime [82]. One may indeed check that this reproduces the linear in T resistivity found for the standard case of quadratic hopping ($r = 2$) and two body inter-dot interactions ($q = 4$) [33]. Below this temperature, there is a crossover into a (heavy) Fermi-liquid $\rho \propto T^2$, which is also typical of cuprates and SYK lattices [33]. The linear resistivity remains as long as the onsite contribution considered is twice the order of the transport $q = 2r$. One would get quadratic resistivity when the onsite is of much higher order $r/q \rightarrow 0$.

We can also find $1 < \alpha < 2$. Such deviations are also experimentally observed in some materials [163, 164], For instance, in the high- T_c cuprate $\text{Pr}_{2-x}\text{Ce}_x\text{CuO}_{4+\delta}$, with an exponent α ranging from 1.2 till 1.8. Such power laws are also found in materials subjected to a magnetic field B , for which one finds modified Kohler's laws for the magnetoresistance (MR) [150, 165–168]

$$\rho_{\text{MR}}(B) = \rho(B)/\rho(B=0) - 1 \propto B^2/(1 + AT^\alpha)^2.$$

A natural question is to what extent the general SYK Hamiltonians capture qualitative aspects of such materials, for instance, whether the models also yield overlapping scalings in the specific heats and Lorentz ratios.

3.4 Analytical results for dynamics on a lattice

In the next included preprint we go on to study the full dynamics of the chain captured by the bilocal flavor averaged Green's functions

$$\mathcal{G}_{ij}(t_1, t_2) \equiv \frac{-1}{\mathcal{N}} \sum_{\alpha=1}^{\mathcal{N}} \langle \mathcal{T} c_{i;\alpha}(t_1) c_{j;\alpha}^\dagger(t_2) \rangle. \quad (3.26)$$

These Green's functions are the solution to Dyson's equation $\hat{\mathcal{G}} = \hat{\mathcal{G}}_0 + \hat{\mathcal{G}}_0 \hat{\Sigma} \hat{\mathcal{G}} = \hat{\mathcal{G}}_0 + \hat{\mathcal{G}} \hat{\Sigma} \hat{\mathcal{G}}_0$. Here $\hat{\Sigma}$ is the $2L$ by $2L$ self-energy matrix, which is diagonal $\hat{\Sigma}_{i,i+d} \equiv \delta_{d0} \Sigma_i$ for the SYK chain. We consider diagonal initial conditions $\hat{\mathcal{G}}_{i,i+d} = \delta_{d0} \mathcal{G}_{ii}$, hence we need to only consider the local Green's functions $\mathcal{G}_i \equiv \mathcal{G}_{ii}$ corresponding to each dot/blob in the lattice.

We develop the general framework for dealing with a chain of large- q SYK dots and $r/2$ -particles hopping to nearest neighbors assuming $r = \mathcal{O}(q^0)$. We start by calculating the effective action in the large- \mathcal{N} limit and derive the Schwinger-Dyson equations, which translate to the Kadanoff-Baym (KB) equations using Langreth rules. We then study the KB equations in the

¹⁷The simplification stems from the ladder/vertex corrections being subleading [162], which is also the case in the large- d limit [160, eq. (271)].

large- q limit, controlling the non-equilibrium dynamics of the system at the leading order in $1/q$. We focus on the symmetric and antisymmetric Green's functions g_i^\pm for dealing with complex fermions and evaluate their equations of motion. The leading order KB equations are expressed in terms of g_i^\pm . We show how the physics of the diffusive $r > 2$ is effectively the same as the kinetic case $r = 2$ at leading order in $1/q$.

We again study the quench dynamics of the system, where the large- q complex SYK blobs would instantaneously thermalize for the disconnected chain. At $t = 0$, the transport coupling of $r/2$ particles to nearest neighbors is switched on. We find closed-form expressions for the local charge transport dynamics. For any finite q , there is a local change in charge density of order $\mathcal{O}(Q/q)$, which vanishes as $q \rightarrow \infty$.

Considering a single large- q SYK model that instantaneously thermalizes [80], one may wonder whether their chain behaves similarly given the fluctuations in charge density vanish. Via proof by contradiction, we may show that the chain does not instantaneously thermalize. We generalize the framework and all results to an arbitrary d -dimensional nearest neighbor lattice of size $(2L)^d$.

3.4.1 Preprint: Dynamics and Charge Fluctuations in Large- q Sachdev-Ye-Kitaev Lattices

Reprinted preprint with permission from

R. Jha and Jan C. Louw

Phys. Rev. B 107, 235114 (2023)

<https://doi.org/10.1103/PhysRevB.107.235114>

Author contributions J. C. L. set up an early outline of the manuscript, having set up the analytic equations to be solved. Both authors together found the main results and revised the manuscript.

Dynamics and charge fluctuations in large- q Sachdev-Ye-Kitaev lattices

Rishabh Jha* and Jan C. Louw†

Institute for Theoretical Physics, Georg-August-Universität Göttingen, Friedrich-Hund-Platz 1, 37077 Göttingen, Germany

(Received 17 April 2023; accepted 30 May 2023; published 6 June 2023)

It is known that the large- q complex Sachdev-Ye-Kitaev dot thermalizes instantaneously under rather general dynamical protocols. We consider a lattice of such dots coupled together, allowing for $r/2$ body hopping of particles between nearest neighbors. We develop a rather general analytical framework to study the dynamics to leading order in $1/q$ on such a lattice, allowing for arbitrary time-dependent couplings, hence general dynamical protocols. We find that the physics of the diffusive case $r > 2$ is effectively the same as the kinetic case $r = 2$, assuming $r = O(q^0)$. Remarkably, we find that the local charge densities Q_i form a closed set of equations. They, however, only show fluctuations of the order $O(Q_i/q)$, hence remaining constant in the limit $q \rightarrow \infty$. Despite this effective lack of charge dynamics, the dots do not in fact behave as isolated lattice sites which would thermalize instantaneously. Indeed, we show via a proof by contradiction that such instantaneously thermalization is not generally possible for a connected lattice. Importantly, the results are shown to be independent of the dimensionality of the lattice.

DOI: [10.1103/PhysRevB.107.235114](https://doi.org/10.1103/PhysRevB.107.235114)**I. INTRODUCTION**

The Sachdev-Ye-Kitaev (SYK) model is a generalization of Sachdev-Ye model [1] proposed by Kitaev [2] as a model for quantum holography where q Majorana fermions interact via random matrix coupling in a total of N particles. The SYK model is a $(0 + 1)$ -dimensional strongly coupled quantum field theory. Given this, it has attracted attention due to its analytical tractability in the large- N limit where the Schwinger-Dyson equations can be written in a closed form. This is despite the model being maximally chaotic [3].

To bring the model closer in contact with a condensed matter system, one usually considers complex charged fermions [4–6]. Such a natural generalization is known as the complex SYK model. Unlike the Majorana case, here the number of particles is a definable quantity associated with a conserved $U(1)$ charge due to the presence of fermionic charges. This charge may be varied by introducing a chemical or mass potential term in the Hamiltonian. When considering this model at charge neutrality, the Majorana case is recovered.

Despite its simplification at large N , the model is usually only fully solvable via numerics. At low energies, an emergent conformal symmetry does, however, allow one to extract certain analytical results [6]. In considering q -body interactions, one may in fact analytically solve the model order by order in $1/q$ [7]. The leading-order results are often qualitatively reflective of the $q \geq 4$ models. For instance, quantitatively and qualitatively similar phase transitions are observed at all $q \geq 4$ [8–11]. This system has a tendency to thermalize rapidly [12]. In particular, given a general nonequilibrium protocol to a single large- q SYK model, the system will

thermalize instantaneously [13]. A better understanding of this thermalization process is still lacking. For instance, under which conditions would a large- q SYK model not thermalize instantaneously?

Moreover, one may for instance study charge transport along a chain of complex SYK dots. In this setup each lattice site (or blob for a better physical picture) is occupied by a complex SYK model. The blobs are connected by transport terms with nearest-neighbor hopping. Such a one-dimensional chain is intimately connected to strongly correlated quantum matter and strange metals, which are considered to be at the heart of modern condensed matter theory. They have been shown to exhibit non-Fermi-liquid transport behavior [5,14,15], for instance, a linear in T resistivity [5]. In other words, their behavior is not captured by a quasiparticle picture.

One analytically tractable construction considers such a chain where each lattice site is occupied by large- q complex SYK model. Naturally, this construction has been studied in the literature [16], where the transport terms also include $q/2$ -body hopping. The analytically tractable property of the large- q SYK model is then exploited to extract exact analytical results. This then provides analytical insight into strongly correlated matter. For instance, by imposing uniform temperature and chemical potential gradients, thermoelectric transport properties may be calculated.

In this work, we consider a similar construction: a one-dimensional lattice where each blob has large- q complex SYK model and the blobs are connected by $r/2$ -particle transport between nearest neighbors. Standard (quadratic) hopping would correspond to $r = 2$, while we also allow for diffusive hopping $r > 2$. We consider r to be order of $O(q^0)$. Due to analytic tractability, this has become one of the prototypical examples for analytic calculations of various transport properties. We develop a rather general framework required to

*rishabh.jha@uni-goettingen.de

†jan.louw@theorie.physik.uni-goettingen.de

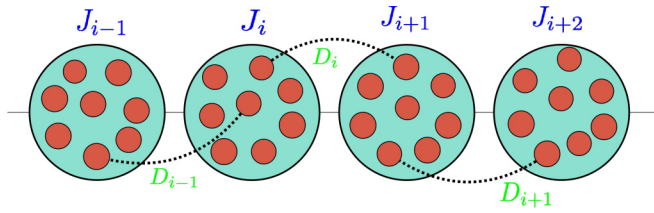


FIG. 1. One-dimensional chain where each blob contains large- q complex SYK model with onsite strength for i th site is given by J_i while the nearest-neighbor coupling strength is given by D_i .

study the dynamical properties of this system. Our framework is well suited to handle general dynamical protocols such as quenches and ramps in order to study the nonequilibrium behavior of the system. Such dynamical protocols will be the focus of this work, instead of temperature and chemical potential gradients considered in [16]. The $1/q$ expansion drastically simplifies the analysis. For instance, we find that to leading order in $1/q$, the equation of motion for the charge is closed under the charge density. In other words, the complicated Green’s functions do not enter.

With this, we may analytically calculate the charge transport dynamics in the system. In particular, we focus on a quench from a disconnected, with transport terms switched off, to a connected chain. We find a discrete wave equation for the charge transport. Solving this equation, we show how current flows directly after transport is switched on. We find, however, in the large- q limit, that the local charge remains constant. From this, one might assume that each dot behaves as an isolated (instant thermalizing) large- q SYK system. We show that this is in fact not the case. This is done via a proof by contradiction. Assuming the chain does thermalize instantaneously, implies a certain consistency relation. This relation is not satisfied for our quench, hence, the system cannot thermalize instantaneously. One may, however, consider when the consistency relation would be fulfilled. This would then provide a set of conditions under which instantaneous thermalization cannot be ruled out. One of these cases is when all transport coefficients are set to zero. Thus, our proof is consistent with the instantaneous thermalization of isolated blobs of large- q complex SYK models [13].

Lastly, we show that these results are immediately generalizable to a d -dimensional lattice.

II. MODEL AND FRAMEWORK

A. Model

We consider a chain consisting of $2L$ lattice blobs where each blob is occupied by a large- q complex SYK model. The Hamiltonian is given as follows (see Fig. 1):

$$\mathcal{H}(t) = \sum_{i=1}^{2L} (\mathcal{H}_i(t) + \mathcal{H}_{i \rightarrow i+1}(t) + \mathcal{H}_{i+1 \rightarrow i}^\dagger(t)), \quad (1)$$

where the onsite large- q complex SYK Hamiltonian is given by

$$\mathcal{H}_i(t) = J_i(t) \sum_{\substack{\{\mu\}_1^{q/2} \\ \{\nu\}_1^{q/2}}} X(i)^\mu c_{i;\mu_1}^\dagger \dots c_{i;\mu_{q/2}}^\dagger c_{i;\nu_{q/2}} \dots c_{i;\nu_1} \quad (2)$$

summing over $\{\nu\}_1^{q/2} \equiv 1 \leq \nu_1 < \dots < \nu_{q/2} \leq N$. The transport of $r/2$ fermions from site i to $i + 1$ is given by

$$\mathcal{H}_{i \rightarrow i+1}(t) = D_i(t) \sum_{\substack{\{\mu\}_1^{r/2} \\ \{\nu\}_1^{r/2}}} Y(i)^\mu c_{i+1;\mu_1}^\dagger \dots c_{i+1;\mu_{r/2}}^\dagger c_{i;\nu_{r/2}} \dots c_{i;\nu_1}. \quad (3)$$

The operators $c_{i;\alpha}^\dagger$ and $c_{i;\alpha}$ are spinless fermionic creation and annihilation operators (associated with lattice site i and flavor α), respectively. Here $J_i(t)$ and $D_i(t)$ are the coupling strengths of the onsite and the transport interactions, respectively. Both $X(i)^\mu$ and $Y(i)^\mu$ are independent random matrices whose components are derived from Gaussian ensemble with zero mean and variances

$$\begin{aligned} \overline{|X|^2} &= \frac{q^{-2} [(q/2)!]^2}{(N/2)^{q-1}} \\ \overline{|Y|^2} &= \frac{1}{q} \frac{(1/r)^2 [(r/2)!]^2}{(N/2)^{r-1}}. \end{aligned} \quad (4)$$

In order to introduce competition between the transport terms and the onsite interactions, we need to introduce a $1/q$ scaling in the variance for the random matrix $Y(i)^\mu$. For $r = 2$, the hopping is kinetic while $r > 2$ corresponds to a *diffusive*-type transport. We also allow for a local mass term of the form

$$\mathcal{H}_0(t) = - \sum_i \dot{\eta}_i(t) N \mathcal{Q}_i, \quad \mathcal{Q}_i \equiv \frac{1}{N} \sum_{\alpha=1}^N [c_{i;\alpha}^\dagger c_{i;\alpha} - 1/2], \quad (5)$$

where \mathcal{Q}_i is the local charge density on the i th blob, $\eta_i(t)$ is an arbitrary function playing a role as of chemical potential, and N is the number of particles on the blob. Using the benefit of the hindsight, we have introduced the derivative $\dot{\eta}_i(t)$ here. With this, the total Hamiltonian would be $\mathcal{H}(t) + \mathcal{H}_0(t)$. Although the Hamiltonian is of diffusive type, it is an interesting feature of charged SYK lattices that their transport properties are more dependent on the ratio between r and q . For instance, one may show that, beyond the coherent regime, that the resistivity behaves as $\rho \sim T^{2(r/q-1)}$ [17]. In other words, for large q , the properties will not be strongly affected by the order of the transport. To have qualitative and quantitative diffusive transport, in the large- q limit, one would thus have to scale r with q .

We can assume both periodic as well as nonperiodic boundary conditions over the lattice. If we assume periodic boundary conditions, then we consider the blob $2L + 1 \equiv_{2L} 1$ where the subscript $2L$ denotes the periodicity. For non-periodic boundary conditions, we set the coupling strength transporting fermions from blobs $2L \rightarrow 2L + 1$ equal to zero.

B. Schwinger-Dyson equations

Our main interest is in the nonequilibrium dynamics of our chain. We consider the general time evolution along the Keldysh contour \mathcal{C} , with focus on the flavor-averaged Green’s functions which are defined as follows:

$$\mathcal{G}_{ij}(t_1, t_2) \equiv \frac{-1}{N} \sum_{\alpha=1}^N \langle \mathcal{T}_{\mathcal{C}} c_{i;\alpha}(t_1) c_{j;\alpha}^\dagger(t_2) \rangle. \quad (6)$$

Here \mathcal{T}_C is the time-ordering operator with respect to C . We are in the Heisenberg picture in the Keldysh formalism where the averaging is taken with respect to the initial noninteracting Hamiltonian [18]. These Green's functions are the solution to Dyson's equation $\hat{G} = \hat{G}_0 + \hat{G}_0 \hat{\Sigma} \hat{G} = \hat{G}_0 + \hat{G} \hat{\Sigma} \hat{G}_0$. Here $\hat{\Sigma}$ is the $2L \times 2L$ self-energy matrix, which is diagonal $\hat{\Sigma}_{i,i+d} \equiv \delta_{d0} \Sigma_i$ for the SYK chain. We consider diagonal initial conditions $\hat{G}_{i,i+d} = \delta_{d0} \mathcal{G}_{ii}$, hence, we need to only consider the local Green's functions $\mathcal{G}_i \equiv \mathcal{G}_{ii}$ corresponding to each blob in the lattice.

Similar to one complex SYK model, we write the partition function corresponding to the Hamiltonian in Eq. (67), introduce the fields \mathcal{G}_i and Σ_i through delta functions, and then integrate out the fermions to get

$$\mathcal{Z} = \int \mathcal{D}\mathcal{G}_i \mathcal{D}\Sigma_i e^{-NS_{0i}[\mathcal{G}, \Sigma] - NS_{Ii}[\mathcal{G}, \Sigma]}, \quad (7)$$

where S_{0i} is the effective action on i th blob while S_{Ii} is the effective transport action corresponding to the transport from blobs $i-1$ and $i+1$ to and from the i th blob. They are given by¹

$$S_{0i} = -\ln \text{Tr} (\mathcal{G}_{0i}^{-1} - \Sigma_i) - \int dt_1 dt_2 \left(\Sigma_i(t_1, t_2) \mathcal{G}_i(t_2, t_1) + \frac{J_i(t_1) J_i(t_2)}{2q^2} [-4\mathcal{G}_i(t_1, t_2) \mathcal{G}_i(t_2, t_1)]^{\frac{q}{2}} \right) \quad (8)$$

as well as

$$S_{Ii} \equiv \int dt_1 dt_2 \mathcal{L}_{Ii}[\mathcal{G}](t_1, t_2), \quad (9)$$

where the Lagrangian \mathcal{L}_{Ii} corresponding to the Hamiltonian [Eq. (67)] is given by

$$\mathcal{L}_{Ii}[\mathcal{G}] = \frac{D_{i-1}^*(t_1) D_{i-1}(t_2)}{qr} [-4\mathcal{G}_{i-1}(t_1, t_2) \mathcal{G}_i(t_2, t_1)]^{r/2} + \frac{D_i(t_1) D_i^*(t_2)}{qr} [-4\mathcal{G}_{i+1}(t_1, t_2) \mathcal{G}_i(t_2, t_1)]^{r/2}. \quad (10)$$

This is similar to that found in [16]. The differences lie only in a redefinition of the couplings and allowing them to be time dependent. Clearly when $D_i = 0 \forall i$, we obtain the disconnected SYK blobs whose effective action is given by Eq. (8) as expected. Therefore, the total effective action is given by

$$S_{\text{eff},i} = S_{0i} + S_{Ii}, \quad (11)$$

where S_{0i} and S_{Ii} are given in Eqs. (8) and (9) and (10), respectively.

Having obtained the effective action in the large- N limit for the Hamiltonian [Eq. (67)], we take its functional derivative to get the local self-energy Σ_i . We see that there are two contributions to the local self-energy Σ_i , namely, $\Sigma_{J,i}$ and $\Sigma_{D,i}$ where $\Sigma_{J,i}$ is the onsite contribution and $\Sigma_{D,i}$ is the transport contribution at the i th blob. Thus, we can write

$$\Sigma_i(t_1, t_2) = \Sigma_{J,i}(t_1, t_2) + \Sigma_{D,i}(t_1, t_2), \quad (12)$$

where

$$q\Sigma_{J,i} = 2J_i(t_1) J_i(t_2) \mathcal{G}_i(t_1, t_2) [-4\mathcal{G}_i(t_1, t_2) \mathcal{G}_i(t_2, t_1)]^{\frac{q}{2}-1} \quad (13)$$

and

$$q\Sigma_{D,i} = D_{i-1}^*(t_1) D_{i-1}(t_2) [-4\mathcal{G}_i(t_2, t_1) \mathcal{G}_{i-1}(t_1, t_2)]^{\frac{q}{2}-1} \times 2\mathcal{G}_{i-1}(t_1, t_2) + D_i(t_1) D_i^*(t_2) [-4\mathcal{G}_i(t_2, t_1) \times \mathcal{G}_{i+1}(t_1, t_2)]^{\frac{q}{2}-1} 2\mathcal{G}_{i+1}(t_1, t_2) \quad (14)$$

from which one can read off the same conjugate relation $\Sigma_i(t_1, t_2)^* = \Sigma_i(t_2, t_1)$ as the Green's functions.

C. Kadanoff-Baym equations

Using Langreth rules [19], Dyson's equations yield the Kadanoff-Baym (KB) equations which can be expressed as follows where we take $t_2 >_C t_1$ without loss of generality (chosen to lie on different halves of C) [13]:

$$[\partial_{t_1} - t \dot{\eta}_i(t_1)] \mathcal{G}_i^{\geq}(t_1, t_2) = \int_{t_1}^{t_2} dt_3 (\Sigma_i^{\geq}(t_1, t_3) \mathcal{G}_i^A(t_3, t_2)) - \frac{t}{2q} \alpha_i(t_1, t_2). \quad (15)$$

Here the forward (backward) Green's functions \mathcal{G}_i^{\geq} correspond to t_1 being ahead (behind) of t_2 on the Keldysh contour C , respectively. They are defined as

$$\mathcal{G}_i^{\geq}(t_1, t_2) \equiv -\frac{1}{N} \sum_{\mu=1}^N \langle c_{i;\mu}(t_1) c_{i;\mu}^\dagger(t_2) \rangle, \quad \mathcal{G}_i^{\leq}(t_1, t_2) \equiv \frac{1}{N} \sum_{\mu=1}^N \langle c_{i;\mu}^\dagger(t_2) c_{i;\mu}(t_1) \rangle. \quad (16)$$

For $t_2 >_C t_1$ the advanced Green's function is given by

$$\mathcal{G}_i^A(t_1, t_2) = \mathcal{G}_i^{\leq}(t_1, t_2) - \mathcal{G}_i^{\geq}(t_1, t_2), \quad (17)$$

while it is zero otherwise. Finally, α_i in Eq. (15) is defined as

$$\alpha_i(t_1, t_2) \equiv t \int_{t_0}^{t_1} dt_3 q \Sigma_i^{\geq}(t_1, t_3) 2\mathcal{G}_i^{\leq}(t_3, t_2) - t \int_{t_0-t\beta}^{t_1} dt_3 q \Sigma_i^{\leq}(t_1, t_3) 2\mathcal{G}_i^{\geq}(t_3, t_2),$$

where we define the forward and backward self-energies Σ_i^{\geq} in the same manner as the Green's functions \mathcal{G}_i^{\geq} whose explicit expressions can be obtained using Eqs. (12)–(14) as

¹A combinatorial argument to get the effective action (consequently, the Schwinger-Dyson equations) is provided in Appendix A.

follows:

$$\begin{aligned}
q\Sigma_i^>(t_1, t_2) &= 2J_i(t_1)J_i(t_2)[-4\mathcal{G}_i^>(t_1, t_2)\mathcal{G}_i^<(t_2, t_1)]^{q/2-1}\mathcal{G}_i^>(t_1, t_2) + 2D_{i-1}(t_2)D_{i-1}^*(t_1)[-4\mathcal{G}_{i-1}^>(t_1, t_2)\mathcal{G}_i^<(t_2, t_1)]^{r/2-1}\mathcal{G}_{i-1}^>(t_1, t_2) \\
&\quad + 2D_i(t_1)D_i^*(t_2)[-4\mathcal{G}_{i+1}^>(t_1, t_2)\mathcal{G}_i^<(t_2, t_1)]^{r/2-1}\mathcal{G}_{i+1}^>(t_1, t_2), \\
q\Sigma_i^<(t_2, t_1) &= 2J_i(t_1)J_i(t_2)[-4\mathcal{G}_i^>(t_1, t_2)\mathcal{G}_i^<(t_2, t_1)]^{q/2-1}\mathcal{G}_i^<(t_2, t_1) + 2D_{i-1}(t_1)D_{i-1}^*(t_2)[-4\mathcal{G}_i^>(t_1, t_2)\mathcal{G}_{i-1}^<(t_2, t_1)]^{r/2-1}\mathcal{G}_{i-1}^<(t_2, t_1) \\
&\quad + 2D_i(t_2)D_i^*(t_1)[-4\mathcal{G}_i^>(t_1, t_2)\mathcal{G}_{i+1}^<(t_2, t_1)]^{r/2-1}\mathcal{G}_{i+1}^<(t_2, t_1). \tag{18}
\end{aligned}$$

From them one can see $\Sigma_i^{\gtrless}(t_1, t_2)^* = \Sigma_i^{\gtrless}(t_2, t_1)$. The first term in both the expressions is the onsite contribution to the self-energies while the second and the third terms are the transport contributions. Also for the kinetic case where $r = 2$, these expressions considerably simplify, although we will always consider a general $r [= O(q^0)]$ in this work. We assume the weakening of initial conditions at initial time $t_0 \rightarrow -\infty$ (Bogoliubov principle) [20,21]. Under this assumption, the imaginary part of the contour in α_i in Eq. (18) is ignored. Considering equal times ($t_2 \rightarrow t_1$), the KB equations in Eq. (15) reduce to

$$\alpha_i(t_1, t_1) = 2\iota q[\partial_{t_1} - \iota\dot{\eta}_i(t_1)]\mathcal{G}_i^<(t_1, t_1^+), \tag{19}$$

where the limit $t_1^+ \rightarrow t_1$ is taken only after differentiating.

D. Expectation values of energy

We are interested in finding the expectation values of local onsite energy as well as the transport energy. Considering the explicit definition of the backward Green's function, we get for the right-hand side of Eq. (19)

$$2\iota q[\partial_{t_1} - \iota\dot{\eta}_i(t_1)]\mathcal{G}_i^<(t_1, t_1^+) = \frac{2q}{N} \left\langle \sum_{\alpha} c_{i,\alpha}^{\dagger} [c_{i,\alpha}, \mathcal{H}] \right\rangle (t_1). \tag{20}$$

We can further evaluate using the identity $[c, \mathcal{H}] = \partial_{c^{\dagger}}\mathcal{H}$ where $\partial_{c^{\dagger}}$ anticommutes with fermionic operators. This leads to

$$2 \sum_{\alpha} c_{i,\alpha}^{\dagger} [c_{i,\alpha}, \mathcal{H}] = q\mathcal{H}_i + r\mathcal{H}_{i \rightarrow i+1}^{\dagger} + r\mathcal{H}_{i-1 \rightarrow i}, \tag{21}$$

where we used the identity for any even n -body interaction term and a generalized Galitskii-Migdal sum rule [13,19] (n can be q or r in our case depending on whether we are dealing with the onsite Hamiltonian or the transport Hamiltonian, respectively) Plugging Eq. (21) in (20), we get

$$\begin{aligned}
&2\iota q[\partial_{t_1} - \iota\dot{\eta}_i(t_1)]\mathcal{G}_i^<(t_1, t_1^+) \\
&= \frac{q^2}{N} \langle \mathcal{H}_i \rangle (t_1) + \frac{qr}{N} \langle \mathcal{H}_{i \rightarrow i+1}^{\dagger} \rangle (t_1) + \frac{qr}{N} \langle \mathcal{H}_{i-1 \rightarrow i} \rangle (t_1). \tag{22}
\end{aligned}$$

According to the equal-time KB equations [Eq. (19)], we know that this expression is equal to $\alpha_i(t, t)$. Accordingly, we define the local and transport expectation values as

$$\epsilon_i(t_1) \equiv \frac{q^2}{N} \langle \mathcal{H}_i \rangle (t_1), \quad \epsilon_{i \rightarrow i+1}(t_1) \equiv \frac{qr}{N} \langle \mathcal{H}_{i \rightarrow i+1} \rangle (t_1). \tag{23}$$

Thus, the equal-time KB equations become

$$\alpha_i(t_1, t_1) = \epsilon_i(t_1) + \frac{r}{q} [\epsilon_{i \rightarrow i+1}^*(t_1) + \epsilon_{i-1 \rightarrow i}(t_1)]. \tag{24}$$

We can extract the correspondence between these expectation values and integrals of the Green's functions and self-energies by taking derivatives of the total effective action [Eqs. (8), (9), and (11)] with respect to the corresponding coupling constants (J_i or D_i). This leads to the following expressions for the onsite and transport contributions:

$$\begin{aligned}
\epsilon_i(t_1) &= \text{Im} \int_{-\infty}^{t_1} dt_2 2J_i(t_1)J_i(t_2) [-4\mathcal{G}_i^<(t_1, t_2)\mathcal{G}_i^>(t_2, t_1)]^{q/2}, \\
\epsilon_{i \rightarrow i+1}(t_1) &= \int_{-\infty}^{t_1} dt_2 \frac{\iota q}{r} D_i^*(t_1)D_i(t_2) [(-4\mathcal{G}_{i+1}^>(t_1, t_2) \\
&\quad \times \mathcal{G}_i^<(t_2, t_1))^{r/2} - (-4\mathcal{G}_i^>(t_2, t_1)\mathcal{G}_{i+1}^<(t_1, t_2))^{r/2}], \tag{25}
\end{aligned}$$

respectively, where Im denotes the imaginary part. This can be verified by plugging these expressions in Eq. (24) and using the definition of α_i in Eq. (18) for $t_1 = t_2$.

E. Functional form of Green's functions

We express our Green's functions in the form

$$g_i^{\gtrless}(t_1, t_2) = \mp \left(\frac{1}{2} \mp \mathcal{Q}_i(t) \right) e^{\iota\eta_i(t_1, t_2) + g_i^{\gtrless}(t_1, t_2)/q}, \tag{26}$$

where we have defined the time average $t \equiv (t_1 + t_2)/2$,² and \mathcal{Q} is defined in Eq. (5). Considering the definitions of Green's functions in Eq. (16) and the local charge density, we have $g_i^{\gtrless}(t, t) = 0$.³ Similar to the Green's functions, for $t_1 > c$ t_2 we have $g_i(t_1, t_2) = g_i^>(t_1, t_2)$ while for $t_1 < c$ t_2 we have $g_i(t_1, t_2) = g_i^<(t_1, t_2)$. Given the expression (26), the proof is shown in [8] that $g_i^{\gtrless} = O(q^0)$, implying that it is a good starting point of a $1/q$ expansion. The exponential form also yields a larger overlap with the exact $q = 4$ solution [7]. In the interaction picture, we have equations of motion such as $\dot{c}(t) = \iota[-\dot{\eta}(t)c^{\dagger}c, c](t) = \iota\dot{\eta}(t)c(t)$ solved by $c(t) = e^{\iota\eta(t)}c$ and similarly $c^{\dagger}(t) = e^{-\iota\eta(t)}c^{\dagger}$. These suggest to conveniently define the following quantity:

$$\eta_i(t_1, t_2) \equiv \eta_i(t_1) - \eta_i(t_2), \tag{27}$$

where the KMS relation for g_i^{\gtrless} provides leading-order scaling in q as $\eta_i = O(\mathcal{Q}) = O(q^{-1/2})$ [11].

As shown in [13], the onsite energy density is bounded as $|\epsilon_i| \leq 2e^{-q\mathcal{Q}^2}J_i$. Thus, for nontrivial interactions, we focus on small charge densities in large- q limit as $\mathcal{Q}_i = O(q^{-1/2})$.

²Sometimes this is also denoted as t_{12}^+ .

³In other words, for $t_1 = t_2 + \epsilon$ and $t_2 = t$, for small ϵ we can write $g_i^{\gtrless}(t + \epsilon, t) \equiv \mathcal{Q}_i(t) - \text{sgn}(\epsilon)/2$.

Accordingly, we can conveniently move the charge densities appearing in Eq. (26) into the exponential as

$$1 \mp 2\mathcal{Q}_i(t) \sim e^{-2\mathcal{Q}_i(t) \mp 2\mathcal{Q}_i(t)} \quad (28)$$

which is correct to quadratic order in charge density. Therefore, plugging this in Eq. (26), we explicitly have for the Green's functions at leading order in $1/q$

$$\begin{aligned} -2\mathcal{G}_i^>(t_1, t_2) &= e^{-2[\mathcal{Q}_i(t) + \mathcal{Q}_i(t)^2] + i\eta_i(t_1, t_2) + g_i^>(t_1, t_2)/q}, \\ 2\mathcal{G}_i^<(t_1, t_2) &= e^{-2[-\mathcal{Q}_i(t) + \mathcal{Q}_i(t)^2] + i\eta_i(t_1, t_2) + g_i^<(t_1, t_2)/q}. \end{aligned} \quad (29)$$

We can use these leading order in $1/q$ results to get the explicit expressions for self-energies $\Sigma_i^{\gtrless}(t_1, t_2)$ using Eq. (18). The final expressions are quite lengthy but straightforward to obtain. We present the following results for the kinetic hopping case where $r = 2$ to leading order in $1/q$ in the large- q limit:

$$\begin{aligned} -q\Sigma_i^>(t_1, t_2) &= J_i(t_1)J_i(t_2)e^{-2q\mathcal{Q}_i(t)^2} e^{(g_i^>(t_1, t_2) + g_i^<(t_2, t_1))/2}, \\ q\Sigma_i^<(t_2, t_1) &= J_i(t_1)J_i(t_2)e^{-2q\mathcal{Q}_i(t)^2} e^{(g_i^>(t_1, t_2) + g_i^<(t_2, t_1))/2}. \end{aligned} \quad (30)$$

Thus, we obtained the functional form for the large- q expansion of Green's functions in Eq. (29) which also led us to the functional form for the large- q expansion of self-energies where we presented the results for kinetic hopping case in Eq. (30). We already know that $g_i^{\gtrless}(t_1, t_2) = O(q^0)$ and $\eta_i = O(q^{-1/2})$. Then starting from Eq. (15), we use these results to obtain the leading-order KB in q in Sec. IV A.

III. CHARGE TRANSPORT

We are interested in studying the nonequilibrium charge transport dynamics in the chain where there is a quench done at $t = 0$. Before we deal with the quench dynamics, we develop a general formalism to study the charge transport. Using the functional form of the Green's functions in Eq. (26) where we know already that $g_i^{\gtrless}(t_1, t_1) = 0$, we have that $\mathcal{G}_i^<(t_1, t_1) = \mathcal{Q}_i(t_1) + 1/2$ implies that

$$\dot{\mathcal{Q}}_i(t_1) = \partial_t \mathcal{G}_i^<(t_1, t_1^+) + \partial_t \mathcal{G}_i^<(t_1^+, t_1), \quad (31)$$

where the limit $t_1^+ \rightarrow t_1$ is taken only after the derivative has been taken. Due to the structure of the right-hand side, we are interested in the real part of the KB equation at equal time in Eq. (15). We note that the mass term η_i is real, the real part of Eq. (15) at equal time takes the following form in terms of the change in local charge density:

$$\dot{\mathcal{Q}}_i(t_1) = \text{Im}[\alpha_i(t_1, t_1)]/q. \quad (32)$$

But we already know the form of α_i from Eq. (24) where using the explicit form of $\epsilon_{i \rightarrow i+1}(t_1)$ from Eq. (25), we get that $\epsilon_{i \rightarrow i+1}(t_1)^* = -\epsilon_{i \rightarrow i+1}(t_1)$. This then yields

$$\dot{\mathcal{Q}}_i(t_1) = \frac{r}{q^2} \text{Im}[\epsilon_{i-1 \rightarrow i}(t_1) - \epsilon_{i \rightarrow i+1}(t_1)]. \quad (33)$$

Using Eq. (25) and the functional form of Green's functions in Eq. (29) up to leading order in $1/q$, we get

$$\begin{aligned} \epsilon_{i-1 \rightarrow i}(t_1) &= \int_{-\infty}^{t_1} dt_2 2t_2 q D_{i-1}^*(t_1) D_{i-1}(t_2) [\mathcal{Q}_{i-1}(t) - \mathcal{Q}_i(t)], \\ \epsilon_{i \rightarrow i+1}(t_1) &= \int_{-\infty}^{t_1} dt_2 2t_2 q D_i^*(t_1) D_i(t_2) [\mathcal{Q}_i(t) - \mathcal{Q}_{i+1}(t)], \end{aligned} \quad (34)$$

where we have previously defined $t \equiv (t_1 + t_2)/2$. By inserting this into Eq. (33), we obtain an explicit differential equation describing the change in local charge density for the leading order in $1/q$ [recall $r = O(q^0)$]:

$$\dot{\mathcal{Q}}(t_1) = \frac{r}{q} \int_{-\infty}^{t_1} dt_2 [\mathbf{H}(t_1, t_2) \mathcal{Q}(t) + O(q^{-1})], \quad (35)$$

where

$$\begin{aligned} H_{ij}(t_1, t_2) &= 2 \text{Re}[D_{i-1}(t_1) D_{i-1}^*(t_2) \delta_{j,i-1} + D_i(t_1) D_i^*(t_2) \delta_{j,i+1} \\ &\quad - (D_{i-1}(t_1) D_{i-1}^*(t_2) + D_i(t_1) D_i^*(t_2)) \delta_{j,i}], \end{aligned} \quad (36)$$

where we note that $q\dot{\mathcal{Q}}(t) = O(\mathcal{Q})$. Note that the above equation is closed under the local charge densities. In other words, the Green's functions do not enter into the expression to leading order in $1/q$. This is a drastic simplification to the general problem. The above equation implies that the local charge density can change on timescales $t = O(q^0)$, but the fluctuations would then be of the order $O(\mathcal{Q}q^{-1})$. Hence, to leading order in $1/q$, the local charge density effectively remains constant.⁴ In other words, if one does *not* consider a rescaled time, $t \neq q^{3/2}\tau$, then for any finite time $t = O(q^0)$, there is no charge flow.

Having obtained this general equation of motion, let us solve it for a particular case, which we will encounter again at a later stage. That is the case of a quench where we switch on the transport interactions at $t = 0$

$$D_i(t) = R_i \Theta(t) \quad (\text{quench at } t = 0), \quad (37)$$

where R_i are any arbitrary real or complex constants. Then taking the second derivative of Eq. (35), we obtain the result for the charge transport dynamics as

$$\ddot{\mathcal{Q}} = \frac{r}{q} \mathbf{H} \mathcal{Q}, \quad (38)$$

where

$$H_{ij} = |R_i|^2 \delta_{j,i+1} + |R_{i-1}|^2 \delta_{j,i-1} - [|R_i|^2 + |R_{i-1}|^2] \delta_{j,i}. \quad (39)$$

We have thus obtained a *discrete wave equation* independent of the onsite interaction strengths and depending only on

⁴The physical reason for such a fine-tuned large- q model construction can be expressed as essentially being a question about which terms will compete with one another. To have a competition between transport terms and onsite interactions on the level of the Green's functions, one must consider "small" transport terms. This leads to the small charge fluctuations, but still keeps the influence of the transport on the level of the Green's functions. To have competition on both levels, one would have to consider r scaling in q , something we plan to study in the future.

the local charge densities as well as the transport coupling strengths. We have taken $R_0 = R_{2L+1} = 0$.

To see explicitly how charge flows, let us consider $R_i = R \forall i$. Then after the quench [Eq. (37)], the solution of Eq. (38) to leading order in $1/q$ is given by

$$Q_i(t) = Q_i(0) + \frac{Q_{i+1}(0) + Q_{i-1}(0) - 2Q_i(0)}{q} 2R^2 t^2 \quad (40)$$

as shown in Appendix B. Note that the only stationary state would correspond to a uniformly charged chain. In general, every site will gain charge assuming the neighboring sites have a combined larger charge density or otherwise lose charge.

IV. A NOTE ON INSTANTANEOUS THERMALIZATION

A. Leading-order Kadanoff-Baym equations

We already have the functional form of the Green's functions [Eqs. (26) and (29)]. The purpose is to plug this in the KB equations [Eq. (15)] and derive a leading order in $1/q$ behavior for the KB equations. We reproduce the KB equations here as following for convenience:

$$\begin{aligned} & [\partial_{t_1} - \imath \dot{\eta}_i(t_1)] \mathcal{G}_i^{\lessgtr}(t_1, t_2) \\ &= \int_{t_1}^{t_2} dt_3 \Sigma_i^{\lessgtr}(t_1, t_3) \mathcal{G}_i^A(t_3, t_2) - \frac{\imath}{2q} \alpha_i(t_1, t_2). \end{aligned} \quad (41)$$

We start by evaluating the left-hand side of the KB equations using the functional form of Green's functions from Eq. (26) where we find that the η_i term cancels out to get

$$\dot{Q}_i(t) e^{\imath \eta_i(t_1, t_2) + g_i^{\lessgtr}(t_1, t_2)/q} + q^{-1} \mathcal{G}_i^{\lessgtr}(t_1, t_2) \partial_{t_1} g_i^{\lessgtr}(t_1, t_2).$$

Plugging back in the KB equations and rearranging yields

$$\begin{aligned} \partial_{t_1} g_i^{\lessgtr}(t_1, t_2) &= \int_{t_1}^{t_2} dt_3 \frac{q \Sigma_i^{\lessgtr}(t_1, t_3) \mathcal{G}_i^A(t_3, t_2)}{\mathcal{G}_i^{\lessgtr}(t_1, t_2)} \\ &\quad - \left(\frac{\imath \alpha_i(t_1, t_2)/2 + q \dot{Q}_i(t) e^{\imath \eta_i(t_1, t_2) + g_i^{\lessgtr}(t_1, t_2)/q}}{\mathcal{G}_i^{\lessgtr}(t_1, t_2)} \right). \end{aligned} \quad (42)$$

Up until this point, everything is exact. Now we start truncating at the leading order in $1/q$. We start by considering the functional form of Green's functions that appears in the denominator above, which at leading order is given by $\mathcal{G}_i^{\lessgtr} \sim \mp 1/2$. We further recall that $Q = O(q^{-1/2})$ while from the charge transport dynamical equation (35), we have $q \dot{Q}_i(t) = O(Q) \Rightarrow \dot{Q}(t) = O(q^{-3/2})$. We also have $\eta_i = O(q^{-1/2})$. Moreover, from the definition of $\alpha(t_1, t_2)$ in Eq. (18), we see that up to leading order, $\mathcal{G}_i^{\lessgtr} \sim \mp 1/2$ there too [recall $\Sigma_i = O(1/q)$], thereby making $\alpha(t_1, t_2)$ lose its t_2 dependence. Finally, using the definition of $\mathcal{G}_i^A(t_1, t_2)$ from Eq. (17), $\mathcal{G}_i^A(t_3, t_2) = \Theta(t_2 - t_3)$ at leading order in $1/q$. Thus, the KB equations at leading order in $1/q$ become

$$\partial_{t_1} \frac{g_i^{\lessgtr}(t_1, t_2)}{2} = \mp \left(\int_{t_1}^{t_2} dt_3 q \Sigma_i^{\lessgtr}(t_1, t_3) \right) \pm \frac{\imath \alpha_i(t_1)}{2}. \quad (43)$$

We can also express the self-energies $\Sigma_i^{\lessgtr}(t_1, t_2)$ appearing here at the leading order using the explicit forms in Eq. (18).

We can write $\Sigma_i^{\lessgtr}(t_1, t_2) = \Sigma_{J,i}^{\lessgtr}(t_1, t_2) + \Sigma_{D,i}^{\lessgtr}(t_1, t_2)$ [Eq. (12)] where the onsite [same as Eq. (30)] and transport contributions at leading order in $1/q$ are as follows:

$$\begin{aligned} q \Sigma_{D,i}^{\lessgtr}(t_1, t_2) &= \mp \mathcal{D}_{\text{eff},i}^2(t_1, t_2), \\ q \Sigma_{J,i}^{\lessgtr}(t_1, t_2) &= \mp \mathcal{J}_{\text{eff},i}^2(t_1, t_2) e^{g_i^{\lessgtr}(t_1, t_2)}, \end{aligned} \quad (44)$$

respectively. Here the effective onsite and transport coupling strengths are

$$\begin{aligned} \mathcal{D}_{\text{eff},i}^2(t_1, t_2) &\equiv D_{i-1}^*(t_1) D_{i-1}(t_2) + D_i(t_1) D_i^*(t_2), \\ \mathcal{J}_{\text{eff},i}^2(t_1, t_2) &\equiv J_i(t_1) J_i(t_2) e^{-2q\mathcal{Q}^2}, \end{aligned} \quad (45)$$

respectively.

B. Symmetric and asymmetric Green's functions

We now introduce (a)symmetric Green's functions

$$g_i^{\pm}(t_1, t_2) \equiv \frac{g_i^{\lessgtr}(t_1, t_2) \pm g_i^{\lessgtr}(t_2, t_1)}{2} \quad (46)$$

which can be inverted to get

$$\begin{aligned} g_i^{\lessgtr}(t_1, t_2) &= g_i^+(t_1, t_2) + g_i^-(t_1, t_2), \\ g_i^{\lessgtr}(t_2, t_1) &= g_i^+(t_1, t_2) - g_i^-(t_1, t_2). \end{aligned} \quad (47)$$

The physical motivation for introducing them comes from the fact that the Green's functions for Majorana fermions are symmetric but they are not symmetric for complex fermions which we are considering. Since Majorana Green's functions are symmetric, accordingly the asymmetric Green's function defined above vanishes for Majorana case, namely, $g_i^- = 0$ [12]. For complex fermions, $g_i^- \neq 0$ and the interpretation is that g_i^- is in a sense a measure of deviations away from charge neutrality.

We express Eq. (43) in terms of these new Green's functions by taking the derivative. Note that the order of taking derivative matters.⁵ Recall $\mathcal{G}_i(t_1, t_2)^* = \mathcal{G}_i(t_2, t_1)$ and consequently $g_i^{\lessgtr}(t_1, t_2)^* = g_i^{\lessgtr}(t_2, t_1)$.⁶ Doing this, we get

$$\begin{aligned} \partial_{t_1} g_i^+(t_1, t_2) &= - \int_{t_1}^{t_2} dt_3 (q \Sigma_i^{\lessgtr}(t_1, t_3) - q \Sigma_i^{\lessgtr}(t_3, t_1)) \\ &\quad + \imath \text{Re}[\alpha_i(t_1)], \\ \partial_{t_1} g_i^-(t_1, t_2) &= - \int_{t_1}^{t_2} dt_3 (q \Sigma_i^{\lessgtr}(t_1, t_3) + q \Sigma_i^{\lessgtr}(t_3, t_1)) \\ &\quad - \text{Im}[\alpha_i(t_1)]. \end{aligned} \quad (48)$$

⁵For instance, if the derivative is to be taken with respect to, say t_2 , which is the second argument in the KB equations, we first need to swap t_1 and t_2 in the arguments to keep t_2 at the first place to take the derivative and then take the conjugate.

⁶As shown in [12,13], $g_i^{\lessgtr}(t_1, t_2) = g_i^{\lessgtr}(t_2, t_1)$ holds true for Majorana fermions which can be derived from the complex SYK case by taking the limit $Q \rightarrow 0$.

Then, we can also evaluate the equal-time KB equations when $t_2 \rightarrow t_1$ at leading order in $1/q$. Equation (48) reduces to

$$\partial_t g_i^+(t_1, t_1^+) = \iota \operatorname{Re}[\alpha_i(t_1)], \quad (49)$$

$$\partial_t g_i^-(t_1, t_1^+) = -\operatorname{Im}[\alpha_i(t_1)], \quad (50)$$

where we take the limit $t_1^+ \rightarrow t_1$ only after taking the derivative. We already know the equal-time KB equations from Eq. (24) where onsite and transport energies are given in Eq. (25). At leading order in $1/q$, we then get

$$\alpha_i(t_1, t_1) = \epsilon_i(t_1) + \frac{r}{q} [\epsilon_{i \rightarrow i+1}^*(t_1) + \epsilon_{i-1 \rightarrow i}(t_1)], \quad (51)$$

where

$$\begin{aligned} \epsilon_i(t_1) &= \operatorname{Im} \int_{-\infty}^{t_1} dt_2 2\mathcal{J}_{\text{eff},i}^2 e^{g_i^+(t_1, t_2)}, \\ \epsilon_{i \rightarrow i+1}(t_1) &= 2[\mathcal{Q}_{i+1}(t) - \mathcal{Q}_i(t)] \int_{-\infty}^{t_1} dt_2 \iota q D_i^*(t_1) D_i(t_2). \end{aligned} \quad (52)$$

From the above expressions (52), we note that the boundary condition on g_i^+ takes the form

$$\partial_t g_i^+(t_1, t_1^+) = \iota \epsilon_i(t_1) + O(q^{-1}), \quad (53)$$

due to $\epsilon_{i \rightarrow i+1}(t_1)$ being imaginary to leading order.

Finally, we take the second derivative of Eq. (48) with respect to t_2 , where we use Eq. (44) for self-energies and the fact that complex conjugate amounts to switching of the two time arguments, to get (recall that partial derivatives commute)

$$\begin{aligned} \partial_{t_1} \partial_{t_2} g_i^+(t_1, t_2) &= 2 \operatorname{Re}[\mathcal{D}_i(t_1, t_2) + \mathcal{J}_{\text{eff},i}^2 e^{g_i^+(t_1, t_2)}], \\ \partial_{t_1} \partial_{t_2} g_i^-(t_1, t_2) &= 2\iota \operatorname{Im}[\mathcal{D}_{\text{eff},i}(t_1, t_2)]. \end{aligned} \quad (54)$$

Let us recall the equation of motion describing the local change in charge density $\operatorname{Im}[\alpha_i(t_1, t_1)] = q \dot{\mathcal{Q}}_i(t_1)$ [Eq. (32)]. Since this was of order $O(\mathcal{Q})$, we note that the same order

appears in the equal time derivative (50). In fact, it is known that for a single disconnected dot, to leading order in $1/q$, $g_i^- = O(\mathcal{Q})$ [13]. From (54), we note that this result only extends over to the chain given real effective transport interactions $\mathcal{D}_{\text{eff},i}^2(t_1, t_2) \in \mathbb{R}$. Since we are restricting our analysis to the nontrivial onsite interactions where the local charge density scales as $\mathcal{Q} = O(q^{-1/2})$, assuming $\mathcal{D}_{\text{eff},i}^2(t_1, t_2) \in \mathbb{R}$, we have to leading order [using Eq. (47)]

$$g_i^>(t_1, t_2) \sim g_i^+(t_1, t_2), \quad g_i^<(t_2, t_1) \sim g_i^+(t_1, t_2). \quad (55)$$

C. Lack of instantaneous thermalization

If $D_i = 0 \forall i$, then we are left with individual disconnected SYK blobs. We already know that a large- q complex SYK model (which exists in each blob) instantaneously thermalizes [13]. A natural question to ask is what happens in the case of our chain where we connect the large- q SYK blobs with $r/2$ -particle nearest-neighbor hopping. We show via proof by contradiction that this is not the case here.

One might argue that since there exist charge fluctuations, the system would clearly not be in thermal equilibrium. However, here we are considering the large- q case, where the Green's functions change over a timescale $t = O(q^0)$, while the fluctuations in charge density are of the order $O(\mathcal{Q}/q)$ at such time. As such, in this limit, the local charge densities are effectively constant, while the Green's functions are not.

For our proof, we again start with the same quench protocol as in Eq. (37): $D_i(t) = R_i \Theta(t)$ where R_i are any arbitrary real or complex constants. Therefore, for $t < 0$, we have disconnected large- q SYK blobs which thermalizes instantaneously thereby causing the whole system to be in equilibrium in prequench. Then at $t = 0$, we connect them with $r/2$ -particle nearest-neighbor hopping term that leads to nonequilibrium dynamics in the system.

We focus on the real part of the transport energies, which is given by Eq. (25):

$$\operatorname{Re}[\epsilon_{i \rightarrow i+1}(t_1)] = \int_0^{t_1} dt_2 |R_i|^2 \left(\frac{-2q}{r} \right) \operatorname{Im} \left[\underbrace{[-4\mathcal{G}_{i+1}^>(t_1, t_2) \mathcal{G}_i^<(t_2, t_1)]^{r/2} - [-4\mathcal{G}_i^>(t_1, t_2) \mathcal{G}_{i+1}^<(t_2, t_1)]^{r/2}}_{rA} \right]. \quad (56)$$

If we plug in the functional form of Green's functions from Eq. (29), we find that where the quadratic in charge density [recall $\mathcal{Q} = O(q^{-1/2})$] terms $\mathcal{Q}_{i+1}^2, \mathcal{Q}_i^2$ cancel, leaving

$$\begin{aligned} A &= 2[\mathcal{Q}_{i+1}(t) - \mathcal{Q}_i(t)] + \frac{g_{i+1}^>(t_1, t_2) + g_i^<(t_2, t_1)}{2q} \\ &\quad - \frac{g_i^>(t_1, t_2)^* + g_{i+1}^<(t_2, t_1)^*}{2q}. \end{aligned}$$

The first term is the leading-order contribution, which consists of local charge densities that are real. Since we are interested in the imaginary part of A , this term drops out. The second and third terms are the next-leading-order contributions of A where clearly the \mathcal{Q}^2 terms cancel out. Recall $t \equiv (t_1 + t_2)/2$. Thus, we are left with the g_i^{\geq} terms in A ,

namely,

$$\frac{1}{2q} [g_{i+1}^>(t_1, t_2) + g_i^<(t_2, t_1) - g_i^>(t_1, t_2)^* - g_{i+1}^<(t_2, t_1)^*]. \quad (57)$$

Note that such a quench to constant couplings yields real effective transport couplings $\mathcal{D}_{\text{eff},i}^2(t_1, t_2) = |R_i|^2 + |R_{i+1}|^2$. As such, the leading-order equation for g_i^- is of order $O(\mathcal{Q})$. Since we are restricting our analysis to the nontrivial onsite interactions where the local charge density scales as $\mathcal{Q} = O(q^{-1/2})$, hence Eq. (55) applies which states that all g_i^{\geq} to leading order are given by their symmetric contributions

leaving

$$\frac{1}{2q} [g_{i+1}^+(t_1, t_2) + g_i^+(t_1, t_2) - g_i^+(t_1, t_2)^* - g_{i+1}^+(t_1, t_2)^*]. \quad (58)$$

This simplifies to

$$\frac{i}{q} \text{Im}[g_{i+1}^+(t_1, t_2) + g_i^+(t_1, t_2)]. \quad (59)$$

Therefore, plugging this back in Eq. (56), we get

$$\text{Re}[\epsilon_{i \rightarrow i+1}(t_1)] = \int_0^{t_1} dt_2 |R_i|^2 \text{Im}[g_{i+1}^+(t_1, t_2) + g_i^+(t_1, t_2)]. \quad (60)$$

In order to prove by contradiction, we now assume that the Green's function instantaneously thermalizes which implies that they can only depend on time differences, namely, $g_i^+(t_1, t_2) = g_i^+(t_1 - t_2) \forall i$. Then the real part of the local transport energy term becomes

$$\begin{aligned} \text{Re}[\epsilon_{i \rightarrow i+1}(t_1)] &= \int_0^{t_1} dt_2 |R_i|^2 \text{Im}[g_{i+1}^+(t_1 - t_2) + g_i^+(t_1 - t_2)] \\ &= \int_0^{t_1} d\tau |R_i|^2 \text{Im}[g_{i+1}^+(\tau) + g_i^+(\tau)]. \end{aligned} \quad (61)$$

But since we have assumed instantaneous thermalization, we know that the time derivative of the real part of the transport energy should be equal to zero. So we proceed to calculate the derivative of $\text{Re}[\epsilon_{i \rightarrow i+1}(t_1)]$ with respect to t_1 :

$$\text{Re}[\dot{\epsilon}_{i \rightarrow i+1}(t_1)] = |R_i|^2 \text{Im}[g_{i+1}^+(t_1) + g_i^+(t_1)]. \quad (62)$$

But, we saw in Eq. (49) that the time derivative of g_i^+ is given as $\partial_t g_i^+(t, t^+) = i \text{Re}[\alpha_i(t)]$. At $t = 0^+$, there are only onsite interactions, therefore, this reduces to [recall the discussion below Eq. (47) that $g_i^+ = O(q^0)$]

$$\dot{g}_i^+(0^+) = i \text{Re}[\epsilon_i(0^+)] + O(q^{-1}) \quad (63)$$

as seen from (53). Finally, taking another derivative of the transport energy, we get

$$\text{Re}[\ddot{\epsilon}_{i \rightarrow i+1}(0^+)] = |R_i|^2 \text{Im}[\dot{g}_{i+1}^+(0^+) + \dot{g}_i^+(0^+)], \quad (64)$$

thereby leading to

$$\text{Re}[\ddot{\epsilon}_{i \rightarrow i+1}(0^+)] = |R_i|^2 (\text{Re}[\epsilon_{i+1}(0^+)] + \text{Re}[\epsilon_i(0^+)]). \quad (65)$$

But, as aforementioned, $\text{Re}[\ddot{\epsilon}_{i \rightarrow i+1}(0^+)] = 0$ if the system thermalizes instantaneously after the quench at $t = 0^+$. This implies that if $R_i \neq 0$, then $\epsilon_{i+1}(0^+)$ and $\epsilon_i(0^+)$ must have opposite signs. However, for any positive temperature, the energy densities are always negative. Hence, the assumption that the system thermalizes instantaneously is false and there is a lack of instantaneous thermalization for the chain even though individual blobs thermalize instantaneously in isolation. This is also captured by the observation that $\text{Re}[\ddot{\epsilon}_{i \rightarrow i+1}(0^+)]$ vanishes when $R_i = 0$ which simply reproduces the result for an individual large- q SYK model as expected [13].

Another interesting possibility is that $J_i = 0 \forall i$ which will also satisfy the condition in Eq. (65). The interpretation of this result is that in case of a pure transport chain of $r/2$ particles

to nearest neighbors *can* lead to instantaneous thermalization. But having obtained the result for local charge density in Eq. (38), we know that there is a flow of current for any *finite* q that shows that the chain cannot be in equilibrium. But in the limit $q \rightarrow \infty$, the local charge density effectively becomes constant. Note that Eq. (65) does not rule out the possibility for a pure transport chain to thermalize instantaneously, in this limit.

Lastly, note that at uniform coupling and charge density our system effectively describes a single SYK dot. This can be seen in all the equations of motion reducing to that of a single dot together with kinetic-type and large- q coupling. As such, the proof by contradiction remains valid for a single dot.

In the general case, however, where we have both onsite and transport terms, the picture would be the following. While the total energy remains conserved, there exist fluctuations between the onsite and kinetic energies [Eq. (23)]

$$\epsilon_i(t_1) \propto \langle \mathcal{H}_i \rangle(t_1), \quad \text{Re}[\epsilon_{i \rightarrow i+1}(t_1)] \propto \text{Re}[\langle \mathcal{H}_{i \rightarrow i+1} \rangle(t_1)], \quad (66)$$

which tend to their final values over a nonzero finite time. A natural question is how, for instance, at what rate, these terms tend to their equilibrium values to attain thermalization. Such an analysis could be carried out by explicitly solving for the Green's functions. Alternatively, one may consider a linear stability analysis around the thermal Green's functions.

V. GENERALIZING THE CHAIN TO A HIGHER-DIMENSIONAL LATTICE

Let us now consider the same model by on a d -dimensional lattice Λ with the nearest-neighbor hopping, where the Hamiltonian is given by

$$\mathcal{H}(t) = \sum_{x \in \Lambda} \mathcal{H}_x(t) + \sum_{\langle x, x' \rangle \in \Lambda} \mathcal{H}_{x \rightarrow x'}(t), \quad (67)$$

where $\langle x, x' \rangle$ denotes nearest-neighbor interactions. The explicit form of \mathcal{H}_x is the same as in Eq. (2) and the transport Hamiltonian from site x to x' is given by

$$\mathcal{H}_{x \rightarrow x'}(t) = \sum_{\substack{\{\mu\}_1^{r/2} \\ \{\nu\}_1^{r/2}}} Y(x, x')_{\nu}^{\mu} c_{x'; \mu_1}^{\dagger} \dots c_{x'; \mu_{\frac{r}{2}}}^{\dagger} c_{x; \nu_{\frac{r}{2}}} \dots c_{x; \nu_1}. \quad (68)$$

Here $D_{xx'}(t)^* = D_{x'x}(t)$ and $[Y(x, x')_{\nu}^{\mu}]^* = [Y(x', x)_{\mu}^{\nu}]$ ensures Hermiticity in the Hamiltonian. In the old notation, we always defined D_i as the coupling corresponding to right hopping. To make it explicitly clear, for $d = 1$ case, we had $D_{i-1}^*(t) = D_{i, i-1}(t)$ while $D_i(t) = D_{i, i+1}(t)$. All expressions remain unchanged, except that we now sum over $z = 2d$ nearest neighbors (which in the one-dimensional case would reduce to two nearest neighbors). So, for instance, the action corresponding to site x [Eqs. (8) and (9)] remains unchanged, only with i being replaced by x . The transport Lagrangian $\mathcal{L}_{i,x}$ in (9), however, gains additional terms due to the now z nearest neighbors

$$\sum_{x': \langle x, x' \rangle} \frac{D_{xx'}(t_1) D_{xx'}^*(t_2)}{qr} [-4\mathcal{G}_{x'}(t_1, t_2) \mathcal{G}_x(t_2, t_1)]^{r/2}. \quad (69)$$

Here $x' : \langle x, x' \rangle$ means summation is over x' such that x' is the nearest neighbor of x . This then yields the new transport

self-energy for site x :

$$q\Sigma_{D,x}(t_1, t_2) = \sum_{x':(x,x')} D_{xx'}(t_1)D_{xx'}^*(t_2) \times [-4\mathcal{G}_x(t_2, t_1)\mathcal{G}_{x'}(t_1, t_2)]^{\frac{r}{2}-1} 2\mathcal{G}_{x'}(t_1, t_2). \quad (70)$$

As an example, for an equilibrium and translationally invariant system $\mathcal{G}_x(t_1, t_2) = \mathcal{G}(t)$, we simply have $q\Sigma_{D,x}(t_1, t_2) = z|D_{12}|^2[-4\mathcal{G}(-t)\mathcal{G}(t)]^{\frac{r}{2}-1} 2\mathcal{G}(t)$.

With this setup for a general nearest-neighbor d -dimensional lattice Λ , we carry out the same analysis for the charge dynamics as in Sec. III. We find that the analysis goes through, and we still are left with a closed-form equation for charge transport to leading order in $1/q$ as in Eq. (35). Explicitly we have for site x

$$\dot{Q}_x(t_1) = \frac{r}{q} \int_{-\infty}^{t_1} dt_2 \sum_{y \in \Lambda} [H_{xy}(t_1, t_2)Q_y(t) + O(q^{-1})], \quad (71)$$

where

$$H_{xy}(t_1, t_2) = \sum_{x':(x,x')} 2 \operatorname{Re}[D_{xx'}^*(t_1)D_{xx'}(t_2)](\delta_{x'y} - \delta_{xy}). \quad (72)$$

Thus, we see that generalizing to higher-dimensional lattice preserves the closed-form relation for charge dynamics.

Moreover, the result for lack of instantaneous thermalization as done in Sec. IV still holds for such a higher-dimensional lattice Λ . We start with the equal-time KB equation as in Eq. (24) for site x which is given by

$$\alpha_x(t_1, t_1) = \epsilon_x(t_1) + \frac{r}{q} \sum_{j=1}^d (\epsilon_{x \rightarrow x+\hat{e}_j}^*(t_1) + \epsilon_{x-\hat{e}_j \rightarrow x}(t_1)), \quad (73)$$

where \hat{e}_j is the unit vector pointing towards positive direction along the dimension j and the sum is over all possible dimensions. Then proceeding in the same manner as in Sec. IV for the same quench considered there [Eq. (37)], we note that Eq. (60) is symmetric under the operation $i \longleftrightarrow i+1$. Therefore, we get a similar equation as in Eq. (60) for site x and some neighboring site x' :

$$\operatorname{Re}[\epsilon_{x \rightarrow x'}(t_1)] = \int_0^{t_1} dt_2 |R_{xx'}|^2 \operatorname{Im}[g_{x'}^+(t_1, t_2) + g_x^+(t_1, t_2)]. \quad (74)$$

Then again to prove by contradiction, we assume instantaneous thermalization after the aforementioned quench so that $g_x(t_1, t_2) = g_x(t_1 - t_2) \forall x \in \Lambda$. We again get

$$\operatorname{Re}[\dot{\epsilon}_{x \rightarrow x'}(0^+)] = |R_{xx'}|^2 (\operatorname{Re}[\epsilon_{x'}(0^+) + \epsilon_x(0^+)]). \quad (75)$$

But due to the assumption of instantaneous thermalization after the quench at $t = 0$, we must have $\operatorname{Re}[\dot{\epsilon}_{x \rightarrow x'}(0^+)] = 0$ and this implies that if $R_{xx'} \neq 0$, then $\epsilon_x(0^+)$ and $\epsilon_{x'}(0^+)$ must have opposite signs. However, the onsite energy for any site $x \in \Lambda$ is always negative for any positive temperature. Thus, our proof for lack of instantaneous thermalization holds true for any higher-dimensional nearest-neighbor lattice consisting of large- q complex SYK models.

VI. CONCLUSION AND OUTLOOK

We considered in this work a chain of large- q SYK dots connected by $r/2$ particles hopping to nearest neighbors. We assumed that r does not scale with q so that $r = O(q^0)$. We already know that the case of $r = 2$ amounts to quadratic hopping, which has been shown to exhibit strange metal behaviors [5]. We considered an even more general case of $r/2$ -particles hopping, where we developed a rather general analytical framework and obtained the dynamical results at leading order in $1/q$. Surprisingly, we found that the physics of the diffusive $r > 2$ is effectively the same as the kinetic case $r = 2$ at leading order in $1/q$, assuming $r = O(q^0)$.

In Sec. II, we have developed a rather general framework of dealing with a general chain as described above. Starting with calculating the effective action in the large- N limit, we calculated the Schwinger-Dyson equations that translated to the Kadanoff-Baym (KB) equations using the Langreth rules. Providing explicit expressions for self-energies, we evaluated the expectation values of energies and showed their connection with the equal-time KB equations. Working with a functional form for Green's functions, we were able to study the KB equations in the large- q limit in Sec. IV A that controls the nonequilibrium dynamics of the system at the leading order in $1/q$. Dealing with complex fermions necessitated the introduction of symmetric and antisymmetric Green's functions g_i^\pm in Sec. IV B where we evaluated their equations of motion. We gave an interpretation for both g_i^\pm and expressed the leading-order KB equations in terms of g_i^\pm .

With this rather general framework developed, we proceeded to study the quench dynamics of the system. The quench is given in Eq. (37) where we have instantaneously thermalized and disconnected large- q complex SYK blobs for $t < 0$. Then, the transport coupling of $r/2$ particles to nearest neighbors is switched on at $t = 0$. We found closed-form expressions for the local charge transport dynamics in a general scenario in Eq. (35) and consequently Eq. (38) for a quench dynamics. The corresponding closed-form result obtained in Eq. (38) is quite fascinating in the sense that this is a discrete wave equation which is completely independent of the onsite couplings J_i . So the $r/2$ -particles charge transport somehow does not feel the onsite coupling strengths of the individual SYK blobs. Furthermore, we see that for any finite q , there is indeed a local change in charge density, albeit of the order $O(Q/q)$. Only in the limit $q \rightarrow \infty$ do these fluctuations become vanishing small.

Having known that a single large- q SYK model instantaneously thermalizes [13], we asked the natural question about our chain in consideration. We again considered the same aforementioned quench and *assumed* that the system does indeed thermalize instantaneously. This led us to the consistency relation (65) which must vanish for the system to be in equilibrium. Thus, we realized that if $R_i \neq 0$ and $J_i \neq 0$, then the onsite energies must have opposite signs to cancel each other but this cannot be true because for any positive temperature, the onsite energy densities are always negative. Hence, by contradiction, we proved that the chain does not instantaneously thermalize. The consistency condition [Eq. (65)] also provides the necessary condition when it is satisfied by either $R_i = 0$ or $J_i = 0$. First considering the case

of $R_i = 0$, this means that the system has disconnected SYK blobs which we already know from [13] that individually all the blobs instantaneously thermalize. The other $J_i = 0$ implies that the system is a pure transport chain of $r/2$ particles hopping to nearest neighbors. But having obtained the result for local charge density in Eq. (38), we know that there is a flow of current for any *finite* q that shows that the chain cannot be in equilibrium. But in the limit $q \rightarrow \infty$, the local charge density effectively becomes constant. Our result obtained in Eq. (65) does not rule out the possibility for a pure transport chain to thermalize instantaneously, in this limit.

Finally, in Sec. V, we generalized our analytical framework from a one-dimensional nearest-neighbor chain to an arbitrary d -dimensional nearest-neighbor lattice Λ . To leading order in $1/q$, we found that the equations describing the local charge density still remain closed, as explicitly shown in Eq. (71). Moreover, our proof by contradiction for the chain to show lack of instantaneous thermalization, after a quench, also holds true for the lattice Λ .

We have solved for the case of $r/2$ -particle hopping. This is the general *diffusive* case where r scales as $O(q^0)$. The subset case of $r = 2$ is the kinetic hopping, which has been studied in [5] to exhibit strange metal behaviors. One of the natural generalizations of this work is when r scales as q such that $r = \kappa q$ where κ is some scalar constant. Moreover, we know that the SYK model shows maximally chaotic behavior [3]. We did not address the chaotic behavior of the chain that might lead to chaotic-integrable phase transitions as observed in a single SYK model [11]. We already know for a single large- q complex SYK model that the critical exponents corresponding to this phase transition belong to the same universality class as that of AdS black holes [8], so a natural question to ask is what happens if we connect those SYK models in the form of a chain as considered in this work. Another crucial feature of the SYK model is that it serves as a model for quantum holography [2]. This begs a natural question as to whether the chain that we have considered does have a holographic dual or not. We leave these to future works.

ACKNOWLEDGMENTS

This work was funded by the Deutsche Forschungsgemeinschaft (DFG, German Research Foundation) Grant No. SFB 1073. We are grateful to S. Kehrein for insightful discussions.

APPENDIX A: COMBINATORIAL ARGUMENT FOR ANY SYK-TYPE EFFECTIVE ACTION

1. Combinatorics of a disordered averaged action

Here we describe the mathematics describing the leading-order SYK action. We do this in a rather abstract combinatorial way and then proceed to relate it to the SYK case.

Let us consider an action $\mathcal{A} = \sum_{i=1}^N S_i$ where S_i are identically distributed and independent random variables with zero mean. They scale as $N^{-1/2}$ which ensures an extensive averaged action. We would like to evaluate the following average:

$$e^{-S_{\text{eff}}} \equiv \overline{e^{\mathcal{A}}} = \sum_{n=0}^{\infty} \frac{t^{2n}}{(2n)!} \overline{\mathcal{A}^{2n}}, \quad (\text{A1})$$

where we have already taken into account that odd powers average to zero due to the zero mean. We note that whenever two random variables average together, this implies that they are the same random variables with the same indices, reducing the number of free summations. For instance, a simple case will be

$$\mathcal{A}^4 = \overline{\sum_{i_1, i_2, i_3, i_4} S_{i_1} S_{i_2} S_{i_3} S_{i_4}}. \quad (\text{A2})$$

There are three ways in which two random variables average together and one way where all of them average together, namely, when $i_1 = i_2 = i_3 = i_4$. This implies that

$$\mathcal{A}^4 = 3 \sum_{i_1, i_2} \overline{S_{i_1}^2 S_{i_2}^2} + \sum_{i_1} \overline{S_{i_1}^4}. \quad (\text{A3})$$

Each sum contributes a factor N , hence, $\overline{S^4} = 3N^2 \overline{S^2}^2 + N \overline{S^4}$. Each power scales as $\overline{S^n} \sim N^{-n/2}$, indicating that the first term is of order $O(N^0)$ while the second term is over order $O(1/N)$, thereby becoming irrelevant for large N . Hence in situations like these, we need only consider the averages between two random variables. The same holds true in the SYK model where to leading order in $1/N$, we only have to consider *two* random variables averaging together (recall that the odd numbers of random variables average to zero). There are $(2n-1)(2n-3)\dots 1$ different pairs of $S_i S_j$. Written differently, this implies that

$$\mathcal{A}^{2n} \sim \frac{(2n)!}{2^n n!} \overline{\mathcal{A}^{2n}}, \quad (\text{A4})$$

hence reducing Eq. (A1) to the effective action $S_{\text{eff}} = \overline{\mathcal{A}^2}/2$. Note that this argument does not rely on having Gaussian random variables.

2. Relation with SYK-type action

The above problem relates to any SYK-type actions where the Hamiltonian is described by the Grassmann expectation value

$$(\overline{\psi}(t_1), \psi(t_1)) = \sum_{i=1}^N X_i F_i(\overline{\psi}(t_1), \psi(t_1)), \quad (\text{A5})$$

where X_i is the random variable and F_i is an arbitrary function of $\overline{\psi}$ and ψ . What this means is that for any SYK-type Hamiltonian, the effective averaged action is given as follows:

$$S_I = \int dt_1 dt_2 \frac{1}{2} \overline{\mathcal{H}(\overline{\psi}(t_1), \psi(t_1)) \mathcal{H}(\overline{\psi}(t_2), \psi(t_2))}. \quad (\text{A6})$$

3. Lagrange multipliers and effective action

Even when we combine many SYK models such as a chain as done in this work, the partition function takes on the form

$$\mathcal{Z} = \int \mathcal{D}(\Psi, \Psi) e^{-S_I[G] + \text{Tr}\{\hat{\mathcal{G}}_0^{-1} \circ G\}}, \quad (\text{A7})$$

where the quadratic field G is given by

$$G_{ij}(t_1, t_2) \equiv -\frac{1}{N} \sum_{\alpha=1}^N \overline{\psi}_{i;\alpha}(t_1) \psi_{j;\alpha}(t_2). \quad (\text{A8})$$

The matrix field multiplication is defined as

$$(\hat{A} \circ \hat{B})(t_1, t_2) = \int_C dt_3 \hat{A}(t_1, t_3) \hat{B}(t_3, t_2) \quad (\text{A9})$$

which defines the trace over matrix fields' time components as

$$\text{Tr}\{\hat{A} \circ \hat{B}\} \equiv \int_C dt_1 (\hat{A} \circ \hat{B})(t_1, t_1). \quad (\text{A10})$$

Lagrange multiplier \mathcal{G} is introduced via a delta functional which further is expressed in terms of another Lagrange multiplier $\hat{\Sigma}$ as follows:

$$\begin{aligned} \mathcal{Z} &= \int \mathcal{D}(\bar{\Psi}, \Psi) \int d\hat{\mathcal{G}} \delta[\hat{\mathcal{G}} - G] e^{\text{Tr}\{\hat{\mathcal{G}}_0^{-1} \circ G\}} e^{-S_I[\hat{\mathcal{G}}]} \\ &= \int \mathcal{D}(\bar{\Psi}, \Psi) \int d\hat{\mathcal{G}} \int d\hat{\Sigma} e^{\text{Tr}\{\hat{\Sigma} \circ [\hat{\mathcal{G}} - G]\}} e^{\text{Tr}\{\hat{\mathcal{G}}_0^{-1} \circ G\}} e^{-S_I[\hat{\mathcal{G}}]} \\ &= \int d\hat{\mathcal{G}} \int d\hat{\Sigma} e^{-S_0[\hat{\mathcal{G}}, \hat{\Sigma}]} e^{-S_I[\hat{\mathcal{G}}]}, \end{aligned}$$

where we have Gaussian-type integrals of Grassmann fields in the definition of G [Eq. (A8)]. After integrating out the Grassmann fields, we get the *effective noninteracting action*

$$S_0[\mathcal{G}, \Sigma] \equiv -\text{Tr}\{\hat{\Sigma} \circ \hat{\mathcal{G}} + \ln[\hat{\mathcal{G}}_0^{-1} - \hat{\Sigma}]\}. \quad (\text{A11})$$

By varying the action with respect to $\hat{\Sigma}$, we obtain the *Dyson's equation*

$$\hat{\mathcal{G}} - [\hat{\mathcal{G}}_0^{-1} - \hat{\Sigma}]^{-1} = 0. \quad (\text{A12})$$

APPENDIX B: CHARGE TRANSPORT SOLUTION

Here we provide the full solution to the vector equation $\dot{\mathcal{Q}} = \mathbf{H} \mathcal{Q}$, with

$$H_{ij} = \frac{4}{q} [R_i^2 \delta_{j,i+1} + R_{i-1}^2 \delta_{j,i-1} - [R_i^2 + R_{i-1}^2] \delta_{ij}], \quad (\text{B1})$$

where $R_0 = R_{2L+1} = 0$ and $R_i = R \forall i$. Then

$$H = -\frac{16R^2}{q} M, \quad (\text{B2})$$

$$M = \frac{1}{2} - \frac{1}{4} \begin{bmatrix} 1 & 1 & 0 & \dots & 0 & 0 \\ 1 & 0 & 1 & 0 & \dots & 0 \\ 0 & 1 & 0 & 1 & 0 & \dots \\ & & & \ddots & & \\ 0 & \dots & 0 & 1 & 0 & 1 \\ 0 & \dots & 0 & 0 & 1 & 1 \end{bmatrix},$$

where charge conservation is seen in all columns summing to zero. The near Toeplitz matrix M can be diagonalized $\Lambda = U M U^\dagger$ via the unitary matrix U_{ij} . With this, the solution to the time-dependent charge density is given by

$$\mathcal{Q}(t) = U^\dagger \cos(\tau \sqrt{\Lambda}) U \mathcal{Q}(0) \quad \left(\tau \equiv \frac{4R}{\sqrt{q}} t \right) \quad (\text{B3})$$

or, explicitly,

$$\mathcal{Q}_i(t) = \sum_{j=1}^{2L} c_{ij}(\tau) \mathcal{Q}_j(0), \quad (\text{B4})$$

$$c_{ij}(\tau) \equiv \sum_{k=1}^{2L} \cos(\tau \sqrt{\Lambda_{kk}}) U_{ik}^\dagger U_{kj}. \quad (\text{B5})$$

Now we need to find an explicit form of U_{ij} . We define $U_{1j} = 1/\sqrt{2L}$ and for $k \neq 1$

$$U_{kj} = \sqrt{\frac{1}{L}} \cos\left(\frac{pk-1}{2}[2j-1]\right), \quad pk \equiv \frac{\pi k}{2L}. \quad (\text{B6})$$

Then the diagonalized matrix Λ is the matrix of eigenvalues which is given by

$$\Lambda_{kk} = \sin^2(p_{k-1}/2). \quad (\text{B7})$$

The coefficients in Eq. (B5) become

$$c_{ij}(\tau) \equiv \sum_{k=1}^{2L} \cos(\tau \sqrt{\Lambda_{kk}}) U_{ik}^\dagger U_{kj} = \frac{1}{L} + d_{ij}(\tau) \quad (\text{B8})$$

with

$$\begin{aligned} d_{ij}(\tau) &\equiv \frac{2}{\pi} \frac{\pi}{4L} \sum_{m=0}^{2L-1} 2 \cos\left[\tau \sin\left[\frac{p_m}{2}\right]\right] \cos\left[\frac{p_m}{2}[2i-1]\right] \\ &\quad \times \cos\left[\frac{p_m}{2}[2j-1]\right], \end{aligned} \quad (\text{B9})$$

where the inner term may be expressed as

$$\begin{aligned} &2 \cos[x[2i-1]] \cos[x[2j-1]] \\ &= \cos[2(i-j)x] + \cos[2(i+j-1)x]. \end{aligned} \quad (\text{B10})$$

Now for large $2L$ the sum

$$\frac{2}{\pi} \frac{\pi}{4L} \sum_{m=0}^{2L-1} \cos[\tau \sin(p_m/2)] \cos(2np_m/2) \quad (\text{B11})$$

can be approximated by the integral

$$\begin{aligned} A_n(\tau) &= \frac{2}{\pi} \int_0^{\pi/2} dx \cos[\tau \sin x] \cos(2nx) \\ &= J_{2n}(\tau), \end{aligned} \quad (\text{B12})$$

where the Bessel functions are defined by

$$J_n(\tau) \equiv \frac{1}{\pi} \int_0^\pi dx \cos(nx - \tau \sin x). \quad (\text{B13})$$

So, we have that for large $2L$

$$c_{ij}(\tau) \sim J_{2|i-j|}(\tau) + J_{2|i+j-1|}(\tau). \quad (\text{B14})$$

Total charge conservation is then ensured by the Bessel function property [22]

$$1 = J_0(\tau) + 2 \sum_{n=1}^{\infty} J_{2n}(\tau) \quad (\text{B15})$$

from which one can show that

$$\mathcal{Q}(t) = \sum_{j=1}^{2L} \sum_{i=1}^{2L} c_{ij}(\tau) \mathcal{Q}_j(0) \quad (\text{B16})$$

is equal to $\mathcal{Q}(t)$, by showing that $\sum_{i=1}^{\infty} c_{ij}(\tau) = 1$. To leading order we have $J_n(\tau) = (\tau/2)^n/n! + O(\tau^{n+2})$. As such, if $\tau =$

$O(q^{-1/2})$, then the dynamics of Q_i are dominated by

$$c_{ii}(\tau) \sim 1 - \tau^2/4, \quad c_{i,i\pm 1}(\tau) \sim \tau^2/8. \quad (\text{B17})$$

Explicitly, we have

$$Q_i(t) = Q_i(0) + [Q_{i-1}(0) - 2Q_i(0) + Q_{i+1}(0)]\tau^2/8. \quad (\text{B18})$$

-
- [1] S. Sachdev and J. Ye, Gapless Spin-Fluid Ground State in a Random Quantum Heisenberg Magnet, *Phys. Rev. Lett.* **70**, 3339 (1993).
- [2] A. Kitaev, in Proceedings of the KITP Program: Entanglement in Strongly-Correlated Quantum Matter, 2015, <http://online.kitp.ucsb.edu/online/entangled15/kitaev/>, <http://online.kitp.ucsb.edu/online/entangled15/kitaev2/>.
- [3] J. Maldacena and D. Stanford, Remarks on the Sachdev-Ye-Kitaev model, *Phys. Rev. D* **94**, 106002 (2016).
- [4] Y. Gu, A. Kitaev, S. Sachdev, and G. Tarnopolsky, Notes on the complex Sachdev-Ye-Kitaev model, *J. High Energy Phys.* **02** (2020) 157.
- [5] X. Y. Song, C. M. Jian, and L. Balents, Strongly Correlated Metal Built from Sachdev-Ye-Kitaev Models, *Phys. Rev. Lett.* **119**, 216601 (2017).
- [6] W. Fu, The Sachdev-Ye-Kitaev model and matter without quasiparticles, Ph.D. thesis, Harvard University, 2018.
- [7] G. Tarnopolsky, Large q expansion in the Sachdev-Ye-Kitaev model, *Phys. Rev. D* **99**, 026010 (2019).
- [8] J. C. Louw and S. Kehrein, Shared universality of charged black holes and the complex large- q Sachdev-Ye-Kitaev model, *Phys. Rev. B* **107**, 075132 (2023).
- [9] F. Ferrari and F. I. Schaposnik Massolo, Phases of melonic quantum mechanics, *Phys. Rev. D* **100**, 026007 (2019).
- [10] T. Azezanagi, F. Ferrari, and F. S. Massolo, Phase Diagram of Planar Matrix Quantum Mechanics, Tensor, and Sachdev-Ye-Kitaev Models, *Phys. Rev. Lett.* **120**, 061602 (2018).
- [11] N. Sorokhaibam, Phase transition and chaos in charged SYK model, *J. High Energy Phys.* **07** (2020) 055.
- [12] A. Eberlein, V. Kasper, S. Sachdev, and J. Steinberg, Quantum quench of the Sachdev-Ye-Kitaev model, *Phys. Rev. B* **96**, 205123 (2017).
- [13] J. C. Louw and S. Kehrein, Thermalization of many many-body interacting Sachdev-Ye-Kitaev models, *Phys. Rev. B* **105**, 075117 (2022).
- [14] D. Chowdhury, Y. Werman, E. Berg, and T. Senthil, Translationally Invariant Non-Fermi-Liquid Metals with Critical Fermi Surfaces: Solvable Models, *Phys. Rev. X* **8**, 031024 (2018).
- [15] D. Chowdhury and E. Berg, Intrinsic superconducting instabilities of a solvable model for an incoherent metal, *Phys. Rev. Res.* **2**, 013301 (2020).
- [16] C. Zanoci and B. Swingle, Near-equilibrium approach to transport in complex Sachdev-Ye-Kitaev models, *Phys. Rev. B* **105**, 235131 (2022).
- [17] P. Cha, A. A. Patel, E. Gull, and E.-A. Kim, Slope invariant T -linear resistivity from local self-energy, *Phys. Rev. Res.* **2**, 033434 (2020).
- [18] A. Kamenev and A. Levchenko, Keldysh technique and non-linear sigma-model: basic principles and applications, *Adv. Phys.* **58**, 197 (2009).
- [19] G. Stefanucci and R. Van Leeuwen, *Nonequilibrium Many-body Theory of Quantum Systems: A Modern Introduction* (Cambridge University Press, Cambridge, 2010).
- [20] D. Semkat, D. Kremp, and M. Bonitz, Kadanoff-Baym equations with initial correlations, *Phys. Rev. E* **59**, 1557 (1999).
- [21] M. Pourfath, Numerical study of quantum transport in carbon nanotube-based transistors, Ph.D. thesis, Technical University of Vienna, 2007.
- [22] M. Abramowitz and I. A. Stegun, *Handbook of Mathematical Functions (Dover Books on Mathematics): With Formulas, Graphs, and Mathematical Tables* (Dover, Mineola, NY, 1965).

Appendix 3.A: Connectedness and upper bound on thermalization rate

The instantaneous thermalization discussed in Sec. 3.2.3 might seem unphysical. Indeed, it might not truly correspond to a thermal state, but rather some pre-thermal state [143]. Here we consider the concept of thermalization from a different perspective which might give some idea as to a possible mechanism for instantaneous thermalization. We will predominantly follow the analysis in [169], restating the relevant parts and their relevance to our large- q SYK model.

We focus on bounds that exist on the minimal thermalization time (inverse thermalization rate). These are based on the speed at which information can move through the system. For both local and long-range models, rigorous bounds may be found on the rate at which the observables thermalize. These results are reasoned through typicality. In resorting to such arguments, an important ingredient is locality [170–175]. This has multiple motivations, one of which is that not all states are equally likely. Since all physical Hamiltonians have a sense of distance built-in, states typically reflect this locality. A different line of reasoning connects to what is experimentally accessible, namely local observables. The class of SYK models we have considered so far, however, have no sense of locality. One can still focus on locally measurable quantities in a certain sense, e.g., the local Green's functions. The idea is that choosing a fixed (e.g., local) Hamiltonian and a typical (random) observable is similar to the reverse: choosing a fixed (e.g., local) observable and a typical (random) Hamiltonian. Considering κ -local observables, one can also provide a bound on information spread in a more abstract space. This is the eigenvalue space of some κ -local observable

$$\hat{O} = \sum_{\mathbb{X} \in \mathcal{N}_\kappa} \omega_{\mathbb{X}}, \quad r_{\text{con}} \equiv \frac{1}{\|\hat{O}\|} \sum_{\mathbb{X}} \|\omega_{\mathbb{X}}\| \geq 1 \quad (3.27)$$

with eigenvalues o_i . We focus on observables that are sufficiently complex to capture both equilibrium and nonequilibrium (NEQ). We then consider the distance metric

$$d_{fi} \equiv \frac{|o_i - o_f|}{2\|\hat{O}\|} \in [0, 1]$$

in this abstract NEQ phase space. For instance, the eigenvalue o_i could live in a typical NEQ subspace. Then we measure how fast this network of eigenstates communicates with one another. In particular, how strongly they are interacting with a particular equilibrium eigenvalue o_f .

Here we consider thermalization from this perspective. We can then compare this to our observed behavior. We start by considering some Hamiltonian $\mathcal{H} = \sum_{\mathbb{X}} h_{\mathbb{X}}$, where \mathbb{X} is a subset of all N lattice sites. We quantify the locality/connectivity of \mathcal{H} through the norm

$$g_{\text{con}} = \frac{1}{\|\mathcal{H}\|} \max_j \left\| \sum_{\mathbb{X} \ni j} h_{\mathbb{X}} \right\|.$$

We work in the eigenbasis of the observable capturing NEQ and EQ. Then for some time evolved initial state $|\psi(t)\rangle$, we consider its amplitudes $x_i(t) \equiv \langle O_i | \psi(t) \rangle$. We are left with the equations of motion

$$x_f(t) = \sum_i U_{fi}(t) x_i(0), \quad U_{fi}(t) \equiv \langle o_f | e^{-it\mathcal{H}} | o_i \rangle \equiv e^{\lambda_{fi}(t) + i\xi_{fi}(t)}.$$

Here we have performed a polar decomposition on $U_{fi}(t)$, such that both λ and ξ functions are real. This allows us to distinguish two different cases. At $t = 0$, we have $U_{fi}(0) \equiv \langle o_f | o_i \rangle = 0$, for $f \neq i$. As such for short times we should expect $U_{fi}(t)$ to be small, corresponding to $\lambda_{fi}(t) \ll 0$, since the two states are uncorrelated. It then takes time for information to spread leading to an increase in the size of $\lambda_{fi}(t)$. When $|U_{fi}(t)| = 1$, then the states f, i are perfectly connected, corresponding to $\lambda_{fi}(t) = 0$, meaning that the system has fully transitioned from $i \rightarrow f$.

We may rewrite this in a more familiar way as

$$\left| \frac{\partial x_f(t)}{\partial x_i(0)} \right| = |U_{fi}(t)| = e^{\lambda_{fi}(t)} \quad \mathbf{c} \equiv \kappa r_{\text{con}} g_{\text{con}}, \quad z \equiv \mathbf{c}\tau, \quad \tau \equiv \|H\|t$$

where the bound on the right is proven via various norms on the commutators [169]. The above may be written in the form of a classical Lieb-Robinson bound. In particular, the influence between the two states is bounded by a scattering rate $\lambda_{fi}(t) \leq \tau \Gamma(d_{fi}/\tau)$. Defining $v \equiv d/\tau$ this is given by [169]

$$\Gamma(v) = 1 + [v - \mathbf{c} + v \ln[\mathbf{c}/v]] \Theta(v - \mathbf{c}).$$

Since this is always positive for $v \leq \mathfrak{c}$, we will focus on the first zero when $v > 0$. The first zero occurs when v is small enough, in particular

$$v = v_{\text{LR}}(\mathfrak{c}) \equiv \frac{1 - \mathfrak{c}}{\mathcal{W}_0[(\mathfrak{c}^{-1} - 1)/e]}.$$

Here \mathfrak{c} captures the connectivity of the system. If $\mathfrak{c} \rightarrow 0$, then the system is unconnected, while if $\mathfrak{c} \rightarrow \infty$, then the system is fully and strongly connected.

Here $\mathcal{W}_0(x)$ is the product log. For small x it is linear $\mathcal{W}_0(x) = x + \mathcal{O}(x^2)$, while for large x it is logarithmic $\mathcal{W}_0(x) \sim \ln x$. So for large connectivity, we have

$$v_{\text{LR}}(\mathfrak{c}) \equiv \frac{1 - \mathfrak{c}}{\mathcal{W}_0[(\mathfrak{c}^{-1} - 1)/e]}.$$

Assuming f is the equilibrium state, this means that the system will remain in said state as soon as $\lambda_{f_i}(t) = 0$. Notice that as expected for early times or large distances large v this bound is negative corresponding to exponential decay in overlap.

We then study the light-cone $t_{\text{LR}}(d) = d/v_{\text{LR}}$ over the distance $d = d_{if}$, where

$$\Gamma(v) = \begin{cases} 0 & \text{for } d < v_{\text{LR}}\tau \\ -|\mathfrak{c} + \mathfrak{c}v \ln v - 1 - \mathfrak{c}v| & \text{for } d \geq v_{\text{LR}}\tau \end{cases}. \quad (3.28)$$

If the light cone flattens to the horizon $v_{\text{LR}} \rightarrow \infty$ then the system can thermalize instantaneously. Indeed, v_{LR} will grow as a function of the connectivity $v_{\text{LR}} \sim \mathfrak{c}$. For small connectivity, we find

$$v_{\text{LR}} \sim \frac{1}{\ln \mathfrak{c}}. \quad (3.29)$$

In particular, we consider the case where the system starts in some nonequilibrium state i , i.e., $x_i(0) = 1$, meaning that by locality.

For the SYK model, we have independence of which flavor we look at, meaning

$$g_{\text{con}} = \frac{1}{\mathcal{N}\|H\|} \sum_{i=1}^{\mathcal{N}} \left\| \sum_{\mathcal{X} \ni i} h_{\mathcal{X}} \right\| \geq \frac{1}{\mathcal{N}\|H\|} \left\| \sum_{i=1}^{\mathcal{N}} \sum_{\mathcal{X} \ni i} h_{\mathcal{X}} \right\| \sim \frac{q}{\mathcal{N}}.$$

As such for $\kappa = \mathcal{N}$, we have $\mathfrak{c} = r_{\text{con}}q \xrightarrow{q \rightarrow \infty} \infty$. In other words, the light cone flattens in the large q limit and information can propagate instantaneously, hence the possibility of instantaneous thermalization. Such an extension κ is necessary if one wishes to quantify equilibrium with respect to non-local states, for instance, the eigenstates of non-local Hamiltonians. Note, however, that this is just an upper bound on the light cone's size. The true size will be smaller, and perhaps even much smaller.

The above analysis gives us an idea of why a model might thermalize instantaneously. Unfortunately, effectively, the bound on light-cone size actually trivially diverges in the thermodynamic limit, $\mathcal{N} \rightarrow \infty$, since

$$\tau = \mathcal{O}(\mathcal{N}t).$$

Considering the generality in the calculations in [169] one might be able to address this issue in the future.

Appendix 3.B: d dimensional lattices in momentum space

The tight-binding model of nearest neighbor hopping operators on a d -dimensional lattice is given by

$$\mathcal{H}_{\text{hop}} = \frac{1}{2} \sum_{|i-j|=1} c_i^\dagger c_j, \quad \sum_{|i-j|=m} \equiv \sum_{\mathbf{i}} \sum_{\substack{\mathbf{j} \\ |i-j|=m}}.$$

It is diagonal in momentum space with the momentum vector $\kappa = 2\pi\mathbf{n}/L$, where $\mathbf{n} = (n_1, n_2, \dots, n_d)$. The creation operators transform as

$$c_{\mathbf{j}} = \frac{1}{L^{d/2}} \sum_{\kappa} e^{i\kappa \cdot \mathbf{j}} c_{\kappa},$$

where for some \mathbf{i} this is $\mathbf{j} \in \{\mathbf{i} \pm m\mathbf{1}^{(1)}, \mathbf{i} \pm m\mathbf{1}^{(2)}, \dots, \mathbf{i} \pm m\mathbf{1}^{(d)}\}$ and $\mathbf{1}_j^{(i)} = \delta_{ij}$.
In momentum space we then have

$$\frac{1}{2} \sum_{|\mathbf{i}-\mathbf{j}|=1} c_i^\dagger c_j = \sum_{\kappa} \lambda(\kappa) n_{\kappa}, \quad \lambda(\kappa) = \sum_{i=1}^d \cos(k_i).$$

Next for the number operator terms $n_i n_j = c_i^\dagger c_j^\dagger c_j c_i$, where we have permuted two fermionic operators past another, we have

$$\sum_{|\mathbf{i}-\mathbf{j}|=m} n_i n_j = \frac{1}{L^{2d}} \sum_{\kappa_1 \kappa_2 \kappa_3 \kappa_4} \sum_{|\mathbf{i}-\mathbf{j}|=m} e^{-i\kappa_1 \cdot \mathbf{i} - i\kappa_2 \cdot \mathbf{j} + i\kappa_3 \cdot \mathbf{j} + i\kappa_4 \cdot \mathbf{i}} c_{\kappa_1}^\dagger c_{\kappa_2}^\dagger c_{\kappa_3} c_{\kappa_4} \quad (3.30)$$

Where we focus on the middle part

$$\begin{aligned} \frac{1}{L^d} \sum_{|\mathbf{i}-\mathbf{j}|=m} e^{i[(\kappa_4 - \kappa_1) \cdot \mathbf{i} + (\kappa_3 - \kappa_2) \cdot \mathbf{j}]} &= \frac{1}{L^d} \sum_{\mathbf{i}} e^{i[\kappa_3 + \kappa_4 - \kappa_1 - \kappa_2] \cdot \mathbf{i}} \lambda(m(\kappa_2 - \kappa_3)) \\ &= \left[\prod_{j=1}^d \frac{1}{L} \sum_{i_j} e^{-i(k_j^1 + k_j^2 - k_j^3 - k_j^4) i_j} \right] \lambda(m(\kappa_2 - \kappa_3)) \\ &= 2\delta[(\kappa_1 + \kappa_2 - \kappa_3 - \kappa_4) \% L] \lambda(m(\kappa_2 - \kappa_3)) \end{aligned}$$

here we are considering the modulus of the integer part of the k vector, so

$$\kappa \% L = \frac{2\pi}{L} (n_1, n_2, \dots, n_d) \% L = (n_1, n_2, \dots, n_d) \% L.$$

Then the interaction term is

$$\sum_{|\mathbf{i}-\mathbf{j}|=m} n_i n_j = \frac{1}{L^d} \sum_{\kappa_1 \kappa_2 \kappa_3 \kappa_4} 2\delta[(\kappa_1 + \kappa_2 - \kappa_3 - \kappa_4) \% L] \lambda(m(\kappa_2 - \kappa_3)) c_{\kappa_1}^\dagger c_{\kappa_2}^\dagger c_{\kappa_3} c_{\kappa_4}. \quad (3.31)$$

For large L , the unit vector \hat{n} can be written in d -spherical coordinates as

$$\hat{n}_1 = \cos(\theta_1) \quad (3.32)$$

$$\hat{n}_2 = \sin(\theta_1) \cos(\theta_2) \quad (3.33)$$

$$\hat{n}_3 = \sin(\theta_1) \sin(\theta_2) \cos(\theta_3) \quad (3.34)$$

$$\vdots \quad (3.35)$$

$$\hat{n}_{d-1} = \sin(\theta_1) \cdots \sin(\theta_{d-2}) \cos(\theta_{d-1}) \quad (3.36)$$

$$\hat{n}_d = \sin(\theta_1) \cdots \sin(\theta_{d-2}) \sin(\theta_{d-1}). \quad (3.37)$$

with $|\kappa| \in \mathbb{R}_+$, $\theta_1, \dots, \theta_{d-2} \in [0, \pi]$ and $\theta_{d-1} \in [0, 2\pi]$.

Appendix 3.C: Kubo's formula for conductivity

A current $J = \sigma E$ is the response to some applied electric field of magnitude E . Here σ is the conductivity and the resulting current can be recast into Ohm's law $I = V/R$, for uniform current in a wire. While the resistance $R = \ell/(\sigma A)$ is dependent on the dimensions of the material, the conductivity is scaled such that it should only be dependent on the material's inherent properties. As such, it should be an intensive quantity not scaling with the length L of the wire. In Sec. 3.2, we considered the linear response to a perturbation $\mathcal{H}_s[E(t)] = E(t)\hat{X}$. Here we wish to study how the total current density along the x -direction $\hat{J}_x^{\mathcal{Q}} = \sum_i \hat{J}_{x;i}^{\mathcal{Q}}$ responds to such a field, where

$$\hat{X} = \sum_{x=1}^L \frac{i}{L} \hat{Q}_{x;i},$$

is some polarization operator. It tells us about the distribution of some total charge, hence serves as a sort of position operator. For instance, if we have a total charge \hat{Q} and we get $X = x_0 \hat{Q}$, then we know that all charge is located at x position x_0 . We consider the case where the system is initially in thermal equilibrium $\varrho = e^{-\beta \mathcal{H}}$. As such without any field there is no charge flow, hence $\langle J \rangle_0 = 0$. In general, the response from some observable \hat{J} to such an applied electric field $E(t)$, in the x -direction, is given by Kubo's formula [137],

$$J_x^{\hat{Q}}(t) = \int dt' E(t') G_X(t, t'), \quad G_X(t, t') \equiv \Theta(t, t') \frac{\langle [\hat{J}_x^{\hat{Q}}(t), \hat{X}(t')] \rangle}{i}, \quad (3.38)$$

where $\hat{X}(t)$ evolves under \mathcal{H} , i.e., the interaction picture. This has also allowed us to write $G_X(t, t')$ as a function of time differences $G_X(0, \tau) \equiv G_X(\tau)$ by commuting the unitary evolution operators within the trace. Kubo's formula then amounts to a convolution which has the Fourier transform $J_x^{\hat{Q}}(\omega) = E(\omega) G_X(\omega)$, where the right term is the optical conductivity $\sigma_{\text{opt}}^{xx}(\omega) = G_X(\omega)$. We next evaluate $G_X(\omega)$ using integration by parts, noting its relation to the current-current correlation function

$$\chi_{xx}(\tau) \equiv \Theta(\tau) \frac{\langle [\hat{J}_x^{\hat{Q}}(0), \hat{J}_x^{\hat{Q}}(-\tau)] \rangle}{iL}, \quad (3.39)$$

$\dot{G}_X(\tau) = -\chi_{xx}(\tau)$, for $\tau > 0$. This is due to the ‘‘velocity’’ expression

$$\partial_t \hat{X} = i[\mathcal{H}, \hat{X}] = \sum_i \frac{i}{L} \partial_t \hat{Q}_i = \frac{1}{L} \sum_i i \hat{J}_{x;i-1}^{\hat{Q}} - i \hat{J}_{x;i}^{\hat{Q}} = \frac{\hat{J}_x^{\hat{Q}}}{L}. \quad (3.40)$$

As such we are left with [160]

$$\sigma_{\text{opt}}^{xx}(\omega) = \int d\tau \left(\frac{e^{i\omega\tau} - 1}{i\omega} \right)' G_X(\tau) = \int d\tau \frac{e^{i\omega\tau} - 1}{-i\omega} \chi_{xx}(\tau) \equiv \frac{i\chi_{xx}^R(\omega) - i\chi_{xx}^R(0)}{\omega}.$$

The retarded correlations $\chi_{xx}^R(\omega) \equiv \chi_{xx}(\omega + i0^+)$ satisfy the Kramers-Krönig relation [21]

$$\chi_{xx}^R(\omega) = \int d\omega' \frac{-\Im \chi_{xx}^R(\omega') / \pi}{\omega - \omega' + i0^+}, \quad (3.41)$$

whereby explicitly writing the trace in terms of the eigenenergies of the Hamiltonian, the Källén-Lehmann representation, one may check that

$$\Im \chi_{xx}^R(\omega) = [1 - e^{-\beta\omega}] \Im \Pi_{xx}^R(\omega), \quad \Pi_{xx}^R(t) \equiv \Theta(t) \frac{\langle \hat{J}_x^{\hat{Q}}(t) \hat{J}_x^{\hat{Q}}(0) \rangle}{iL}.$$

Meaning that

$$\frac{i\chi_{xx}^R(\omega)}{\omega} = \frac{e^{-\beta\omega} - \Im}{\omega} \Im \Pi_{xx}^R(\omega) + \frac{e^{-\beta\omega} - 1}{\pi\omega} \int d\omega' \mathcal{P} \frac{i\Im \Pi_{xx}^R(\omega')}{\omega - \omega'} \quad (3.42)$$

For large lattice dimensions \mathcal{d} , the real part of the optical conductivity is given by [160, eq. (271)]

$$\Re \sigma_{\text{opt}}^{xx}(\omega) = \frac{4}{(2\pi)^{\mathcal{d}}} \int d\mathbf{k} v_{\mathbf{k};x}^2 A_{\mathbf{k}}(\omega') A_{\mathbf{k}}(\omega' + \omega) \frac{n_F(\omega' + \omega) - n_F(\omega')}{\omega} \quad (3.43)$$

where A is the spectral function we encountered before, $n_F(\omega) \equiv \frac{1}{e^{\beta\omega} + 1}$ is the Fermi function and $v_{\mathbf{k};x} = \partial_{k_x} \epsilon_{\mathbf{k}}$. As $\omega \rightarrow 0$, the fraction tends to $n'_F(\omega) = \beta \text{sech}^2(\beta\omega/2)/4$, leaving the DC resistivity (3.25).

Chapter 4

SYK Thermodynamics

Place a ball on top of a hill, a local maximum, like in Fig. 4.1. From experience, we know that any small perturbation would cause it to roll down, i.e., local maxima are unstable fixed points. Energetically favorable processes minimize energy, and the ball will roll until it reaches a (local) minimum potential energy $\ddot{x} \propto \mathcal{V}'(x) = 0$.

It turns out that more complicated systems behave in an analogous way. To make this more precise, consider a system consisting of many atoms inside a box. In the event that the box is isolated, with solid rigid and insulating walls, the system will have a fixed energy E . If these restrictions are relaxed and outside influences are allowed to perturb the system we find that the energy changes according to the fundamental thermodynamic relation $dE = TdS - pdV + \mu dQ$ with volume (per lattice site) V . From this relation, one can understand various processes. For instance, it tells us that pressure is a sort of resistance to adiabatic (no heat transfer $TdS = 0$) compression at constant charge density Q . The higher the pressure, the more energy is required.

While the system, like the ball in Fig. 4.1, wishes to minimize its energy, it also tends to maximize its entropy¹. Assuming the walls are conductive, then both energy and entropy can change. Together, the two principles, minimization of E and maximization of S , combine to the minimization of the thermodynamic potential, in this case, the Helmholtz free energy $\mathcal{F} = E - TS$. For instance, the water-to-ice transition is energetically favorable at room temperature, since kinetic energy is lowered. However, this process also lowers entropy; hence it only spontaneously occurs when $\delta\mathcal{F} = T\delta S - \delta E < 0$, i.e., at lower temperatures. Such macroscopic phase transitions illustrate the importance of the free energy landscape.

If we now also allow the charge density to fluctuate, then we have to consider the grand canonical partition function which is the integral of $e^{-N\beta\mathcal{A}(Q)}$, where $\mathcal{A}(Q) = \mathcal{F}(Q) - \mu Q$, over

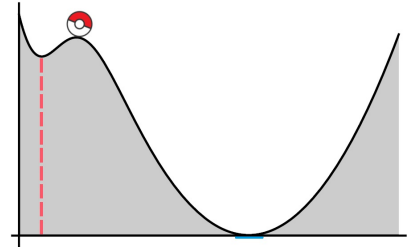


Figure 4.1: Ball on the top of a hill representing the stability of phases in the free energy landscape.

¹If all microstates $|\vec{n}\rangle$ are equally likely (the principle of equal a priori probabilities) then the system will spend most of its time in the macrostate ϱ_{th} corresponding to the most microstates W , thus the largest Boltzmann entropy $S(E) = \ln W(E)$.

all values of Q . Explicitly this is given by

$$\mathcal{Z} = \int dQ e^{-N\beta\mathcal{A}(Q)} \sim \sum_i e^{-N\beta\mathcal{A}^*(Q_i)} \int dQ e^{-N\beta\mathcal{A}^{(2)}(Q_i)(Q-Q_i)^2/2+o(N)}, \quad (4.1)$$

where we have used the initial steps of Laplace's method, i.e., expanding the function around the various fixed points $\mathcal{A}'(Q_i) = 0$, which corresponds to $\mu = \mathcal{F}'(Q)$, which is the equation of state. If there are multiple fixed points, then clearly the one corresponding to the smallest $\mathcal{A}(Q_i)$ dominates. This is the thermodynamically preferred phase. Note, however, that any fixed point corresponding to a local maximum, a concave function forming the top of a hill, will have $\mathcal{A}^{(2)} = \mathcal{F}^{(2)} > 0$, meaning that it is exponentially suppressed. These are the unstable-fixed points. This exponential suppression leads to their exclusion. This is seen in the fact that the grand potential captured by the Legendre-Fenchel transform of the Helmholtz free energy [176]

$$\Omega = \inf_Q \{\mathcal{F}(Q) - \mu Q\}.$$

In other words, it only considers the minima, more generally the infimum, while excluding the maxima corresponding to the unstable fixed points². Substituting this back in, we can express Ω directly in terms of the order parameter Q . A stable fixed point that is not the global minimum is a metastable phase [177]. Like super-cooled water, a big enough perturbation will cause it to transition to the global fixed point.

Non-analytic behavior in Ω is characteristic of a phase transition (PT). In particular, an n th order PT is a point at which the n th derivative diverges. Continuous (second-order) PTs have a diverging correlation length leading to universal behavior. This is characterized by a set of critical exponents which are reflected in the divergent thermodynamic properties close to the critical point, i.e., in their power laws. Their values are defined by the renormalization group flow of the thermodynamic potential [178]. This flow leads to a thermodynamic potential which is a homogeneous function. The fact that the typical power laws are not always directly related to standard thermodynamic observables such as the specific heat is a phenomenon known as field mixing, which we will explore in Sec. 4.3.

4.1 Phase diagram of the complex SYK model

We are particularly interested in the equilibrium thermodynamics of the charged q -body SYK model given in (2.3)

$$\mathcal{H}_q = J_q \sum_{\{\mu\}_1^{q/2}, \{\nu\}_1^{q/2}} X_{\nu_1 \dots \nu_{q/2}}^{\mu_1 \dots \mu_{q/2}} c_{\mu_1}^\dagger \dots c_{\mu_{q/2}}^\dagger c_{\nu_{q/2}} \dots c_{\nu_1}. \quad (4.2)$$

We focus on the grand canonical setting with partition function

$$\mathcal{Z} = \text{tr} \{ e^{-\beta\mathcal{N}[\mathcal{H}_q/\mathcal{N} - \mu\hat{Q}]} \}$$

²Again this is in analogy to the ball rolling down the top of the hill in Fig. 4.1, where the hill is the free energy "landscape".

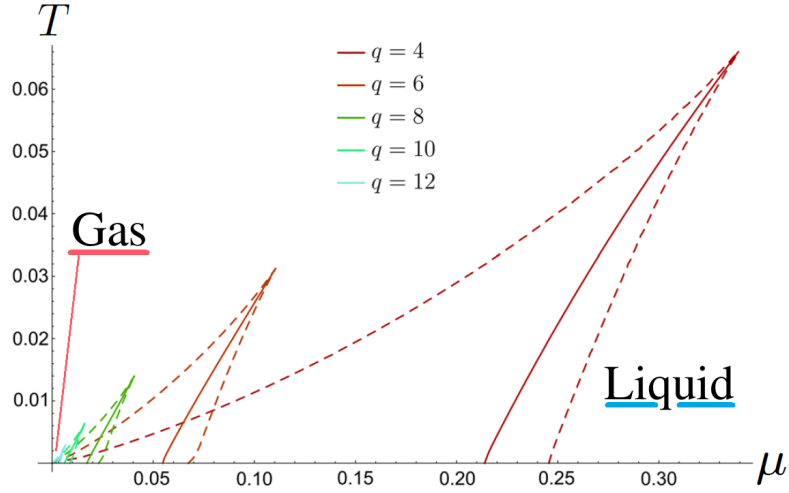


Figure 4.2: Phase diagram of the charged $q/2$ -body SYK models for different values of q adapted from [180]. The solid lines correspond to the coexistence line, over which a first-order phase transition occurs. The dashed lines enclose the stability regime, where both phases are stable, but only one is thermodynamically preferred.

and grand potential $\Omega = -T \ln \mathcal{Z}/\mathcal{N}$. Despite SYK models like (4.2) being tractable in the large \mathcal{N} limit, the thermodynamics can still be difficult to solve analytically, hence one must resort to numerical methods. Such methods have been employed to study the thermodynamics of \mathcal{H}_q for various finite values of q [179–181]. It was found that there exists a liquid-gas type phase transition. Studying the phase diagram for different values of q , plotted in Fig 4.2, it was noted that the part of the phase diagram corresponding to the phase transition shrinks as q becomes larger. As such, it was believed that this phase diagram does not exist in the $q \rightarrow \infty$ limit. One can still attempt to study the model via a $1/q$ expansion. This offers an advantage over the numerical approach, which is plagued by numerical error, a topic we will touch on in a later section. This is the alternate route to numerics we consider here. The $1/q$ expansion yields leading order analytical results which we will contrast to the numerical findings.

4.1.1 Obtaining the equation of state

A good start to studying the phases of a model is to find the equation of state (EOS). In this section, we describe in detail how one obtains this for the large- q cSYK dot (4.2) in the grand canonical setting. The EOS was originally calculated in [80]. In this section, we provide additional mathematical detail on deriving this equation.

Typically, one provides a Hamiltonian \mathcal{H} , specifies a chemical potential μ , and then calculates the particle number density. This particle number density is directly related to the charge density

$$\mathcal{Q} = \sum_{\nu=1}^{\mathcal{N}} \langle c_{\nu}^{\dagger} c_{\nu} \rangle - \frac{1}{2} \quad (4.3)$$

which is a conserved quantity. Thus, one might opt to specify the charge density first and then determine the corresponding chemical potential. This chemical potential will then be a function of the charge density \mathcal{Q} , temperature T , and coupling strength J_q . In other words, by specifying the three quantities μ, T , and J_q we can then find the associated charge density from it; hence it is our equation of state. There are multiple reasons to do this. The main reason is that, in terms of the SYK model, the solutions available to us are the Green's functions

$$\mathcal{G}(t) = -\frac{1}{\mathcal{N}} \sum_{\nu=1}^{\mathcal{N}} \langle \mathcal{T} c_{\nu}(t) c_{\nu}^{\dagger} \rangle = \Theta(t) \mathcal{G}^{\>}(t) + \Theta(-t) \mathcal{G}^{\<}(t). \quad (4.4)$$

Here the time ordering operator $\mathcal{T} c(0^{\pm}) c^{\dagger}$ yields cc^{\dagger} and $-c^{\dagger}c$ respectively. Together with the anti-commutation relation $cc^{\dagger} = 1 - c^{\dagger}c$, we are left with the boundary conditions

$$\mathcal{G}(0^{\pm}) = -\frac{1}{\mathcal{N}} \sum_{\nu=1}^{\mathcal{N}} \langle \mathcal{T} c_{\nu}(0^{\pm}) c_{\nu}^{\dagger} \rangle = \mathcal{Q} \pm \frac{1}{2}. \quad (4.5)$$

In other words, the boundary conditions are *directly* given by the charge density, *not* the chemical potential. The associated chemical potential may then however be extracted from the KMS relation. Let us see how this works for a single fermion $c(t) \equiv e^{t\mathcal{H}} c e^{-t\mathcal{H}}$ and $c^{\dagger}(t) = e^{t\mathcal{H}} c^{\dagger} e^{-t\mathcal{H}}$. The forward and backward Green's functions are

$$\mathcal{G}^{\>}(t) = -\langle c(t) c^{\dagger} \rangle, \quad \mathcal{G}^{\<}(t) = \langle c^{\dagger} c(t) \rangle,$$

where the expectation value is taken with respect to the thermal state $\rho \propto e^{-\beta[\mathcal{H}-\mu\hat{\mathcal{Q}}]}$. The total charge density $\hat{\mathcal{Q}}$ is conserved, $[\mathcal{H}, \hat{\mathcal{Q}}] = 0$, hence we may factor this exponential $e^{-\beta\mathcal{H}} e^{\beta\mu\hat{\mathcal{Q}}}$. Explicitly we have

$$\mathcal{G}^{\>}(t - i\beta) = -\text{Tr}\{e^{\beta\mathcal{H}} c(t) e^{-\beta\mathcal{H}} c^{\dagger} e^{-\beta[\mathcal{H}-\mu\hat{\mathcal{Q}}]}\} / \mathcal{Z} = -\text{Tr}\{c^{\dagger} e^{-\beta[-\mu\hat{\mathcal{Q}}]} c(t) e^{-\beta\mathcal{H}}\} / \mathcal{Z},$$

where we have used the cyclic property of the trace. On the right we insert $e^{\beta\mu\hat{\mathcal{Q}}} e^{-\beta\mu\hat{\mathcal{Q}}}$ and cycle the rightmost term to the left of the trace, leaving $\mathcal{G}^{\>}(t - i\beta) = -\langle e^{-\beta\mu\hat{\mathcal{Q}}} c^{\dagger} e^{\beta\mu\hat{\mathcal{Q}}} c(t) \rangle$, where $e^{-\beta\mu\hat{\mathcal{Q}}} c^{\dagger} e^{\beta\mu\hat{\mathcal{Q}}} = e^{-\beta\mu} c^{\dagger}$, hence

$$\mathcal{G}^{\<}(t) = -e^{\beta\mu} \mathcal{G}^{\>}(t - i\beta). \quad (4.6)$$

Clearly, the above remains true if one averages over \mathcal{N} flavors of such fermions.

4.1.2 Comparing KMS relations

Before proceeding, we should comment on the non-standard nature of the above KMS relation (4.6). Focus is ordinarily placed on the fermionic ‘‘mass’’ term $\mathcal{H} \rightarrow \mathcal{H}_q - \eta\hat{\mathcal{Q}}$ mentioned in Sec. 3.2.2. Such a mass term amounts to a flat banded dispersion relation, $\epsilon_k = \eta$, for all k . Such flat bands³ are seen in magic-angle graphene [70, 71].

³The Bohigas-Giannoni-Schmit conjecture, mentioned in Sec. 1.3.3, states that single particle nonintegrable systems can be modeled via random matrices/tensors after the Ehrenfest time. One can similarly postulate that the quenched-random SYK models capture the typical behavior of nonintegrable flat banded (so essentially without a kinetic term) interacting many-body Hamiltonians.

This mass term is related to the difference of derivatives of the Green's function. In particular, from the Kadanoff-Baym equations from Sec. 3.2.3, together with the generalized Galitskii-Migdal sum rule, one may show that the Green's functions satisfy $\dot{\mathcal{G}}^{\gtrless}(0) - \imath\eta\mathcal{G}^{\gtrless}(0) = -\imath q^2 \langle \mathcal{H}_q / \mathcal{N} \rangle$. Subtracting these two equations from one another, and using the boundary conditions (4.5), leaves us with the mass term

$$\dot{\mathcal{G}}^<(0) - \dot{\mathcal{G}}^>(0) = \imath\eta[\mathcal{G}^<(0) - \mathcal{G}^>(0)] = \imath\eta. \quad (4.7)$$

The standard KMS relation, $\mathcal{G}^<(t) = -\mathcal{G}^>(t - \imath\beta)$, is restored when setting $\mu = 0$ and rather identifying η with the chemical potential $\eta \rightarrow \mu$. Essentially, it occurs when treating the chemical potential term as generating time evolution. While this is a valid definition of μ , it does not yield any extra information, e.g., the equation of state. For our KMS relation (4.6), one does not consider the chemical potential to be part of the Hamiltonian, but only to be part of the state $e^{-\beta(\mathcal{H} - \mu\mathcal{Q})}$. Physically this is motivated over the usual KMS relation since the chemical potential is primarily a thermodynamic variable, hence not necessarily dynamical in nature.

In real-time, the choice difference will only amount to a global phase in the Green's functions $\mathcal{G}^{\gtrless}(t) \rightarrow e^{\imath\eta t}\mathcal{G}^{\gtrless}(t)$. As such, it makes no difference to the thermodynamics, in a sense it is an arbitrary choice. Our choice, however, does provide a clean way to derive a nontrivial relation for chemical potential from the Green's functions, i.e., it yields the equation of state.

4.1.3 Charged SYK Green's functions

Using the KMS relation (4.6), we may extract out the chemical potential given the Green's functions at arbitrary charge density. These were calculated in Sec. 3.2.3, essentially extending the large- q solution from Chapter 2, to non-zero charge [80]

$$\mathcal{G}^>(t) = \left[\mathcal{Q} - \frac{1}{2} \right] e^{[g_+(t) + g_-(t)]/q} \quad \mathcal{G}^<(t) = \left[\mathcal{Q} + \frac{1}{2} \right] e^{[g_+(-t) + g_-(-t)]/q}. \quad (4.8)$$

The main novelty lies in the addition of a linear term $g_-(t) = -4\mathcal{Q}\mathcal{J}(\mathcal{Q}) \sin(\pi v/2)\imath t$ which we stated was zero in the uncharged case. It is indeed zero at charge neutrality $\mathcal{Q} = 0$. Further, the interaction strength gets modified to $\mathcal{J}(\mathcal{Q}) = [1 - 4\mathcal{Q}^2]^{(2-q)/4} J_q$ which we will call the “effective interaction”. The $g_+(t)$ solution remains almost unchanged aside from this the modified interaction

$$e^{g_+(t)} = \left[\frac{\pi v}{\beta \mathcal{J}(\mathcal{Q}) \cos(\pi v(1/2 - \imath t/\beta))} \right]^2. \quad (4.9)$$

At $t = 0$, we have $\mathcal{G}^<(0) = -e^{\beta\mu}\mathcal{G}^>(-\imath\beta)$, where one notices that $g_+(-\imath\beta) = g(0) = 0$, leaving

$$\left[\mathcal{Q} + \frac{1}{2} \right] = -e^{\beta\mu} \left[\mathcal{Q} - \frac{1}{2} \right] e^{-4\mathcal{Q}\mathcal{J}(\mathcal{Q}) \sin(\pi v/2)\beta/q}.$$

With some manipulation, we are left with the equation of state μ as a function of \mathcal{Q} and T :

$$\boxed{\mu = T \ln \left[\frac{1 + 2\mathcal{Q}}{1 - 2\mathcal{Q}} \right] + 4\mathcal{Q}\mathcal{J}(\mathcal{Q}) \sin(\pi v/2)/q.} \quad (4.10)$$

As shown in Sec. 3.1.2, v quantifies the degree of chaos expressed by the model, i.e., the Lyapunov exponent $\lambda_L = 2\pi T v$, and is the solution to

$$\beta \mathcal{J}(\mathcal{Q}) = \pi v \sec(\pi v/2). \quad (4.11)$$

In particular, $v = 1$ indicates that the MSS bound is saturated, hence the system is maximally chaotic, while $v = 0$ indicates that the system is regular/non-chaotic.

4.2 A liquid-gas phase transition in the cSYK model

Before moving on to the main results in Sec. 4.2.1, we first sketch out the thermodynamics, adding some additional comments not given in the included publication [61]. Let us focus on the effective interaction, which may be rewritten as⁴

$$\mathcal{J}(\mathcal{Q}) = e^{(2-q)\frac{|\ln[1-4\mathcal{Q}^2]|}{4}} J.$$

Note that, even for small charge densities $\mathcal{J}(\mathcal{Q}) = e^{-(q-2)[\mathcal{Q}^2 + \mathcal{O}(\mathcal{Q}^4)]} J$. Thus we see that these interactions become weaker under larger charge density. In fact, in the large- q limit, at any non-zero charge, the system tends to a non-interacting harmonic oscillator. This explains why the phase diagram, see Fig. 4.2, appears to shrink away as $q \rightarrow \infty$. However, in considering correspondingly small charge densities $\mathcal{Q} = \tilde{\mathcal{Q}}q^{-1/2}$, nontrivial interaction $\mathcal{J}(\mathcal{Q}) = e^{-\tilde{\mathcal{Q}}^2 + \mathcal{O}(1/q)} J$, is maintained. To achieve such a charge density, we consider rescaled thermodynamic variables in q ,

$$T = \tilde{T}q^{-1}, \quad \mu = \tilde{\mu}q^{-3/2} \quad (4.12)$$

where we keep the tilde'd quantities fixed as we take $q \rightarrow \infty$ to extract the leading order results.

Rmk 1 (Weakening of effective interactions and scattering) *For a system with a sense of locality, such a weakening of interactions can perhaps be understood as charges rearranging themselves in such a way that on average, they partially cancel each other out. In the model we consider here, no such spatial rearrangement can take place. The actual reason for this weakening of interactions is purely due to the limitation of possible scatterings. Due to the exclusion principle, no scattering interactions can occur when every site is filled with a fermion, corresponding to $\mathcal{Q} = 1/2$. In contrast, for half (fermion) filling, corresponding to $\mathcal{Q} = 0$, we obtain the maximum amount of possible scattering events, with $\mathcal{N}/2$ fermions possibly moving onto $\mathcal{N}/2$ empty sites via $q/2$ -body interaction.*

Let us now consider the derived equation of state (4.10), plotted in Fig. 4.3, at various temperatures. It is by doing this that one can now read off when a possible phase transition can occur. To see this, note that $\mu(\mathcal{Q})$ tells us about the state the system finds itself in. In other words, given a known chemical potential and temperature, it tells us the corresponding charge density of the system. However, if this function is no longer one-to-one, then the question becomes; which of

⁴Here we are dropping the subscript q , $J_q \rightarrow J$ since we will only consider a single SYK model.

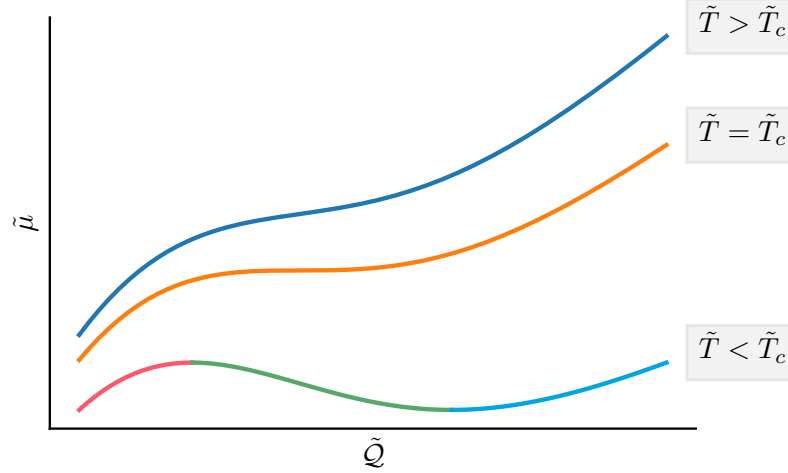


Figure 4.3: Equation of state $\mu(\mathcal{Q})$ for various temperatures in the maximally chaotic regime (4.12).

the multiple densities correspond to the system? So, as plotted in Fig. 4.3, we note that at higher temperatures, the function is one-to-one; hence there is only a single possible phase. At the critical values

$$T_c = 2e^{-3/2}q^{-1}, \quad \mu_c = 2e^{-3/2}\sqrt{3/2}q^{-3/2}, \quad (4.13)$$

however, the equation of state has an inflection point at $\tilde{\mathcal{Q}}_c = \sqrt{3/2}$. This corresponds to a second-order phase transition where several thermodynamic observables will diverge. Below this temperature, the function is three-to-one. Hence, for every pair (μ, T) , there are three possible phases, each with its own charge densities.

Rmk 2 (A comment on the rescaling) *The rescaling (4.12) is analogous to what is done in dynamical mean-field theory (DMFT) where one considers system dimension $d \rightarrow \infty$ [182]. To preserve competition between interaction and kinetic terms one must rescale the hopping $t \rightarrow t d^{-1/2}$. The DMFT framework has often been found to provide an excellent description for real $d = 3$ materials, despite this unusual scaling. It also allows one to then analytically study the Mott-insulator and metallic phases of the Hubbard model and their transition. Our q -rescaling is in the same spirit, it retains the competition between the phases and thereby leads to a nontrivial phase diagram.*

The middle phase, denoted in green, has a negative bulk modulus (inverse compressibility), $\mu'(\mathcal{Q}) < 0$. To see how this is unphysical, let us consider the role which the chemical potential plays by viewing the charge density's response to an increasing chemical potential. Due to the Gibbs-Duhem relation to pressure (per particle) $dP = \mathcal{Q}(\mu)d\mu + SdT$, at constant temperature $dP = \mathcal{Q}(\mu)d\mu$, the bulk modulus is a measure of resistance to compression. In other words, it tells us how the density changes as a response to an applied pressure. As such, the middle phase has a decreased density when a pressure is applied. This behavior is not seen in ordinary materials.

This brings us back to the question of which phase is the physical one in which the system finds itself. The thermodynamically favorable state is, in fact, selected out by the saddle point of the action $\beta\Omega = \bar{S}[\mathcal{G}, \Sigma]$. The grand potential Ω is important because it is the quantity that is minimized by the thermal state. For rescaled quantities (4.12), hence small charge density $Q = \tilde{Q}q^{-1/2}$, we have the free energy

$$\tilde{\mathcal{F}}(\tilde{Q}) = -2J e^{-\tilde{Q}^2} + 2\tilde{Q}^2\tilde{T}.$$

The function $\mathcal{A}(\tilde{Q}) = \tilde{\mathcal{F}}(\tilde{Q}) + \tilde{\mu}\tilde{Q}$ was, in fact, plotted in Fig. 4.1. This illustrates the different phases. The unphysical phase is the top of the hill which is an unstable-fixed point that can be ignored [61], as seen in the next section where the publication is included below in Sec. 4.2.1. The details on the numerics required to reproduce the phase diagrams are given in App. 4.A.

4.2.1 Publication: Shared universality of charged black holes and the complex large- q Sachdev-Ye-Kitaev model

Reprinted article with permission from

Jan C. Louw and Stefan Kehrein


Phys. Rev. B 107, 075132 (2023)

<https://doi.org/10.1103/PhysRevB.107.075132>


Copyright (2023) by the American Physical Society.

Author contributions J. C. L. suggested the direct rescaling of the charge density $Q \rightarrow \tilde{Q}q^{-1/2}$, did the analytic calculations, and wrote the article. S. K. suggested rescaling the chemical potential as $\mu = \hat{\mu}q^{-1/2}$, which inspired the consideration of multiple eventual rescalings in the paper, and also provided input on the manuscript. Both authors discussed the results and possible interpretations.

Shared universality of charged black holes and the complex large- q Sachdev-Ye-Kitaev model

Jan C. Louw  and Stefan Kehrein

Institute for Theoretical Physics, Georg-August-Universität Göttingen, Friedrich-Hund-Platz 1, 37077 Göttingen, Germany

 (Received 20 June 2022; revised 31 January 2023; accepted 31 January 2023; published 13 February 2023)

We investigate the charged $q/2$ -body interacting Sachdev-Ye-Kitaev (SYK) model in the grand-canonical ensemble. By treating q as a large parameter, we are able to analytically study its phase diagram. By varying the chemical potential or temperature, we find that the system undergoes a phase transition between low and high entropies in the maximally chaotic regime. A similar transition in entropy is seen in charged anti-de Sitter (AdS) black holes transitioning between a large and small event horizon. Approaching zero temperature, we find a first-order chaotic-to-nonchaotic quantum phase transition, where the finite extensive entropy drops to zero. This again has a gravitational analog—the Hawking-Page transition between a large black hole and thermal radiation. An analytical study of the critical phenomena associated with the continuous phase transition provides us with mean-field van der Waals critical and effective exponents. We find that all analogous power laws are shared with several charged AdS black hole phase transitions. Together, these findings indicate a connection between the charged $q \rightarrow \infty$ SYK model and black holes.

DOI: [10.1103/PhysRevB.107.075132](https://doi.org/10.1103/PhysRevB.107.075132)

I. INTRODUCTION

The analysis of condensed-matter systems lacking quasiparticles is hindered by the unamenability of Fermi-liquid theory. One successful approach is via a class of disordered Sachdev-Ye-Kitaev (SYK) models [1,2] or their related disorderless planar/tensor matrix models [3,4]. Despite their nonintegrability, one may find exact relations between the self-energy and Green's function \mathcal{G} [5]. This reduces the exponential complexity of the problem to a single Dyson equation purely in terms of \mathcal{G} . Although some analytical results exist in the infrared limit [6], the full solutions are obtained numerically.

There is also a framework in which one may find exact analytical solutions. This is by considering $q/2$ -body interactions, for large q , and treating $1/q$ as an expansion parameter. In this work we present a study of such a model [2,7],

$$\mathcal{H} = J \sum_{\substack{1 \leq i_1 < \dots < i_{q/2} \leq N \\ 1 \leq j_1 < \dots < j_{q/2} \leq N}} X_{j_1 \dots j_{q/2}}^{i_1 \dots i_{q/2}} c_{i_1}^\dagger \dots c_{i_{q/2}}^\dagger c_{j_{q/2}} \dots c_{j_1}, \quad (1)$$

with a conserved U(1) charge density $\hat{Q} = \frac{1}{N} \sum_i c_i^\dagger c_i - 1/2$, with expectation values $Q \in [-1/2, 1/2]$. Here c^\dagger, c are Dirac/complex fermionic creation and annihilation operators, respectively. We will study this model in the grand-canonical ensemble with partition function $Z = \text{Tr}\{e^{-\beta[\mathcal{H} - \mu N \hat{Q}]}\}$. The couplings, X , are complex random variables with zero mean and a variance $\overline{|X|^2} = [q^{-1}(q/2)!]^2 [2/N]^{q-1}$. Such models have the advantage of being amenable to analytical solutions. At neutral charge, $Q = 0$, its thermodynamics reduces to its Majorana ($c^\dagger = c$) counterpart [6]. The inclusion of nonzero charge brings Eq. (1) in closer contact with electronic systems [1,8,9]. By varying a chemical potential μ , the conjugate to Q , we find that this model exhibits a phase transition similar

to its finite- q equivalents [3,10]. In contrast to the numerical results in the finite- q case, we are able to analytically study its phase diagram in the large- q limit. This is done by considering suitable polynomial scaling (in q) thermodynamic variables such as T, μ . Such q scalings have also previously been considered for two coupled Majorana SYK models [11] in the $q \rightarrow \infty$ limit. The analytical solutions to the equilibrium Green's functions \mathcal{G} and a proof that they remain valid for our considered scaling is given in Appendix A.

The Green's functions are key to studying the phase diagram. This is because the Kubo-Martin-Schwinger (KMS) relation, $\mathcal{G}(\tau + \beta) = -e^{-\beta\mu}\mathcal{G}(\tau)$ [12, Appendix B], allows one to extract the exact equation of state [7, Eq. (43)],

$$\mu(Q) = 2T \tanh^{-1}(2Q) + 4Q\mathcal{J}(Q) \sin(\pi v/2)/q, \quad (2)$$

for large q with effective coupling strength

$$\mathcal{J}(Q) \equiv J[1 - 4Q^2]^{(q-2)/4} \quad (3)$$

and the Lyapunov exponent $\lambda_L = 2\pi vT$, found by solving $\mathcal{J}/T = \pi v \sec(\pi v/2)$ [6]. Note that for any nonzero $Q = \mathcal{O}(q^0)$, the interaction is suppressed for large q , $\mathcal{J} \xrightarrow{q \rightarrow \infty} 0$.

One is able to retain nonzero (constant) effective coupling \mathcal{J} by adjusting the model to have Q -dependent coupling $J(Q) \propto [1 - 4Q^2]^{(2-q)/4}$ [13]. This allows the interactions to remain relevant at all charge densities. Notice, however, that with this adjustment the Hamiltonian inherits a temperature dependence from the charge density [8]. In this case there is no phase transition. In contrast, by a suitable q -dependent rescaling introduced below, we will find that the phase transition of the Hamiltonian (1), without adjustments, persists even for $q \rightarrow \infty$.

In particular, we find a van der Waals (vdW)-like phase diagram [14,15], with a line of first-order phase transition

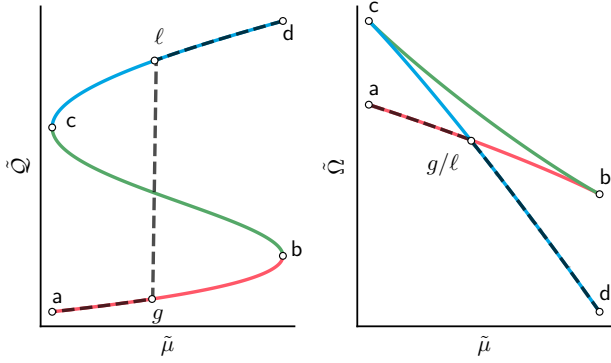


FIG. 1. The three solutions to Eq. (5) distinguished by color for $\tilde{T} < \tilde{T}_{\text{crit}}$. The dashed line indicates the thermodynamically favorable solution.

terminating at a critical end point where the transition is continuous. Associated with this are multiple power laws, the critical exponents of which we are able to calculate analytically. Comparing exponents, we find that our model shares such a universality class with a wide range of models, including numerous AdS black holes, a nonexhaustive list of which is in Refs. [15–22]. These similarities between black holes and the complex large- q SYK model extend even beyond the shared universality class. For instance, over the phase transition there is a drop in entropy reminiscent of the large-to-small horizon transition in Reissner-Nordström (RN), charged and nonrotating, black holes. Such systems also appear in the study of non-Fermi liquids under the name RN metals [23].

Phase diagram. We start our analysis by considering two extremes. At zero charge density we are left with a strongly interacting pure Majorana-like SYK model, while at any finite charge density $Q = \mathcal{O}(q^0)$ the interaction (3) is trivial, $\mathcal{J} \rightarrow 0$, leaving a Fermi gas. Somewhere in between these two extremes must lie a regime where interactions and density terms in (2) compete in a nontrivial way. Indeed, such a competition is found for thermodynamic quantities which scale like

$$T = \tilde{T}q^{-1}, \quad \mu = \tilde{\mu}q^{-3/2}, \quad (4)$$

where tilde'd quantities are held fixed as $q \rightarrow \infty$. In turn, the charge densities scales like $Q = \tilde{Q}q^{-1/2}$, hence yielding a finite effective interaction (3), $\mathcal{J}(Q) \xrightarrow{q \rightarrow \infty} e^{-\tilde{Q}^2}J$. This scaling corresponds to the maximally chaotic regime where $v = 1 - 2\tilde{T}/(q\mathcal{J}) + \mathcal{O}(1/q^2)$ saturates the universal (chaos) bound $\lambda_L \rightarrow 2\pi T$ [24]. Using the scaling (4) thus simplifies equation of state (2) to

$$\tilde{\mu}(\tilde{Q}) = 4\tilde{Q}[\tilde{T} + Je^{-\tilde{Q}^2}] + \mathcal{O}(1/q). \quad (5)$$

Plotting this, as in Fig. 1, one notes that there exists a critical temperature, $\tilde{T}_{\text{crit}} = 2Je^{-3/2}$, below which three solutions exist instead of one. The solution from point b-c has unphysical negative compressibility. Such behavior is also seen in the vdW liquid-gas transition. Due to the difference in (charge) density and similarities to the vdW system, we shall refer to the two physical solutions as the gaseous and liquid phases, given in pink and blue, respectively.

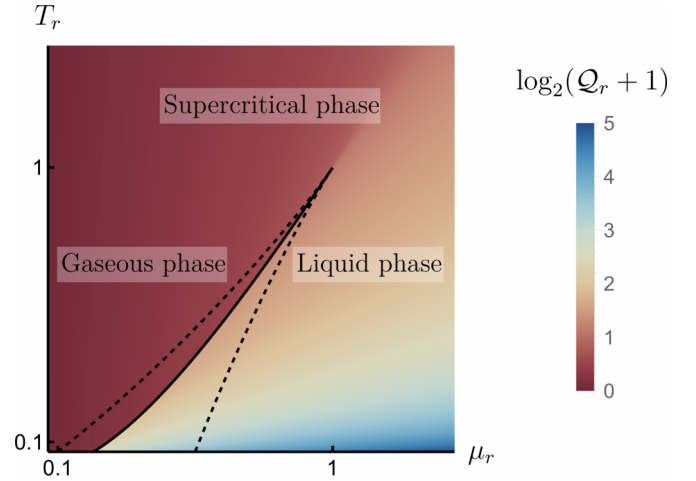


FIG. 2. Phase diagram, for scaling (4), in terms of reduced variables $T_r = \tilde{T}/\tilde{T}_{\text{crit}}$, $\mu_r = \tilde{\mu}/\tilde{\mu}_{\text{crit}}$, and $Q_r = \tilde{Q}/\tilde{Q}_{\text{crit}}$. The solid and dashed lines denote the coexistence and stability curves, respectively. The color corresponds to the thermodynamically favorable charge density.

Out of the three, the thermodynamically favorable solution corresponds to the smallest grand potential (per lattice site) $\Omega = -T \ln Z/N$. Considering the partition function, we observe the relations $J\partial_J\Omega = E$ and $\partial_\mu\Omega = -Q$, where the energy density is given by [7]

$$E = -2(1 - 4Q^2)\mathcal{J} \sin(\pi v/2)/q^2,$$

which defines a set of differential equations. From the relation $\Omega = E - \mu Q - T\mathcal{S}$, we observe that the entropy density \mathcal{S} is the only unknown. We may find \mathcal{S} by solving the set of differential equations for the scaling (4), i.e., in the maximal chaotic regime $v \rightarrow 1$, $\partial_{\tilde{\mu}}q^2\Omega = -\tilde{Q}$ and $\partial_Jq^2\Omega = -2e^{-\tilde{Q}^2}$. One may then verify by substitution that $\mathcal{S} = \ln 2 - 2\tilde{Q}^2/q + \mathcal{O}(1/q^2)$, where the constant is found by using the free fermion solution at $J = 0$. The corresponding grand potential is the written as $q^2\Omega = \tilde{\Omega} - q\tilde{T} \ln 2$, with

$$\tilde{\Omega} \equiv -2\tilde{Q}^2\tilde{T} - 2[1 + 2\tilde{Q}^2]Je^{-\tilde{Q}^2} + \mathcal{O}(1/q). \quad (6)$$

Considering $\tilde{\Omega}$ for these three solutions, plotted in Fig. 1, we find that the favorable charge density necessarily jumps between g and ℓ , missing the unphysical solution. Also note the distinct swallowtail shape, from catastrophe theory, which is also common to RN phase transitions. This shape is indicative of a first-order phase transition, in this case from a low (charge) density gaseous phase to the dense liquid phase. This is induced either by increasing the chemical potential or decreasing the temperature, as seen from the phase diagram in Fig. 2. The stability limit curves, enclosing the region where both phases can coexist, coincide at the critical point $(\tilde{\mu}_{\text{crit}}, \tilde{T}_{\text{crit}})$, with charge density $\tilde{Q}_{\text{crit}} = \sqrt{3/2}$. Here the two turning points b and c merge into an inflection point, where there is a continuous (second-order) phase transition. Above this lies the supercritical phase, identified by a single unique solution.

Universality. Approaching the critical point, i.e., for small shifted variables $m \equiv \mu_r - 1$, $\rho \equiv Q_r - 1$, and $t \equiv T_r - 1$, we find that various thermodynamic quantities display power

TABLE I. Table of critical exponents.

α	β	γ	δ
0	1/2	1	3

laws. To study this we shift and rescale the grand potential (6) and consider it close to this point,

$$f = \frac{\tilde{\Omega} - \tilde{\Omega}_{\text{crit}}}{\tilde{\mu}_{\text{crit}} \tilde{Q}_{\text{crit}}} + t/3 + m = -\rho^2 \frac{t + (3\rho/2)^2}{3} + \mathcal{O}(\rho^5), \quad (7)$$

which satisfies $\partial_m f = -\rho$, stemming from $\partial_{\tilde{\mu}} \tilde{\Omega} = -\tilde{Q}$. Further, the linear shift t will not affect the specific heat.

In particular, we focus on the minimized grand potential corresponding to the dashed line in Fig. 1. One may show that in terms of some ordering field \hbar , it is homogeneous $f(t, \hbar) = t^{2-\alpha} f(1, \hbar t^{\beta-2+\alpha})$, where α and β are the critical exponents characterizing the power laws. Models which share the same scale-invariant form f under the renormalization group flow are said to belong to the same universality class.

The homogeneity property is satisfied for the ordering field $\hbar = m - 2t/3$, which restricts the form of \hbar up to a scaling constant. This leaves the singular function

$$f(t, \hbar) = -\frac{|t|^{2-\alpha}}{6} - |\hbar| |2t/3|^\beta - \frac{3\hbar^2}{2} |t|^{-\gamma} + \mathcal{O}(\hbar^3 |t|^{-5/2})$$

for small \hbar and $f(t, \hbar) = -\frac{3}{4} |\hbar|^{1+1/\delta} [1 + \mathcal{O}(t\hbar^{-2/3})]$ for small t . The details of this calculation are given in Appendix C. Here $\alpha, \beta, \gamma, \delta$ are the classical mean-field critical exponents, given in Table I. As such, our model falls into the vdW universality class. From $\rho(t, \hbar) = -\partial_{\hbar} f(t, \hbar)$, we have $\rho(0, \hbar) = \hbar^{1/\delta}$, and

$$\rho(t, \hbar) = \text{sgn}(\hbar) |2t/3|^{1/2} + 2\hbar |2t/3|^{-1} + \mathcal{O}(\hbar^2 t^{-5/2}) \quad (8)$$

for small \hbar . The remaining critical exponents characterize the power laws along the line $\hbar = 0$: the order parameter $\rho(t, 0) \propto |t|^\beta$, specific heat $C_{\hbar} \propto -\partial_t^2 f(t, 0) \propto |t|^{-\alpha}$, and susceptibility $\chi_{\hbar} \propto \partial_{\hbar}^2 f(t, \hbar)|_{\hbar=0} \propto |t|^{-\gamma}$.

Effective exponents. The particular power law can be dependent on the line along which the critical point is reached. This feature is due to the mixing of chemical potential and temperature in the ordering field \hbar [25]. Since the corresponding exponents do not enter into the scale-invariant form of the model, they are not the critical exponents which define the universality class. However, these *effective* exponents still describe physically relevant processes. As an example, let us consider the specific heat. For constant μ , we have $C_{\mu} \propto -\partial_t^2 f(t, -2t/3) \propto |t|^{-2/3}$, i.e., $\alpha_{\mu} = 2/3$. Here, the subscripts indicate which quantity is set to its critical value. In contrast, for constant Q , we use the identity $C_Q = (\partial_T E)_Q$. In the chaotic regime, the energy behaves as $E \propto T^2 + \text{const.}$, leaving $C_Q \propto T \sim t^0$. While often associated with Fermi-liquid behavior, such as a Sommerfeld, linear in T , specific heat also appears in RN [23] and cuprate [26–28] strange metals for a range of doping levels. The remaining *effective* exponents can be obtained from (8) and are listed in Tables II(a) and II(b).

Relation to gravity. By comparing order parameters and their conjugates, one can make various analogies between

TABLE II. Tables of effective exponents.

(a)	α_{μ}	β_{μ}	γ_{μ}
	2/3	1/3	2/3
(b)	α_Q	γ_Q	
	0	1	

the models listed in Table III. The similarities are strongest when comparing our model to RN black holes. These systems are defined by a charge q_B , an event horizon radius r , and electrical potential $\Phi = q_B r^{2-d}$ [22]. One may also consider such systems in an *extended* AdS $_{d+1}$ space [15,29], where the cosmological constant Λ and its conjugate quantity, the volume V , are treated as thermodynamic variables. Here V , like in the vdW case, is the order parameter, while $-\Lambda$ acts as the pressure term P .

These analogies are quantitative in the sense that all effective exponents also match. By this we mean that by keeping order parameters fixed, both exponents match II(b). Then, while keeping the conjugates fixed, we find three exponents matching II(a). All models listed in Table III also share the same critical exponents. As such, our model, the vdW liquid [15], and multiple RN AdS $_{d+1}$ black holes [15,17,22,29] all share a universality class, as well as having the same effective exponents.

Besides sharing a universality class, these analogous models also have an abundance of qualitative commonalities. This is particularly apparent at low energies where the suppression by large charge densities leaves a relatively weakly interacting, $\mathcal{J} \sim e^{-Q^2} J$, liquid phase. The extreme of this is seen by considering a different rescaling,

$$T = \bar{T} q^{-2}, \quad \mu = \bar{\mu} q^{-2}, \quad (9)$$

where the system transitions to a finite nonrescaled charge density $Q = 0 \rightarrow \sqrt{1 - e^{-4J/\bar{T}}}/2$, shown in Appendix B. This suppresses the effective interaction $\mathcal{J} = e^{-qJ/\bar{T}} J \rightarrow 0$, yielding a free integrable ($v \rightarrow 0$) system. As such, small perturbations, stemming from $\bar{\mu}$ to the $Q = 0$ symmetric-Majorana state, induce a jump to a Fermi gas at finite (positive or negative) charge density, hence breaking the U(1) symmetry. This transition is thus from a maximally chaotic to a nonchaotic state. Such a Fermi gas has an entropy $S = -\beta\mu Q - \ln \sqrt{1/4 - Q^2}$. To leading order in $\bar{T} \equiv \bar{\beta}^{-1}$, this indicates a drastic drop in entropy, $\ln 2 \rightarrow \bar{\beta} J e^{-4\bar{\beta} J}$. Such an instability is also seen in RN black holes at low temperatures [30,31]. The RN transition is from a large black hole to a small one. Since the Bekenstein-Hawking entropy is proportional to the surface area, this also corresponds to a drop in entropy.

TABLE III. Analogies between models with shared universality class.

Model	SYK	vdW	RN-AdS	
			[15,29]	[17]
Order parameter	Q	V	V	Φ
Conjugate	μ	P	$-\Lambda$	q_B

Lastly, both RN and SYK transitions also include an unstable solution with a negative bulk modulus.

For $\bar{T} = o(q^0)$, there is a first-order quantum phase transition from $\mathcal{Q} = 0$ to maximum density $\mathcal{Q} = 1/2$ at $\bar{\mu}_0 = 4J$. If $\bar{\mu} < \bar{\mu}_0$, then we are left with a Majorana SYK ground-state solution with an extensive entropy. Such a finite entropy, at $T = 0$, is also the defining property of RN metals [23]. If $\bar{\mu} > \bar{\mu}_0$, we are left with a zero-entropy harmonic oscillator vacuum state. This first-order quantum phase transition is also observed in the finite- q equivalent models [3,10]. Such a transition is again related to gravity, this time the classical HP transition [32], which has a large black hole to (noninteracting) thermal radiation with a zero entropy transition.

Also of note is the conjecture of black holes being the fastest scramblers [33] and as such chaotic [6,34,35]. Assuming this holds, the gravitational analogies extend over to a chaotic-to-chaotic RN transition, as we found in the scaling regime (4). It would further include a chaotic-to-nonchaotic HP transition, where the nonchaotic phase is (noninteracting) thermal radiation, corresponding to our observed low-temperature crossover (9).

It is quite remarkable that there are at least two RN models which also qualitatively match our phase diagram [17,21] by terminating at a first-order phase transition at $(q_B, \beta) = (0, \beta_Z)$. This is reminiscent of how our coexistence line terminates at $(\bar{T}, \bar{\mu}) = (0, \bar{\mu}_0)$. This is in contrast to extended-space RN black holes and vdW, with coexistence lines extending to the point (0,0). At the other end, both models terminate at a second-order transition. Of note is that [21] has the same effective exponents matching II(a) [22].

All these similarities are perhaps not so surprising from the perspective of holography. This is because the SYK model is a $(0+1)$ -dimensional conformally symmetric theory at low temperatures. As such, from the anti-de Sitter/conformal field theory (AdS/CFT) correspondence, one would conjecture that it is a CFT on the boundary of some AdS_{1+1} space. Standard $(1+1)$ -dimensional gravity is topological and displays only trivial physics; hence we consider nonstandard gravity, the simplest of which are the Jackiw-Teitelboim (JT) black holes. They may be viewed as the dimensional reduction, or the near-horizon theory of near-extremal (minimal mass) higher-dimensional black holes [36–38]. One such model [18] even has a phase transition with calculated effective exponents matching that of II(b) and $\beta = 1/2$.

II. CONCLUSION

We presented an analytic study of the complex large- q SYK model, showing that it displays an RN-like phase transition. Prior numerical analyses of the finite- q case have observed that the phase diagram scales away at larger values of q [3,10]. We showed that if one considers rescaled quantities as described by (4) and (9), then the transition in fact still exists at infinite q .

One can further study the overlap of our large- q results with that of the finite- q numerical results [10]. A natural choice is to consider the relative error between their respective critical values. Such an analysis is provided in Appendix D, where we found relative errors which appear to converge to

zero rather quickly as q increases. This supports the relevance of the $q \rightarrow \infty$ limit for finite- q models.

In contrast to the finite- q case, which has asymmetric (differing over the coexistence line) irrational exponents [3,10], we found symmetric rational numbers. One should note that Refs. [3,10] actually determined effective exponents because the ordering field was assumed to be the chemical potential. However, as we have seen in our analysis, field mixing needs to be taken into account to determine the universality class and the critical exponents. The only exception where field mixing plays no role is β . The small deviation from the mean-field value $1/2$ in Refs. [3,10] might be due to numerical error, and as such whether the finite- q SYK model also falls into the vdW universality class remains an open question.

By comparing the critical exponents to other models, we found that the complex large- q SYK model and many RN black holes find themselves in the same mean-field vdW universality class. Further, in the low-reduced-temperature regime, defined by the scaling (9), we found a jump between maximally chaotic and nonchaotic phases, also observed in generalized/coupled SYK models [11,39–43]. The coexistence line dividing the two phases terminates at a first-order quantum phase transition from a Majorana ground state to a Fermi gas, and hence a drop from nonzero residual entropy down to zero. This feature is shared with the first-order Hawking-Page (HP) transition between a large black hole and thermal radiation [32]. As such, the gravitational analogies extend to the low-temperature regime.

From the perspective of AdS/CFT, these similarities between our model and charged black holes are perhaps not too surprising. This is because the SYK model is conformally symmetric in the infrared limit [6]. However, the details narrow down the list of possible gravity duals to the SYK model [44]. The analytical expressions derived in this work, the power laws, equation of state, and grand potential serve as a guide towards finding this dual.

We conclude with the natural question of whether any columns in Table III or other mentioned analogies are part of an AdS/CFT dictionary. In other words, is there (asymptotic) equivalence between any of the partition functions?

ACKNOWLEDGMENTS

We would like to thank Peter Sollich for helpful discussions on field mixing, critical exponents, and scaling relations. This work was funded by the Deutsche Forschungsgemeinschaft (DFG, German Research Foundation) - 217133147/SFB 1073, Project B03, and the Deutsche akademische Austauschdienst (DAAD, German Academic Exchange Service).

APPENDIX A: VALIDITY OF q RESCALING

The thermal Green's function $\mathcal{G}(\tau - \tau') \equiv \mathcal{G}(\tau, \tau') = -\mathcal{T}(c(\tau)c^\dagger(\tau'))$ is the solution to Dyson's equation:

$$[\mathcal{G} - \mathcal{G}_0](\tau, \tau') = \int_0^\beta d\tau_1 dt \mathcal{G}(\tau, t) \Sigma(t, \tau_1) \mathcal{G}_0(\tau_1, \tau'), \quad (\text{A1})$$

with noninteracting Green's function $\mathcal{G}_0(\tau) = \langle c^\dagger c \rangle_0 - \Theta(\tau)$ and self-energy Σ . For the $q/2$ -body interacting SYK model, $\Sigma(t) = \mathcal{G}(t)2J^2[-4\mathcal{G}(t)\mathcal{G}(-t)]^{q/2-1}/q$ [2]. We write $\mathcal{G}(\tau) = [\mathcal{Q} - \text{sgn}(\tau)/2]e^{\Delta\mathcal{G}(\tau)}$, with $\Delta \equiv 1/q$, leaving $q\Sigma = 2\mathcal{J}^2 e^{(1-2\Delta)\mathcal{G}_+} \mathcal{G}$. Here we have it split into symmetric/asymmetric parts $\mathcal{g}_\pm(-\tau) = \pm\mathcal{g}_\pm(\tau)$ and defined the charge density $\mathcal{Q} \equiv \frac{1}{N} \sum_i \langle c_i^\dagger c_i \rangle - 1/2$.

Claim 1. In the large- q limit, we *claim* that for any thermodynamic variables which scale subexponentially in q , the solution to (A1) is given by $\mathcal{g}_-(\tau) = 2\mathcal{Q}\dot{\mathcal{g}}_+(0)\tau$ and

$$e^{[1-2\Delta]\mathcal{g}_+(\tau)} = \frac{[\pi v/\lambda]^2}{\cos^2[\pi v(1/2 - |\tau|/\beta)]}, \quad \frac{\pi v/\lambda}{\cos[\pi v/2]} = 1, \quad (\text{A2})$$

where $\lambda = \beta\mathcal{J}\sqrt{1-2\Delta}$ and $\mathcal{J} \equiv [1-4\mathcal{Q}^2]^{(q-2)/4}/J$. Note that for nonrescaled variables, they take on the standard known forms given for neutral charge $\mathcal{Q} = 0$ in [6] or at finite charge in [7].

Proof. We take the approach of substituting the claimed solutions \mathcal{g}_\pm into the full Dyson equation. We then gather the nonzero (error) terms ΔR_i and show that, given sub-exponentially scaling, $\Delta R_i \xrightarrow{\Delta \rightarrow 0} 0$. Using (A1), $q\partial_\tau \ln \mathcal{G}(\tau, \tau')|_{\tau=0}$, for $\tau \geq 0$, reduces to

$$\dot{\mathcal{g}}(\tau) - \mathcal{J}^2 \int_0^\beta dt [\text{sgn}(\tau-t) - 2\mathcal{Q}] e^{\mathcal{g}_+(\tau-t) + \Delta\varphi_t(\tau)} = 0, \quad (\text{A3})$$

with $\varphi_\tau(t) \equiv \mathcal{g}(\tau-t) - \mathcal{g}(\tau) - \mathcal{g}(-t)$. By differentiating again we obtain the two equations

$$\ddot{\mathcal{g}}_+ = 2\mathcal{J}^2 e^{[1-2\Delta]\mathcal{g}_+} [1 + \Delta R], \quad \ddot{\mathcal{g}}_- = \Delta 2\mathcal{Q}\mathcal{J}^2 R_3,$$

with $R \equiv R_1 + R_2$. Ignoring the error terms, we have $\mathcal{g}_-(\tau) \sim \epsilon\tau$, while $\dot{\mathcal{g}}_+$ reduces to a Liouville equation with solution (A2). The boundary condition in (A2) enforces $\mathcal{G}(0^+) = \mathcal{Q} - 1/2$. By substituting the solutions back into (A3), one finds the error terms

$$R_1(\tau) = -[e^{-(1/2-\Delta)\mathcal{g}_+(\tau)} \dot{\mathcal{g}}_+(\tau)/\mathcal{J}]^2/2, \quad (\text{A4})$$

$$R_2(\tau) = e^{-(1+\Delta)\mathcal{g}_+(\tau)} \frac{\mathcal{I}_\tau(t)|_0^\tau - \mathcal{I}_{\tau+\beta}(t)|_\tau^\beta}{2}, \quad (\text{A5})$$

$$R_3(\tau) = -[\mathcal{I}_\tau(t)|_0^\tau + \mathcal{I}_{\tau+\beta}(t)|_\tau^\beta] - \frac{\dot{\mathcal{g}}_+(\tau) \dot{\mathcal{g}}_-(\tau)}{\mathcal{J} 2\mathcal{Q}\mathcal{J}}, \quad (\text{A6})$$

where we have defined the indefinite integral

$$\mathcal{I}_\tau(t) \equiv \int dt \dot{\mathcal{g}}_+(\tau-t) e^{\Delta\mathcal{g}_+(\tau-t) + (1-\Delta)\mathcal{g}_+(t)}. \quad (\text{A7})$$

We would next like to find the q -dependent scaling conditions on λ for which all $\Delta R_i \xrightarrow{\Delta \rightarrow 0} 0$. Using (A2), the bound $|R_1| \lesssim 2$ follows from

$$\frac{\dot{\mathcal{g}}_+(\tau)}{\mathcal{J}} = -\frac{2 \sin[\pi v(1/2 - \tau/\beta)]}{\sqrt{1-2\Delta}} e^{(1/2-\Delta)\mathcal{g}_+(\tau)}.$$

To bound (A5) and (A6), we first evaluate the integral (A7). To simplify the analysis we would like to replace exponentials like $e^{(1+\Delta)\mathcal{g}_+}$ with $e^{\mathcal{g}_+}$, under the integral, which is justified if the corresponding function, e.g., $e^{\Delta\mathcal{g}_+}$, remains differentiable under said limit. To see when this holds, we note that $(\pi v/\lambda)^{2\Delta} \leq e^{\Delta(1-2\Delta)\mathcal{g}_+(\tau)} \leq 1$ saturates for $|\ln[v/\lambda]| \lesssim q$. In

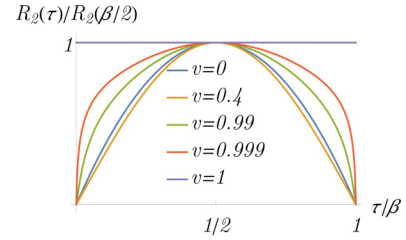


FIG. 3. The error plotted for various values of v .

this case, (A7) evaluates to

$$\begin{aligned} \mathcal{I}_\tau(t) &= \int dy \tan[\pi v/2 - (x-y)] \frac{-2 \cos^2(\pi v/2)}{\cos^2[\pi v/2 - y]} \\ &= 2 \cot[\pi v - x] \sin y \frac{\cos[\pi v/2]}{\cos[\pi v/2 - y]} \\ &\quad + 2 \left[\frac{\cos(\pi v/2)}{\sin(\pi v - x)} \right]^2 \ln \frac{\cos[\pi v/2 - (x-y)]}{\cos(\pi v/2 - y)}, \end{aligned} \quad (\text{A8})$$

where $x = \pi v\tau/\beta$ and $y = \pi vt/\beta$. This yields the error (A5)

$$\begin{aligned} R_2(\tau) &\sim \left[\frac{\csc^2[\pi v - x] + \csc^2 x}{2} \mathcal{g}_+(\tau) - 1 \right. \\ &\quad \left. + \frac{2 \sin^2[\pi v/2]}{\sin[\pi v - x] \sin x} \right] 2 \cos^2[\pi v/2 - x], \end{aligned}$$

which, seen in Fig. 3, has a maximum at $\tau = \beta/2$ given by

$$R_2(\beta/2) = 2 + 2 \frac{\ln[\pi v/\lambda]^2}{1 - [\pi v/\lambda]^2}.$$

The final error term (A6) is bounded by using (A3) to write

$$\dot{\mathcal{g}}_-(\tau) \xrightarrow{\Delta \rightarrow 0} -2\mathcal{Q}\mathcal{J}^2 \int_0^\beta dt e^{\mathcal{g}_+(t)} = -\mathcal{Q} \int_0^\beta dt \ddot{\mathcal{g}}_+(t),$$

which integrates to $\dot{\mathcal{g}}_-(\tau) = 2\mathcal{Q}\dot{\mathcal{g}}_+(0)$, hence matching the postulated solution. Together with (A8), one may show that this leaves an error with maximum magnitude of $4 \sin^2(\pi v/2)$ at $\tau = 0$.

With all three of these error terms, one notices that $\Delta R_i \xrightarrow{q \rightarrow \infty} 0$ as long as large $|\ln[v/\lambda]| \lesssim q$. For large λ , the relation (A2) implies that $v \sim 1$. This means our solutions remains valid for any $\ln \beta\mathcal{J} \ll q$, which includes the polynomial scalings $\beta\mathcal{J} \sim q^\alpha$ considered in the work, i.e., $T = \tilde{T} q^{-1}$ and $T = \tilde{T} q^{-2}$, with $J = \mathcal{O}(q^0)$. ■

APPENDIX B: LOW-TEMPERATURE CHARGE TRANSITION

Claim 2. At small reduced temperature $T_r \equiv \tilde{T}/\tilde{T}_{\text{crit}}$, where $\tilde{T}_{\text{crit}} = 2e^{-3/2}J$, the charge density jumps as

$$\mathcal{Q}_g = \frac{\cosh^{-1}[e^{2\tilde{\beta}J}]}{q2\tilde{\beta}J} \rightarrow \mathcal{Q}_\ell = \frac{\sqrt{1 - e^{-4\tilde{\beta}J}}}{2}. \quad (\text{B1})$$

For convenience, we have defined $\tilde{T} \equiv q^{-1}\bar{T}$, $\tilde{\mu} \equiv q^{-1/2}\bar{\mu}$.

As a special case, if we consider \tilde{T} , $\tilde{\mu}$ fixed in the large- q limit, we find a transition from $\mathcal{Q} = 0 \rightarrow \sqrt{1 - e^{-4\tilde{\beta}J}}/2$, i.e.,

a transition to a finite nonrescaled charge density as discussed in the work.

Proof. Consider the grand and chemical potentials

$$\tilde{\Omega} = -2\mathcal{J} - 2\tilde{Q}^2[2\mathcal{J} + \tilde{T}], \quad \tilde{\mu} = 4\tilde{Q}[\mathcal{J} + \tilde{T}], \quad (\text{B2})$$

at low reduced temperature. In other words, consider the asymptotic behavior for $\tilde{T} \ll J$ of the charge densities on both sides of the coexistence line. Though we do not have explicit forms for these charge densities, we can gain some insight by considering Fig. 1 from the work. Here we note that the gaseous solution must be smaller than the charge density at the first turning point of $\tilde{\mu}(\tilde{Q})$, $\tilde{Q}_g < \tilde{Q}_b$, while the liquid charge density must be larger than the second turning point $\tilde{Q}_\ell > \tilde{Q}_c$. These turning points are

$$\tilde{Q}_b = \sqrt{\frac{1}{2} - w_0 \left[\frac{-T_r}{e} \right]}, \quad \tilde{Q}_c = \sqrt{\frac{1}{2} - w_{-1} \left[\frac{-T_r}{e} \right]}, \quad (\text{B3})$$

where $w(x)$ is the product log satisfying $w e^w = x$. Here the subscripts indicate the various branches, with w_0 corresponding to the principal branch.

On the gaseous side we have $\tilde{Q}_b = \sqrt{1/2} + \mathcal{O}(T_r)$, implying relatively small charge densities $\tilde{Q}_g < \sqrt{1/2}$. As such, the strong coupling $\mathcal{J}_g \equiv J e^{-\tilde{Q}_g^2} = \mathcal{O}(T_r^0)$ dominates in (B2),

$$\tilde{\Omega}_g = -2\mathcal{J}_g - 4\tilde{Q}_g^2[\mathcal{J}_g + \mathcal{O}(T_r)], \quad \tilde{\mu}_g = 4\tilde{Q}_g[\mathcal{J}_g + \mathcal{O}(T_r)]. \quad (\text{B4})$$

For the liquid phase we have $\tilde{Q}_c = \sqrt{\ln[\beta_r \ln \beta_r]} + \mathcal{O}(1)$, with $\beta_r \equiv 1/T_r$. As such, we have a relatively large charge density $\tilde{Q}_\ell > \tilde{Q}_c$, hence a large suppression in the coupling $\mathcal{J}_\ell \lesssim \tilde{T} / \ln \beta_r$. With this (B2) reduces to

$$\tilde{\Omega}_\ell = -2\tilde{T} \tilde{Q}_\ell^2 [1 + \mathcal{O}(\mathcal{J}_\ell/\tilde{T})], \quad \tilde{\mu}_\ell = 4\tilde{Q}_\ell \tilde{T} [1 + \mathcal{O}(\mathcal{J}_\ell/\tilde{T})], \quad (\text{B5})$$

where $\mathcal{J}_\ell/\tilde{T} = \mathcal{O}(1/\ln \beta_r)$. Here, the weakly interacting phase (B5) is in fact the leading-order solution to free fermions,

$$\tilde{\Omega}_0 = \frac{\tilde{T}}{2} \ln [1 - 4Q_\ell^2], \quad \tilde{\mu}_0 = 2 \frac{\tilde{T}}{\sqrt{q}} \tanh^{-1}[2Q_\ell], \quad (\text{B6})$$

i.e., expanding (B6) for small nonrescaled charge densities $Q \equiv \tilde{Q}/\sqrt{q}$ yields (B5) to leading order. These are the full solutions at large charge densities, since this yields small effective interactions. An analysis using (B5), while valid at infinite q , for fixed tilde'd variables yields the incorrect zero-temperature limit expressions for large finite q . As such, we focus on phase transitions from (B4) to (B6), which includes the previous analysis as a solution under the appropriate limit. The phase transition occurs at the point of equal grand and chemical potential. Equating the expressions in (B4) and (B6) yields the equations

$$\ln(1 - 4Q_\ell^2) = -4\tilde{\beta} \mathcal{J}_g [1 + 2\tilde{Q}_g^2], \quad 2Q_\ell = \tanh[2\tilde{Q}_g \tilde{\beta} \mathcal{J}_g],$$

where $\tilde{Q} \equiv q^{-1/2} \tilde{Q}$. The solution to these two are the roots of

$$F(\tilde{Q}_g) = 1 + 2\tilde{Q}_g^2 - \frac{\ln \cosh[2\tilde{\beta} \mathcal{J}_g \tilde{Q}_g]}{2\tilde{\beta} \mathcal{J}_g}. \quad (\text{B7})$$

As $\tilde{T} \rightarrow 0$, the root is at $\tilde{Q}_g = 1 + 2\tilde{Q}_g^2 \sim 1$. Together with (B4), this suggests that there is a first-order transition at

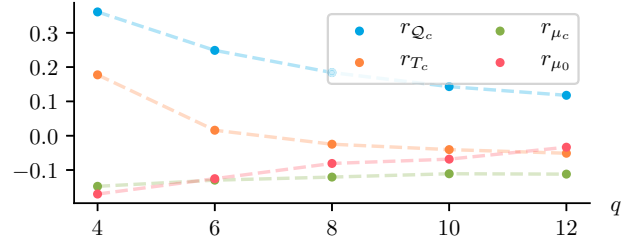


FIG. 4. Plots of the relative errors (D1) between the large- q estimated critical points and the numerically calculated critical points for various finite q values.

$\tilde{\mu}_0 = 4J$. Above zero temperature, for any $\tilde{Q}_g = o(q^0)$ we simply have $\mathcal{J}_g \sim J$ and as such the root of F , \tilde{Q}_g , and the corresponding liquid charge density as given in (B1). ■

APPENDIX C: SCALE-INVARIANT GRAND POTENTIAL

Claim 3. Consider the shifted rescaled grand potential from the work

$$f = -\rho^2[3\rho^2/4 + t/3] + \mathcal{O}(\rho^5). \quad (\text{C1})$$

Here ρ is the solution to the equation of state (B5) around the critical point

$$m - 2t/3 = \rho(2t/3 + \rho^2) + \mathcal{O}(\rho^4), \quad (\text{C2})$$

with m, t , and ρ defined in the work. We claim that in terms of the ordering field $\tilde{h} = m - 2t/3$ that (C1) is homogeneous $f(t, \tilde{h}) = t^2 f(1, \tilde{h}|t|^{-3/2})$.

Proof. The above function f satisfies $\partial_m f = -\rho$. We may rewrite f in terms of $\rho \equiv -|t|^{1/2} \Psi$, as $f = |t|^2 \Psi$, where for $t < 0$,

$$\Psi \equiv -\dot{\Psi}^2[3\dot{\Psi}^2/4 - 1/3] + \mathcal{O}(\rho^5).$$

To prove homogeneity, we must show that $\dot{\Psi}$ is a function only of $\omega \equiv \tilde{h}|t|^{-3/2}$, hence leaving $\Psi(\omega) \equiv f(1, \omega)$. From (C2) we have the relation $\omega = \dot{\Psi}(\Psi^2 - 2/3)$. This implies that $\dot{\Psi}$ is indeed purely a function of ω . One may further show that $\partial_\omega \Psi(\omega) = \dot{\Psi}(\omega)$. The liquid phase solution is

$$\dot{\Psi}_\ell(\omega) = \begin{cases} [2/3]^{1/2} + 3\omega/4 - (3/2)^{7/2} \omega^2/4 + \mathcal{O}(\omega^3) \\ \omega^{1/3} + 2\omega^{-1/3}/9 + \mathcal{O}(\omega^{-5/3}). \end{cases}$$

Over the range $\dot{\Psi} \leq 2^{3/2}/3$, $\omega(\dot{\Psi})$ is three-to-one, with the two remaining solutions $\dot{\Psi}_{b-c}(\omega) = \dot{\Psi}_\ell(-\omega) - \dot{\Psi}_\ell(\omega)$ and $\dot{\Psi}_g(\omega) = -\dot{\Psi}_\ell(-\omega)$, where the latter corresponds to the gaseous phase. Explicitly,

$$\Psi_\ell(\omega) = \begin{cases} -1/9 - \sqrt{2/3}\omega - 3\omega^2/8 + \mathcal{O}(\omega^3) \\ -\frac{3}{4}\omega^{4/3} - \frac{\omega^{2/3}}{3} - \frac{2}{27} + \mathcal{O}(\omega^{-2/3}). \end{cases}$$

Considering the grand potential, one notes that the gaseous solution is thermodynamically preferred for $\omega < 0$ while the liquid solution is preferred for $\omega > 0$, i.e., $\dot{\Psi}^*(\omega) = \text{sgn}(\omega)\dot{\Psi}_\ell(|\omega|)$. ■

APPENDIX D: OVERLAP WITH FINITE- q MODEL

We can test the extent to which our large- q results capture the finite- q physics by comparing our derived quantities to the

numerically derived ones in [10, Table I]. We focus on the relative error

$$r_x = \frac{x}{x^{(q)}} - 1, \quad (\text{D1})$$

where x is the large- q estimation, while $x^{(q)}$ corresponds to the numerical results. The particular quantities we compare are the critical values

$$\mathcal{Q}_c = \sqrt{\frac{3}{2q}}, \quad T_c = \frac{2J e^{-3/2}}{q} \quad \mu_c = 6\mathcal{Q}_c T_c, \quad \mu_0 = \frac{4J}{q^2}$$

derived in the work. We choose a matching coupling constant to [10], $J = \sqrt{q} 2^{1-q}$. As such, all the critical values become functions of q , which we compare with their numerically derived values in Fig. 4.

The comparison is given for $q \in \{4, 6, 8, 10, 12\}$. From this we note that the estimated values appear to converge to their finite q values rather fast as q increases. In order to reduce the relative error at smaller values of q , for instance, $q = 4$, one would have to consider $1/q^2$ corrections to the Green's functions [45].

-
- [1] S. Sachdev, Bekenstein-Hawking Entropy and Strange Metals, *Phys. Rev. X* **5**, 041025 (2015).
- [2] W. Fu, The Sachdev-Ye-Kitaev model and matter without quasiparticles, Ph.D. thesis, Harvard University, 2018.
- [3] T. Azeyanagi, F. Ferrari, and F. I. Schaposnik Massolo, Phase Diagram of Planar Matrix Quantum Mechanics, Tensor, and Sachdev-Ye-Kitaev Models, *Phys. Rev. Lett.* **120**, 061602 (2018).
- [4] E. Witten, An SYK-like model without disorder, [arXiv:1610.09758](https://arxiv.org/abs/1610.09758).
- [5] S. Sachdev and J. Ye, Gapless Spin-Fluid Ground State in a Random Quantum Heisenberg Magnet, *Phys. Rev. Lett.* **70**, 3339 (1993).
- [6] J. Maldacena and D. Stanford, Remarks on the Sachdev-Ye-Kitaev model, *Phys. Rev. D* **94**, 106002 (2016).
- [7] J. C. Louw and S. Kehrein, Thermalization of many many-body interacting Sachdev-Ye-Kitaev models, *Phys. Rev. B* **105**, 075117 (2022).
- [8] C. Zanoci and B. Swingle, Near-equilibrium approach to transport in complex Sachdev-Ye-Kitaev models, *Phys. Rev. B* **105**, 235131 (2022).
- [9] X. Y. Song, C. M. Jian, and L. Balents, Strongly Correlated Metal Built from Sachdev-Ye-Kitaev Models, *Phys. Rev. Lett.* **119**, 216601 (2017).
- [10] F. Ferrari and F. I. Schaposnik Massolo, Phases of melonic quantum mechanics, *Phys. Rev. D* **100**, 026007 (2019).
- [11] J. Maldacena and X. Qi, Eternal traversable wormhole, [arXiv:1804.00491](https://arxiv.org/abs/1804.00491).
- [12] N. Sorokhaibam, Phase transition and chaos in charged SYK model, *J. High Energy Phys.* **07** (2020) 055.
- [13] R. A. Davison, W. Fu, A. Georges, Y. Gu, K. Jensen, and S. Sachdev, Thermoelectric transport in disordered metals without quasiparticles: The Sachdev-Ye-Kitaev models and holography, *Phys. Rev. B* **95**, 155131 (2017).
- [14] W. Cho, D. Kim, and J. Park, Isobaric critical exponents: Test of analyticity against NIST reference data, *Front. Phys.* **6**, 00112 (2018).
- [15] D. Kubizňák and R. B. Mann, P-V criticality of charged AdS black holes, *J. High Energy Phys.* **07** (2012) 033.
- [16] B. R. Majhi and S. Samanta, P-V criticality of AdS black holes in a general framework, *Phys. Lett. B* **773**, 203 (2017).
- [17] B. P. Dolan, Pressure and compressibility of conformal field theories from the AdS/CFT correspondence, *Entropy* **18**, 169 (2016).
- [18] S. Cao, Y.-C. Rui, and X.-H. Ge, Thermodynamic phase structure of complex Sachdev-Ye-Kitaev model and charged black hole in deformed JT gravity, [arXiv:2103.16270](https://arxiv.org/abs/2103.16270).
- [19] A. Dehyadegari, B. R. Majhi, A. Sheykhi, and A. Montakhab, Universality class of alternative phase space and Van der Waals criticality, *Phys. Lett. B* **791**, 30 (2019).
- [20] A. Mandal, S. Samanta, and B. R. Majhi, Phase transition and critical phenomena of black holes: A general approach, *Phys. Rev. D* **94**, 064069 (2016).
- [21] A. Chamblin, R. Emparan, C. V. Johnson, and R. C. Myers, Charged AdS black holes and catastrophic holography, *Phys. Rev. D* **60**, 064018 (1999).
- [22] C. Niu, Y. Tian, and X.-N. Wu, Critical phenomena and thermodynamic geometry of Reissner-Nordström-anti-de Sitter black holes, *Phys. Rev. D* **85**, 024017 (2012).
- [23] J. Zaanen, Y. Liu, Y.-W. Sun, and K. Schalm, *Holographic Duality in Condensed Matter Physics* (Cambridge University Press, Cambridge, England, 2015).
- [24] J. Maldacena, S. H. Shenker, and D. Stanford, A bound on chaos, *J. High Energy Phys.* **08** (2016) 106.
- [25] J. Wang and M. A. Anisimov, Nature of vapor-liquid asymmetry in fluid criticality, *Phys. Rev. E* **75**, 051107 (2007).
- [26] J. W. Loram, K. A. Mirza, J. R. Cooper, and W. Y. Liang, Electronic Specific Heat of $\text{YBa}_2\text{Cu}_3\text{O}_{6+x}$ from 1.8 to 300 K, *Phys. Rev. Lett.* **71**, 1740 (1993).
- [27] B. Michon, C. Girod, S. Badoux, J. Kačmarčík, Q. Ma, M. Dragomir, H. A. Dabkowska, B. D. Gaulin, J.-S. Zhou, S. Pyon, T. Takayama, H. Takagi, S. Verret, N. Doiron-Leyraud, C. Marcenat, L. Taillefer, and T. Klein, Thermodynamic signatures of quantum criticality in cuprate superconductors, *Nature (London)* **567**, 218 (2019).
- [28] A. Legros, S. Benhabib, W. Tabis, F. Laliberté, M. Dion, M. Lizaire, B. Vignolle, D. Vignolles, H. Raffy, Z. Z. Li *et al.*, Universal T-linear resistivity and Planckian dissipation in overdoped cuprates, *Nat. Phys.* **15**, 142 (2019).
- [29] D. Kubizňák, R. B. Mann, and M. Teo, Black hole chemistry: Thermodynamics with lambda, *Class. Quantum Gravity* **34**, 063001 (2017).
- [30] S. A. Hartnoll, C. P. Herzog, and G. T. Horowitz, Holographic superconductors, *J. High Energy Phys.* **12** (2008) 015.
- [31] U. Karahasanovic, F. Krüger, and A. G. Green, Quantum order-by-disorder driven phase reconstruction in the vicinity of ferromagnetic quantum critical points, *Phys. Rev. B* **85**, 165111 (2012).
- [32] S. W. Hawking and D. N. Page, Thermodynamics of black holes in anti-de Sitter space, *Commun. Math. Phys.* **87**, 577 (1983).
- [33] Y. Sekino and L. Susskind, Fast scramblers, *J. High Energy Phys.* **10** (2008) 065.

- [34] S. H. Shenker and D. Stanford, Black holes and the butterfly effect, *J. High Energy Phys.* **03** (2014) 067.
- [35] J. Engelsöy, T. G. Mertens, and H. Verlinde, An investigation of AdS₂ backreaction and holography, *J. High Energy Phys.* **07** (2016) 139.
- [36] P. Nayak, A. Shukla, R. M. Soni, S. P. Trivedi, and V. Vishal, On the dynamics of near-extremal black holes, *J. High Energy Phys.* **09** (2018) 048.
- [37] U. Moitra, S. K. Sake, S. P. Trivedi, and V. Vishal, Jackiw-Teitelboim gravity and rotating black holes, *J. High Energy Phys.* **11** (2019) 047.
- [38] U. Moitra, S. P. Trivedi, and V. Vishal, Extremal and near-extremal black holes and near-CFT₁, *J. High Energy Phys.* **07** (2019) 055.
- [39] Z. Luo, Y.-Z. You, J. Li, C.-M. Jian, D. Lu, C. Xu, B. Zeng, and R. Laflamme, Quantum simulation of the non-Fermi-liquid state of Sachdev-Ye-Kitaev model, *npj Quantum Inf.* **5**, 1 (2019).
- [40] A. M. Garcia-Garcia, B. Loureiro, A. Romero-Bermúdez, and M. Tezuka, Chaotic-Integrable Transition in the Sachdev-Ye-Kitaev Model, *Phys. Rev. Lett.* **120**, 241603 (2018).
- [41] J. Kim and X. Cao, Comment on “Chaotic-Integrable Transition in the Sachdev-Ye-Kitaev Model,” *Phys. Rev. Lett.* **126**, 109101 (2021).
- [42] I. R. Klebanov, A. Milekhin, G. Tarnopolsky, and W. Zhao, Spontaneous breaking of U(1) symmetry in coupled complex SYK models, *J. High Energy Phys.* **11** (2020) 162.
- [43] S. Sahoo, E. Lantagne-Hurtubise, S. Plugge, and M. Franz, Traversable wormhole and Hawking-Page transition in coupled complex SYK models, *Phys. Rev. Res.* **2**, 043049 (2020).
- [44] V. Rosenhaus, An introduction to the SYK model, *J. Phys. A: Math. Theor.* **52**, 323001 (2019).
- [45] G. Tarnopolsky, Large q expansion in the Sachdev-Ye-Kitaev model, *Phys. Rev. D* **99**, 026010 (2019).

4.3 Scaling and field mixing

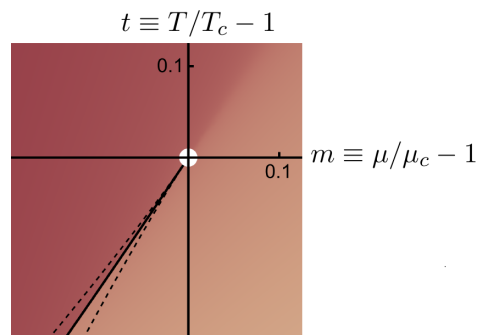


Figure 4.4: The region around the critical point denoted in the white dot at the origin

Let us now focus more on the region around the critical point, i.e., we zoom in on this region as illustrated in Fig. 4.4. Close to a second-order phase transition various measurable quantities display power laws with associated *effective* exponents. To define a universality class, one must find the *critical* exponents associated with the second-order phase transition. These are often read off from the temperature scaling in various thermodynamic observables. This is not always sufficient, however. The reason is that the critical exponents are not necessarily the same as the power laws displayed in the thermodynamics quantities. This is because they are defined by something more fundamental, namely the scaling laws associated with the relevant thermodynamic potential. In particular, under the renormalization group flow, in the presence of a second-order phase transition, the thermodynamic potential will flow towards the corresponding fixed point [178, 183]. Close to this fixed point, its secular contribution f is a homogeneous function of the scaling fields. To fit this to experiment one requires enough flexibility in this scaling form for the free energy. One may then read off the critical exponents from it. The key factor is to allow various fields, such as chemical potential and temperature, to mix in possibly nonlinear ways in the homogeneous form of the free energy. This is the revised scaling hypothesis⁵ [187]. This then allows one to correctly fit the form of f and its dependence on a non-linear mixture of the bare fields. Without taking field mixing into account one can erroneously mistake effective exponents for critical exponents [61].

For our analysis, we only need to focus on the mixing of two bare fields, namely the temperature and conjugate (to the order parameter) fields

$$t \equiv T/T_c - 1, \quad m \equiv \mu/\mu_c - 1 \quad (4.14)$$

respectively. The scaling fields which enter into f , the ordering field \hbar_1 , and the thermal field \hbar_2 can then mix in a complicated non-linear way with m, t [188, 189]. The thermodynamic potential is then a homogeneous function of these fields

$$f(\hbar_2, \hbar_1) = |\hbar_2|^{2-\alpha} \Psi \left(\frac{\hbar_1}{|\hbar_2|^{2-\alpha-\beta}} \right), \quad \hbar_2 < 0. \quad (4.15)$$

The standard associations of critical exponents with thermodynamic observables hold in the case when the bare and scaling fields equal another $m = \hbar_1, t = \hbar_2$. Here, for instance, m could be the magnetic field. As an example, consider a simple quartic free energy density $f = \min_{\phi} \{t\phi^2/2 + 4\phi^4 - m\phi\}$. It has the homogeneous form

$$f(t, m) = -|t|^2 \Psi(m/|t|^{3/2}), \quad (4.16)$$

⁵The generalization of this is the complete scaling hypothesis [184] which also allows for pressure mixing. This is important in understanding certain divergences lattice gases [184–186].

where the scaling function is

$$\Psi(\omega) = \begin{cases} 1/4 + \omega + \omega^2/4 + \mathcal{O}(\omega^3) \\ \omega^{4/3}(3/4 + \mathcal{O}(\omega^{-2/3})) \end{cases} . \quad (4.17)$$

From this, together with (4.15), we can immediately read off $\alpha = 0$ and $\beta = 1/2$. One can then check that the specific heat $C_\mu = -\partial_t^2 f(t, 0)$ and the order parameter, $\phi = \partial_m f$, at critical field strength $m = 0$ ($\mu = \mu_c$), indeed have power laws in t with exponents $\alpha_\mu = 0$ and $\beta_\mu = 1/2$ respectively. Here we have used subscripts to denote the corresponding power laws while holding a specific field fixed. Next, by considering the susceptibility $\chi_\mu(t) = \partial_m^2 f(t, m)|_{m=0}$ one finds $\gamma_\mu = 1/3$. Finally, the relation between the order parameter and conjugate, $\mathcal{M} \propto m^3$ yields the final exponent $\delta = 3$. For such a model without field mixing, one sees how these exponents are fully determined by α , β and hence force the Rushbrooke, $\alpha + \gamma + 2\beta = 2$, and Widom, $\gamma = \beta(\delta - 1)$, identities⁶. Further, as tabulated in Table 4.5, they are clearly the same as the critical exponents.

Mean field critical exponents	$\alpha = 0$	$\beta = 1/2$	$\gamma = 1/3$	$\delta = 3$
Quartic model effective exponents	$\alpha_\mu = 0$	$\beta_\mu = 1/2$	$\gamma_\mu = 1/3$	not applicable
large- q SYK effective exponents	$\alpha_\mu = 2/3$	$\beta_\mu = 1/3$	$\gamma_\mu = 2/3$	not applicable

Figure 4.5: Table of critical and effective exponents of two different mean field models.

In general, however, the above analysis should be done in the same way but with the replacement $t \rightarrow \hbar_2$, $m \rightarrow \hbar_1$. Take for instance the SYK model which has essentially the same scaling function, however, with the ordering field $\hbar_1 = m - 2t/3$. This field mixing yields comparatively different power laws when keeping the bare (conjugate) ordering field fixed, tabulated in Table 4.5, which do not match the critical exponents from the mean-field universality class⁷. Calculating the same quantities, however, at critical ordering field $\hbar_1 = 0$ would yield the critical exponents as it did for the quartic example.

4.3.1 Comparison to numerics

Given the discussion of field mixing and effective exponents, we now return to the topic of the numerically calculated power laws. Since we know from our analytical results that the SYK model does have field mixing, one should be careful not to mistake effective exponents for critical exponents. Since the numerical studies focused on power laws of observables, rather than the scaling form of the grand potential, they, in fact, calculated these effective exponents. While some effective exponents can at times overlap with the critical exponents, this is not a general rule, as is seen in the large- q SYK model. Further, the calculation of such power laws is numerically a highly

⁶These scaling laws are universal in nature [190]. Remarkably, in many experiments and exactly solved models, the Rushbrooke inequality saturates to equality. The Widom equality holds for magnetic systems and fluids.

⁷For strongly correlated systems, if the interactions are long ranged, the system often has a mean-field description [191–193]. Since the SYK model is not only long-ranged but has all-to-all coupling, such mean-field critical exponents might be expected.

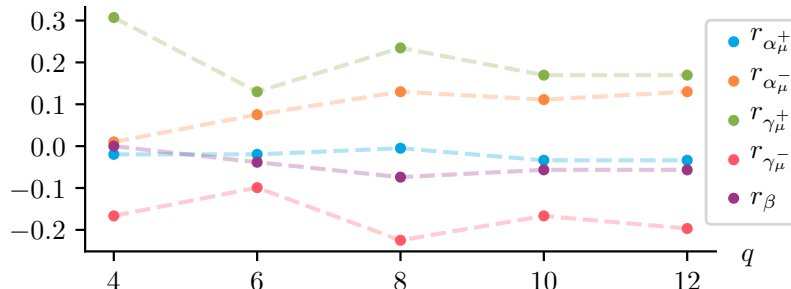


Figure 4.7: Relative error $r_\sigma(q) = \sigma^{(\infty)}/\sigma^{(q)} - 1$ for the effective exponents, where $\sigma^{(q)}$ are the finite q values tabulated in [180].

non-trivial task, with large numerical errors. This is reflected in the fact that three different studies found three different sets of effective exponents.

Source	α_μ^+	α_μ^-	β	γ_μ^+	γ_μ^-
[179]	0.61 ± 0.01	0.71 ± 0.01	0.52 ± 0.02	0.51 ± 0.01	0.80 ± 0.05
[180]	0.68 ± 0.02	0.66 ± 0.02	0.50 ± 0.02	0.51 ± 0.01	0.80 ± 0.01
[181]	0.6388	0.6644	0.6397	0.5815	0.7537

Figure 4.6: Numerically calculated effective exponents corresponding to the $q = 4$ cSYK model.

Note that the finite- q studies find asymmetric effective exponents. In other words, the exponents are direction dependent. For instance $C_\mu(\pm|t|) \sim |t|^{\alpha_\pm}$, where α_+ is for $t > 0$ and α_- is for $t < 0$. In general, the subscript $+$ indicates the limit from above the critical point, and a subscript $-$ indicates the limit from below the critical point.

Note that the final study [181], corresponding to the final row, did not mention the numerical error. Importantly, however, the values calculated in [181], hardly ever fall within the range of the numerical error estimated in the first two studies [179, 180]. Further, though the numerical error was calculated in the first two studies, this error was underestimated. This can be seen in the error range of α_μ^\pm not overlapping.

Let us however ignore this problem of numerical error for now. Here we wish to just gain some idea of how close our analytic results are to the approximate numerical results. Here we will still study the overlap of these results with our analytical results when setting $q = 4$. To do this, we just compare to $\alpha_\mu^\pm = 0.61, 0.71$; $\gamma_\mu^\pm = 0.51, 0.80$; $\beta = 0.52$ and $\alpha_\mu^\pm = 0.64, 0.66$; $\gamma_\mu^\pm = 0.58, 0.75$; $\beta = 0.64$, respectively. In comparing to the average exponents, we find relative errors, $r_x = x/\bar{x} - 1$, $r_{\alpha_\mu} = 0.01$, $r_{\gamma_\mu} = 0.01$, $r_\beta = 0.03$, and $r_\beta = 0.04$, which are all rather close to zero. Considering the finite $q = 4 \rightarrow 12$ results for the effective exponents, we note that there are significant finite q fluctuations around our critical exponents seen in Fig. (4.7). However, compared to the average, the relative error always remains below 5%.

4.4 Motivation for studying the large- q case

Let us close the chapter by giving a few additional motivations for considering the large- q cSYK model. We start by summarizing what we have seen throughout the thesis. In Sec. 2.1 we gave some mathematical motivation in terms of viewing the $1/q$ expansions as a fast converging series. This is in agreement with the analytically proved error bound in the appendix of Louw *et. al.* [61], included in Sec. 4.2.1. The key point is that these results are reflective of the $q \geq 4$ results and even predictive in the sense that one often obtains small differences when setting $q = 4$ in the results which were derived under the large- q limit. Throughout the thesis, this was reflected in various results. We saw how well the large- q results overlapped with the $q \geq 4$ IR results in Sec. 2.4.1. The overlap continued in the Lyapunov exponents discussed in Sec. 3.1.2 and even the electrical and thermal conductivity discussed in Sec. 3.3.1.1.

We next discuss the motivation for studying such a $1/q$ expansion in the grand canonical ensemble. The derived exact analytical results, including the scale invariant form of the grand potential, have allowed us to unambiguously classify the universality class. This scale invariant form also illustrates that one must take field mixing into account when calculating the critical exponents. Such often overlooked field mixing implies that one should be careful to distinguish the power laws found in observables, which we have called effective exponents, from the critical exponents. We showed that the phase transition falls into the mean-field van der Waals liquid universality class. While most power laws in observables are also found to overlap with mean-field, some do not, highlighting the aforementioned field mixing. This is in contrast to the power laws found in the numerical studies of the finite q case ([179–181]) which were non-mean-field. One should note that all three of these studies found different power laws, which is reflective of the notoriously large numerical error involved in such numerical algorithms used to calculate the effective exponents.

Our results are thus in line with the belief that all-to-all models are mean-field. This statement is not only in the sense of the power laws but also in the particular structure of the free energies [191, 192] and dynamical properties [193].

The aforementioned mean-field van der Waals-like critical behavior is also found in charged non-rotating, Reissner–Nordström (RN), black holes [194–196]. As such, our result may be viewed from the perspective of the AdS/CFT correspondence, first introduced by Maldacena in [197]. In fact, the SYK model owes its renewed interest to possibly being a simple example of such a holographic principle [56]. This mean-field behavior of most (if not all⁸) black holes, is a well-known property. As such, the fact that the large- q limit is mean-field-like can be seen as an additional verification that a dual exists, and hence a consequence of holography. Typically, such a mapping corresponds to a weak-strong duality. Since their rescaled phase diagram corresponds to the extremely low temperature in terms of the original variable, hence corresponding to strong coupling. It is thus expected that the dual black hole should have a semiclassical (weakly curved) gravitational description which is generically mean-field.

A detailed correspondence with the phase transition in (charged) RN black holes can further constrain the type of gravity theory that the large- q complex SYK model might be dual too. These

⁸Some possible exceptions exist [198, 199], however, one should note the listed power laws, are, in fact, the effective exponents, rather than the critical exponents, defining the scaling function.

results further encourage the use of holography further away from zero temperature. It narrows down the list of possible gravity duals to the SYK model [98]. The analytically derived expressions, the power laws, the equation of state, and grand potential, serve as a guide towards finding this dual. Indeed, as we will discuss next in Chapter 5, one may, in fact, find the exact bulk dual gravitational model to the charge large- q SYK model. Such an exact, non-trivial connection between statistical mechanics and gravity, has the potential of pointing the way to new developments in holography.

Appendix 4.A: Numerical calculation of the phase diagram

Here we give the details surrounding the numerical calculations required to produce the phase diagram. Note that we already have the analytical expressions for both the EOS and the grand potential. As such, we only need to find the value of $\tilde{\mu}$ where the grand potential intersects for each temperature \tilde{T} , illustrated in Fig. 4.8. If one rather focuses on the temperatures where $\tilde{\Omega}$ intersects, then we find the coexistence/binodal curve. This is the line over which the first-order phase transition occurs. In other words we have to solve the problem

$$\tilde{\Omega}(\tilde{Q}_\ell, \tilde{T}) = \tilde{\Omega}(\tilde{Q}_g, \tilde{T}), \quad \tilde{\mu}(\tilde{Q}_\ell, \tilde{T}) = \tilde{\mu}(\tilde{Q}_g, \tilde{T}).$$

This is simply done by inverting the function $\tilde{\mu}(\tilde{Q}, \tilde{T})$ for each of the three segments given in pink, blue, and green, and then solving the problem by finding the root.

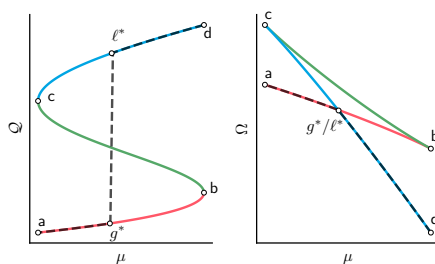


Figure 4.8: Three solutions to the equation of state. The dashed line denotes the solution which minimizes the grand potential, i.e., it is the thermodynamically preferred state.

Doing this, one finds the following results: Near the critical point $\mu_R \in [10^{-2}, 1]$, this curve is given by $T_R^* = T_{R,\text{num}}^* \pm 1.5 \cdot 10^{-3}$, where

$$T_{R,\text{num}}^*(\mu_R) \equiv 1 + \frac{\sqrt{b(b/4 - 1)(\mu_R^2 - 1) + (1 - b/2)^2} + 1 - b/2}{b/2 - 2}, \quad b = \tilde{Q}_c^3 \tilde{\mu}_c. \quad (4.18)$$

Here we have defined the reduced temperature and chemical potential as

$$T_R = T/T_c, \quad \mu_R = \mu/\mu_c.$$

For $\mu_R \in [10^{-2}, 1]$, the relative numerical error $r(T_R^*) = |T_R^*(\mu_R)/T_{R,\text{num}}^*(\mu_R) - 1| \in [0, 0.5 \cdot 10^{-2}]$. It begins to diverge at smaller chemical potentials. With the approximate coexistence line $T_{R,\text{num}}^*(\mu_R)$, the numerics involved to verify it become rather simple.

Chapter 5

Black hole thermodynamics

A standard layman’s description of black holes is that they are objects with such a strong gravitational pull that not even light can escape. However, in the 1970s, Hawking showed that black holes are not quite so “black” after all. In fact, they can emit thermal radiation [200, 201]. This then allows one to associate a temperature with them. For a Schwarzschild (uncharged and non-rotating) black hole, this is simply given by [202]

$$T_{\text{H}} = 1/(8\pi M). \quad (5.1)$$

Such Hawking temperatures thus generated the novel field of black hole thermodynamics.

In black hole thermodynamics one focuses on asymptotically anti-de Sitter (AdS) spaces with negative cosmological constant $\Lambda < 0$. To understand why, let us consider our universe. Here $\Lambda > 0$ acts as a negative pressure, leading to inflation. This leads to an additional horizon, the cosmic horizon, the boundary between the observable universe and the region that is causally disconnected from it. This seemingly innocent observation makes it very difficult to define a well-behaved global energy. In the asymptotically AdS $_{d+1}$ case, however, there is no cosmic horizon and one can define the energy as that seen by an observer at asymptotic infinity¹.

5.1 Bekenstein bound and the implication of holography

On top of a temperature, one can even associate an entropy with black holes known as the Bekenstein-Hawking entropy [203]

$$S_{\text{BH}} = A/(4\ell_P^2). \quad (5.2)$$

The entropy, á la Boltzmann, is a measure of multiplicity $S = k_{\text{B}} \ln W$, i.e., a measure of the number of microstates W that describe the macrostate. By the no-hair theorem, we know that any (classical) black hole is *fully* described by *only* three parameters, namely its mass M , charge Q_{B}

¹Due to the cosmic horizon in dS there is no well-behaved boundary at infinity. Further, the cosmic horizon is associated with a nonzero temperature, i.e., it emits its own Hawking radiation. This energy competes with the gravitational energy of the system, making it difficult to isolate the energy content attributed solely to the mass distribution. Given a black hole the two horizons would exchange thermal radiation.

and angular momentum [204]. In other words, classically, there would be very few microscopic degrees of freedom. As such, a somewhat naive assumption would be that black holes cannot have any significant entropy, since they appear devoid of any structure. However, the size of the Planck length ℓ_P is of the order 10^{-35} m, hence even a small black hole is associated with a stupendous number of microscopic degrees of freedom. The appearance of the Planck length $\ell_P^2 = \hbar G_N / c^3$, highlights that this is a semi-classical result stemming from quantum corrections. This entropy, as a measure of microscopic degrees of freedom corresponding to macroscopic observables, would imply that the degrees of freedom are quantum gravitational in nature.

Stranger even, this entropy is proportional to its horizon surface area A rather than its volume V . In fact (5.2) serves as a bound on entropy [205]. To see this, consider an ordinary quantum system with mass² $M - \delta M$ and entropy S_0 , filling a sphere with area A . By forcing δM energy into the sphere, so keeping A fixed, with entropy δS , the system necessarily collapses into a black hole with mass M . From the second law, the entropy must increase: $S_0 + \delta S \leq S_{\text{BH}}$, and we conclude that $S_0 \leq S_{\text{BH}}$. In other words, S_{BH} is the maximum entropy that can reside in a region of area A . To see how strange this is, let us consider a lattice of N particles. For large temperatures, the von Neumann entropy is proportional to the effective degrees of freedom $S = \alpha N \ln 2$. Since the Hilbert space dimension is 2^N , the maximum entropy would correspond to $\alpha = 1$. For a spherical lattice with lattice spacing a , the volume is approximated by $V = a^3 N$ [206]. Hence, the typical entropy for a quantum system satisfies a volume law, which will, at astronomical volumes, overshoot (5.2). As such, a theory of quantum gravity would naturally have to yield an enormous reduction in effective degrees of freedom. In other words, a quantum gravitational system of volume V must be fully encodable on its surface of area A . This is the holographic principle [207].

The goal of holography is to find the lower dimensional model living on the surface. This is typically done in string theory, for instance, the first AdS/CFT correspondence [197]. Finding and understanding such mappings is a very difficult task. We have a more modest goal: to find a quantum mechanical model which shares some aspects of gravity at the semi-classical level [126]. Here we focus on a condensed matter-gravity duality. Such dualities have been studied in the past to understand non-Fermi liquids in $(2 + 1)$ -dimensions, so-called holographic strange metals [52, 208–210].

5.1.1 Simplest model for holography

Here we focus on the simplest example, namely the $(0 + 1)$ -dimensional cSYK model. We start by motivating that such a duality exists by identifying non-trivial universal behaviors in gravity, then seeing if these features are matched by the cSYK model. The gravitational features should ideally be shared with all black holes. The original universal feature which was shared by both the condensed matter model (SYK) and gravity was the saturation of the chaos bound discussed in Chapter 2 [56]. The simplest illustration of where this MSS Lyapunov exponent occurs is in the trajectories of a test particle at a fixed point close to the event horizon as illustrated in Fig. 5.1. A linear stability analysis would then yield a Lyapunov exponent saturating the MSS bound $\lambda_L = 2\pi T_{\text{H}}$, where T_{H} is the Hawking temperature of the black hole [134].

²Here we are still using the same symbols as the paragraph before, so M is the mass of a black hole which would have area A .

Based on holography, the focus was placed on $(1 + 1)$ -dimensional gravity. Indeed, the simplest non-trivial example of such a gravitational model, known as Jackiw-Teitelboim (JT) gravity, has the same infrared symmetry breaking as the SYK model [212]. Both of these shared features are in the IR limit, meaning one focuses in on the low-temperature regime, meaning the near-extremal limit of the black hole.

In this chapter, we extend the picture of holography to all temperatures. An indication that this might be possible lies in the fact that second-order phase transitions also occur in charged non-rotating, i.e., Reissner-Nordström (RN), black holes. The connection arises in that their universality class directly overlaps with that of the charged SYK model [61]. To understand this, we start by introducing the formalism of black hole thermodynamics.

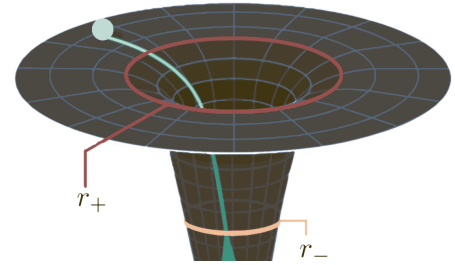


Figure 5.1: Schematic representation of a particle and its geodesic near the outer horizon r_+ of a black hole. Image adapted from [211].

5.2 Regularity of the spherically symmetric metric

Our main focus is on *non-rotating* black holes in $(d + 1)$ -dimensional space-time. As such we do not mention the case of non-zero angular momentum in the work, however, most results can be extended to such cases [195]. Due to rotational symmetry, the metric takes on the rather simple form [195]

$$ds^2 = -f(r)dt^2 + f(r)^{-1}dr^2 + r^2d\Omega_{d-1}^2, \quad (5.3)$$

where $d\Omega_n^2$ is the metric on the round unit n -sphere S^n . These are the kinds of static metrics we will focus on throughout this chapter. They are defined by their (em)blackening factor $f(r)$, which has a root at the event horizon $r = r_+$ of the black hole, effectively “blacking out” the region behind the horizon from the outside observer’s view. With this, the metric becomes singular, hence the radial coordinate r loses its meaning as a distance measure. A standard charged black hole has two roots $f(r_{\pm}) = 0$, the largest of which is the event horizon, while the smaller $r_- < r_+$ corresponds to the Cauchy horizon illustrated in Fig. 5.1.

5.2.1 Black hole temperature from the Euclidean-trick

Black hole thermodynamics is studied in Euclidean time $\tau = it$ (Wick rotating). In the near-horizon regime $r = r_+ + \delta r$, we find an effective two-dimensional metric $ds_{\text{eff}}^2 = dR^2 + R^2d\Theta^2$, where

$$R \equiv \frac{2}{\sqrt{f'(r_+)}}\sqrt{\delta r} \quad \Theta \equiv \frac{\tau f'(r_+)}{2}.$$

As such, given a negative cosmological constant, the space maps from $\text{AdS}_{d+1} \rightarrow \text{AdS}_2 \times S^{d-1}$, where S^{d-1} is the $(d - 1)$ -sphere. Here the metric ds_{eff}^2 is that of flat two-dimensional Euclidean space, viewed as polar coordinates of a sheet of paper. If you cut a wedge, then you remove part of the range of Θ . Connecting the paper, one is left with a cone, which has a singularity at the

tip ($R = 0$), where the radial coordinate vanishes. The space is locally flat everywhere, except at this conical singularity, where the curvature is infinite. Such an irregular Euclidean metric at the horizon would yield a divergent Euclidean path integral; hence an undefined partition function used to determine the thermodynamic properties of the black hole. As such, we impose the regularity condition, which imposes a constraint on the imaginary time coordinate. In particular, the conical singularity only disappears if we take it to be periodic with a periodicity of $\Theta = 2\pi$. The metric is then that of a circle $d\Omega_1$. We identify the corresponding value of τ with the temperature of the black hole

$$\beta_H = 4\pi/f'(r_+), \quad (5.4)$$

which is analogous to the period in the KMS relation identifying the temperature. This is the so-called Euclidean trick, which is one of many simplified ways to derive rather non-trivial results in the field of black hole thermodynamics. Take for instance an uncharged black hole in $d = 3$, with $f(r) = 1 - 2M/r$. From this, $f'(r_+) = 1/(2M)$, with a horizon at $r_H = 2M$. With this, one can directly verify that it yields the same temperature $T_H = 1/(8\pi M)$ as the Hawking radiation formula (5.1). This gives us all the requirements to derive the Bekenstein-Hawking entropy. From the relation of entropy to energy (mass), we know that $\partial_M S = \beta = 8\pi M$. Hence, we are left with³ $S = 4\pi M^2 = A/4$. We will see another example of such a simplified trick in Sec. 5.3.1.1, which will yield a relation between the mass and other thermodynamic quantities.

5.3 Phase transitions in black holes

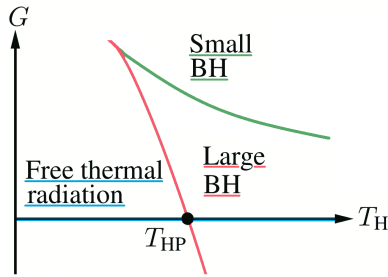


Figure 5.2: Schematic plot of Gibbs free energy for a black hole with a Hawking-Page transition.

In studying Schwarzschild (nonrotating, uncharged) black holes in AdS, one finds a Gibbs free energy [213] as plotted in Fig. 5.2. Note that there exist two black hole phases, one small, and one large. The small black hole always has a larger Gibbs free energy than the large black hole; hence it is never thermodynamically favored. However, as the larger black hole's temperature decreases, it becomes unstable. Here one then finds one additional phase, which one might suspect from black hole evaporation through thermal Hawking radiation. Below a temperature T_{HP} , the (chaotic) larger black hole will spontaneously evaporate into a (regular) radiation phase. This is the non-zero to zero entropy Hawking-Page transition⁴[200]. We saw such an entropy drop in Chapter 4 in the SYK chaotic-to-regular transition. Because of these similarities with black-hole phase transitions, analogies have been drawn to the gravitational collapse of branes, with extended (non-point-like) singularities, [179] and the Hawking-Page transition [215, 216]. This is, however, a first-order phase transition; hence

³While we derived this in the case of a simple uncharged non-rotating black hole, remarkably the same area law is found in all standard black holes.

⁴There are also non-zero entropy quantum corrections; thus one should perhaps be careful to specify that we are focusing on the classical HP transition with a zero entropy phase. This PT can also be connected to quark-gluon confinement-deconfinement transitions [214].

there are no associated critical exponents. Since we want to compare universality classes, we must consider charged black holes.

5.3.1 Black hole chemistry in vacuum pressure

Our main focus will be on RN (non-rotating charged) black holes in $(d + 1)$ dimensional space-time, under a variable Λ [194–196, 198, 199, 217]. Given that the cosmological constant Λ induces a vacuum pressure in spacetime, one can associate it with a thermodynamic pressure $P = -\Lambda/(8\pi)$. Since this pressure couples to the curvature, it also enters into the blackening factor [196, 217]

$$f(r) = 1 - 2\gamma_d M r^{2-d} + Q_B^2 r^{2d-4} + v_d P r^2, \quad (5.5)$$

where the mass M is given by the Smarr relation which we will discuss in Sec. 5.3.1.1. The thermal AdS solution corresponds to $M = Q_B = 0$. Here the proportionality constants

$$\gamma_d = \frac{4\Gamma(d/2)}{(d-1)\pi^{(d-2)/2}}, \quad v_d = \frac{16\pi}{d(d-1)}, \quad (5.6)$$

enforce the first law of black hole thermodynamics

$$dM = T_H dS_{\text{BH}} + \Phi_{\text{th}} dQ_B + V_{\text{th}} dP. \quad (5.7)$$

Here Φ_{th} is the surface electrical potential of the black hole corresponding to a charge Q_B .

Seeing as this vacuum pressure defines the asymptotic curvature of the theory, thermodynamics over multiple values of Λ amounts to an ensemble over different geometries. A strong interpretation of this might be that this implies that we are doing thermodynamics over different universes, which indeed sounds rather absurd. There are, however, multiple motivations for considering a variable Λ [194]. For one, physical constants can correspond to vacuum expectation values, which can in principle fluctuate. For instance, its value might be at a local minimum of the free energy, but not the global minimum. One would then have to include variations of these expectation values in the first law (5.7) to obtain the full equilibrium picture.

A second motivation is that, in allowing for a variable Λ , one obtains a richer phase diagram for charged black holes. The unstable small black hole phase remains, however, because of charge conservation, the black hole cannot fully evaporate via uncharged Hawking radiation. It can radiate up until a point, leading to another smaller black hole. This is the third phase, and it again becomes thermodynamically favorable below some transition temperature. These results are rather universal in that they are fairly independent of dimension d as long as $d > 2$. Most (if not all) of these black hole PTs [194, 196] fall into the *same universality class* as the SYK model [61]. In the extended space, the phase transitions are between a small and large BH [194] as plotted in Fig. 5.3.

An extremal black hole is characterized by having the minimum possible mass (the smallest black hole) before evaporating, given charge and angular momentum. As the black hole approaches

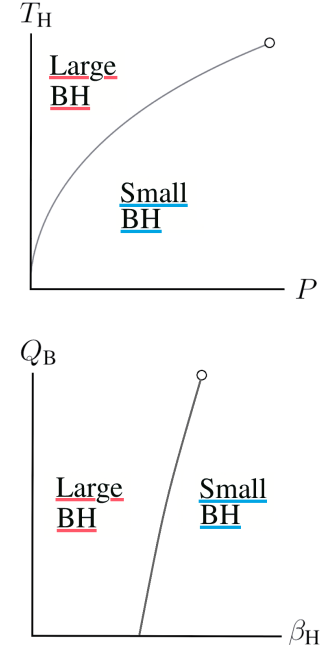


Figure 5.3: Black hole chemistry phase diagrams adapted from [194].

extremality the two roots r_{\pm} of $f(r)$ merge into a turning point $f'(r_H) = 0$. Recalling that this is directly proportional to the Hawking temperature, we note that the black hole is extremal when $T_H \rightarrow 0$. Note that in all of these examples, the order parameter is always a function of the horizon radius r_H .

5.3.1.1 Mass from the Smarr relation derivation

A third motivation for introducing a thermodynamic pressure is that such fluctuations must be included to have consistency with the scaling of the Smarr relation and the first law of black hole thermodynamics. The black hole mass M is then the total energy required to create a black hole and place it in a cosmological (negative Λ) environment, i.e., the enthalpy. The pressure P is then the conjugate to the ‘‘thermodynamic volume’’

$$V_{\text{th}} = \left(\frac{\partial M}{\partial P} \right)_{S, Q_B}. \quad (5.8)$$

While this volume often overlaps with the volume enclosed by the event horizon radius r_+ , deviations occur in lower dimensions. This is the reason we call it the ‘‘thermodynamic volume’’.

We now present a standard method to derive the Smarr relation $M = \mathcal{M}_{\text{Sm}}(A, P, Q_B)$ in $d > 1$ for the mass [218]. Let us consider the mass from a dimensional analysis perspective. To do this, define a dimensionless re-scaling of the radius $\varphi_+ = r_+/\ell$. Doing so, one would imagine that the units in which we are measuring length ℓ should *only* affect the mass by a proportionality factor. This is because, in our natural Planck units, the mass will scale with length as ℓ^{d-2} . This argument provides some motivation for the assumption that \mathcal{M}_{Sm} should be a homogeneous function

$$\mathcal{M}_{\text{Sm}}(\lambda^{\Delta_A} A, \lambda^{\Delta_P} P, \lambda^{\Delta_Q} Q_B) = \lambda^{\Delta_M} \mathcal{M}_{\text{Sm}}(A, P, Q_B). \quad (5.9)$$

This often holds, for instance, in the case of a charged black hole in $d = 3$ [194] the mass is $M = S_{\text{BH}} T_H - 2PV_{\text{th}} + Q_B \Phi_{\text{th}}$ with

$$S_{\text{BH}} = \pi \ell^2 \varphi_+^2, \quad T_H = \frac{1}{4\pi \ell \varphi_+} - \frac{Q_B^2}{4\pi \ell^3 \varphi_+^3} + 2P\ell \varphi_+, \quad V_{\text{th}} = \frac{4\pi \ell^3 \varphi_+^3}{3}, \quad \Phi_{\text{th}} = \frac{Q_B}{\ell \varphi_+}. \quad (5.10)$$

If we now change the length scale $\ell \rightarrow \lambda \ell$, we see how all other quantities scale in return. In particular, we find $X \rightarrow \lambda^{\Delta_X} X$, $\Delta_P = -2$, $\Delta_Q = 1$, together with conjugate scalings $\Delta_V = 3$, $\Delta_\Phi = 0$, which altogether sums to 1 and leads to $\Delta_M = 1$.

In general, the scaling dimensions may be read off from dimensional analysis on (5.5)⁵

$$\Delta_A = d - 1, \quad \Delta_P = -2, \quad \Delta_Q = \Delta_M = d - 2.$$

Differentiating (5.9) w.r.t. λ , and setting $\lambda = 1$ yields Euler’s theorem

$$\Delta_M M = \Delta_A A \partial_A M + \Delta_P P \partial_P M + \Delta_Q \partial_{Q_B} M. \quad (5.11)$$

⁵To a condensed matter physicist it might seem strange to find mass (for $d = 3$) scaling with length, given the Compton wavelength $\lambda \propto 1/M$, the larger the mass, the more localized it becomes. Restoring units around this mass however yields $M G_N / c^2$, which has dimension length. Here G_N / c^2 has dimension length squared in (condensed matter) natural units ($\hbar = c = 1$); thus there is no contradiction here.

Using the first law of black hole thermodynamics (5.7) and identifying the Bekenstein-Hawking entropy as $S_{\text{BH}} = A/4$ yields the relation

$$M = \frac{\Delta_A}{\Delta_M} S_{\text{BH}} T_{\text{H}} - \frac{2}{\Delta_M} P V_{\text{th}} + Q_{\text{B}} \Phi_{\text{th}}. \quad (5.12)$$

5.4 JT gravity and SYK

Based on AdS/CFT, the SYK dual should be a $(1+1)$ -dimensional model of gravity. One can already see from the divergences in (5.6), that the $d = 1$ case needs to be treated differently. The $(1+1)$ -dimensional Einstein-Hilbert action is given by

$$S = \frac{1}{G_N} \int d^2x \sqrt{-g} \mathcal{L}$$

where \mathcal{R}_2 is the two-dimensional Ricci scalar (curvature) and g is the determinant of the metric tensor. For the standard Lagrangian $\mathcal{L} \propto \varphi_0 \mathcal{R}_2$, this action is trivial⁶ in the sense that the solutions are invariant under any conformal deformations. Thus, for ordinary Einstein gravity, every metric is a valid solution and it has no phase transitions. As such, in search of this dual, we consider gravity coupled to a dynamical dilaton field φ . The simplest of such theories is that of uncharged JT gravity $\mathcal{L} \propto \varphi[\mathcal{R}_2 - 8\pi P]$ in AdS₂. The fluctuations in φ weakly break the conformal symmetry down to $\text{SL}_2(\mathbb{R})$, a feature which should sound familiar from the discussion in Sec. 2.3.2. Indeed, JT gravity is believed to be the low energy gravitational dual to the Majorana fermionic SYK model [56]. It is also possible to obtain the low-energy dual to the SYK model, by dimensional reduction⁷ of higher dimensional theories [220–222]. This reduction yields the above JT action together with a Schwarzian boundary term [96].

The $\text{SL}_2(\mathbb{R})$ invariance of JT gravity is also reflected in the metric $ds^2 = -f(r)d\tau_E^2 - f(r)^{-1}dr^2$, given here in Euclidean time. To start, let us consider the metric in terms of the tortoise coordinates $dr/dr_T = -f(r)$

$$r_T = \int_r^\infty dx f(x)^{-1}.$$

Now the metric takes the simple diagonal form $ds^2 = f(r)[d\tau_E^2 + dr_T^2]$. We can write our metric on the conformal gauge form $ds^2 = e^{2w(t_1, t_2)} dt_1 dt_2$ by transforming to the coordinates $t_1(z)$ and $t_2(-\bar{z})$, where $z = r_T + i\tau_E$, i.e., transforming to coordinates⁸ $u_1(t_1) = z$ and $u_2(t_2) = \bar{z}$. This yields

$$e^{2w(t_1, t_2)} = \frac{f(r)}{\dot{t}_1 \dot{t}_2} = -\frac{\dot{u}_1(t_1) \dot{u}_2(t_2)}{dr_T/dr}.$$

⁶The scalar curvature is proportional to the Euler characteristic, and thus the model is also sometimes said to be topological. If we also consider a non-zero cosmological constant $\mathcal{R}_2 \rightarrow \mathcal{R}_2 - 8\pi P$ the analysis becomes more complicated, since the Euler-Lagrange equations imply a degenerate metric.

⁷In particular, this is a so-called Kaluza-Klein reduction since it is of the same spirit as Kaluza's original dimensional reduction from $d = 4$ to $d = 3$ [219].

⁸A particular case of such coordinates are the Kruskal coordinates [223, 224] $t_1 = e^{\kappa z}$ $t_2 = -e^{\kappa \bar{z}}$, which leaves $\dot{t}_1 \dot{t}_2 = -\kappa^2 e^{2\kappa r_T}$. Note that $i\tau_E \pm r_T$ almost takes on the form of light-cone coordinates, however, we have changed from the proper distance r for an observer at infinity, to r_T . Here $\kappa = 2\pi T$ is the surface gravity as well as the maximal Lyapunov exponent

The above metric takes on the Poincaré form

$$ds^2 = \mathcal{R}_2^2 \frac{d\tau_E^2 + dr_T^2}{r_T^2},$$

in the case of simple JT gravity we have $f(r) = -8\pi P(r - r_H)^2$ [96]. Such a metric may be explicitly written in an $SL_2(\mathbb{R})$ (the isometry group of AdS_2) invariant form

$$ds^2 = -(8\pi P)^2 \frac{4\dot{u}_1(t_1)\dot{u}_2(t_2)}{[u_1(t_1) - u_2(t_2)]^2} dt_1 dt_2.$$

In the case where $u_1(t_1) = e^{i\pi(v/2+1)+\sigma t_1}$ and $u_2(t_2) = e^{-i\pi(v/2+1)+\sigma t_2}$, where $\sigma = \kappa v$, we are left with the function

$$e^{w(t_1, t_2)} = \frac{\sigma 8\pi P}{\sec(\pi v/2 - i\sigma(t_1 - t_2)/2)}.$$

In other words, the metric is invariant under any Möbius transformation

$$u \rightarrow \frac{au + b}{cu + d}, \quad a, b, c, d \in \mathbb{R}, ad - bc = 1.$$

5.4.1 Eulerian-trick for AdS_2

We are interested in the Smarr relation for $d = 1$, corresponding to the cSYK dual. Consider the first parameter in \mathcal{M}_{Sm} , the “area” A . A re-scaling in length is only captured by A when it is dimensionful. In $d = 1$ the area, however, lacks dimension as well as a clear interpretation. To get around this one can consider $d = 1 + \epsilon$ dimension for small ϵ , one is left with an entropy $S_{\text{BH}} = 2A_p/4 + \mathcal{O}(\epsilon)$, where the “area” $A_p = 1$ is that of a “point” [225]. In the limit as $\epsilon \rightarrow 0$ the above formalism could then argue that $M = 2T_H S_{\text{BH}} - 2V_{\text{th}} P$ for the uncharged case.

There is however a more fundamental generalization of the Bekenstein-Hawking entropy known as the Wald entropy [226]. For two-dimensional JT gravity, this entropy is proportional to the dilaton $\mathcal{S}_W = \varphi_+$ [227, 228]. Here the dilaton is proportional to the radius $\varphi = \gamma r$, where we set $\gamma = 1/\ell$ without loss of generality, to reflect the fact that the entropy, while being proportional to the radius, is, in fact, dimensionless. Let us consider a charged black hole⁹ with mass, volume, and surface electrical potential given by

$$M = PV_{\text{th}} + Q_B \Phi_{\text{th}}/2, \quad V_{\text{th}} = \ell \varphi_+^2/2, \quad \Phi_{\text{th}} = -\ell Q_B \varphi_+, \quad (5.13)$$

respectively. The last factor of a half in the above mass M means that this is inconsistent with (5.12). The mistake arises from $\Delta_A = 0$, where the concept of an area does not have a clear meaning. One might attempt to remedy this by focusing rather on the Wald entropy. It, however, has the same scaling dimension $\Delta_S = 0$, so the same problem.

⁹The particular Lagrangian will be discussed in Sec. 5.5.1. This case corresponds to $\mathcal{U}(\varphi) = \varphi$, $\mathcal{W}(\varphi) = 1$, we have $Q_B = -\partial_r A_t = \partial_r \Phi$ and $V = \partial_r \mathcal{U}$, implying that $\Phi_{\text{th}} = Q_B \varphi_+/\gamma$ and $V_{\text{th}} = \varphi_+^2/(2\gamma)$.

5.4.2 Motivation from changing length scale

To get a more in-depth understanding of these results, let us first provide additional motivation for the homogeneous Smarr relation and see what this implies for the $\mathcal{d} = 1$ case.

We now propose a more general formalism which rather considers the homogeneous function $\mathcal{M}_{\text{Sm}}(\ell, P, Q_{\text{B}})$, i.e., the role of A is replaced by the length scale ℓ . The same application of Euler's theorem modifies the expression (5.12) to

$$M = \frac{1}{\Delta_M} \ell \partial_\ell M - \frac{2}{\Delta_M} P V_{\text{th}} + Q_{\text{B}} \Phi_{\text{th}}, \quad (5.14)$$

where $\Delta_\ell = 1$. For the standard $\mathcal{d} > 1$ case everything stays the same, since ℓ and φ_+ always enter the M as powers of $r_+ = \ell \varphi_+$, for which $\ell \partial_\ell (\ell \varphi_+)^n = \partial_{r_+} r_+^n$. Then via the chain rule

$$\ell \frac{\partial M}{\partial \ell} = r_+ \frac{\partial M}{\partial r_+} = (\mathcal{d} - 1) r_+^{\mathcal{d}-1} \frac{\partial M}{\partial r_+^{\mathcal{d}-1}} = \Delta_A A \frac{\partial M}{\partial A}.$$

This can also be verified directly for the example (5.10). The results do, however, change for $\mathcal{d} = 1$ where the dilaton coupling introduces another length-scale γ , which we set equal to $1/\ell$, $M = 2P V_{\text{th}} + Q_{\text{B}} \Phi_{\text{th}} - \ell \partial_\ell M$, where the right-hand side reduces to

$$\ell \partial_\ell M = \ell \frac{P \varphi_+^2 + Q_{\text{B}}^2 \varphi_+}{2} = P V_{\text{th}} + Q_{\text{B}} \Phi_{\text{th}}/2 \quad (5.15)$$

which indeed yields the expression (5.13). The same result is obtained for the most general deformed JT gravity coupled with a Maxwell field, as we will see in Chapter 5.5.1.

5.5 Holographic mappings beyond the zero temperature limit

Thus far the focus of holography in the SYK model has been on the strongly coupled (IR) regime $\beta \mathcal{J} \rightarrow \infty$. Straying away from this regime means that one no longer has a conformal symmetry. As such, away from the IR regime, based on AdS/CFT, one would not necessarily expect there to be any gravitational dual (for any q). For ordinary Majorana SYK models, this dual appears to be the simplest $(1 + 1)$ -dimensional gravity with a dilaton field, namely Jackiw–Teitelboim (JT) gravity. For the complex SYK model, one would further consider coupling JT gravity to a Maxwell field.

In the below-included preprint, in Sec. 5.5.1, we extend the holographic mapping. We do this by again focusing on the large- q cSYK model for which the full partition function can be calculated. This is in contrast to the finite q case, where the only analytical solutions are in the IR regime. We show that perhaps the most important universal feature, the universality class, is also shared between the cSYK model and gravity. However, we require two adjustments to the proposed JT gravity. Even for some standard variants of Einstein gravity in $\mathcal{d} = 1$, there is no second-order phase transition (PT) [217, 229, 230], including ordinary JT gravity. As such we deform the model of JT gravity and coupled it to a Maxwell field, with the resulting Lagrangian

$$\mathcal{L}(\varphi, A) = \frac{\varphi}{4\pi} \mathcal{R}_2 + P \mathcal{U}(\varphi) - \frac{\mathcal{W}(\varphi)}{4} F(A)^2. \quad (5.16)$$

The resulting model not only has a second-order phase transition with the same critical and effective exponents, i.e., the same field mixing, but it also has the same partition function [130].

We also go beyond matching the partition functions and also consider the Lyapunov exponents on the gravitational side via linear stability analysis. In the maximally chaotic regime, we get perfect overlap. In the low-temperature regime, where the condensed matter system has a chaotic-to-regular PT, the results are inconclusive due to the back action being ignored.

5.5.1 Preprint: Matching partition functions of deformed JT gravity and the charged SYK model

Reprinted article with permission from
Jan C. Louw, Sizheng Cao, and Xian-Hui Ge

Author contributions J. C. L. did the analytic calculations and wrote the manuscript. S. C. verified some of the analytical calculations and produced all figures. X-H. G. revised parts of the manuscript and suggested linear stability analysis to extract the Lyapunov exponent. All authors contributed parts to the manuscript and discussed the results.

Matching partition functions of deformed JT gravity and cSYK model

Jan C. Louw¹,² Sizheng Cao,² and Xian-Hui Ge^{2,3}

¹*Institute for Theoretical Physics, Georg-August-Universität Göttingen, Friedrich-Hund-Platz 1, 37077 Göttingen, Germany*

²*Department of Physics, College of Sciences, Shanghai University, 99 Shangda Road, 200444 Shanghai, China*

³*Shanghai Key Laboratory of High Temperature Superconductors, Shanghai University, 99 Shangda Road, Shanghai 200444, China*

(Dated: May 19, 2023)

Motivated by recent analogies between the large- q cSYK model and charged black holes, we aim to find a concrete gravitation theory with a matching partition function. Our main focus is to match the thermodynamics of the $(0+1)$ -dimensional cSYK model, with that of a $(1+1)$ -dimensional gravitational model. We focus on a model of deformed JT gravity, characterized by some unknown dilaton potential function and unknown dilaton-to-Maxwell field coupling. By finding the general solutions, we are able to find the Lagrangian which produces the same partition function and equation of state as that of the considered SYK model. We go beyond showing that the thermodynamics overlaps by also showing that the Lyapunov exponents, characterizing the degree of chaos, overlap close to the second-order phase transition. In the low-temperature rescaled regime, there remain open questions about the Lyapunov exponents, given that our analysis ignores the black hole back action which can be large in this regime.

I. INTRODUCTION AND OUTLINE

The Sachdev-Ye-Kitaev (SYK) model is a simple quantum model that proposes a gravity-condensed matter correspondence. One of its key findings is the emergence of conformal symmetry with nearly AdS₂ geometry in its configuration space of reparametrization modes [1], which is also observed in black holes. Both systems are also maximally chaotic [2, 3]. Significant progress has been made in understanding this duality, including the discovery that fluctuations away from conformality are described by a Schwarzian action [4], which is also the boundary theory of Jackiw-Teitelboim (JT) gravity. There is a wealth of literature on the connections between the SYK models and JT gravity [3–15]. The chaotic-integrable transition in the SYK model can be achieved by introducing a generalized SYK model with an additional one-body infinite-range random interaction [16]. This transition is interpreted as the Hawking-Page (HP) phase transition in the bulk gravity [16].

Attempts have been made to extend such holographic analogies to charged black holes by considering complex SYK (cSYK) models [17]. The cSYK model exhibits a second-order phase transition in the maximally chaotic regime, which is believed to be associated with a universal class of phase transitions in spherical Reissner-Nordström (RN)-anti-de Sitter (AdS) black holes [18, 19]. On a thermodynamic level, analogies have been drawn between RN black holes and van der Waals liquid-gas phase transition, and recently also to the phase transition found in the cSYK models [17, 18]. Similar phase transitions can be found in $(1+1)$ -dimensional deformed JT gravity if a dilaton coupling is included [7]. The power laws associated with the continuous phase transition match those of the cSYK model. Given this, it is natural to ask how explicit one can make such analogies. For instance, would it be possible to have a gravitational model with the exact same thermodynamic potential and equation of state? Similar questions can be asked about the Lyapunov exponents reflecting the degree of chaos found in the respective models.

In this paper, we give partial answers to these questions.

We explore the phase structure of deformed JT gravity and the cSYK model by comparing their partition functions. Our focus is on the on-shell physics, which corresponds to the solutions that minimize the action and characterize the leading order thermodynamics. To achieve this, we consider the $q/2$ -body interacting complex SYK model. One can then derive the exact thermodynamic potential in powers of $1/q$. On the cSYK side, we place emphasis on the fluctuations away from on-shell, described by the Schwarzian [20], by neglecting the q -dependent contributions. In the context of holography, the focus is usually placed on these off-shell fluctuations [21, 22]. Typically, these fluctuations cannot be ignored at nonzero temperatures. The resulting action can be expanded around the conformal solution to yield fluctuations described by the Schwarzian action. However, by expanding in $1/q$, we find that they are sub-leading, in orders of $1/q$, to the on-shell contributions [20]. The $1/q$ expansion, however, goes beyond this, also providing information about the harmonic oscillator-like phase, where conformal symmetry is strongly broken [23, 24]. This is because it provides the full phase diagram to leading order in $1/q$, hence it is not restricted to certain charge densities or low temperatures.

As for finding the candidate bulk dual, we start with a rather general model of deformed JT gravity. It is characterized by a dilaton potential energy \mathcal{U} and a dilaton coupling \mathcal{W} to Maxwell fields. In the context of the charged SYK model, such a theory has been proposed before as the low-energy dual [8]. Since the focus was placed on the low-energy limit, the considered deformations, were power laws. To capture the thermodynamics away from the strictly low-energy limit, we must consider more general deformations \mathcal{W} and \mathcal{U} . This is possible, since, like large- q cSYK, the generally deformed model admits exact solutions [25]. Starting with some unknown potentials \mathcal{W} and \mathcal{U} , we calculate various quantities. For instance, we find the general form of the equation of state (EOS), which is related to the Hawking temperature T_H , the Wald entropy S_W and the Arnowitt-Deser-Misner (ADM) mass M . We also find the associated Gibbs free energy G . All of these quantities are given in terms of the unknown functions

\mathcal{U} and \mathcal{W} , which we constrain such that we obtain the same thermodynamics as the cSYK model.

By expressing the charge density as a function of the entropy, we are able to show that the same thermodynamic relations hold for both models. This relation allows us to identify the enthalpy on the SYK side, while the ADM mass corresponds to the enthalpy on the gravitational side. Equating these two enthalpies, we show that the equations of states also match. This requirement then fixes the potentials, identifying the sought deformation. It is further shown that their partition functions exactly match $Z_{\text{cSYK}} = Z_{\text{dT}}$, in the regimes of interest. With this bulk dual, we go on to describe its gravitational properties, such as its scalar curvature, and how it relates to the condensed matter system.

We find two different dictionaries which still provide the same thermodynamics. These correspond to the two different analogies that one can draw between the van der Waals liquid, RN black holes, and the complex SYK model [18, 24].

II. THE q -DEPENDENT CSYK MODEL

We start from the $q/2$ -body interacting cSYK model [26]

$$\hat{\mathcal{H}} = J \sum_{\substack{1 \leq i_1 < \dots < i_{q/2} \leq N \\ 1 \leq j_1 < \dots < j_{q/2} \leq N}} X_{j_1 \dots j_{q/2}}^{i_1 \dots i_{q/2}} c_{i_1}^\dagger \dots c_{i_{q/2}}^\dagger c_{j_{q/2}} \dots c_{j_1}, \quad (1)$$

with a conserved U(1) charge density $\hat{\mathcal{Q}} = \frac{1}{N} \sum_i c_i^\dagger c_i - 1/2$, with expectation values $\mathcal{Q} \in [-1/2, 1/2]$, where c^\dagger, c are fermionic creation and annihilation operators, respectively. Here N is the number of lattice sites, hence the thermodynamic limit corresponds to taking $N \rightarrow \infty$. The couplings, X , are complex random variables with zero mean, and a variance $\overline{|X|^2} = [q^{-1}(q/2)!]^2 [2/N]^{q-1}$. We will work in the grand canonical ensemble

$$Z_{\text{cSYK}} = \text{tr} \exp(-\beta[\hat{\mathcal{H}} - \mu N(\hat{\mathcal{Q}} - 1/2)]).$$

By considering $q/2$ -body interactions instead of two-body interactions, one may solve the SYK model exactly, treating $1/q$ as an expansion parameter. It was first pointed out by Davison et al. in [21] that the equilibrium state described by \mathcal{H} (1) tends to free fermions, for any non-zero charge density $\mathcal{Q} = \mathcal{O}(q^0)$, in the large q limit. This can be seen in the effective interaction strength

$$\mathcal{J}(\mathcal{Q}) \equiv J[1 - 4\mathcal{Q}^2]^{q/4-1/2} \quad (2)$$

going to zero as $q \rightarrow \infty$. Even for small charge densities $\mathcal{J}(\mathcal{Q}) \sim e^{-q\mathcal{Q}^2} J$. To avoid this tendency, Davison et al. considered an altered Hamiltonian $H_{\text{alt}}(\beta\mu)$, where the bare system coupling $J \rightarrow J_{\text{alt}}(\beta\mu)$ grows as a function of inverse temperature β and chemical potential μ to compensate for the effective suppression. The acquired $\beta\mu$ -dependence of $H_{\text{alt}}(\beta\mu)$, however, leads to starkly different thermodynamics from \mathcal{H} (1), for any q [23, 27], as discussed in App. E.

By not making any changes to the Hamiltonian (1), we preserve the non-trivial thermodynamics at small fluctuations

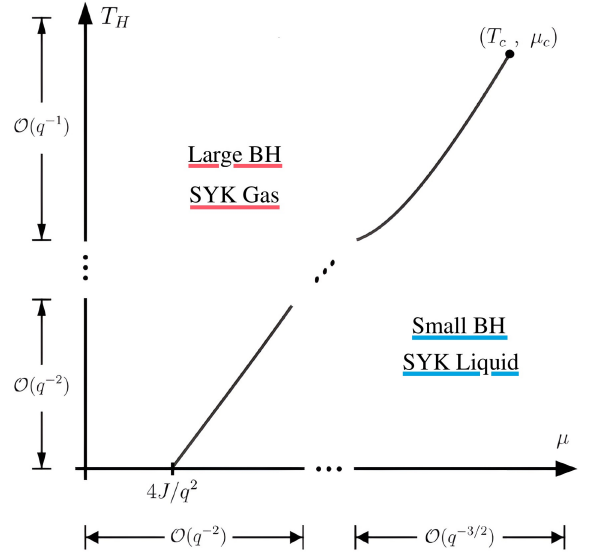


FIG. 1. Schematic phase diagram for our particular deformed JT and cSYK models in different q -scaling regimes under the large- q limit condition. The upper regime encompasses the critical endpoint of the coexistence line. Close to the origin, there is a near-extremal phase transition.

$\mathcal{Q} = \mathcal{O}(q^{-1/2})$ away from $\mathcal{Q} = 0$ [17]. Remarkably, this unaltered cSYK model leads to a liquid-gas phase diagram which bares a striking resemblance to the small-large black hole phase diagrams found in black hole thermodynamics. The “liquid” and “gaseous” phases reflect their respective (charge) densities. In particular (1) exhibits a phase transition below a critical temperature $T_c = \mathcal{O}(q^{-1})$ or critical chemical potential $\mu_c = \mathcal{O}(q^{-3/2})$ [17] because the temperature is q -dependent and the scaling transformation given in [21] is broken. Explicitly the critical point is at

$$T_c = 2\mathcal{J}(\mathcal{Q}_c)/q, \quad \mu_c = 6T_c\mathcal{Q}_c, \quad \mathcal{Q}_c = \sqrt{3/(2q)}. \quad (3)$$

Regarding the relation to gravity, there are two regimes of interest, the first considers a scaling $T = q^{-1}\tilde{T}$, $\mu = q^{-3/2}\tilde{\mu}$, with tilde'd quantities are q -independent. Around the transition point, the strongly coupled cSYK model dominates due to the relatively small charge densities. This rescaled regime corresponds to the IR regime, small $\beta\mathcal{J}$, hence both phases are maximally chaotic, reflected in their Lyapunov exponents saturating the Maldacena-Shenker-Stanford (MSS) bound $\lambda_L \rightarrow 2\pi T$ [3]. This feature is shared with black holes. In particular, it is shared by both large and small black hole phases in the extended space [18]. The corresponding phase transition also shares a universality class with that of the cSYK model. Both cases have mean-field critical exponents.

We further consider a second rescaled regime $T = q^{-2}\bar{T}$, $\mu = q^{-2}\bar{\mu}$, where barred quantities are held fixed as $q \rightarrow \infty$, with the corresponding phase diagram given in fig. 1. The gaseous phase in this regime corresponds to an uncharged, $\mathcal{Q} = 1/q$ (in the large q limit), and maximally chaotic SYK

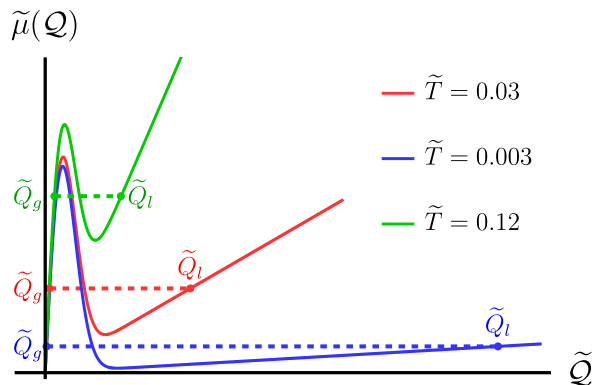


FIG. 2. The chemical potential $\tilde{\mu}$ as a function of the charge density \tilde{Q} , the dash lines of different colors represent the real physically acceptable solution which satisfies the Maxwell area law.

model. The liquid phase becomes incompressible and has an exponentially small entropy which tends to zero. The incompressibility stems from it reaching a maximal charge density, which is of the order $Q = \mathcal{O}(q^0)$. As noted before, such a large density fully suppresses the SYK interactions, yielding a free non-interacting model. The non-zero to zero entropy drop is analogous to the black hole to the thermal radiation Hawking-Page transition. In the large q limit, the jump in charge density from $1/q$ to $1/2$, caused by a small perturbation $\mu_0 = 4J/q^2$ to the chemical potential, is reminiscent of spontaneous symmetry breaking. To see how this behavior of the charge density nearby the coexistence line emerges, we can go back to the first scaling regime and plot the chemical potential $\tilde{\mu}$ as a function of charge density \tilde{Q} . One can directly find that as the decreasing of the temperature \tilde{T} , the charge density of liquid phase \tilde{Q}_l goes to infinity which implies that the corresponding non-rescaled charge density Q_l is the order of $\mathcal{O}(q^0)$ as the rescaled temperature \tilde{T} goes to zero. At the same time, the charge density of the gas phase vanishes. This phenomenon indicates the jump in the charge density we described above. This highlights a difference between the two rescaled regimes. In the first regime, close to the critical point, the liquid and gaseous charge densities are of the same order. As such, for the specific rescaled quantities $(\tilde{\mu}, \tilde{T}, \tilde{Q})$, the limit as $q \rightarrow \infty$ is well-defined.

In the regime associated with the zero T limit, we have two different scalings in the charge density, namely $Q = \mathcal{O}(1/q)$ and $Q = \mathcal{O}(q^0)$. As such, the two charge densities diverge from one another. For any finite, but large q , the phase transition still exists. In the limit $q \rightarrow \infty$, one can, however, argue that this phase transition no longer makes sense due to this diverging separation. Similarly, the limit of a spherical to a flat Euclidean space as the parameter $k \rightarrow 0$ [28], the phase transition also disappears, in which the parameter k represents the topological parameter of the RN-AdS black hole [29]. In this sense, one might be able to associate k with $1/q$.

III. THE DEFORMED JT GRAVITY MODEL

We consider general deformed JT gravity [30] together with coupling to a Maxwell field [25], with action

$$I[\varphi, A] = G_N^{-1} \int_M d^2x \sqrt{-g} \mathcal{L}(\varphi, A) + I_{\text{bdy}}.$$

Here the boundary action contribution I_{bdy} , described in App. A 2, regularizes the theory. In (1+1)-dimensions, the constant G_N is dimensionless in natural units $\hbar = c = 1$. Its inverse will play the role of the large parameter N selecting out the on-shell solution in the classical limit. To have a well-defined limit, we must focus on "intensive" quantities, for instance focusing on the intensive bulk Lagrangian density

$$\mathcal{L}(\varphi, A) = \frac{\varphi}{4\pi} \mathcal{R}_2 + P\mathcal{U}(\varphi) - \frac{\mathcal{W}(\varphi)}{4} F(A)^2, \quad (4)$$

instead of \mathcal{L}/G_N . Here $F_{\mu\nu} = \partial_\mu A_\nu - \partial_\nu A_\mu$ is the electromagnetic tensor and \mathcal{R}_2 is the 2-dimensional Ricci scalar. The dilaton φ couples to the electromagnetic field via a term $\mathcal{W}(\varphi)$. The field also has its own potential energy $P\mathcal{U}(\varphi)$, where we have a thermodynamic pressure term P . This pressure is associated with a negative cosmological constant [19], which is the pressure of empty space. Since the characteristic length scale is associated with the scalar curvature at the conformal boundary, we would assume it to be related in some way to the interacting contribution of the quantum system.

We assume the black hole solution, in the Schwarzschild gauge, takes the form $ds^2 = -f(r)dt^2 + dr^2/f(r)$. Solving the Euler-Lagrange equations, see App. A, we find the dilaton field solution (A11) $\varphi = \gamma r$, where γ is the dilaton coupling strength. Setting $\gamma = 1$ amounts to measuring distance in units of γ . We also have the emblackening factor (A15)

$$f(r)/(4\pi) = -M + PV(r) - Q_B A_t(r)/2, \quad (5)$$

for some integration constant M and black hole charge Q_B . Here we have defined the anti-derivatives

$$V(r) = \int dr \mathcal{U}(r), \quad A_t(r) = Q_B \int dr \frac{1}{\mathcal{W}(r)}. \quad (6)$$

By definition, the event horizon is at the root $r = r_H$ of $f(r)$, i.e., $f(r_H) = 0$. With this, (5) implies

$$M = PV_{\text{th}} + Q_B \Phi_{\text{th}}/2, \quad V_{\text{th}} \equiv V(r_H), \quad \Phi_{\text{th}} \equiv -A_t(r_H), \quad (7)$$

where we have defined the thermodynamic quantities as (6) evaluated at the horizon $\varphi_0 = r_H$. For instance, in black hole chemistry, the pressure is conjugate to the volume [31] leading to the identification of V_{th} as the thermodynamic volume. We identify, as usual, the Hawking temperature as $T_H \equiv f'(r_H)/(4\pi)$ which is the conjugate to the Wald entropy [32] $S_W = r_H$. As such the function $M(S, P, Q_B)$ satisfying the differential relation

$$dM = \Phi_{\text{th}} dQ_B + V_{\text{th}} dP + T_H dS_W, \quad (8)$$

which is the first law of (black hole) thermodynamics [19], which also serves to define the thermodynamic volume. Indeed, it can be identified as the ADM mass [33]. In considering Φ_{th} to be the black hole's chemical potential [25], we may also view it as an enthalpy. From (8), using $\mathcal{S}_W = r_H$, we may also obtain the EOS

$$T_H = \left(\frac{\partial M}{\partial \mathcal{S}_W} \right)_{P, Q_B} = PV'(r_H) - \frac{Q_B}{2} A'_t(r_H), \quad (9)$$

where, unless specified otherwise, derivatives are evaluated keeping P and Q_B constant, $V'(r_H) \equiv (\partial_{r_H} V(r_H))_{P, Q_B}$.

The thermodynamic potential which selects out the favorable state is the Gibbs free energy [19] $G(T_H, P, Q_B) = M - T_H \mathcal{S}_W$. This is identified with the on-shell action (A24) of the uncharged black hole dual to the described charged system. All other expressions would remain unchanged if we had instead worked with this uncharged dual from the start. The Gibbs free energy also arises naturally in the dimensionality reduction of $(3+1)$ -dimensional charged black holes [25].

IV. MATCHING THE PARTITION FUNCTIONS

Our goal is to find the gravitational Lagrangian dual to the cSYK model, which is defined by the yet to be determined potentials U, \mathcal{W} . Equivalently, we may focus on the related anti-derivatives V, A_t defined in (6). We do this by focusing on the large q cSYK model's grand potential

$$\Omega \equiv -T \ln Z_{\text{cSYK}}/N = E + (1/2 - \mathcal{Q})\mu - T\mathcal{S}, \quad (10)$$

with the interaction energy [24]

$$E \sim -2\epsilon(\mathcal{Q})/q^2, \quad \epsilon(\mathcal{Q}) \equiv \mathcal{J}(\mathcal{Q}) \sin(\pi v/2) \quad (11)$$

and entropy density $\mathcal{S} = \mathcal{S}_2(\mathcal{Q}) - (\pi v/q)^2/2$, as shown in App. C, where

$$\mathcal{S}_2(x) \equiv -\frac{1-2x}{2} \ln \left| \frac{1-2x}{2} \right| - \frac{1+2x}{2} \ln \left| \frac{1+2x}{2} \right|, \quad (12)$$

which is an even function of x . Here v is the solution to the closure relation $\mathcal{J}(\mathcal{Q})/T = \pi v \sec(\pi v/2)$ [20], which is also related to the Lyapunov exponent as $\lambda_L = 2\pi T v$.

The phase transition is reflected in the EOS [24, eq.(43)]

$$T = \frac{\mu - 4\mathcal{Q}\epsilon/q}{2 \tanh^{-1}(2\mathcal{Q})}, \quad (13)$$

becoming three-to-one for $T < T_c$, or $\mu < \mu_c$, where the critical temperature and critical chemical potential scales as $T_c = \mathcal{O}(1/q)$ and $\mu_c = \mathcal{O}(q^{-3/2})$. Equation (13) is q -dependent since for example, it breaks the scaling symmetry $T \rightarrow T/q^2$, $\mu \rightarrow \mu/q^2$, and $\mathcal{Q} \rightarrow \mathcal{Q}/q$. Note that this equation is invalid for $\mathcal{Q} = 0$, amounting to division by zero, in which case the temperature becomes an independent free parameter. One may show that this EOS remains valid for large q , for any polynomial (in q) scaling for temperature and chemical potential [17], i.e., the cases we consider.

TABLE I. Dictionary between the thermodynamics of the q -dependent cSYK model and deformed JT (dJT) gravity. Each row identifies the two quantities which equate to another.

Model	cSYK	dJT
large parameter	N	$1/G_N$
enthalpy	H (9)	M (7)
entropy density	\mathcal{S}	\mathcal{S}_W
temperature	T (13)	T_H (9)
thermodynamic potential	Ω (10)	G

To have matching thermodynamics, we not only require the same thermodynamic potentials Ω, G , but also matching equations of states. If the quantity $\Omega + T\mathcal{S}$:

$$H \sim -2\epsilon(\mathcal{Q})/q^2 + (1/2 - \mathcal{Q})\mu \quad (14)$$

satisfies the same relation as the mass (9)

$$T = \left(\frac{\partial H}{\partial \mathcal{S}} \right)_{\mu, J} = \left(\frac{\partial \mathcal{Q}}{\partial \mathcal{S}} \right)_{\mu, J} \left(\frac{\partial H}{\partial \mathcal{Q}} \right)_{\mu, J}, \quad (15)$$

i.e., yields the same EOS, then it can also be identified with the enthalpy. The above relation may be rewritten as

$$\beta \left(\frac{\partial H}{\partial \mathcal{Q}} \right)_{\mu, J} = \left(\frac{\partial \mathcal{S}}{\partial \mathcal{Q}} \right)_{\mu, J} = -2 \tanh^{-1}(2\mathcal{Q}) - \partial_{\mathcal{Q}} \frac{(\pi v/q)^2}{2} \quad (16)$$

where unless specified otherwise, we assume that μ, J are kept constant, meaning that $v'(\mathcal{Q}) \equiv (\partial_{\mathcal{Q}} v(\mathcal{Q}))_{\mu, J}$. Using the closure relation $\beta \mathcal{J}(\mathcal{Q}) \cos(\pi v/2) = \pi v$, the left-hand-side of (16) reduces to

$$-2\beta\epsilon'(\mathcal{Q})/q^2 - \beta\mu = 4\mathcal{Q}\beta\epsilon(\mathcal{Q})/q - \pi^2 v'(\mathcal{Q})v/q^2 - \beta\mu.$$

Finally, from (13), we have $4\mathcal{Q}\beta\epsilon/q = \beta\mu - 2 \tanh^{-1}(2\mathcal{Q})$, which leaves the right-hand side of (16), thus finished the proof identifying H as an enthalpy. Considering (9) and (15) we note that the same equation of state is obtained if we identify the temperatures and entropies and enthalpies with another which also then implies that $G = \Omega$, since $G = M - T_H \mathcal{S}_W$ and $\Omega = H - T\mathcal{S}$. This (partial) dictionary is summarized in table I. With these identifications, one finds not only an isomorphism between the EOS's and thermodynamic potentials, but *equivalent* partition functions

$$Z_{\text{dJT}} = e^{-\beta N G} = Z_{\text{cSYK}} = e^{-\beta N \Omega}.$$

Since the thermodynamics is uniquely encoded by the partition function and EOS, we also have the exact phase diagram matching Fig. 1. The same holds true in the maximally chaotic regime, where the phase diagram has been given in [17].

To further specify the dictionary, we consider the differential relations of the two models. For the cSYK model, we have

$$\left(\frac{\partial \Omega}{\partial J} \right)_{\mu, T} = \frac{E}{J}, \quad \left(\frac{\partial \Omega}{\partial \mu} \right)_{J, T} = \frac{1}{2} - \mathcal{Q} \quad (17)$$

TABLE II. Dictionary relations for parameter and conjugate pairs

cSYK	dJT (a)	dJT (b)
$\mu, 1/2 - Q$	$Q_B^2, \frac{\Phi_{\text{th}}}{2Q_B}$	P, V
$J, E/J$	P, V	$Q_B^2, \frac{\Phi_{\text{th}}}{2Q_B}$

while for the gravitational model's Gibbs free energy, we have

$$\left(\frac{\partial G}{\partial Q_B^2}\right)_{P,T} = \frac{\Phi_{\text{th}}}{2Q_B}, \quad \left(\frac{\partial G}{\partial P}\right)_{Q_B,T} = V_{\text{th}}. \quad (18)$$

By comparing these two, we note the two possible options given in Table. II.

This choice will *not* influence the thermodynamics, except for its interpretation on the black hole side. Such that we do not restrict ourselves to a particular choice, we typically use the notation on the condensed matter side. These two options in fact directly overlap with the two different analogies which can be drawn between the van der Waals liquid, RN black holes, and the charged SYK model [18, 24].

A. Equivalence of thermodynamics

Since we know the thermodynamics match, we can consider the equation of state (13) in the context of the black hole's thermodynamics. Below a critical chemical potential, associated with either charge (dictionary II.a) or pressure (dictionary II.b), or temperature, (13) becomes three-to-one. The Wald entropy is equal to the horizon radius, but also equal to the cSYK entropy $r_H = \mathcal{S}(Q)$, given the dictionary table. I. As such the three different charge densities Q correspond to three different entropies (horizon radii), i.e., three different states as plotted in fig. 3. These entropies

$$\mathcal{S} \in \{\mathcal{S}_{\text{large BH}}, \mathcal{S}_{\text{unstable BH}}, \mathcal{S}_{\text{small BH}}\},$$

correspond to three different horizon radii; hence we have a large black hole, a small unstable black hole and a small stable black hole, as expected from a charged extended space system [18]. Those with a positive specific heat, corresponding to negative horizon curvature, are the stable phases [30].

These entropies exactly correspond to the phases of the gaseous, unstable liquid, and stable liquid phases of the cSYK model, reflected in the different charge densities Q . These three phases are seen in the three-to-one behavior in the rescaled chemical potential $\tilde{\mu}(Q)$ (or temperature) as a function of entropy $\tilde{\mathcal{S}}(Q)$. Between the temperature $\tilde{\mu}_1 \sim \tilde{\mu}_2$, there are three different phases corresponding to the three different horizon radii. The thermodynamically preferred radius corresponds to the minimum Gibbs free energy between the three.

It is important to note that since the partition functions and equations of states exactly overlap, given the dictionary I, we are guaranteed to have equivalent thermodynamics for both dual models. This means that they share the same critical exponents, given in table III, hence the same universality class.

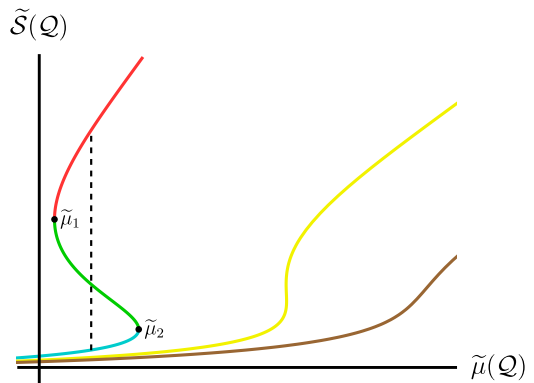


FIG. 3. The red, green, and blue curves represent the three phases of black hole, small, medium, and large, respectively. The dashed line stands for the thermodynamically favorable solution, in which the area of both sides is the same (Maxwell area law). The yellow line and brown lines are for $\tilde{T} = \tilde{T}_{\text{crit}}$ and $\tilde{T} > \tilde{T}_{\text{crit}}$ respectively.

Here we take a moment to describe the thermodynamics from the gravitation perspective. This is done by translating the known results for the q body cSYK model [17] into gravitational language via the dictionary.

TABLE III. Tables of critical (left) and effective (right) exponents

α	β	γ	δ
0	1/2	1	3

α_μ	β_μ	γ_μ	α_Q	γ_Q
2/3	1/3	2/3	0	1

To get some idea of the interpretations on the gravitational side, let us for the moment consider Table II.b. The charge density is provided in color on these diagrams and is then directly related to the thermodynamic volume of the black hole $V_{\text{th}} = 1/2 - Q$. Note that when we approach the boundary, we consider smaller values of Q , corresponding to larger volumes.

Various power laws emerge as the critical point (P_c, T_c) is reached which can differ from the critical exponents. This is due to a feature well known in the field of statistical mechanics known as field mixing [34]. The prototypical example is that of the van der Waals liquid. These *effective* power laws are still physically relevant. For instance, the specific heat will diverge as $C_P \propto |T - T_c|^{-2/3}$, i.e. $\alpha_P = 2/3$. Given its relation to the Ricci scalar (25), we note that this ensures a finite horizon curvature. It remains well-defined at constant volume $C_V \propto T \sim t^0$, as is common to RN system [35]. The remaining *effective* exponents can be obtained from [17], and are listed in III.

The equivalence is over the entire coexistence line, meaning that we have the same thermodynamics also in the regime where the quantum model has a chaotic-to-nonchaotic transition $T = \mathcal{O}(q^{-2})$, $P = \mathcal{O}(q^{-2})$. Here the chaotic phase corresponds to the maximally large black hole $r_H = r_{\text{max}}$. The nonchaotic phase on the quantum side corresponds to an evaporated black hole, where the horizon radius goes to zero $r_H \rightarrow 0$. This transition occurs at a pressure $P_0 = 4Q_B/q^2$. We will further consider the degree of chaos, a dynamical

property, in the next section.

V. METRIC DUAL TO THE CSYK MODEL

To make the mapping more explicit, we must fully specify the functions \mathcal{U} and \mathcal{W} which define the dJT model. Extending the identification $r_{\text{H}} = \mathcal{S}(\mathcal{Q})$ to all radii, we have the equation $r = \mathcal{S}(x)$, or the inverse $x(r) = \mathcal{S}^{-1}(r)$. When evaluated at the horizon, we find the order parameter $\mathcal{Q} = x(r = r_{\text{H}})$. We perform this inversion in various regimes in App.C 1. Given the above, we can fully specify the functions V and A_t , hence \mathcal{U} and \mathcal{W} , given (6). In other words, we can fully specify the particular deformation. Using the relations in (6), we have that

$$\mathcal{Q}'(r_{\text{H}}) = \begin{cases} -2/\mathcal{W}(r_{\text{H}}) & (a) \\ -\mathcal{U}(r_{\text{H}}) & (b) \end{cases}$$

which is equal to $1/\mathcal{S}'(\mathcal{Q})$. With this, we note that $\mathcal{S}'(\mathcal{Q})$ measures the coupling to the Maxwell fields given dictionary (a), while dictionary (b) yields the reciprocal dilaton potential. Hence, (a) identifies the U(1) charges on the gravitational side with that of the condensed matter side. Using either of the tables II.a or II.b would yield the enthalpy “functions”

$$PV(r) - Q_{\text{B}}A_t(r)/2 = \mu[1/2 - x(r)] - 2\epsilon(x(r))/q^2. \quad (19)$$

Here the second term stems from the relation with the interaction energy density function (11)

$$\epsilon(x) \equiv \mathcal{J}(x) \sin(\pi v(x)/2), \quad \mathcal{J}(x) \sim [1 - 4x^2]^{q/4} J. \quad (20)$$

Using (19) we find the metric corresponding to the cSYK model, defined by the emblackening factor (5) written directly in terms of the dual condensed matter model’s parameters

$$f(r)/(4\pi) = \mu[\mathcal{Q} - x(r)] + 2\epsilon(\mathcal{Q})/q^2 - 2\epsilon(x(r))/q^2. \quad (21)$$

The roots of this function yield the horizons. The largest root is the event horizon r_{H} of the black hole, i.e., $x(r_{\text{H}}) = \mathcal{Q}$. The smaller root r_- , corresponding to large x , is the Cauchy horizon. For instance, where the interaction energy becomes exponentially small $\epsilon(x) \sim e^{-qx^2}$ we have a root at $x(r_-) = \mathcal{Q} + 2\epsilon(\mathcal{Q})/(\mu q^2)$.

As before, the temperature is obtained from the function $f'(r_{\text{H}})$. For other values of r , we define the function

$$\mathcal{T}(x) \equiv \frac{f'(r(x))}{4\pi} = \frac{\mu - 4x\epsilon(x)/q}{2 \tanh^{-1}(2x)} \quad (22)$$

where $T = \mathcal{T}(\mathcal{Q})$. With this, the closure relation becomes

$$\mathcal{J}(x)/\mathcal{T}(x) = \pi v(x) \sec(\pi v(x)/2). \quad (23)$$

Solving (23) in the limiting cases, we find

$$\frac{\epsilon(x)}{\mathcal{J}(x)} \sim \begin{cases} 1 + \mathcal{O}(\mathcal{T}^2(x)/\mathcal{J}^2(x)), \\ \frac{\mathcal{J}(x)}{\mu} \tanh^{-1}(2x), \end{cases} \quad \text{for } x = \mathcal{O}(q^0). \quad (24)$$

Evaluating (22) at the horizon, where $x(r_{\text{H}}) = \mathcal{Q}$, yields the cSYK EOS (13) as expected from a dual theory.

Evaluated at the horizon, the curvature may be written as

$$\mathcal{R}_2(r_{\text{H}}) = -4\pi \left(\frac{\partial T_{\text{H}}}{\partial \mathcal{S}_W} \right)_{\mu, J} = -\frac{4\pi T_{\text{H}}}{C_{\mu}}, \quad (25)$$

where C_{μ} is the heat capacity at constant chemical potential

$$C_{\mu} \equiv T_{\text{H}} \left(\frac{\partial \mathcal{S}_W}{\partial T_{\text{H}}} \right)_{\mu, J}. \quad (26)$$

For $\mathcal{Q} = \mathcal{O}(q^0)$, the SYK interactions are suppressed, yielding a near-free system $\mathcal{Q} \sim \tanh(\beta\mu/2)/2$ with specific heat $C_{\mu} \sim 2(\beta\mu)^2 e^{-\beta\mu}$ as entropy tends to zero ($\mathcal{Q} \rightarrow 1/2$). This means that the curvature at the horizon blows up as the dual system becomes a free Fermi gas, as was found in [36]. In this sense, the mapping is a weak-strong duality. An analogy would be how the shear viscosity diverges in the free theories with holographic duals considered in [37, 38].

Given the above discussion, we can now gain an idea of the metric dual to the cSYK model. Recall that the stable phases have positive specific heat. Noting that $f^{(1)}(r_{\text{H}}) = 4\pi T_{\text{H}}$ and $f^{(2)}(r_{\text{H}}) = 4\pi T_{\text{H}}/C_{\mu}$, we may express the near-horizon emblackening factor as

$$f(r_{\text{H}} + \delta) = 4\pi T_{\text{H}} \delta (1 + \delta/(2C_{\mu})) + \mathcal{O}(\delta^3). \quad (27)$$

As such the stable phases, above and near the horizon, will have a positive concave-up emblackening factor.

A. Need for an IR cutoff

As $x \rightarrow 1/2$, the interaction energy contributions are fully suppressed, leaving a free theory. As such, we need only invert $\mathcal{S}_2(x)$, which yields

$$x(r) \sim \frac{1}{2} - \frac{r}{\ln(1/r)} \xrightarrow{r \rightarrow 0^+} 1/2. \quad (28)$$

We have $r_{\text{H}} = 0$ corresponding to $\mathcal{Q} = 1/2$. We, however, exclude this point from our space, i.e., $r > 0$. From this, we also note that $r \geq r_{\text{H}}$, i.e., when $x(r) \leq \mathcal{Q}$. A naive calculation of x , when x is small, yields the inverse $x(r) \sim \sqrt{(\ln 2 - r)/2}$. The diverging second derivative at $r = \mathcal{S}(0)$ would also yield a diverging scalar curvature $\mathcal{R}_2(r) = -f^{(2)}(r)$. This simple expression is due to the simplicity of the two-dimensional static metric we have, yielding simple Christoffel symbols.

As mentioned in Sec. IV, the EOS (13) is not valid for $\mathcal{Q} = 0$, seen in its diverging temperature. This is because, on the condensed matter side, it determines the chemical potential

$$\mu = 2T \tanh(2\mathcal{Q}) + 4\mathcal{Q}\epsilon/q$$

rather than the temperature. As such, $\mathcal{Q} = 0$, directly implies $\mu = 0$, leaving T a free variable. In the form of (13), we are thus effectively dividing by zero, when $\mathcal{Q} = 0$. Since this corresponds to a zero charge SYK model, this point

$r = \ln 2$ is also where the EOS (13) fails. We fix this by limiting our scope to small but non-zero charge densities. On the gravitational side, this means that we consider a minimal $x = x_{\min} \neq 0$. This is equivalent to introducing an IR cutoff radius r_{\max} . The square root is then modified to

$$x(r) \sim \sqrt{x_{\min}^2 + (r_{\max} - r)/2} \xrightarrow{r \rightarrow r_{\max}} x_{\min} \quad (29)$$

As such, to have a well-defined theory, we should have some non-zero minimum value $\mathcal{Q} = x_{\min}$. Such a minimum appears when considering a particular IR cutoff r_{\max} . We choose this cutoff such that our theory will satisfy two conditions:

(I) Given the cutoff we have access to the full liquid-gas coexistence line of the SYK model.

(II) The scalar curvature $\mathcal{R}_2(r_{\max})$ remains finite for any finite value of q . This condition would, for instance, be violated given an emblackening factor $f(r) \propto \sqrt{r_{\max} - r}$, which has both a diverging temperature function (related to $f'(r)$) and scalar curvature (related to $f^{(2)}(r)$).

One choice in cutoff is such that we include the minimum charge density which occurs along the coexistence line in the cSYK model, $x_{\min} = 1/q$ [17]. Given that the entropy function relates x to the radius, we substitute this value to find

$$r_{\max} = \ln 2 - \frac{4 + \pi^2 + \mathcal{O}(q^{-2})}{2q^2}. \quad (30)$$

Note that for both the first or second rescaled regimes

$$\mu = q^{-3/2}\tilde{\mu} = \mathcal{O}(q^{-3/2}), \quad \mu = q^{-2}\bar{\mu} = \mathcal{O}(q^{-2}) \quad (31)$$

we are guaranteed a small temperature function at the cutoff

$$\mathcal{T}(x_{\min} = 1/q) \sim q\mu/4 - J/q + \mathcal{O}(q^{-3/2}). \quad (32)$$

Further motivations for this choice are provided in App.D. From the above, we also note the endpoint of the coexistence line $\mu_0 = 4J/q^2$, corresponding to zero temperature. At the boundary $\mathcal{T}(x_{\min})$, (26) is given by $\beta C_\mu \sim 16/\mu$, for μ of order $q^{-3/2}$ or lower. Now using (26), we find the scalar curvature $\mathcal{R}_2(r_{\text{H}}) = -4\pi T/C_\mu$, yielding the boundary curvature $\mathcal{R}_2(r_{\max}) = -\pi q^3 \mu/4$ which is indeed finite for any finite q , hence our chosen cutoff satisfies condition (II). The dictionary II.b is required if we wish to identify the pressure with the cosmological constant, as standard in black hole chemistry [19]. A different cutoff would yield a different curvature. Since the cutoff is not unique, one could view this specific cutoff as being the most appropriate in that it yields the expected curvature.

From the above, we note that the near-extremal limit, we are left with $f(r) \propto -\pi q J(r - r_{\text{H}})^2$. Close to the cutoff, for small $\delta = q^2(r - r_{\max})$, we have (D8) $f'(r) = q\pi\mu(1 - \delta/2)^{-1/2} - q\pi\mu_0$, implying the emblackening factor

$$f(r) = f(r_{\max}) + q\pi[\mu - \mu_0]\delta/2 + \frac{q\pi\mu}{8}\delta^2 + \mathcal{O}(\delta^3) \quad (33)$$

working to explicit order $\mathcal{O}(q^{-1})$.

There are multiple other choices of cutoffs that would satisfy both above conditions. One could also consider UV cutoffs to regularize the theory at smaller distances.

VI. COMPARISON OF LYAPUNOV EXPONENTS

In this section, we wish to compare the dynamical properties of the two models with matching thermodynamics. While it was true that the choice of particular dictionary in Table II did not affect the thermodynamics, the same cannot be said about the dynamics. This is because we are choosing which cSYK term should be identified with the electrical field. Here we will consider both cases. We focus on their Lyapunov exponents measuring the sensitivity to initial conditions. We write the Lyapunov exponent as $\lambda_L = 2\pi v T$. For the SYK model, v is the solution to the closure relation (23) $\beta\mathcal{J}(\mathcal{Q}) = \pi v \sec(\pi v/2)$. In the maximally chaotic regime $T = q^{-1}\tilde{T}$, $\mu = q^{-3/2}\tilde{\mu}$ with tilde'd quantities are q -independent, it is solved by

$$v = 1 - 2q^{-1}\tilde{T}/\mathcal{J}(\mathcal{Q}) + \mathcal{O}(q^{-2}) \xrightarrow{q \rightarrow \infty} 1. \quad (34)$$

The liquid phase becomes near-integrable in the second rescaled regime $\beta = q^2\bar{\beta}$, $\mu = q^{-2}\bar{\mu}$, where barred quantities are held fixed as $q \rightarrow \infty$. In this same regime, the gaseous phase remains maximally chaotic. The tendency to integrability is driven by its large charge density $\mathcal{Q} = \mathcal{O}(q^0)$ which suppresses the effective coupling $\mathcal{J}(\mathcal{Q}) \sim J e^{-q\mathcal{Q}^2}$, leading to an exponentially small Lyapunov exponent $v = q^2\bar{\beta}\mathcal{J}(\mathcal{Q})/\pi \xrightarrow{q \rightarrow \infty} 0$.

For a non-extremal black hole, the maximal Lyapunov exponent is usually given by the surface gravity $\kappa = f'(r_{\text{H}})/2 = 2\pi T_{\text{H}}$ [39] which is MSS bound [3]. We find λ_L by focusing on the near-horizon trajectory of a charged particle close to the black hole. The corresponding equations of motion are [40] $\dot{r} = \pi_r f$, $\dot{t} = -[\pi_t + Q_e A_t]/f$ and

$$\dot{\pi}_r = -\pi_r^2/(2f') - \dot{t}^2 f'/2 - Q_e A_t' \dot{t}, \quad (35)$$

where π_t and π_r are the t and r components of particle momentum, respectively. The particle's charge is given by Q_e and $A_t = -\Phi$. Note that we are focusing on the particle's geodesic for a non-dynamic metric. As such, an implicit assumption is the particle's back-reaction on the metric can be ignored.

The two-velocity's normalization condition $\dot{x}_\nu \dot{x}^\nu = -1$, for massive particles, implies that $1 = f\dot{t}^2 - \dot{r}^2/f$. Substituting the above expressions leaves the two solutions $\dot{t} = \sqrt{\pi_r^2 + 1/f}$. Using this, the equations of motion of $\rho = (r, \pi_r)$ are $\partial_t \rho = \dot{\rho}/\dot{t} = \mathbf{F}(\rho)$, with

$$F_1(\rho) = \frac{\pi_r f}{\sqrt{\pi_r^2 + 1/f}},$$

$$F_2(\rho) = -\frac{\pi_r^2/f'}{2\sqrt{\pi_r^2 + 1/f}} - f' \frac{\sqrt{\pi_r^2 + 1/f}}{2} - Q_e A_t'.$$

We next linearize these equations around the fixed point ρ_0 , $\mathbf{F}(\rho_0) = 0$, to first order $\mathbf{F}(\rho) = K(\rho_0)(\rho - \rho_0)$, where

$$K(\rho_0) = \begin{bmatrix} \partial_r F_1 & \partial_{\pi_r} F_1 \\ \partial_r F_2 & \partial_{\pi_r} F_2 \end{bmatrix} \Big|_{\rho=\rho_0} \quad (36)$$

is the Jacobian matrix. Slight perturbations away from a fixed point the dynamics is described by $\rho = e^{tK(\rho_0)}\rho_0$. In terms of the phase space (r, π_r) , we have a fixed point at $\pi_r = 0$ and for massive particles the additional condition that

$$Q_e = -\frac{f'(r_i)}{2f(r_i)^{1/2}A_t'(r_i)}. \quad (37)$$

From here we can either find the corresponding initial r_i given a charge Q_e , or we can just consider any r_i , but set the charge accordingly. The results are equivalent, but the analysis is simpler for the latter. For massive particles, the matrix K is off-diagonal $K_{11} = K_{22} = 0$, with $K_{12} = f^{3/2}$ and

$$K_{21} = f^{-3/2} \left[(f'/2)^2 - Q_e A_t^{(2)} f^{3/2} - f f^{(2)}/2 \right]. \quad (38)$$

It has eigenvalues $\lambda_{\pm} = \pm\sqrt{\det K}$, where the largest eigenvalue is the Lyapunov exponent λ_+ . To get a measure of how much MSS bound is saturated, we focus on $v_{dT} \equiv \lambda_+/\kappa$, explicitly given by

$$v_{dT} = \frac{f'(r_i)}{f'(r_H)} \sqrt{1 + \frac{2f(r_i)}{f'(r_i)} \left[\frac{A_t^{(2)}(r_i)}{A_t'(r_i)} - \frac{f^{(2)}(r_i)}{f'(r_i)} \right]}, \quad (39)$$

which is 1 if the system is maximally chaotic, in the sense of saturating the MSS bound.

Using the near horizon emblackening factor, we find (27)

$$\frac{2f(r_H + \delta)}{f'(r_H + \delta)} \sim \delta \frac{2C_\mu + \delta}{C_\mu + \delta}, \quad \frac{f^{(2)}(r_H + \delta)}{f'(r_H + \delta)} \sim \frac{1}{C_\mu + \delta}. \quad (40)$$

Let us further assume that

$$\frac{A_t^{(2)}(r_H + \delta)}{A_t'(r_H + \delta)} = \frac{1}{\Phi_{\text{th}}'(r_H)/\Phi_{\text{th}}^{(2)}(r_H) + \delta} \quad (41)$$

is of order $\mathcal{O}(\delta^0)$. If we now take the limit as $\delta \rightarrow 0$, without specifying any dependent on q, T_H we get one of two results. For $T \neq 0$, we have a non-extremal black-hole and $v_{dT}(\delta) = \sqrt{1 + \mathcal{O}(\delta)} \rightarrow 1$. In other words, at finite β , we obtain a Lyapunov exponent saturating the MSS bound. This is in both phases, which agrees with the Lyapunov exponents of the gaseous and liquid phases in the rescaled regime $T = q^{-1}\tilde{T}$, $\mu = q^{-3/2}\tilde{\mu}$ of the cSYK model [17].

A. Near-extremal case

We now wish to compare to the results in the second rescaled regime $T = q^{-2}\tilde{T}$, $\mu = q^{-2}\tilde{\mu}$. As $T_H \rightarrow 0$, so does the specific heat, meaning that

$$\frac{2f(r_H + \delta)}{f'(r_H + \delta)} \rightarrow \delta, \quad \frac{f^{(2)}(r_H + \delta)}{f'(r_H + \delta)} \rightarrow \frac{1}{\delta}. \quad (42)$$

With this (39) reduces to

$$v_{dT}(\delta) = \sqrt{1 + \delta[\mathcal{O}(\delta^0) - \delta^{-1}]} \rightarrow 0. \quad (43)$$

corresponding to an extremal black-hole with emblackening factor $f(r) = f^{(2)}(r_H)\delta^2/2$. An exception to the above occurs if the electrical potential contribution leads to a perfect cancelation such that v remains equal to 1. We have assumed that (41) remains of order δ^0 . To assess the validity of this assumption we calculate (41) for both possible dictionaries II.a and II.b. We write this as deviations from the specific heat

$$C^{(a/b)} \equiv \frac{\Phi_{\text{th}}^{(1)}(r_H)}{\Phi_{\text{th}}^{(2)}(r_H)} = C_\mu - \delta_{\pm}^{(a/b)} \quad (44)$$

Here we use the a/b to denote the cases given the two dictionaries in Table II. In this notation, a perfect cancelation will occur if $\delta_{\pm}^{(a/b)}$ goes to zero. Here $\Phi_{\text{th}} \propto \mathcal{Q} - 1/2$ for dictionary II.a and $\Phi_{\text{th}} \propto E = H + (\mathcal{Q} - 1/2)\mu$ for dictionary II.b. With this, we have

$$\Phi_{\text{th}}^{(1)}(r_H) = \begin{cases} \mathcal{Q}'(r_H) & (a) \\ T + \mu\mathcal{Q}'(r_H) & (b) \end{cases}$$

where we have used the enthalpy relation $\partial_S H = T$. Further, recalling that $C_\mu = T\partial_T \mathcal{S}$, we have the second derivatives

$$\Phi_{\text{th}}^{(2)}(r_H) = \begin{cases} \mathcal{Q}^{(2)}(r_H) & (a) \\ T/C_\mu + \mu\mathcal{Q}^{(2)}(r_H) & (b), \end{cases}$$

where $\mathcal{Q}^{(2)}(\mathcal{S}) = -\mathcal{S}^{(2)}(\mathcal{Q})/S'(\mathcal{Q})^3$. For the non-interaction system we find $S_0' = -\bar{\beta}\tilde{\mu}$ and $S_0^{(2)} = -(\bar{\beta}\tilde{\mu})^2 C_\mu^{(0)}$. As such, without any interactions, one finds that (44) is exactly equal to $C_\mu^{(0)}$, in other words, the same term as in (40). However, there are still contributions stemming from the interactions. Now for the lower boundary $\mathcal{Q} \rightarrow 1/2$, where $C_\mu^{(0)} \sim 2(\bar{\beta}\tilde{\mu})^2 e^{-\bar{\beta}\tilde{\mu}}$,

$$\delta_-^{(a)} \sim \frac{(\pi v/2)^2}{2} (\bar{\beta}\tilde{\mu})^2, \quad \delta_-^{(b)} \sim C_\mu^{(0)}/2$$

and for the upper boundary $\mathcal{Q} \rightarrow 1/q$, we find

$$\delta_+^{(a/b)} \sim 2\frac{v-1}{q} + \frac{2(2+\pi^2)/q^2}{\pi^4 - 4\pi^2 - 2} \quad (45)$$

From the above, a perfect cancelation in the larger black hole if we first take the $q \rightarrow \infty$ limit in (45). This then implies that the large black hole is still maximally chaotic in the sense that $v_{dT} \rightarrow 1$. This result would then match with the gaseous Majorana-like ($\mathcal{Q} = 0$) SYK phase at low temperature.

The same can happen in the smaller black hole depending on how the limit is taken. The smaller black hole seems rather badly behaved in terms of the emblackening factor. Especially when considering the black hole charge to be the conjugate driving the phase transition, one should also consider a possible free AdS phase. In other words, one should perform a similar analysis to that of Hawking and Page [41], examining the free energy of the pure AdS solutions to determine when and how this crossover occurs. This would modify the interpretation of the low-temperature regime.

Given the above analysis, one should also note its possible limitation. This lies in the fact that for the extremal black hole the charge of the test particle (37) tends to diverge at the fixed point. For such a diverging charge, it is unlikely that one can ignore the back-reaction from the charged particle [42].

VII. CONCLUSION

Previous analogies between RN-AdS black holes with spherical event horizons and the van der Waals liquid past due to their similar phase structure [18]. However, on the dual field theory side, there is a lack of equivalent holographic descriptions in the literature. In this work, we provided such a holographic description between the $(0 + 1)$ -dimensional cSYK model and $(1 + 1)$ -dimensional JT gravity with a particular deformation. In particular, we have provided a deformed JT gravitational model with a matching partition function to the $q/2$ -body interacting cSYK model for large q . Moreover, together with matching equations of states, we have an exact equivalence in the thermodynamics. We achieved this by introducing a deformed JT gravity model characterized by a dilaton potential $\mathcal{U}(\varphi)$ and dilaton-to-Maxwell field coupling $\mathcal{W}(\varphi)$, and deriving the black hole metric in terms of the physical quantities of the cSYK model.

One of the original reasons for believing that the SYK model should have a holographic dual was its maximal Lyapunov exponent, which is also found in gravitation theories [2]. As such, we went beyond the thermodynamic description and also considered the chaotic nature of the black hole. Close to the second-order phase transition, both liquid and gaseous phases of the cSYK model are maximally chaotic. We estimated the Lyapunov exponent on the gravitational side via linear stability analysis. This indicated the standard maximal Lyapunov exponents associated with both large and small black hole phases. As such, in the first rescaled regime of the

phase diagram, we not only found the same thermodynamics but also the same Lyapunov exponents.

It is known that the Lyapunov exponents of black holes in the extremal limit tend to zero. This is a side effect of the bound $2\pi T$ tending to zero since the extremal limit corresponds to the zero temperature limit. As such we focused on the ratio $v = \lambda_L/(2\pi T)$. For the cSYK model, the liquid phase would remain maximally chaotic $v = 1$, while the gaseous phase becomes regular $v \rightarrow 0$. Depending on the choice of dictionary, and how the limits are taken, one can get different results for the small and large black holes. This highlights the need for a more in-depth analysis taking the black hole back action into account. Open questions also remain in terms of the appropriate UV and IR cutoffs to prevent unphysical behavior in the black hole. As an example, for ordinary $(1 + 3)$ -dimensional black hole chemistry the smaller black hole's radius does not shrink to zero [18]. When setting the charge to zero, the black hole no longer exists at $T = 0$. A natural question is whether some interpretation changes could yield similar results.

The provided dictionaries directly overlap with the analogies between the charged SYK model and charged black holes provided in [17]. As such this paper directly serves as an answer to said paper, by both showing that the analogies can be used as dictionaries. In conclusion, our results encourage the use of holography away from the low-temperature regime, i.e., beyond the near-extremal regime.

ACKNOWLEDGEMENTS

We would like to thank Wenhe Cai, Yicheng Rui, and Rishabh Jha for their helpful discussions. This work is partly supported by NSFC, China (Grant No. 12275166 and No. 11875184) and partly by the Deutsche Forschungsgemeinschaft (DFG, German Research Foundation) - SFB 1073.

-
- [1] G. Sarosi, in *Proceedings of XIII Modave Summer School in Mathematical Physics — PoS(Modave2017)*, Vol. 323 (SISSA Medialab, 2018) p. 001.
 - [2] A. Kitaev, “A simple model of quantum holography,” (2015), talks given at “Entanglement in Strongly-Correlated Quantum Matter,” (Part 1, Part 2), KITP (2015).
 - [3] J. Maldacena, S. H. Shenker, and D. Stanford, *J. High Energy Phys.* **2016**, 106 (2016).
 - [4] D. A. Trunin, *Phys.-Usp.* **64**, 219 (2021).
 - [5] D. Anninos and D. A. Galante, *J. High Energy Phys.* **2021**, 1 (2021).
 - [6] D. Anninos, D. A. Galante, and S. U. Sheorey, *arXiv* (2022), 10.48550/arXiv.2212.04944, 2212.04944.
 - [7] S. Cao, Y.-C. Rui, and X.-H. Ge, *arXiv* (2021), 2103.16270.
 - [8] D. Chowdhury, A. Georges, O. Parcollet, and S. Sachdev, *Rev. Mod. Phys.* **94**, 035004 (2022).
 - [9] A. Kitaev and S. J. Suh, *J. High Energy Phys.* **2018**, 1 (2018).
 - [10] A. Almheiri and J. Polchinski, *J. High Energy Phys.* **2015**, 1 (2015).
 - [11] J. Maldacena, D. Stanford, and Z. Yang, *Prog. Theor. Exp. Phys.* **2016**, 12C104 (2016).
 - [12] K. Jensen, *Phys. Rev. Lett.* **117**, 111601 (2016).
 - [13] G. Mandal, P. Nayak, and S. R. Wadia, *J. High Energy Phys.* **2017**, 1 (2017).
 - [14] A. Lala and D. Roychowdhury, *Phys. Rev. D* **100**, 124061 (2019).
 - [15] A. Lala, H. Rathi, and D. Roychowdhury, *Phys. Rev. D* **102**, 104024 (2020).
 - [16] A. M. Garcia-Garcia, B. Loureiro, A. Romero-Bermúdez, and M. Tezuka, *Phys. Rev. Lett.* **120**, 241603 (2018).
 - [17] J. C. Louw and S. Kehrein, *Phys. Rev. B* **107**, 075132 (2023).
 - [18] D. Kubizňák and R. B. Mann, *J. High Energy Phys.* **2012**, 033 (2012).
 - [19] D. Kubizňák, R. B. Mann, and M. Teo, *Classical Quantum Gravity* **34**, 063001 (2017).
 - [20] J. Maldacena and D. Stanford, *Phys. Rev. D* **94**, 106002 (2016).
 - [21] R. A. Davison, W. Fu, A. Georges, Y. Gu, K. Jensen, and S. Sachdev, *Phys. Rev. B* **95**, 155131 (2017).

- [22] A. Gaikwad, K. K. Joshi, G. Mandal, and S. R. Wadia, *J. High Energy Phys.* **2020**, 033 (2020).
- [23] T. Azeyanagi, F. Ferrari, and F. I. Schaposnik Massolo, *Phys. Rev. Lett.* **120**, 061602 (2018).
- [24] J. C. Louw and S. Kehrein, *Phys. Rev. B* **105**, 075117 (2022).
- [25] R.-G. Cai, S. He, S.-J. Wang, and Y.-X. Zhang, *J. High Energy Phys.* **2020**, 1 (2020).
- [26] W. Fu, *The Sachdev-Ye-Kitaev model and matter without quasi-particles*, Ph.D. thesis, Harvard University (2018).
- [27] F. Ferrari and F. I. Schaposnik Massolo, *Phys. Rev. D* **100**, 026007 (2019).
- [28] A. Chamblin, R. Emparan, C. V. Johnson, and R. C. Myers, *Phys. Rev. D* **60**, 064018 (1999).
- [29] M. Ammon and J. Erdmenger, *Gauge/Gravity Duality: Foundations and Applications* (Cambridge University Press, 2015).
- [30] E. Witten, *arXiv* (2020), 2006.03494.
- [31] B. P. Dolan, *Entropy* **18**, 169 (2016).
- [32] R. M. Wald, *Phys. Rev. D* **48**, R3427 (1993).
- [33] J. Gegenberg, G. Kunstatter, and D. Louis-Martinez, *Phys. Rev. D* **51**, 1781 (1995).
- [34] J. Wang and M. A. Anisimov, *Phys. Rev. E* **75**, 051107 (2007).
- [35] J. Zaanen, Y. Liu, Y.-W. Sun, and K. Schalm, *Holographic Duality in Condensed Matter Physics* (Cambridge University Press, Cambridge, England, UK, 2015).
- [36] G. Ruppeiner, *Entropy* **20**, 460 (2018).
- [37] G. Policastro, D. T. Son, and A. O. Starinets, *Phys. Rev. Lett.* **87**, 081601 (2001).
- [38] D. T. Son and A. O. Starinets, *Annu. Rev. Nucl. Part. Sci.* **57**, 95 (2007).
- [39] K. Hashimoto and N. Tanahashi, *Phys. Rev. D* **95**, 024007 (2017).
- [40] Y.-Q. Lei and X.-H. Ge, *Phys. Rev. D* **105**, 084011 (2022).
- [41] S. W. Hawking and D. N. Page, *Commun. Math. Phys.* **87**, 577 (1982).
- [42] E. Poisson, *Living Rev. Relativ.* **7**, 1 (2004).
- [43] “General Relativity Lecture Notes: Matthias Blau,” (2020), [Online; accessed 22. Aug. 2022].
- [44] D. Grumiller and R. McNees, *J. High Energy Phys.* **2007**, 074 (2007).
- [45] M. V. Fedoryuk, in *Analysis I* (Springer, Berlin, Germany, 1989) pp. 83–191.

Appendix A: Extremizing the action

In this section, we find and solve the Euler-Lagrange equations associated with the deformed JT gravity action

$$I[\varphi, A] = \frac{1}{G_N} \int_M d^2x \sqrt{-g} \mathcal{L}(\varphi, A) + I_{\text{bdy}},$$

with boundary action contribution I_{bdy} , described in sec. A 2, which cancels any divergences. The bulk Lagrangian (4) is given by

$$\mathcal{L}(\varphi, A) = \frac{\varphi}{4\pi} \mathcal{R}_2 + PU(\varphi) - \frac{\mathcal{W}(\varphi)}{4} F(A)^2, \quad (\text{A1})$$

with dimension ℓ^{-2} and a dimensionless dilaton field φ . We assume the black hole solution, in the Schwarzschild gauge, takes the form $ds^2 = -f(r)dt^2 + dr^2/f(r)$ in Lorentzian signature. For such a metric, in $(1+1)$ -dimensions, the Ricci

scalar takes the form

$$\mathcal{R}_2(r) = -f^{(2)}(r). \quad (\text{A2})$$

Varying with A yields $\nabla_\mu \mathcal{W} F^{\mu\nu}$. Due to the symmetry of the Christoffel symbols and the asymmetry of $F_{\mu\nu} = 2\partial_{[\mu} A_{\nu]}$, this reduces to $\partial_\mu \mathcal{W} F^{01} = 0$ which is solved by

$$F^{01} = Q_B/\mathcal{W}, \quad F^2 = -2Q_B^2/\mathcal{W}^2. \quad (\text{A3})$$

Varying with φ yields $PU' - \mathcal{W}' F^2/4 = -\mathcal{R}_2/(4\pi)$, which together with the on-shell relation (A3) and (A2) becomes

$$f^{(2)}(r) = 2\pi\partial_\varphi[2PU(\varphi) - Q_B^2/\mathcal{W}(\varphi)]. \quad (\text{A4})$$

Noting that the Einstein tensor is zero in 2-dimensions, varying with g leaves only [25]

$$\nabla_\mu \nabla_\nu \frac{\varphi}{\pi} = g_{\mu\nu} \left[\nabla^2 \frac{\varphi}{\pi} - 2PU + \mathcal{W} \frac{F^2}{2} \right] - 2\mathcal{W} F_{\mu\rho} F_\nu^\rho \quad (\text{A5})$$

Here we have used the identity [43, 20.22]

$$\delta\mathcal{R}_2 = [\mathcal{R}_2]_{\mu\nu} \delta g^{\mu\nu} - (\nabla_\mu \nabla_\nu - g_{\mu\nu} \square) \delta g^{\mu\nu}$$

and used integration by parts. Using (A4), the dilaton equation (A5) reduces to the coupled set of differential equations

$$f'(r) \partial_\tau^2 \varphi = -2\partial_\tau [f(r) \partial_\tau^2 \varphi], \quad \partial_\tau^2 \varphi = f(r)^2 \partial_\tau^2 \varphi \quad (\text{A6})$$

where we have performed a Wick rotation to imaginary time $t \rightarrow i\tau$. Together, these equations reduce to $\partial_r^2 \varphi = 2c f(r)^{-3/2}$ and $\partial_\tau^2 \varphi = 2c \sqrt{f(r)}$, for some constant c . The latter equation is solved by

$$\varphi(\tau, r) = \tau(b + c\tau) \sqrt{f(r)} + R(r), \quad (\text{A7})$$

for some τ independent function $R(r)$ and constants b, c . Inserting (A7) into the former equation $f(r)^{3/2} \partial_\tau^2 \varphi = 2c$,

$$2c = f(r)^{3/2} R^{(2)}(r) - \tau(b + c\tau) \frac{f'(r)^2 - 2f(r)f^{(2)}(r)}{4}. \quad (\text{A8})$$

Note that *only* the last term in (A8) has time dependence. Since this equation should hold for all τ , these τ dependent parts must cancel, i.e., either $b = c = 0$ or $f'(r)^2 = 2f(r)f^{(2)}(r)$. The latter equation is solved by $f_{\text{ext}}(r) = z^{-2}$, where $z = m/(r - r_H)$, where m is some constant and r_H is the event horizon radius. In the JT case where $\mathcal{W} = 0$ (or the charge $Q_B = 0$) and $\mathcal{U} = \varphi$, we would find that

$$f_{\text{JT}}(r) = 2\pi P(r - r_+)(r - r_-). \quad (\text{A9})$$

Hence, we note that the solution $f_{\text{ext}}(r)$ is that of an extremal (zero temperature) black hole $r_\pm \rightarrow r_H$. However, as $r \rightarrow \infty$, we also find that $f_{\text{JT}}(r) \rightarrow f_{\text{ext}}(r)$. This leaves the most general extremal solution to the dilaton (A7)

$$\varphi_{\text{extr}}(\tau, r) = \frac{a + b\tau + c[\tau^2 + m^2 z^2]}{z} + d. \quad (\text{A10})$$

In general, however, for non-zero temperatures, the solution must therefore have $c = b = 0$, i.e., $\varphi(r) = R(r)$, with (A6) indicating that $\varphi^{(2)}(r) = 0$, which is solved by

$$\varphi(r) = \gamma r + \varphi_0 \quad (\text{A11})$$

for some coupling strength γ . For such a time-independent solution, (A3)

$$F^{01} = Q_B/\mathcal{W}(\varphi) = \partial_t A_r - \partial_r A_t \quad (\text{A12})$$

is also time-independent. As such, we may choose the gauge $\partial_t A_r = 0$, meaning that A_t is the antiderivative

$$A_t(r) = \frac{Q_B}{\gamma} \int d\varphi \frac{1}{\mathcal{W}(\varphi)}. \quad (\text{A13})$$

1. Emblackening factor solutions in the non-extremal case

From (A11), $\gamma dr = d\varphi$, and we may integrate (A4) over r to yield

$$\gamma f'(r)/(2\pi) = 2PU(\varphi) - Q_B^2/\mathcal{W}(\varphi) + 2T_0. \quad (\text{A14})$$

Here we have allowed for the possibility of some integration constant $4\pi T_0$ would amount to a shift in temperature T_0 and adding a linear term $T_0\varphi_0$ to the enthalpy. We will later see that this term has no effect on the physics. Integrating once more yields

$$\gamma f(r)/(2\pi) = 2PV(r) - Q_B A_t(r) + 2T_0 r - 2M, \quad (\text{A15})$$

where M is some to-be-determined/interpreted integration constant, and we have defined the anti-derivatives

$$V(r) = \gamma^{-1} \int d\varphi \mathcal{U}(\varphi), \quad \Phi(r) = -A_t(r), \quad (\text{A16})$$

where $\Phi(r) = -A_t(r)$ is the electrical potential at r , w.r.t. the horizon. Further, at the horizon r_H , $f(r_H) = 0$, we find

$$M = PV_{\text{th}} + Q_B \Phi_{\text{th}}/2 + T_0 r_H, \quad (\text{A17})$$

where $V_{\text{th}} \equiv V(r_H)$ is the thermodynamic volume and $\Phi_{\text{th}} \equiv \Phi(r_H)$. Setting $\gamma = 1$, amounts to measuring r in units of γ .

2. Free energy

While working in Euclidean signature $\tau_E = it$, the periodicity $\beta_H = 4\pi/f'(r_H)$ in the metric is required to avoid a conical singularity. We associate the free energy with the on-shell action $\mathcal{F}/G_N = I_E^*/\beta_H + I_{\text{bdy}}^*/\beta_H$. Substituting the on-shell solutions into the bulk Lagrangian density (A1) yields

$$\mathcal{L} = -\frac{r + \varphi_0}{4\pi} f^{(2)}(r) + PV'(r) - Q_B \Phi'(r)/2. \quad (\text{A18})$$

which may be rewritten as

$$\mathcal{L} = -\frac{[(r + \varphi_0)f^{(1)}(r) - f(r)]'}{4\pi} + \partial_r [PV - Q_B A_t/2] \quad (\text{A19})$$

Further, the Euclidean action takes the form

$$G_N I_E^* = -\int_0^{\beta_H} d\tau \int_{r_H}^{r_{\text{max}}} dr \mathcal{L} \quad (\text{A20})$$

which, together with (B3) and (B4), leaves us with the on-shell action

$$\mathcal{F} = -\frac{[r_H + \varphi_0]f'(r_H) - f(r_H)}{4\pi} + PV_{\text{th}} - Q_B \Phi_{\text{th}}/2 + C \quad (\text{A21})$$

We leave the proof that the appropriate boundary terms allow us to set $C = 0$, for App. B. Noting $f'(r_H) = 4\pi T_H$ allows us to identify the conjugate to the temperature $\mathcal{S}_W = r_H + \varphi_0$ with the Wald entropy. Since we expect zero entropy when the black hole evaporates to zero $r_H \rightarrow 0$, we set $\varphi_0 = 0$. Lastly since $f(r_H) = 0$, we are then left with the free energy

$$\mathcal{F} = M - Q_B \Phi_{\text{th}} - T_H \mathcal{S}_W. \quad (\text{A22})$$

Having identified the entropy and temperature, one may show that M , defined in (A17), is the mass [25, 33]. From this, one may obtain the Hawking temperature $T_H \equiv 1/\beta_H$ as

$$\left(\frac{\partial M}{\partial \mathcal{S}_W}\right)_{Q_B, P} = T_H = PV'_{\text{th}}(\mathcal{S}_W) + Q_B \Phi'_{\text{th}}(\mathcal{S}_W)/2 + T_0, \quad (\text{A23})$$

Together (A22) and (A23) define the thermodynamics of the system. We note that T_0 shifts the definition of temperature. Due to our freedom in choosing the potentials defining the temperature relation, we may set $T_0 = 0$ without loss of generality.

3. The Gibbs free energy and the uncharged dual

In black hole chemistry, the pressure and thermodynamic volume are conjugate to another [31]. This leads to the identification of the ADM mass with the enthalpy, indicating that $Q_B \Phi_{\text{th}}/2$ is the interaction energy. Further, the thermodynamic potential which selects out the favorable state is the Gibbs free energy [19]

$$G = M - T_H \mathcal{S}_W, \quad (\text{A24})$$

with differential $dG = -\mathcal{S}_W dT_H + V_{\text{th}} dP + \Phi_{\text{th}} dQ_B$.

Let us now consider the uncharged case by setting the term $\mathcal{W}(\varphi)F(A)^2$ equal to zero in (4). Following this, we make the replacement $PU \rightarrow PU - Q_B^2/(2\mathcal{W})$. One may note that this leaves all the equations of motion the same as the charged case [25, 44]. Such a replacement is also equivalent to replacing the varying Maxwell field with its on-shell part in the action. This replacement does, however, yield a single difference—a sign flip in the above on-shell action (A22) in the charged term

$$\frac{G_N I_{\text{uncharged dual}}^*}{\beta_H} = PV_{\text{th}} + Q_B \Phi_{\text{th}}/2 - T_H \mathcal{S}_W. \quad (\text{A25})$$

Recalling the expression for the ADM mass (A17) we note that (A25) is the Gibbs free energy G . This is somewhat reminiscent of the relations between the canonical ensembles. In the first case, we originally allowed the electromagnetic field to vary, leading to the \mathcal{F} . Instead, replacing the Maxwell field by its on-shell part, we no longer treat it as its own independent parameter. This then yields the Gibbs free energy.

Appendix B: Low energy effective action and counter terms

1. Gravitational boundary term

Here we show how the appropriate boundary term counters perfectly the divergences to yield a constant part in (A21)

$$C = \frac{\varphi_{\max} f'(r_{\max}) - f(r_{\max})}{4\pi} - [PV - Q_B \Phi/2]_{r=r_{\max}} + \frac{I_{\text{bdy}}}{\beta_H} \quad (\text{B1})$$

which is perfectly canceled by the boundary action $I_{\text{bdy}} = I_{\text{ct}} + I_{\text{GHY}}$. This is composed of two parts, counter and the Gibbons-Hawking-York (GHY) terms given by

$$I_{\text{ct}} \equiv \frac{1}{G_N} \int_{\partial M} d\tau \sqrt{h} \mathcal{L}_{\text{ct}}, \quad I_{\text{GHY}} \equiv -\frac{1}{G_N} \int_{\partial M} d\tau \sqrt{h} \varphi K, \quad (\text{B2})$$

respectively. The induced metric and extrinsic curvature of the boundary $r = r_{\max}$ entering the above are given by $h = f(r_{\max})$ [7] and $K = -\partial_{r_{\max}} \sqrt{h}$ respectively, yielding (B2)

$$\frac{G_N I_{\text{GHY}}^*}{\beta_H} = -\frac{\varphi(r_{\max}) f'(r_{\max})}{4\pi}. \quad (\text{B3})$$

The on-shell counter Lagrangian, on the boundary, we require is

$$\mathcal{L}_{\text{ct}} = \frac{\sqrt{f(r_{\max})}}{4\pi} + \frac{PV - Q_B \Phi/2}{\sqrt{f(r_{\max})}},$$

which yields the on-shell contribution

$$\frac{G_N I_{\text{ct}}^*}{\beta_H} = \frac{f(r_{\max})}{4\pi} + [PV - Q_B \Phi/2]_{r=r_{\max}}. \quad (\text{B4})$$

Substituting (B3) and (B4) into (B1), we see how the divergences cancel to zero $C = 0$.

Appendix C: cSYK entropy form

In this section, we show that the complex SYK model has an entropy of the form

$$\boxed{\mathcal{S}(\mathcal{Q}) = \mathcal{S}_2(\mathcal{Q}) - (\pi v/q)^2/2}. \quad (\text{C1})$$

We do this by using the Maxwell relation

$$- \left(\frac{\partial \mathcal{S}}{\partial \mathcal{Q}} \right)_{T,J} = \left(\frac{\partial \mu}{\partial T} \right)_{\mathcal{Q},J}, \quad (\text{C2})$$

together with the EOS

$$T = \frac{\mu - 4\mathcal{Q}\epsilon/q}{2 \tanh^{-1}(2\mathcal{Q})}, \quad (\text{C3})$$

rewritten in the form

$$\mu = 2T \tanh^{-1}(2\mathcal{Q}) + 4\mathcal{Q}\epsilon/q, \quad (\text{C4})$$

where $\epsilon \equiv \mathcal{J}(\mathcal{Q}) \sin(\pi v/2)$ and the non-interacting part corresponds to $\mathcal{S}'_2(\mathcal{Q}) = -2 \tanh^{-1}(2\mathcal{Q})$. As such, we are left to show that the corrections $\mathcal{S}_I = \mathcal{S} - \mathcal{S}_2$ satisfy

$$-q \left(\frac{\partial \mathcal{S}_I}{\partial \mathcal{Q}} \right)_{T,J} = \left(\frac{\partial \mathcal{Q}\epsilon}{\partial T} \right)_{\mathcal{Q},J} \quad (\text{C5})$$

or explicitly, for (C1) to hold, we must show that

$$(\partial_{\mathcal{Q}} v)_{T,J} \pi^2 v/q = 2\pi \mathcal{Q} \mathcal{J}(\mathcal{Q}) \cos(\pi v/2) (\partial_T v)_{\mathcal{Q},J}. \quad (\text{C6})$$

From the closure relation (23)

$$\beta \mathcal{J}(\mathcal{Q}) = \pi v \sec(\pi v/2) \quad (\text{C7})$$

this relation reduces to $(\partial_{\mathcal{Q}} v)_{T,J}/q = 2\mathcal{Q} T (\partial_T v)_{\mathcal{Q},J}$. To find the derivatives of v , we differentiate both sides of the closure relation with respect to some variable x

$$\partial_x \ln[\beta \mathcal{J}(\mathcal{Q})] = \partial_x \ln[\pi v \sec(\pi v/2)] = a(v) \partial_x \ln v,$$

where $1/b(v) \xrightarrow{v \rightarrow 0} v$ and $1/b(v) \xrightarrow{v \rightarrow 1} 1 - v$ is explicitly given by $b(v) = a(v)/v$ with

$$a(v) \equiv 1 + \pi v \tan(\pi v/2)/2 = 1 + \beta\epsilon/2.$$

So we have $(\partial_{\mathcal{Q}} v)_{T,J} = b(v)^{-1} \partial_{\mathcal{Q}} \ln \mathcal{J}(\mathcal{Q})$ and $(\partial_T v)_{\mathcal{Q},J} = -b(v)^{-1} \partial_T \ln T$. As such, we only have left to show that $\partial_{\mathcal{Q}} \ln[\mathcal{J}(\mathcal{Q})]/q = -2\mathcal{Q}$, which follows from the definition of effective interaction, for small charge densities, $\ln \mathcal{J}(\mathcal{Q}) \sim -q\mathcal{Q}^2$. For larger charge densities, the SYK contribution is exponentially suppressed in q and the theory is only described by the non-interacting part. As such, we have shown that (C1) holds.

One may show that this entropy remains correct even for zero charge density. This may be verified using the differential (17) at $\mu = \mathcal{Q} = 0$ together with the closure relation (C7).

1. Inverse function of two-state entropy

Here we find the inverse function $r = \mathcal{S}_2^{-1}(x)$ to the two-state entropy function (12)

$$\mathcal{S}_2(x) \equiv -\frac{1-2x}{2} \ln \left| \frac{1-2x}{2} \right| - \frac{1+2x}{2} \ln \left| \frac{1+2x}{2} \right|. \quad (\text{C8})$$

For $x = 1/2 - \sigma$, $\mathcal{S}_2(x) = \sigma[1 - \ln \sigma] + \mathcal{O}(\sigma^2)$, where $r = \sigma_{1/2}[1 - \ln \sigma_{1/2}]$ is solved by $\sigma_{1/2} = e^{1+\mathcal{W}_{-1}(-r/e)}$, which is the product log function [45]

$$\mathcal{W}_{-1}(-r) = \ln(r) - \ln(-\ln(r)) + \mathcal{O}\left(\frac{\ln(-\ln(r))}{\ln(r)}\right) \quad (\text{C9})$$

With this, the solution may be written as $\sigma_{1/2}(r) \sim -r/\ln r$. Around $x = 0$, $\mathcal{S}_2(x) = \ln 2 - 2x^2 + \mathcal{O}(x^4)$, solved by

$$x(r) = \sqrt{[\ln 2 - r]/2} + \mathcal{O}(\ln 2 - r)^{3/2}. \quad (\text{C10})$$

Close to the IR cutoff $x(r \rightarrow r_{\max}) = x_{\min}$, for $x = \mathcal{O}(q^{-2})$, we should consider the full entropy function (C1)

$$\mathcal{S}(x) = \ln 2 - \frac{4\bar{x}^2 + (\pi v)^2}{q^2} + \mathcal{O}(q^{-4})$$

Assuming $\mathcal{T}(x) = o(q^0)$, we have $v(x) = 1 + o(q^0)$. Here we are using little o notation, where $o(q^0)$, means sub-leading in q^0 , e.g., $1/\ln q$. In terms of the radii we have the equation $r(x) \sim r_{\max} + 2(x_{\min}^2 - x^2)$, which is solved by

$$x(r) \sim \sqrt{x_{\min}^2 + (r_{\max} - r)/2} \quad (\text{C11})$$

2. Specific heat

The typical Majorana SYK model has thermodynamics matching the cSYK model at half-filling $\mathcal{Q} = 0$. For this case, we note that the entropy is merely given by $\mathcal{S} = \ln 2 - (\pi v/q)^2/2$. The corresponding specific heat $C_\mu = T\partial_T\mathcal{S}$, is then found by considering how v changes with temperature, as described by the closure relation (C7). Such an analysis eventually reveals $C_\mu \sim 2(\pi/q)^2 T/J$ as $T \rightarrow 0$. Since the equation of state, as written in (C3), is no longer valid for $\mathcal{Q} = 0$, a natural question is whether this specific heat can still be obtained from the general analysis. Here we show that this is indeed the case.

For the full specific heat, we consider

$$\left(\frac{\partial\mathcal{S}}{\partial T}\right)_{\mu,J} = \left(\frac{\partial\mathcal{Q}}{\partial T}\right)_{\mu,J} \mathcal{S}'_2(\mathcal{Q}) - \left(\frac{\partial v}{\partial T}\right)_{\mu,J} \left(\frac{\pi}{q}\right)^2 v.$$

As before, we will assume, unless stated otherwise, that μ, J is kept constant. We find relate $\partial_T v$ to $\partial_T \mathcal{Q}$, by considering both the EOS and the closure relation (C7) yielding

$$\left(\frac{\partial v}{\partial T}\right)_{\mu,J} = -\frac{\beta + 2q\mathcal{Q}\partial_T\mathcal{Q}}{b(v)}$$

and

$$\left(\frac{\partial\mathcal{Q}}{\partial T}\right)_{\mu,J} \sim \frac{1 - 4\mathcal{Q}^2}{4} \frac{\beta\mathcal{S}'_2(\mathcal{Q}) - \mathcal{Q}\partial_T(\pi v)^2/q}{1 + (1 - 2q\mathcal{Q}^2)\beta\epsilon/q}$$

which together yields

$$\left(\frac{\partial\mathcal{Q}}{\partial T}\right)_{\mu,J} = \frac{1 - 4\mathcal{Q}^2}{4T} \frac{\mathcal{S}'_2(\mathcal{Q}) + 2\pi^2\mathcal{Q}[v/b(v)]/q}{1 + \beta\epsilon/q - \mathcal{Q}^2[2\beta\epsilon + \pi^2v/b(v)]}.$$

The general expression reads

$$q^2 C_\mu = T \left(\frac{\partial\mathcal{Q}}{\partial T}\right)_{\mu,J} \left[q^2 \mathcal{S}'_2(\mathcal{Q}) + 2q\mathcal{Q} \frac{\pi^2 v}{b(v)} \right] + \frac{\pi^2 v}{b(v)}. \quad (\text{C12})$$

As $\mathcal{Q} \rightarrow 0$, only the final expression $\pi^2 v/b(v) \rightarrow 2\pi^2 T/J$ remains where $v = 1 - 2T/J + \mathcal{O}^2(T/J)$, hence specific heat $C_\mu \sim 2(\pi/q)^2 T/J$. This corresponds to a large negative curvature $\mathcal{R}_2(\ln 2) \sim -2Jq^2/\pi$.

Appendix D: IR cutoff details

We choose this cutoff such that our theory will satisfy two conditions:

(I) Given the cutoff we have access to the full coexistence line of the SYK model.

(II) The scalar curvature $\mathcal{R}_2(r_{\max})$ remains finite for any finite value of q . This condition would, for instance, be violated given an emblackening factor $f(r) \propto \sqrt{r_{\max} - r}$, which has both a diverging temperature function (related to $f'(r)$) and scalar curvature (related to $f^{(2)}(r)$).

With these conditions in mind, let us consider the radius as a function of x_{\min} when $x_{\min} = \bar{x}_{\min}/q$. This can be done since the entropy function relates these two $r = \mathcal{S}(x)$. Expanding the entropy function around $\bar{x}_{\min} \leq \mathcal{O}(q^0)$, we find

$$r_{\max} = \ln 2 - \frac{4\bar{x}_{\min}^2 + (\pi v(x_{\min}))^2 + \mathcal{O}(q^{-2})}{2q^2}. \quad (\text{D1})$$

Note that this maximal event horizon radius tends to the maximal entropy of a two-state system $r_{\max} = \mathcal{S}_{\max} \xrightarrow{q \rightarrow \infty} \ln 2$, which is also the von Neumann entropy of maximally entangled Bell states.

1. Condition (I): Physics along the coexistence line

For \bar{x}_{\min}/q , we will find a temperature function (22) of the order $\mathcal{T}(x_{\min}) = o(q^0)$, for $\mu \leq \mathcal{O}(q^{-3/2})$, which includes the entire coexistence line. Let us see this explicitly. In the second order PT regime $\mu = \tilde{\mu}q^{-3/2}$, yielding

$$\mathcal{T}(x_{\min}) \sim \frac{q^{-1/2}\tilde{\mu}}{4\bar{x}_{\min}} - J e^{-\bar{x}_{\min}^2/q}/q \quad (\text{D2})$$

which is of the order $\mathcal{O}(1/q)$ for the chaotic-to-nonchaotic PT regime, $\mu = \bar{\mu}/q^2$.

For $\mathcal{T}(x_{\min}) = o(q^0)$ the closure relation (23) yields $v(x_{\min}) = 1 + o(q^0)$. This also shows how, on the quantum side, the maximally large black hole ($r_{\text{H}} = r_{\max}$) corresponds to a maximally chaotic SYK model. This is seen in the Lyapunov exponent $\lambda_L = 2\pi T v$ saturating the MSS bound $2\pi T$ for $v(x(r_{\text{H}})) \rightarrow 1$. As such we are left with

$$r_{\max} = \ln 2 - \frac{4\bar{x}_{\min}^2 + \pi^2 + o(q^0)}{2q^2}. \quad (\text{D3})$$

The second condition can only be violated for certain choices of x_{\min} . As example would be to demand that x_{\min} be an exact root of \mathcal{T} , i.e., when $\mu = 4x\epsilon(x)/q$. Due to the closure relation (23), we know that this root ($\mathcal{T}(x) = 0$) implies that $v(x) = 1$, i.e., $\mu = 4x\mathcal{J}(x)/q$. For small $x = \tilde{x}/\sqrt{q}$, this yields the equation $\tilde{\mu}/(4J) = \tilde{x}e^{-\tilde{x}^2}$. This is solved by the product log function \mathcal{W}_0

$$\tilde{x} = \sqrt{\frac{-\mathcal{W}_0(-\tilde{\mu}^2/(8J^2))}{2}} \xrightarrow{\tilde{\mu} \rightarrow 0} \tilde{\mu}/(4J)$$

which is real for $\tilde{\mu}/J \leq (8/e)^{1/2} < 2$. Limiting ourselves to only such values of the chemical potential unfortunately

would limit our scope to only the line of first-order phase transitions. This is because the second order phase transition occurs at $\tilde{\mu}_c/J = (6/e)^{3/2} > 3$.

There does, however, exist one case where $\mathcal{T}(x_{\min})$ should be close to zero. This is when the $r_{\text{H}} = r_{\text{max}}$, i.e., for a near-extremal maximally large black hole. This phase is stable when $\mu_0 = \tilde{\mu}_0/q^2$. Here $\tilde{\mu}_0 = 4J$ is the endpoint of the coexistence line plotted in Fig. 1. This phase should have a temperature of order q^{-2} , $T = \bar{T}q^{-2}$. Substituting this into (D2), for a maximally large black hole, we find

$$\mathcal{T}(x_{\min}) \sim J \frac{1 - \bar{x}_{\min}(1 - \bar{x}_{\min}^2/q)}{\bar{x}_{\min}q} \quad (\text{D4})$$

which is of order q^{-2} when

$$\bar{x}_{\min} = 1 + \frac{1 - \bar{y}/J}{q}, \quad (\text{D5})$$

for some ‘‘freely’’ chosen \bar{y} . Substituting this result back into (D4), we find that $\mathcal{T}(x_{\min}) = \bar{y}/q^2$. This allows us to consider charge densities up to the minimum charge density which occurs along the coexistence line $x_{\min} = 1/q$ [17]. Substituting (D5) into (D3) we are left with

$$r_{\text{max}} = \ln 2 - \frac{4 + \pi^2 + \mathcal{O}(q^{-2})}{2q^2}. \quad (\text{D6})$$

which is independent of μ/J . We also have

$$\mathcal{T}(x_{\min} = 1) \sim q^{-1/2}\tilde{\mu}/4 - J/q + \mathcal{O}(q^{-3/2}) \quad (\text{D7})$$

Note that while we have written this equation for the scaling $\mu = \mathcal{O}(q^{-3/2})$, it remains valid for $\mu = \mathcal{O}(q^{-2})$. In that case, it may be written as $\mathcal{T}(x_{\min} = 1) \sim [\tilde{\mu}/4 - J]/q$, which is zero at the endpoint of the coexistence line $\tilde{\mu} = 4J$.

Together with the expression (C11), we have near the cut-off, so small $\delta = q^2(r - r_{\text{max}})$,

$$f'(r) = q\pi\mu(1 - \delta/2)^{-1/2} - q\pi\mu_0 \quad (\text{D8})$$

which yields the scalar curvature $-f^{(2)}(r_{\text{max}})/2 = q^3\mu/4$.

Now using (26), we find the scalar curvature $\mathcal{R}_2(r_{\text{H}}) = -4\pi T/C_\mu$. At the IR boundary $\mathcal{Q} = 1/q$, $\beta\epsilon \rightarrow$

$\pi v \tan(\pi v/2)$, for which (C12) reduces to

$$q^2 C_\mu \sim \frac{\pi^2 v}{b(v)} + \frac{4}{1 + \beta\epsilon/q} \sim \frac{2\pi^2}{\beta J} + \frac{4}{1 + \beta J/q}, \quad (\text{D9})$$

where we have replaced $\beta\epsilon/q = \beta J/q + \mathcal{O}(T/q)$ and $v/b(v) \rightarrow 2T/J$. We may evaluate this at the boundary using (D9)

$$\mathcal{R}_2(r_{\text{max}}) \sim -4\pi q^2 / \left[\frac{2\pi^2}{J} + \frac{4}{\mathcal{T}(r_{\text{max}}) + J/q} \right], \quad (\text{D10})$$

yielding

$$\mathcal{R}_2(r_{\text{max}}) \sim -\pi q^{3/2}\tilde{\mu}/4, \quad (\text{D11})$$

Note that this is in agreement with the above result (D8).

Appendix E: Altered v.s. standard SYK model

Here, we discuss the thermodynamic analysis of the *altered* large- q SYK model $H_{\text{alt}}(\beta\mu)$ introduced by Davison et al. in [21, App. C: Large q expansion of the SYK model].

TABLE IV. Comparison between the standard [17] and altered [21, App. C] SYK models.

Model	Altered SYK	Standard SYK
Hamiltonian	$H_{\text{alt}}(\beta\mu)$ [21]	\mathcal{H} [17]
Phase transition	No	Yes
Interactions at $\mathcal{Q} = \mathcal{O}(q^0)$	Non-trivial	Trivial
Ground state energy density	$\mathcal{O}(q^{-2})$	$e^{-q\mathcal{Q}^2} \mathcal{O}(q^{-2})$

Since the models are identical up to a choice in coupling, the self-energies are also equivalent. The difference arises in the effective coupling from [21, C.8] $\mathcal{J}(\mathcal{Q}) = J(\beta\mu)/c(\beta\mu)$, where $c(\beta\mu) \equiv [2 \cosh(\beta\mu/2)]^{q/2-1} \sim e^{2q[\beta\mu/4]^2}$ for large q , for any $\beta\mu = \mathcal{O}(q^0)$. To counteract this one can rescale the bare coupling, which directly enters the Hamiltonian, as $J(\beta\mu) \rightarrow J_0 c(\beta\mu)$. This yields an altered Hamiltonian $H_{\text{alt}}(\beta\mu)$. This $\beta\mu$ dependent Hamiltonian drastically changes the thermodynamics of the standard temperature-independent SYK Hamiltonian with some differences listed in table IV. For instance, the lack of a negative compressibility [21, C22] in $H_{\text{alt}}(\beta\mu)$, is an indication that $H(\beta\mu)$ *does not* have a phase transition. In contrast, the unaltered Hamiltonian (1) has a quantitatively and qualitatively similar phase diagram to its finite q equivalents [17, 23, 27].

Chapter 6

Summary and outlook

Throughout this thesis, we have discussed the various aspects of the quenched disordered complex Sachdev-Ye-Kitaev (cSYK) models. These models are interesting as maximally chaotic systems which lack quasiparticles. These types of Hamiltonians are remarkable in the sense that, despite their chaotic nature, they are still tractable. We showed how considering $q/2$ -body interactions yielded a powerful non-perturbative way to extract analytical results. Our novel results included in this thesis [61, 80, 81, 130] are all concerned with a $1/q$ expansion. We provided multiple examples of how well such a resummed series yields results that are remarkably qualitatively and quantitatively reflective of the $q \geq 4$ cases. A summary of this was given in Sec. 4.4.

In Chapter 3 we focused on the nonequilibrium properties of the model. We started by considering a single cSYK dot. Using a rather general dynamical protocol (including ramps and quenches),

$$\mathcal{H}(t) = \mathcal{H}_2(t) + \sum_{\kappa} \mathcal{H}_{\kappa q}(t),$$

illustrated in Fig. 3.6, we knocked the system out of equilibrium. We analytically showed that given the post-quench system consists of only a single large- q cSYK term $\mathcal{H}(t > 0) = \mathcal{H}_q$, then the local Green's function will instantaneously be thermal [80]. The final state $\varrho(t = 0)$ is then fully determined by the energy density and the charge density. In this sense, a single $q \rightarrow \infty$ cSYK-term acts as a perfect thermalizer for a large class of states ϱ . The result was shown via conservation laws, namely that of the q -body interaction energy and charge density, in combination with the Galitskii-Migdal sum rule.

Given that the finite q SYK model thermalizes at a rate proportional to its final temperature, we note that this is a property unique to the infinite q limit. As an outlook one could consider the next leading order corrections in q , possibly finding a finite scattering rate that scales with q , hence

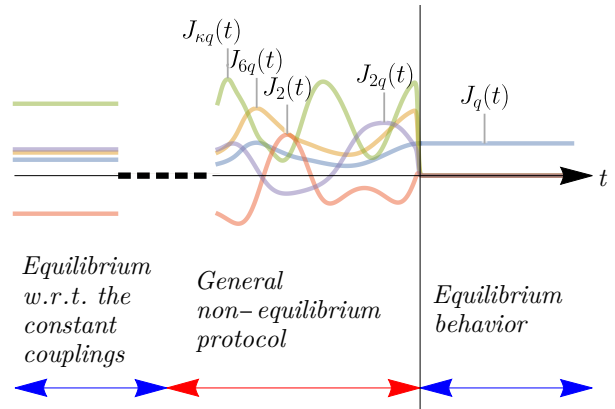


Figure 6.1: Various time protocols leading to instantaneous thermalization

the instantaneous thermalization as $q \rightarrow \infty$. Further, one could consider this model to be a perfect thermalizer; hence it would be interesting to consider it as a bath to another system.

To study aspects of strange metals we further considered a connected d -dimensional lattice Λ of SYK dots. The coupling terms are of order $r = \mathcal{O}(q^0)$, thus corresponding to $r/2$ -particle hopping, between the individual SYK dots allow for transport, i.e., a change in local charge density. This allows one to study its relation to experiment, for instance, the T -linear resistivity characteristic of strange metals. Again a $1/q$ expansion simplified the problem yielding a closed set of equations for the local charge densities

$$\dot{Q}_x(t_1) = \frac{r}{q} \int_{-\infty}^{t_1} dt_2 \sum_{y \in \Lambda} \left[H_{xy}(t_1, t_2) \mathcal{Q}_y \left(\frac{t_1 + t_2}{2} \right) + \mathcal{O}(q^{-1}) \right] \quad (6.1)$$

where the coupling matrix $\hat{H}(t_1, t_2)$ is of order q^0 [81]. This allows one to analytically solve for the charge density fluctuations for a wide range of dynamical protocols. Note that these fluctuations are of order $1/q$, hence suppressed by large q . Since the large- q limit indicates a lack of charge fluctuations, one might suspect that the dots become isolated. We analytically showed that this cannot be the case [81]. This was done by assuming the chain to instantaneously be in thermal equilibrium given a quench that couples the lattice. This would be the case for isolated large- q cSYK dots [80]. This assumption yielded a contradiction, implying that the chain necessarily thermalizes at a finite rate. It would be interesting to calculate this rate in the large- q limit. As an outlook, one could consider $r = q/2$, leading to a linear in T resistivity. The equations for $\dot{Q}_x(t_1)$ will then no longer be closed under the charge density, leading to more complicated, but also richer dynamics. For instance, one might find a chaotic-to-regular phase transition in the chain. Another option is to consider the holographic dual to the chain.

Table 6.1: Analogies between models with shared universality class.

Model	cSYK [80]	RN-AdS [194, 195, 199]	
Order parameter	\mathcal{Q}	Thermodynamic volume V_{th}	Surface electric potential Φ_{th}
conjugate	μ	Vacuum pressure P	Black hole charge Q_B

In Chapter 4 we considered the thermodynamics of the charged SYK model in the grand canonical ensemble $Z = \text{Tr}\{e^{-\beta\mathcal{H} + \beta\mu\mathcal{N}\mathcal{Q}}\}$. By considering rescaled in q quantities, we showed that the finite- q liquid-gas phase transition (PT) [179] persists at infinite q [61]. This is contrary to previous numerical studies being interpreted to suggest otherwise [180]. The analytically obtained large- q results again overlapped strongly with previous numerically obtained finite q results. The differences between the analytical and the numerical results indicated an oversight in previous studies which did not take field mixing into account.

The cSYK phase diagram, shown in Fig. 6.2, was found to bear a striking similarity to those PTs found in Reissner-Nordström (RN), non-rotating and charged, black holes [61]. The large- q cSYK model, like many (if not all) RN black holes, was shown to belong to the mean-field van der Waals universality class. Close to the second order PT $T = \mathcal{O}(q^{-1})$ both liquid and gas phases are maximally chaotic. In the low reduced temperature regime ($T = q^{-2}\bar{T}$, $\bar{T} = \mathcal{O}(q^0)$), the model exhibits a jump between maximally chaotic and non-chaotic phases. We also observed a first-order

Table 6.2: Dictionary between the thermodynamics of the q -dependent cSYK model and deformed JT (dJT) gravity. Each row identifies the two quantities which equate to another.

Model	cSYK	dJT	
Large parameter	N	$1/G_N$	
Entropy density	S	S_W	
Temperature	T	T_H	
Thermodynamic potential	Ω	G	
		dJT (a)	dJT (b)
Conjugate	μ	Q_B^2	P
Oder parameter	$1/2 - Q$	$\frac{\Phi_{th}}{2Q_B}$	V_{th}
Coupling	J	P	Q_B^2
Energy density	E/J	V_{th}	$\frac{\Phi_{th}}{2Q_B}$

quantum phase transition from a Majorana ground state with entropy density $\ln 2$ to a harmonic oscillator with zero entropy density, in the limit as $\bar{T} \rightarrow 0$. This drop in entropy and Lyapunov exponents is characteristic of the first-order Hawking-Page (HP) transition from a black hole to a free thermal gas[231].

Considering the similarities to black hole PTs we collected the quantities which behaved analogously seen in Fig. 6.1. The natural question was whether the table could perhaps be more than just analogies, i.e., whether it could be a holographic (AdS/CFT) dictionary [98]. Investigating this we focused on the gravitational side, starting with a brief review of black hole thermodynamics given in Chapter 5. This gave us the tools needed to extend the holographic duality in the $(0+1)$ -dimensional cSYK dot away from zero temperature. We did this by considering a rather general theory of charged deformed Jackiw-Teitelboim (dJT) gravity, which is a $(1+1)$ -dimensional theory of gravity. Focusing on its thermodynamics, we found the correct deformation and dilaton-Maxwell field coupling required to reproduce the same partition function

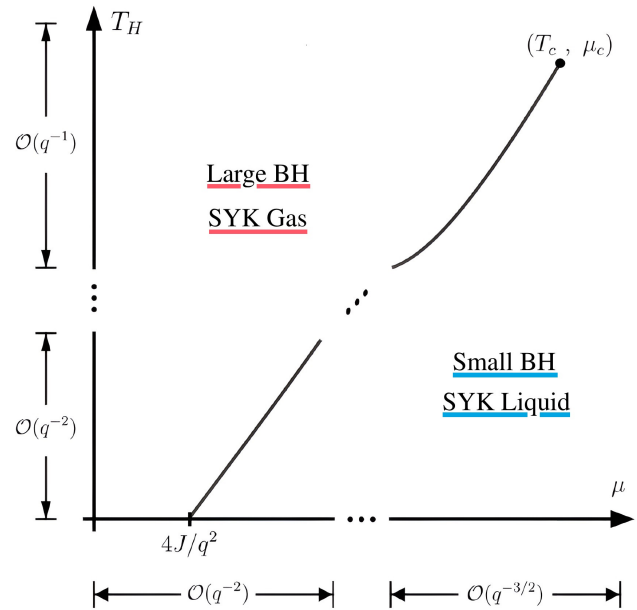


Figure 6.2: Phase diagram of the cSYK model and charged dJT gravity [130].

$Z_{\text{dT}} = Z_{\text{cSYK}}$ and equation of state as the cSYK model

$$T = \left(\frac{\partial H}{\partial \mathcal{S}} \right)_{\mu, J} = T_{\text{H}} = \left(\frac{\partial M}{\partial \mathcal{S}} \right)_{P, Q_{\text{B}}},$$

where $H = \Omega + T\mathcal{S}$ and the ADM mass is given by $M = G + T_{\text{H}}\mathcal{S}_{\text{W}}$. The dictionary is provided in Table 6.2. We noted that there were two different choices for conjugates to the order parameters.

The two choices did not change the thermodynamics, with the same phase diagram as plotted in Fig. 6.2. The choice does have a bearing on the dynamics and interpretation of the gravitational system. In the maximally chaotic regime, we reproduced the maximal Lyapunov exponents, found in the liquid and gas phases of the cSYK model, for both small and large black hole phases. We did this via linear stability analysis of a test particle placed at an unstable fixed point. As the temperature decreases the black hole becomes extremal. The charge of the test particle at the fixed point diverges in this case, implying that our analysis becomes invalid without taking the back action into account. As such, an outlook would be to extract the Lyapunov exponent for the second rescaled regime (close to the origin of the axes in Fig. 6.2), via a different method, for instance, a shock-wave analysis [148].

Before concluding, let us consider a few possible future directions one can go with the SYK-type model we discussed throughout the thesis. The first direction directly relates to the above paragraph. As a simple and exactly solvable model, the large- q cSYK model can be used to see how far one can push holography. This is because both sides of the dual are exactly solvable, allowing one to gain a more concrete understanding of these holographic mappings.

The second direction considers its link to experiments. Key ingredients of all these models are the randomness and all-to-all character of the couplings. Although these features can be mimicked in experiments, as was discussed in Sec. 1.3.4, neither are truly present in real materials. As such a strong physical link to microscopic models is currently lacking. Aside from matching a particular microscopic model, one can view this from the perspective of the Bohigas-Giannoni-Schmit (BHS) conjecture discussed in Sec. 1.3.3. Where the BHS considers the link between single-body Hamiltonians and random matrices, the SYK model is a many-body system. Similarly, one might ask whether the SYK-type Hamiltonians capture aspects of most flat-banded nonintegrable many-body models. In this direction is also the question of fitting to experimental results, e.g., aspects like Kohler scaling resistivities, Lorenz ratios, and specific heats. In other words, can one use the SYK models to more qualitatively match with real materials?

Bibliography

- [1] T. Gaumnitz, A. Jain, Y. Pertot, M. Huppert, I. Jordan, F. Ardana-Lamas, and H. J. Wörner, *Opt. Express* **25**, 27506 (2017).
- [2] J. W. Rohlf, *Modern Physics from alpha to Z0* (Wiley, 1994).
- [3] J. G. Bednorz and K. A. Müller, *Z. Phys. B: Condens. Matter* **64**, 189 (1986).
- [4] D. Chowdhury, A. Georges, O. Parcollet, and S. Sachdev, *Rev. Mod. Phys.* **94**, 035004 (2022).
- [5] R. D. Mattuck, *A Guide to Feynman Diagrams in the Many-Body Problem* (Dover Publications Inc., 1992).
- [6] B. Skinner, *Gravity and Levity: The miracle of Fermi liquid theory* (2015), gravityandlevity.wordpress.com.
- [7] D. Bertrand, *An Experimentally Motivated Study of Electric Fields in Superconductors*, Université catholique de Louvain (2005).
- [8] D. C. Mattis and E. H. Lieb, *J. Math. Phys.* **6**, 304 (1965).
- [9] A. Lerda, *Anyons: Quantum mechanics of particles with fractional statistics*, Vol. 14 (Springer Science, 2008).
- [10] E. S. Coakley and V. Rokhlin, *Appl. Comput. Harmon. Anal.* **34**, 379 (2013).
- [11] S. Kehrein, *The Flow Equation Approach to Many-Particle Systems* (Springer, 2006).
- [12] P. Coleman, *Introduction to Many-Body Physics* (Cambridge University Press, 2015).
- [13] E. Fradkin, *Condensed matter physics ii: Chapter 5: Landau theory of the fermi liquid* (2015), lecture notes for Physics 561.
- [14] K. Andres, J. E. Graebner, and H. R. Ott, *Phys. Rev. Lett.* **35**, 1779 (1975).
- [15] D. van der Marel, J. L. M. van Mechelen, and I. I. Mazin, *Phys. Rev. B* **84**, 205111 (2011).
- [16] X. Wang, V. Askarpour, J. Maassen, and M. Lundstrom, *J. Appl. Phys.* **123**, 055104 (2018).

- [17] A. Lavasani, D. Bulmash, and S. Das Sarma, *Phys. Rev. B* **99**, 085104 (2019).
- [18] C. Kittel, *Introduction to Solid State Physics, 8th Edition* (Wiley, 2004).
- [19] G. S. Kumar, G. Prasad, and R. O. Pohl, *J. Mater. Sci.* **28**, 4261 (1993).
- [20] N. W. Ashcroft and N. D. Mermin, *Solid State Physics* (Saunders College Publishing, 1976).
- [21] T. Giamarchi, A. Iucci, and A. Berthod, *Introduction to many body physics* (2013), lecture notes.
- [22] T. Valla, A. V. Fedorov, P. D. Johnson, and S. L. Hulbert, *Phys. Rev. Lett.* **83**, 2085 (1999).
- [23] W. L. McMillan, *Phys. Rev.* **167**, 331 (1968).
- [24] K. Cho, M. Kończykowski, S. Ghimire, M. A. Tanatar, L.-L. Wang, V. G. Kogan, and R. Prozorov, *Phys. Rev. B* **105**, 024506 (2022).
- [25] M. Baggioli, *Gravity, holography and applications to condensed matter*, PhD Thesis, Universitat Autònoma de Barcelona (2016).
- [26] C. Varma, *Nature* **468**, 184 (2010).
- [27] R. H. McKenzie, *Science* **278**, 820 (1997).
- [28] S. A. Hartnoll, *Nat. Phys.* **11**, 54 (2015).
- [29] J. McGreevy, *Physics* **3** (2010).
- [30] M. Nakajima, S. Ishida, T. Tanaka, K. Kihou, Y. Tomioka, T. Saito, C. H. Lee, H. Fukazawa, Y. Kohori, T. Kakeshita, A. Iyo, T. Ito, H. Eisaki, and S. Uchida, *Sci. Rep.* **4**, 1 (2014).
- [31] S. A. Hartnoll and A. Karch, *Phys. Rev. B* **91**, 155126 (2015).
- [32] J. Crossno, J. K. Shi, K. Wang, X. Liu, A. Harzheim, A. Lucas, S. Sachdev, P. Kim, T. Taniguchi, K. Watanabe, T. A. Ohki, and K. C. Fong, *Science* **351**, 1058 (2016).
- [33] X. Y. Song, C. M. Jian, and L. Balents, *Phys. Rev. Lett.* **119**, 216601 (2017).
- [34] N. Doiron-Leyraud, P. Auban-Senzier, S. René de Cotret, C. Bourbonnais, D. Jérôme, K. Bechgaard, and L. Taillefer, *Phys. Rev. B* **80**, 214531 (2009).
- [35] A. Legros, S. Benhabib, W. Tabis, F. Laliberté, M. Dion, M. Lizaire, B. Vignolle, D. Vignolles, H. Raffy, and Z. Z. Li *et al.*, *Nat. Phys.* **15**, 142 (2019).
- [36] S. Sachdev, *Quantum Phase Transitions* (Cambridge, 1999).
- [37] S. Goldstein, T. Hara, and H. Tasaki, *New J. Phys.* **17**, 045002 (2015).
- [38] S. A. Hartnoll and A. P. Mackenzie, *Rev. Mod. Phys.* **94**, 041002 (2022).

- [39] J. M. Luttinger, Phys. Rev. **119**, 1153 (1960).
- [40] O. Parcollet, A. Georges, G. Kotliar, and A. Sengupta, Phys. Rev. B **58**, 3794 (1998).
- [41] Y.-H. Su and H.-T. Lu, Front. Phys. **13**, 1 (2018).
- [42] K.-S. Chen, S. Pathak, S.-X. Yang, S.-Q. Su, D. Galanakis, K. Mielson, M. Jarrell, and J. Moreno, Phys. Rev. B **84**, 245107 (2011).
- [43] R. P. Smith, M. Sutherland, G. G. Lonzarich, S. S. Saxena, N. Kimura, S. Takashima, M. Nohara, and H. Takagi, Nature **455**, 1220 (2008).
- [44] Y. Kakehashi and P. Fulde, Phys. Rev. Lett. **94**, 156401 (2005).
- [45] J. Maldacena and D. Stanford, Phys. Rev. D **94**, 106002 (2016).
- [46] M. L. Mehta, *Random matrices and matrix models* (Pramana, 1997).
- [47] K. Efetov, *Supersymmetry in Disorder and Chaos* (Cambridge University Press, 1996).
- [48] A. Pandey and R. Ramaswamy, Phys. Rev. A **43**, 4237 (1991).
- [49] M. V. Berry and M. Tabor, Proc. R. Soc. Lond. A. **356**, 375 (1977).
- [50] J. Polchinski and V. Rosenhaus, J. High Energy Phys. **2016** (4), 1.
- [51] S. Sachdev and J. Ye, Phys. Rev. Lett. **70**, 3339 (1993).
- [52] S. Sachdev, J. Stat. Mech.: Theory Exp. **2010** (11), P11022.
- [53] S. Sachdev, Phys. Rev. X **5**, 10.1103/PhysRevX.5.041025 (2015).
- [54] A. M. Garcia-Garcia and J. J. M. Verbaarschot, Phys. Rev. D **94**, 126010 (2016).
- [55] Y.-Z. You, A. W. W. Ludwig, and C. Xu, Phys. Rev. B **95**, 115150 (2017).
- [56] A. Kitaev, A simple model of quantum holography (2015), talks given at “Entanglement in Strongly-Correlated Quantum Matter,” (Part 1, Part 2), KITP (2015).
- [57] Y. Gu, A. Kitaev, S. Sachdev, and G. Tarnopolsky, J. High Energy Phys. **2020** (2), 1.
- [58] S. Sachdev, SYK models, strange metals, and black holes (2016).
- [59] D. Chowdhury and E. Berg, Phys. Rev. Res. **2**, 013301 (2020).
- [60] Y. Wang and A. V. Chubukov, Phys. Rev. Res. **2**, 033084 (2020).
- [61] J. C. Louw and S. Kehrein, Phys. Rev. B **107**, 075132 (2023).
- [62] W. Fu and S. Sachdev, Phys. Rev. B **94**, 035135 (2016).
- [63] O. Bohigas, M. J. Giannoni, and C. Schmit, Phys. Rev. Lett. **52**, 1 (1984).

- [64] O. Bohigas, M. J. Giannoni, and C. Schmit, *J. Physique. Lett.* **45**, 1015 (1984).
- [65] J. Maldacena, S. H. Shenker, and D. Stanford, *J. High Energy Phys.* **2016** (8).
- [66] H. A. Kramers and G. H. Wannier, *Phys. Rev.* **60**, 252 (1941).
- [67] J. Behrends and B. Béri, *Phys. Rev. Lett.* **128**, 106805 (2022).
- [68] R. Babbush, D. W. Berry, and H. Neven, *Phys. Rev. A* **99**, 040301 (2019).
- [69] L. Garcia-Álvarez, I. L. Egusquiza, L. Lamata, A. del Campo, J. Sonner, and E. Solano, *Phys. Rev. Lett.* **119**, 040501 (2017).
- [70] S. Lisi, X. Lu, T. Benschop, T. A. de Jong, P. Stepanov, J. R. Duran, F. Margot, I. Cucchi, E. Cappelli, A. Hunter, A. Tamai, V. Kandyba, A. Giampietri, A. Barinov, J. Jobst, V. Stalman, M. Leeuwenhoek, K. Watanabe, T. Taniguchi, L. Rademaker, S. J. van der Molen, M. P. Allan, D. K. Efetov, and F. Baumberger, *Nat. Phys.* **17**, 189 (2021).
- [71] D. Marchenko, D. V. Evtushinsky, E. Goliias, A. Varykhalov, Th. Seyller, and O. Rader, *Sci. Adv.* **4**, eaau0059 (2018).
- [72] C. Wei and T. A. Sedrakyan, *arXiv 10.48550/arXiv.2205.09766* (2022), 2205.09766 .
- [73] D. Leykam, A. Andreanov, and S. Flach, *Advances in Physics: X* **3**, 1473052 (2018).
- [74] A. Chen, R. Ilan, F. de Juan, D. I. Pikulin, and M. Franz, *Phys. Rev. Lett.* **121**, 036403 (2018).
- [75] C. Wei and T. A. Sedrakyan, *Phys. Rev. A* **103**, 013323 (2021).
- [76] A. Chew, A. Essin, and J. Alicea, *Phys. Rev. B* **96**, 121119 (2017).
- [77] M. Fremling and L. Fritz, *Phys. Rev. B* **105**, 085147 (2022).
- [78] D. I. Pikulin and M. Franz, *Phys. Rev. X* **7**, 031006 (2017).
- [79] I. Danshita, M. Hanada, and M. Tezuka, *Prog. Theor. Exp. Phys.* **2017**, 083101 (2017).
- [80] J. C. Louw and S. Kehrein, *Phys. Rev. B* **105**, 075117 (2022).
- [81] R. Jha and J. C. Louw, *Phys. Rev. B* **107**, 235114 (2023).
- [82] P. Cha, A. A. Patel, E. Gull, and E.-A. Kim, *Phys. Rev. Res.* **2**, 033434 (2020).
- [83] G. Tarnopolsky, *Phys. Rev. D* **99**, 026010 (2019).
- [84] E. S. Swanson, *AIP Conf. Proc.* **1296**, 75 (2010).
- [85] R. A. Davison, W. Fu, A. Georges, Y. Gu, K. Jensen, and S. Sachdev, *Phys. Rev. B* **95**, 155131 (2017).

- [86] J. O. Fjærestad, *Introduction to green functions and many-body perturbation theory* (2016), lectures notes.
- [87] J. P. Blaizot and G. Ripka, *Quantum Theory of Finite Systems* (MIT Press, 1986).
- [88] S. W. Hawking, *Nature* **248**, 30 (1974).
- [89] G. Gur-Ari, R. Mahajan, and A. Vaezi, *J. High Energy Phys.* **2018** (11), 1.
- [90] H. Nishimori, *Statistical physics of spin glasses and information processing: an introduction* (Oxford University Press, 2001).
- [91] N. Read and S. Sachdev, *Nucl. Phys. B* **316**, 609 (1989).
- [92] A. Georges, O. Parcollet, and S. Sachdev, *Phys. Rev. B* **63**, 134406 (2001).
- [93] T. Castellani and A. Cavagna, *J. Stat. Mech.: Theory Exp.* **2005** (05), P05012.
- [94] C. L. Baldwin and B. Swingle, *Phys. Rev. X* **10**, 031026 (2020).
- [95] Y. Gu, X.-L. Qi, and D. Stanford, *J. High Energy Phys.* **2017** (5), 1.
- [96] D. A. Trunin, *Phys.-Usp.* **64**, 219 (2021).
- [97] E. J. Marcus, *Black Holes and Revelations: Investigating Black Holes using String Theory, SYK-Models and Quark-Gluon Plasmas* (Utrecht University, Utrecht, The Netherlands, 2021).
- [98] V. Rosenhaus, *J. Phys. A: Math. Theor.* **52**, 323001 (2019).
- [99] M. Tsutsumi, *J. Math. Anal. Appl.* **76**, 116 (1980).
- [100] A. M. Garcia-Garcia, B. Loureiro, A. Romero-Bermúdez, and M. Tezuka, *Phys. Rev. Lett.* **120**, 241603 (2018).
- [101] L. Boltzmann, in *The Kinetic Theory of Gases*, Vol. 1 (Imperial College Press, 2003).
- [102] A. Peres, *Phys. Rev. A* **30**, 1610 (1984).
- [103] N. Pottier, *Nonequilibrium Statistical Physics* (Oxford University Press, 2014).
- [104] T. Kinoshita, T. Wenger, and D. S. Weiss, *Nature* **440**, 900 (2006).
- [105] M. Rigol, V. Dunjko, and M. Olshanii, *Nature* **452**, 854 (2008).
- [106] T. Langen, S. Erne, R. Geiger, B. Rauer, T. Schweigler, M. Kuhnert, W. Rohringer, I. E. Mazets, T. Gasenzer, and J. Schmiedmayer, *Science* **348**, 207 (2015).
- [107] J. C. Louw, M. Kastner, and J. N. Kriel, *Phys. Rev. B* **102**, 094430 (2020).
- [108] S. Popescu, A. J. Short, and A. Winter, *Nat. Phys.* **2**, 754 (2006).

- [109] M. Srednicki, Phys. Rev. E **50**, 888 (1994).
- [110] J. M. Deutsch, Rep. Prog. Phys. **81**, 082001 (2018).
- [111] S. H. Strogatz, *Nonlinear Dynamics and Chaos: With Applications to Physics, Biology, Chemistry, and Engineering* (Taylor & Francis, Andover, UK, 2019) publication Title: Taylor & Francis.
- [112] C. Rouvas-Nicolis and G. Nicolis, Scholarpedia **4**, 1720 (2009).
- [113] J. S. Cotler, D. Ding, and G. R. Penington, Ann. Phys. **396**, 318 (2018).
- [114] A. I. Larkin and Y. N. Ovchinnikov, Sov Phys JETP **28**, 1200 (1969).
- [115] M. B. Hastings, arXiv 10.48550/arXiv.1008.5137 (2010), 1008.5137 .
- [116] D. A. Roberts and B. Swingle, Phys. Rev. Lett. **117**, 091602 (2016).
- [117] D. A. Roberts and B. Yoshida, J. High Energy Phys. **2017** (4), 1.
- [118] N. Tsuji and P. Werner, Phys. Rev. B **99**, 115132 (2019).
- [119] Y. Liao and V. Galitski, Phys. Rev. B **98**, 205124 (2018).
- [120] B. Kobrin, Z. Yang, G. D. Kahanamoku-Meyer, C. T. Olund, J. E. Moore, D. Stanford, and N. Y. Yao, Phys. Rev. Lett. **126**, 030602 (2021).
- [121] D. Bagrets, A. Altland, and A. Kamenev, Nucl. Phys. B **921**, 727 (2017).
- [122] W. Fu, *The Sachdev-Ye-Kitaev model and matter without quasiparticles*, PhD Thesis, Harvard University (2018).
- [123] P. Uhrich, S. Bandyopadhyay, N. Sauerwein, J. Sonner, J.-P. Brantut, and P. Hauke, arXiv 10.48550/arXiv.2303.11343 (2023), 2303.11343 .
- [124] Y. Sekino and L. Susskind, J. High Energy Phys. **2008** (10), 065.
- [125] C. Murthy and M. Srednicki, Phys. Rev. Lett. **123**, 230606 (2019).
- [126] A. Kitaev, Black holes and the SYK model (2015), talks given at ‘It from Qubit School, IB-CAB’ (Black holes and the SYK model), Instituto Balseiro (2018).
- [127] A. A. Patel, *Transport, criticality, and chaos in fermionic quantum matter at nonzero density*, Ph.D. thesis, Harvard University (2019).
- [128] K. Hashimoto and N. Tanahashi, Phys. Rev. D **95**, 024007 (2017).
- [129] S. H. Shenker and D. Stanford, J. High Energy Phys. **2015** (5), 1.
- [130] J. C. Louw, S. Cao, and X.-H. Ge, arXiv 10.48550/arXiv.2305.05394 (2023), 2305.05394 .

- [131] E. B. Rozenbaum, S. Ganeshan, and V. Galitski, *Phys. Rev. Lett.* **118**, 086801 (2017).
- [132] S. Pilatowsky-Cameo, J. Chávez-Carlos, M. A. Bastarrachea-Magnani, P. Stránský, S. Lerma-Hernández, L. F. Santos, and J. G. Hirsch, *Phys. Rev. E* **101**, 010202 (2020).
- [133] A. Romero-Bermúdez, K. Schalm, and V. Scopelliti, *J. High Energy Phys.* **2019** (7), 1.
- [134] Y.-Q. Lei and X.-H. Ge, *Phys. Rev. D* **105**, 084011 (2022).
- [135] R. Bhattacharya, S. Chakrabarti, D. P. Jatkar, and A. Kundu, *J. High Energy Phys.* **2017** (11), 1.
- [136] C. Choi, M. Mezei, and G. Sárosi, *J. High Energy Phys.* **2021** (5), 1.
- [137] H. Bruus and K. Flensberg, *Many-Body Quantum Theory in Condensed Matter Physics: An Introduction (Oxford Graduate Texts)* (Oxford University Press, 2004).
- [138] A. Kamenev, *Field Theory of Non-Equilibrium Systems* (Cambridge University Press, 2011).
- [139] M. Pourfath, *Numerical study of quantum transport in carbon nanotube-based transistors*, PhD Thesis, Technical University of Vienna (2007).
- [140] G. Stefanucci and R. Van Leeuwen, *Nonequilibrium many-body theory of quantum systems: A modern introduction*, Vol. 9780521766173 (Cambridge University Press, 2010) publication Title: Nonequilibrium Many-Body Theory Quantum Syst. A Mod. Introd.
- [141] D. Semkat, D. Kremp, and M. Bonitz, *Phys. Rev. E* **59**, 1557 (1999).
- [142] T. Langen, R. Geiger, and J. Schmiedmayer, *Annu. Rev. Condens. Matter Phys.* **6**, 201 (2015).
- [143] A. Eberlein, V. Kasper, S. Sachdev, and J. Steinberg, *Phys. Rev. B* **96**, 205123 (2017).
- [144] J. Steinberg, N. P. Armitage, F. H. L. Essler, and S. Sachdev, *Phys. Rev. B* **99**, 035156 (2019).
- [145] N. Sorokhaibam, *J. High Energy Phys.* **2020** (7), 55.
- [146] T. Samui and N. Sorokhaibam, *J. High Energy Phys.* **2021** (4), 1.
- [147] T. Samui and N. Sorokhaibam, *J. High Energy Phys.* **2021** (4), 157.
- [148] J. Engelsöy, T. G. Mertens, and H. Verlinde, *J. High Energy Phys.* **2016** (7), 1.
- [149] J. A. N. Bruin, H. Sakai, R. S. Perry, and A. P. Mackenzie, *Science* **339**, 804 (2013).
- [150] S. A. Grigera, R. S. Perry, A. J. Schofield, M. Chiao, S. R. Julian, G. G. Lonzarich, S. I. Ikeda, Y. Maeno, A. J. Millis, and A. P. Mackenzie, *Science* **294**, 329 (2001).
- [151] B. Bertini, F. Heidrich-Meisner, C. Karrasch, T. Prosen, R. Steinigeweg, and M. Žnidarič, *Rev. Mod. Phys.* **93**, 025003 (2021).

- [152] S. R. Manmana, S. Wessel, R. M. Noack, and A. Muramatsu, Phys. Rev. Lett. **98**, 210405 (2007).
- [153] C. Zanoci and B. Swingle, Phys. Rev. B **103**, 115148 (2021).
- [154] C. Zanoci and B. Swingle, Phys. Rev. B **105**, 235131 (2022).
- [155] I. Esin, C. Kuhlenskamp, G. Refael, E. Berg, M. S. Rudner, and N. H. Lindner, arXiv 10.48550/arXiv.2203.01313 (2022), 2203.01313 .
- [156] A. A. Patel, D. Chowdhury, S. Sachdev, and B. Swingle, Phys. Rev. X **7**, 031047 (2017).
- [157] A. Haldar, S. Banerjee, and V. B. Shenoy, Phys. Rev. B **97**, 241106 (2018).
- [158] D. Chowdhury, Y. Werman, E. Berg, and T. Senthil, Phys. Rev. X **8**, 031024 (2018).
- [159] J. de Woul, *Fermions in Two Dimensions and Exactly Solvable Models*, PhD Thesis, Royal Institute of Technology (KTH) (2011).
- [160] A. Georges, G. Kotliar, W. Krauth, and M. J. Rozenberg, Rev. Mod. Phys. **68**, 13 (1996).
- [161] W. Ding, R. Žitko, P. Mai, E. Perepelitsky, and B. S. Shastry, Phys. Rev. B **96**, 054114 (2017).
- [162] A. A. Patel and S. Sachdev, Phys. Rev. Lett. **123**, 066601 (2019).
- [163] M. Brinkmann, H. Bach, and K. Westerholt, Physica C **292**, 104 (1997).
- [164] T. Tomita, K. Kuga, Y. Uwatoko, P. Coleman, and S. Nakatsuji, Science **349**, 506 (2015).
- [165] Y. Ando and T. Murayama, Phys. Rev. B **60**, R6991 (1999).
- [166] Z. Konstantinović, Z. Z. Li, and H. Raffy, Phys. Rev. B **62**, R11989 (2000).
- [167] J. Levallois, K. Behnia, J. Flouquet, P. Lejay, and C. Proust, Europhys. Lett. **85**, 27003 (2009).
- [168] P. W. Phillips, N. E. Hussey, and P. Abbamonte, Science **377**, eabh4273 (2022).
- [169] D. Nickelsen and M. Kastner, Phys. Rev. Lett. **122**, 180602 (2019).
- [170] J. Goold, M. Huber, A. Riera, L. del Rio, and P. Skrzypczyk, J. Phys. A: Math. Theor. **49**, 143001 (2016).
- [171] P. Zanardi, J. Math. Phys. **55**, 082204 (2014).
- [172] Y. Nakata and T. J. Osborne, Phys. Rev. A **90**, 050304 (2014).
- [173] W. W. Ho and S. Choi, Phys. Rev. Lett. **128**, 060601 (2022).
- [174] D. Poulin, A. Qarry, R. Somma, and F. Verstraete, Phys. Rev. Lett. **106**, 170501 (2011).

- [175] H. Wilming and I. Roth, arXiv 10.48550/arXiv.2202.01669 (2022), 2202.01669 .
- [176] M. Costeniuc, R. S. Ellis, H. Touchette, and B. Turkington, Phys. Rev. E **73**, 026105 (2006).
- [177] H. Touchette, M. Costeniuc, R. S. Ellis, and B. Turkington, Physica A **365**, 132 (2006).
- [178] H. Nishimori, G. Ortiz, H. Nishimori, and G. Ortiz, *Elements of Phase Transitions and Critical Phenomena* (Oxford University Press, 2015).
- [179] T. Azeyanagi, F. Ferrari, and F. I. Schaposnik Massolo, Phys. Rev. Lett. **120**, 061602 (2018).
- [180] F. Ferrari and F. I. Schaposnik Massolo, Phys. Rev. D **100**, 026007 (2019).
- [181] S. Cao, Y.-C. Rui, and X.-H. Ge, arXiv 10.48550/arXiv.2103.16270 (2021), 2103.16270 .
- [182] D. Vollhardt, Ann. Phys. **524**, 1 (2012).
- [183] M. Ley-Koo and M. S. Green, Phys. Rev. A **23**, 2650 (1981).
- [184] M. E. Fisher and G. Orkoulas, Phys. Rev. Lett. **85**, 696 (2000).
- [185] C. N. Yang and C. P. Yang, Phys. Rev. Lett. **13**, 303 (1964).
- [186] C. E. Bertrand, J. F. Nicoll, and M. A. Anisimov, Phys. Rev. E **85**, 031131 (2012).
- [187] J. J. Rehr and N. D. Mermin, Phys. Rev. A **8**, 472 (1973).
- [188] J. Wang, C. A. Cerdeiriña, M. A. Anisimov, and J. V. Sengers, Phys. Rev. E **77**, 031127 (2008).
- [189] J. A. Plascak and P. H. L. Martins, Comput. Phys. Commun. **184**, 259 (2013).
- [190] H. E. Stanley, *Introduction to Phase Transitions and Critical Phenomena* (Oxford University Press, Oxford, England, UK, 1987).
- [191] P. A. Pearce and C. J. Thompson, Commun. Math. Phys. **41**, 191 (1975).
- [192] T. Mori, Phys. Rev. E **82**, 060103 (2010).
- [193] L. Erdős and B. Schlein, J. Stat. Phys. **134**, 859 (2009).
- [194] D. Kubizňák and R. B. Mann, J. High Energy Phys. **2012** (7), 033.
- [195] D. Kubizňák, R. B. Mann, and M. Teo, Classical Quantum Gravity **34**, 063001 (2017).
- [196] C. Niu, Y. Tian, and X. Wu, Phys. Rev. D **85**, 024017 (2012).
- [197] J. Maldacena, Int. J. Theor. Phys. **38**, 1113 (1999).
- [198] B. P. Dolan, Classical Quantum Gravity **28**, 125020 (2011).
- [199] B. P. Dolan, Entropy **18**, 169 (2016).

- [200] S. W. Hawking, *Commun. Math. Phys.* **43**, 199 (1975).
- [201] S. Hawking, *The universe in a nutshell* (Bantam, 2001).
- [202] M. C. LoPresto, *Phys. Teach.* **41**, 299 (2003).
- [203] J. D. Bekenstein, *Phys. Rev. D* **7**, 2333 (1973).
- [204] C. W. Misner, K. S. Thorne, and J. A. Wheeler, *Gravitation* (Princeton University Press, 2017).
- [205] J. D. Bekenstein, *Phys. Rev. D* **23**, 287 (1981).
- [206] J. E. Mazo and A. M. Odlyzko, *Monatsh. Math.* **110**, 47 (1990).
- [207] M. Ammon and J. Erdmenger, *Gauge/Gravity Duality: Foundations and Applications* (Cambridge University Press, Cambridge, England, UK, 2015).
- [208] S. A. Hartnoll, arXiv 10.48550/arXiv.1106.4324 (2011), 1106.4324 .
- [209] K. Jensen, *Phys. Rev. Lett.* **117**, 111601 (2016).
- [210] H. Liu, J. McGreevy, and D. Vegh, *Phys. Rev. D* **83**, 065029 (2011).
- [211] K. Hartnett and R. L., *Mathematicians Disprove Conjecture Made to Save Black Holes* (2021).
- [212] G. Sarosi, in *Proceedings of XIII Modave Summer School in Mathematical Physics — PoS(Modave2017)*, Vol. 323 (SISSA Medialab, 2018) p. 001.
- [213] C. Promsiri, E. Hirunsirisawat, and W. Liewrian, *Phys. Rev. D* **104**, 064004 (2021).
- [214] E. Witten, arXiv 10.48550/arXiv.hep-th/9803131 (1998), hep-th/9803131 .
- [215] J. Maldacena and X.-L. Qi, arXiv 10.48550/arXiv.1804.00491 (2018), 1804.00491 .
- [216] J. Maldacena and A. Milekhin, *J. High Energy Phys.* **2021** (4), 1.
- [217] A. Chamblin, R. Emparan, C. V. Johnson, and R. C. Myers, *Phys. Rev. D* **60**, 064018 (1999).
- [218] K. Hajian, H. Özsahin, and B. Tekin, *Phys. Rev. D* **104**, 044024 (2021).
- [219] T. Kaluza, *Int. J. Mod. Phys. D* **27**, 1870001 (2018).
- [220] A. Gaikwad, K. K. Joshi, G. Mandal, and S. R. Wadia, *J. High Energy Phys.* **2020** (2), 033.
- [221] S. R. Das, A. Ghosh, A. Jevicki, and K. Suzuki, *J. High Energy Phys.* **2018** (2), 1.
- [222] D. Roychowdhury, *Phys. Lett. B* **797**, 134818 (2019).
- [223] D. Stanford and L. Susskind, *Phys. Rev. D* **90**, 126007 (2014).

-
- [224] S. He, Y. Sun, L. Zhao, and Y.-X. Zhang, *J. High Energy Phys.* **2022** (5), 1.
- [225] A. M. Frassino, R. B. Mann, and J. R. Mureika, *Phys. Rev. D* **92**, 124069 (2015).
- [226] R. M. Wald, *Living Rev. Relativ.* **4**, 1 (2001).
- [227] J. Gegenberg, G. Kunstatter, and D. Louis-Martinez, *Phys. Rev. D* **51**, 1781 (1995).
- [228] A. J. M. Medved, *Classical Quantum Gravity* **20**, 2147 (2003).
- [229] Y. S. Myung, *Phys.Lett.B* **624**, 297 (2005).
- [230] B.-Y. Su, Y.-Y. Wang, and N. Li, *Eur. Phys. J. C* **80**, 1 (2020).
- [231] S. W. Hawking and D. N. Page, *Commun. Math. Phys.* **87**, 577 (1982).

Acknowledgments

I am deeply grateful to my supervisor, Stefan Kehrein, for providing me the opportunity to undertake this project, as well as for the wide range of freedom to explore various directions. I appreciate his invaluable guidance, patience, and advice. I am also sincerely thankful for the financial support during my studies, and the encouragement to present my results at several scientific conferences, including the academic exchange at Caltech.

On that topic, I owe a significant debt of gratitude to Iliya Esin, my collaborator from Caltech, for his steadfast support during my visit and throughout our numerous Zoom meetings. I also extend my appreciation to Fabian Heidrich-Meisner for assuming the duties of Second Referee. His humor and positivity were always appreciated.

I would also like to thank Michael Kastner and Daniel Nickelsen for detailed discussions on thermalization in connected graphs and Lieb-Robinson bounds.

I would like to acknowledge Rishabh Jha, Philip Urich, Johan du Buisson, and Jad Halimeh for our enriching discussions on the SYK model and holography. I would like to thank Xian-Hui Ge and Sizheng Cao for guiding me through my first paper on general relativity and holography.

I am immensely grateful to those who proofread parts of my thesis, namely Rishabh Jha, Manuel Kreye, Alexander Osterkorn, and Niklas Bölter. My thanks also go out to my friend and housemate, Tim Schoof, for showing consistent interest in my research and sharing excitement over each new finding, big or small.

Lastly, my heartfelt appreciation goes out to my family, friends and, in particular, to Sahar. Their love, moral support, and shared excitement with every new paper released onto the arXiv have been a source of strength and motivation for me.

This doctoral research was partially funded by the Deutsche Forschungsgemeinschaft (DFG, German Research Foundation) - 217133147/SFB 1073, project B03 and the Deutsche akademische Austauschdienst (DAAD, German Academic Exchange Service).

Nationality South African

Languages

Afrikaans Mother tongue, fluently spoken and written
English Mother tongue, fluently spoken and written
German Fairly spoken and written

Academic Education

Nov - Dec 2022 Research stay at California institute for technology (Caltech)
2019–2023 **PhD (Theoretical Physics) active**, *Georg-August-Universität Göttingen*, Germany
Research based, with additional coursework and teaching requirements, three-year project.
Title *Analytic studies on the SYK models*
Supervisor *Prof. Dr. Stefan Kehrein*
2017–2019 **MSc (Theoretical Physics) cum laude¹**, *Stellenbosch University*, South Africa
Research based, with additional coursework, two-year project.
Title *Thermalization of a two-species condensate coupled to a bosonic bath*
Supervisors *Prof. Dr. Michael Kastner and Dr. Johannes Kriel*
2016 **BScHons (Theoretical Physics) cum laude**, *Stellenbosch University*, South Africa
2013–2015 **BSc (Theoretical Physics) cum laude**, *Stellenbosch University*, South Africa

¹ *Cum laude is the highest possible grade allotted at Stellenbosch University*

Funding and accolades

- PhD ○ DAAD Doctoral Research grant for study in Germany (2020-2021)
- MSc ○ *Rector's award* for excellent achievement in the field of academics (2019). Received for being the top 2018 graduate in the science faculty.
○ Chosen to attend the *69th Nobel Laureate Meeting* in Lindau (2019).
○ Best MSc book prize. Given to *top MSc student* in physics (2019).
○ *Best MSc presentation* during NITheP bursary workshop (2018).
○ SU Merit Bursary. Awarded to the top students who have passed their previous year with distinctions.
○ National Research Foundation (NRF) *Grant-holder Bursary* (2017).
○ National Institute for Theoretical Physics (*NITheP*) *MSc Bursary*.
- BScHons ○ Meiring Naudé Medal for best BScHons Physics student at Stellenbosch University.
○ Helpmekaar Medal for highest academic achievement.
○ National Institute for Theoretical Physics (NITheP) Bursary.
○ SU Merit Bursary.
- BSc ○ *Rector's award* for excellent achievement in the field of academics (2016). Awarded to the top science graduate of 2015.
○ 2014 – 2015: SU Merit Bursary. Awarded to the top students who have passed their previous year with distinctions.